PXY collaboration with other cambial regulators, ER, and MP, is essential for secondary growth

KRISTINE SAMVEL BAGDASSARIAN

PXY collaboration with other cambial regulators, ER, and MP, is essential for secondary growth

By Kristine Samvel Bagdassarian

A thesis submitted for the degree of Doctor of Philosophy

Department of Bioscience

Durham University

July 2021

Declaration

I declare that the material contained within this thesis has not previously been submitted for a degree at Durham University or any other university. The research in this thesis has been conducted by me unless otherwise stated.

Acknowledgements

Many people have helped me along the way to completing this thesis. First and foremost, I would like to thank my husband Thomas, who I met at the start of my third year of PhD, and who has been my rock and solace ever since. I could not have done this without him, his ability to make me laugh when I most need it, or without his cooking.

I would also like to thank my supervisors Peter Etchells and Natasha Savage for their endless support and patience. Thank you for believing in my work even when I wasn't sure I did.

Many thanks for my family and friends, who have been there throughout this entire process and always told me I can.

Abstract

Plants grow both in height, and in width. The process of radial expansion, known as secondary growth, generates the majority of the plant biomass through expansion of the vasculature, the plant's water and nutrient conducting tissues. It is therefore imperative to understand how vascular growth is regulated. Secondary growth is facilitated by a collection of stem cells present in a meristem called the vascular cambium. The cambium gives rise to the water-conducting xylem and nutrient conducting phloem, on opposing sides via periclinal cell divisions. A receptor-like kinase PXY has been found to promote cell division in the cambium, and to control its ability to maintain distinct domains for xylem and phloem. Loss of PXY results in interspersal of these cell types.

PXY interacts with other components in regulating secondary growth. It was seen to genetically interact with another receptor-kinase and its family of genes, *ER*. However, comprehensive exploration of how these two genes and their families interact had not been determined. Similarly, PXY was shown to indirectly suppress the transcription factor MP in stem, but to be promoted by MP in root. Both components were also found to be localized in the same domain on the xylem side of the cambium, where the hormone auxin was shown to accumulate. Disruption of the auxin pattern or removal of *PXY* or *MP* results in defects in cambial function, but the basis of these interactions is not fully understood.

To address the questions surrounding *PXY*'s role in secondary growth, a bespoke method for measuring cell sizes and shapes from cross-sections of plants was developed. This method was employed to analyse *PXY* and *ER* families single and combinatorial mutants. Finally, a theoretical three-cell mathematical model was proposed examining PXY's relationship with the transcription factor MP in controlling the accumulation of auxin in the cambium.

The results of these studies demonstrated that loss of *PXY* and *ER* families results in different consequences in stem and hypocotyl. In hypocotyl and in the absence of the *PXY* family, ER and its genetic paralogues promote hypocotyl radial growth in part, compensating for loss of PXY by promoting cell size increases, but this was not observed in stem. Moreover,

loss of all of the *PXY* and *ER* genes results in complete suspension of secondary growth, suggesting that these two genetic pathways are required for the transition between primary and secondary growth. In the investigation of PXY's relationship with the transcription factor MP in root, it was shown both numerically and analytically that a negative feedback loop between the two provides stability to the system, thus generating a more stable auxin gradient in the cambium. Thus, PXY interacts with both ER and MP to maintain vascular organisation and growth, and these interactions are essential for the induction of secondary expansion, as well as hormone patterning in order to promote cambial activity.

Contents

Foreword

The focus of this thesis is the study of plant vascular development during secondary growth, otherwise known as the radial increase of plant organs. Here, I target the underlying signalling mechanisms which govern both this expansion and the associated tissue patterning in plants. In the centre of the investigation is the cambium - the meristem that generates secondary growth in plants - and a receptor-kinase PHLOEM INTERCALATED WITH XYLEM (PXY) expressed in the cambium, and coordinating the cell division rate and cell division plane. This thesis addresses gaps in the literature associated with PXY's activity in interacting with its own genetic paralogues and other components responsible for secondary growth and patterning. I argue that in order to fulfil its role, PXY collaborates with several key regulators of secondary growth, including other receptor families and hormonal downstream components.

To address the question of how PXY performs its function, I employ: first, a theoretical investigation; second, I develop a bespoke image analysis method to analyse and compare mutants with *PXY* family background; third, I construct a mathematical model to test PXY's role in promoting cambial activity (divisions in the cambium) during secondary growth. I conclude that PXY is involved in several complex relationships cross-tissue and in the cambium, in order to coordinate the proliferation and organisation of the vasculature.

This thesis consists of a compilation of both published and unpublished work, utilising conceptual research, image analysis techniques and mathematical modelling to pursue deeper understanding of the regulation of secondary growth and organization. Below, I will summarise the structure, chapter by chapter.

The first chapter describes the relevant research background and is comprised of three parts. The first part discusses a general overview of vascular tissue in plants and the importance of the cambium for secondary growth. The second part covers signalling mechanisms that regulate the activity of the cambium. The final part of the chapter summarises several important papers in biology which use computational techniques in order to support their testing of hypothesis in plant science. Together, the subsections of Chapter 1 provide the necessary knowledge-base required to conduct the bulk research of this thesis.

The following three chapters discuss the methods and results of my investigations. To

elucidate the relationship between the *PXY* gene family and another receptor-kinase *ERECTA (ER)* and its paralogues, I needed to study different loss-of-function plant mutants from these gene families and compare their phenotypical variation. For this, quantification of cell measurements such as area, perimeter and elongation were required of cells from cross-sections of the various genotypes. In Chapter 2, I will introduce a research approach capable of acquiring and evaluating such information from images. The original use of this method for investigating the *PXY* and *ER* interaction in vascular development will be covered in Chapter 3. Chapter 4's focus is the formulation of a mathematical model to test the PXY and MP relationship for the regulation of cambial activity. The model was explored both analytically and numerically to propose insights into the mechanisms governing hormone patterning in plants. In the last chapter of this thesis I offer a discussion on my research work, outputs and limitations.

This thesis takes a multi-disciplinary approach to science and explores the different pathways that can be used to build upon current understandings in a field. From reviewing existing publications and identifying a gap in the literature, to employing a bespoke method for analysis of phenotypical variation between plant mutants and finally composing a mathematical model for exploring the internal logic of a signalling system, I have approached vascular tissue development from several different angles. As such, I believe I have contributed to the field and hope you enjoy my work.

Chapter 1: Research Background

Multi-disciplinary research requires insight into several distinct types of existing literature. In this chapter, I will explore the three different research backgrounds necessary to provide foundation for this thesis.

The first section will cover a brief review of vascular tissue structure, function and its role in secondary growth. In the second part, I will tackle sub-cellular regulation, consisting of my published review of the signalling mechanisms underlying vascular establishment and maintenance. Finally, I will examine some of the major multi-disciplinary studies that combine mathematical modelling with biology. This third section will offer evidence of the value of mathematical techniques in unravelling complex questions in biology.

Read together, this three-part chapter will demonstrate how experimental and analytical tools can be combined to provide deeper understanding of research questions and hypothesis.

1.1 Plant vascular tissue

1.1.1 Overview

Plants are integral for supporting all life on Earth. They play an important part in sustaining ecosystems [4-6], providing vital habitats [4, 6], nutrients[7-11] and improving soil quality [4, 5, 7, 12]. For humans, plants are a source of fuel [13-15] and food [4, 7, 16, 17], presently rising in importance for the ever-increasing global population. Plant tissues and the chemical compounds they produce are key ingredients in the making of medicines [7, 18-22], paper[23-25] and clothing [26]. Plants are used in the manufacturing of many everyday items and furniture[25-28], and furthermore contribute to our well-being and relationship with nature[7, 29-31]. In our fight against climate change, they are some of our most powerful allies [8, 9, 32-35]. By absorbing carbon dioxide, storing it and producing oxygen, they purify the air we breathe [32-36]. The study of plant development contributes to identifying new, more sustainable resources[37, 38], boosting crop production[7, 8, 11, 17, 39-42], discovering

cures for diseases [7, 18-22] and enhancing our understanding of the world.

In general, three main groups of tissues can be distinguished in plants: dermal (which serves as a protective mechanism between the plant and the external environment) [43], vascular (which facilitates nutrient and water transport, as well as providing mechanical support) [43-45] and ground tissue (constituting all remaining tissues) [43-45]. Ground tissues sustain several functions, including surrounding and supporting the vascular bundles (the discrete structural units of the vascular tissue), partaking in regeneration processes and contributing to nutrient storage and photosynthesis [43-45].

Zones of actively dividing cells in the plant, known as meristems, are responsible for the development of all plant tissues [43-45]. Apical meristems located at the root and shoot tips facilitate primary growth, i.e. elongation of the plant body. These are known as root (RAM) and shoot (SAM) apical meristems [43, 44]. These primary meristems give rise to the primary body of the plant [44]. Many vascular (or land) plants are formed entirely of primary tissues (most monocots and a number of small dicots, to be explained later) [44]. However, other vascular plants expand radially as well. This process, called secondary growth, is facilitated through of the activity of a lateral meristem, the cambium, which bidirectionally gives rise to a strictly organised internal structure of the plant[43-45]. Here, xylem and phloem, the two main types of transporting tissues, are differentiated on either side of the cambium and are spatially separated [43-45]. Xylem is formed on the inner side of the cambium, while phloem is formed on the outer side of the cambium[43-45]. The resulting increase in organ thickness contributes to the vascular tissue making up the majority of plant biomass. It is therefore imperative to understand how these tissues are established and maintained. Such research efforts must be based on understanding both the physical properties of the vascular tissue, and the molecular interactions that govern it. In this section, I will tackle the former, providing an overview of the structure and function of the vasculature, along with the key cells which comprise it [43-45].

.

1.1.2 Secondary growth as a feature of dicots

The two major classes of flowering plants in nature are monocots and dicots. Monocots and dicots differ in several aspects, with the presence of one or two cotyledons, i.e. embryonic leaves in the seed, marking a major such distinction. Other features include,

respectively for monocots and dictots, leaf venation (parallel vs 'branched'), number of flowers in a cluster (three vs four or five) and root (upper-soil mass of splayed out thin roots of approximately equal length vs a deeper-growing thicker main root with lateral roots) [44]. In primary stems, there is also a distinction between vascular bundle organisation. In monocots, the vascular bundles are scattered, while in dicots they are arranged in a ring (Figure 1) [44].

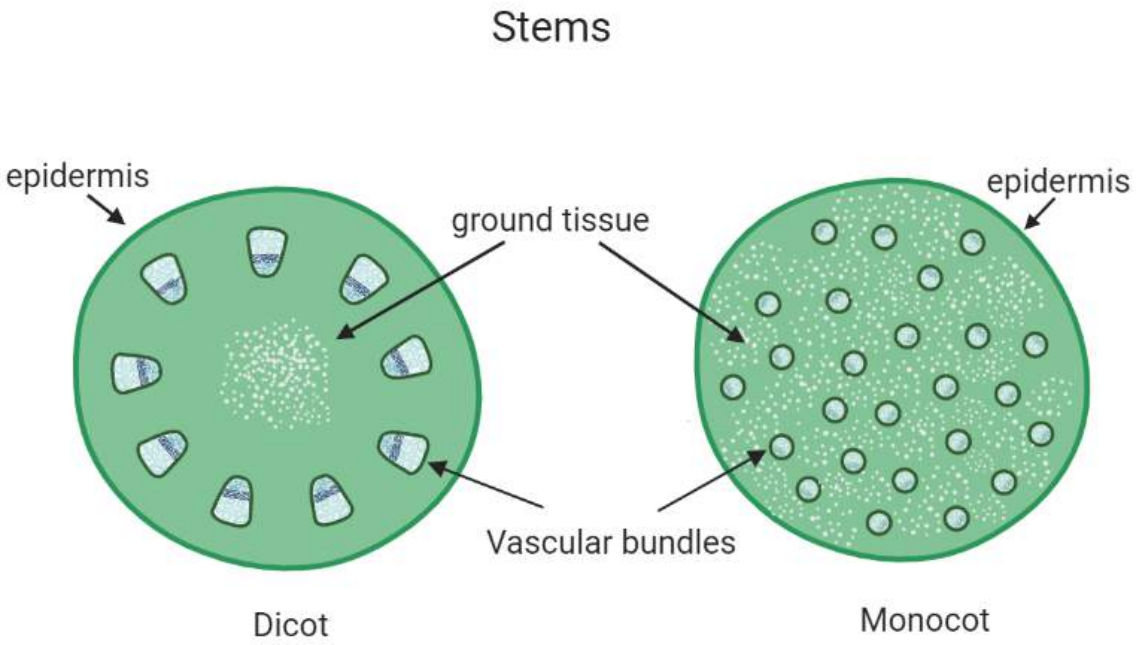

Figure 1: Primary vascular tissue organisation in dicot stems (on the left) vs monocot stems (on the right). Vascular bundles in dicots form a ring around the circumference of the stem with ground tissue in the middle, whereas monocots have scattered vascular bundles surrounded by

Secondary growth which results in the formation of secondary xylem and phloem for organ thickening, is not a typical trait of monocots. In the few monocot species where radial expansion is observed (such as in palm trees and *Yucca* plants), the underlying mechanisms involve what is called *anomalous secondary growth*, i.e. processes such as proliferation in the parenchyma or the functioning of a cambial variant which behaves irregularly to the typical vascular cambium. Since the focus of this study is the regulation of vascular tissue during secondary growth, unless otherwise specified, I will focus on the dicot model plant *Arabidopsis thaliana*, whose genome is small and well annotated. In *Arabidopsis thaliana,* secondary growth occurs in root, hypocotyl and stem [1] In what follows, the concepts of primary and secondary vascular pattern will be described, as well as organisation of the vascular tissue patterns in these three *Arabidopsis* organs.

1.1.2.1 Primary vascular pattern in root and hypocotyl

Development of the vasculature is broadly understood as a continuous process [1] (Figure 2). The formation post-fertilization of the complete plant embryo is known as embryogenesis and is consisted of several stages: embryo sac, zygote, one, eight and sixteen cell stage, early and late globular, transition stage, heart stage and finally seedling. The correct patterning of xylem and phloem can be traced back to the globular stage, when post-fertilization the meristematic tissues are first formed [46, 47].

Root and hypocotyl follow a similar developmental process in terms of both primary and secondary vascular patterning (Figure 2) [48-50]. In *Arabidopsis thaliana*, organisation of the vasculature is offset by four initial cells that undergo periclinal cell division [46, 47]. The subsequent primary pattern represents a template for the establishment of the mature vasculature and is comprised of two protoxylem poles linked by a bridge of metaxylem cells, thus creating a central xylem axis (Figure 2) [47]. This xylem axis is flanked by procambium

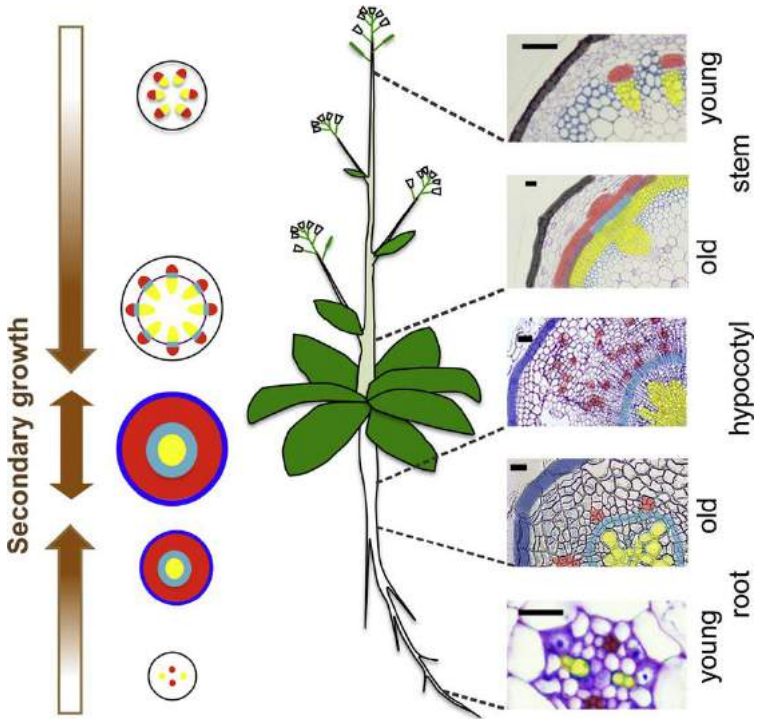

Figure 2: From: Ragni & Greb (2017) **[1]**. Fig 2. Layout of vascular tissue organisation in higher plants in young and old root, hypocotyl and stem.Left-hand side is a schematic. The right-hand side is the cross sections of images. Based on Ragni & Greb (2017) **[1]**, red is phloem, light blue is cambium, purple is interfascicular cambium, yellow is xylem, black is epidermis, blue is periderm. Scale bar iss 50 μm. In this diagram, young is primary growth, old is secondary.

cells, on the other side of which resides a single pole of phloem cells to be expanded into a ring with the offset of secondary growth [47, 51]. In this way, the xylem axis creates a cross-like shape with the two phloem poles positioned at 3 and 9 o'clock relative to the centrally spanning 12 to 6 o'clock xylem axis (Figure 2). This bisymmetric (diarch) pattern is essential for the normal establishment of the mature root/hypocotyl [1, 52].

1.1.2.2 Secondary vascular pattern in root and hypocotyl

The diarch pattern described above is a characteristic of both root and hypocotyl primary vascular organisation [43]. In the next stage of development, secondary vascular tissues are produced via periclinal cell divisions from the lateral cambium [43, 53, 54]. This is marked by the growth of the procambium into mature cambium and expansion of the two phloem poles to create a ring around the circumference of the root and hypocotyl. From its initial axis, the xylem also grows, eventually becoming restricted to the central vascular cylinder (Figure 2) [55, 56]. This process of seconday growth results in the full secondary vascular pattern, constituting a ring of cambial cells which generate xylem on their inward-facing side and phloem on their outward-facing side [43-45]. Notably, hypocotyls are a particularly good model for observing secondary growth due to their large radial expansion during this stage, paired with lack of elongation [55-58].

1.1.2.3 Primary and secondary vascular pattern in stems

Unlike the root and the hypocotyl, the primary vascular pattern in stem consists of several vascular bundles arranged in a ring [1, 59, 60]. This is known as a collateral pattern (Figure 1, left; Figure 2). Each bundle within this arrangement is characterized by a central collection of cambial (fascicular) cells, an inner layer of xylem cells and outer layer of phloem cells [1, 59, 60]. This collateral pattern, however, is changed as radial expansion is triggered. During the process of secondary growth, cells between the vascular bundles obtain a cambial identity (becoming the so-called interfascicular cambium) and connect the individual vascular bundles [1, 59, 60] (Figure 2). As a result of this, continuous rings emerge and, similarly to mature root and hypocotyl, a connected secondary vascular pattern is formed (Figure 2).

1.1.2.4 Similarities and differences in vascular pattern in *Arabidopsis* organs

As discussed above, mature secodary vascular patterns in root, hypocotyl and stem are similar (Figure 2). Notably, in root and stem, the transition to secondary growths forms a gradient, with observable primary pattern at the tips gradually expanding into a secondary pattern [48, 59]. By contrast, hypocotyl secondary growth is mostly uniform[1, 49]. Common regulatory mechanisms have been identified between root, hypocotyl and stem growth and development [61-64], suggesting that many of the mechanisms identified in different organs during secondary growth may overlap. In all three organs, the cambium regulates the radial expansion, directing the differentiation of new cells according to positional information and thus determining which side the phloem and xylem are generated on [65]. In the next section, I will give an overview of the key cells in the vasculature and discuss their structure and functional specificity[43-45]

1.1.3 Main cell types

Typically, xylem cells, with their role in fluid transport and plant mechanical support, occupy the inner perimeter of the cambium. Phloem, on the other hand, is a carrier of nutrients throughout the plant and is located on the outer cambial ring [43-45]. Derivation from the cambium of both these types of cells happens in an oriented manner, with the division occurring mostly periclinally down the long axis of cambial cells, pushing old cells outward and away from the cambial ring [43-45]. This strict architecture of the division plane is preserved through the entirety of the plant's life and is essential for the maintenance of normal physiological functions of the organism [43-45]. It is therefore crucial to gain a better understanding of the mechanisms responsible for this cell patterning.

1.1.3.1 Xylem

Conduction of water is essential for terrestrial plants. Approximately 500 million years ago, as organisms adapted to life on land, structural changes took place in order to provide plants with the necessary tools to exist aboveground rather than in water [66]. The evolution of xylem marks this transition[66]. The new conditions of life required an inner transporting system that was mechanically strong and able to extract water from the ground and distribute

it throughout increasingly taller plants [66]. Xylem tissues served such functions.

In flowering plants (angiosperms), xylem is composed of conductive tracheary elements (TE) divided into xylem vessels and tracheids, as well as xylem parenchyma and xylem fibres [43-45]. TEs are essentially 'dead', lignified cells that have lost their protoplast (Figure 3 B,C) [43-45]. Of these, vessels constitute a majority; they are shorter and larger cells, with perforation end plates and pits (Figure 3 C). When stacked up, vessels form columns of hollow tubes that act as channels for moving water throughout the plant. Such perforated end plates are lacking in tracheids (Figure 3 B), the second type of TEs [43-45]. However, tracheids still have pits on their shared walls, which, along with their elongated shape, allows them to use adhesion to retain water against gravity[67]. Xylem fibres are smaller cells, with thicker lignified cell walls. Just like TE's, they are dead cells (Figure 3 A) [43-45]. They can be found around TEs, thus primarily operating as mechanical support and protection of the major water-conducting cells within the plant body [43-45]. Xylem parynchema is the only 'living' part of the xylem (Figure 3 D) [43-45]. It largely serves storage purposes, but it is also responsible for some short-distance transport, such as radial conduction of water [43-45]. With its role in transport and mechanical strength, xylem constitutes the bulk of plant biomass and in trees, it is known as 'wood' [44].

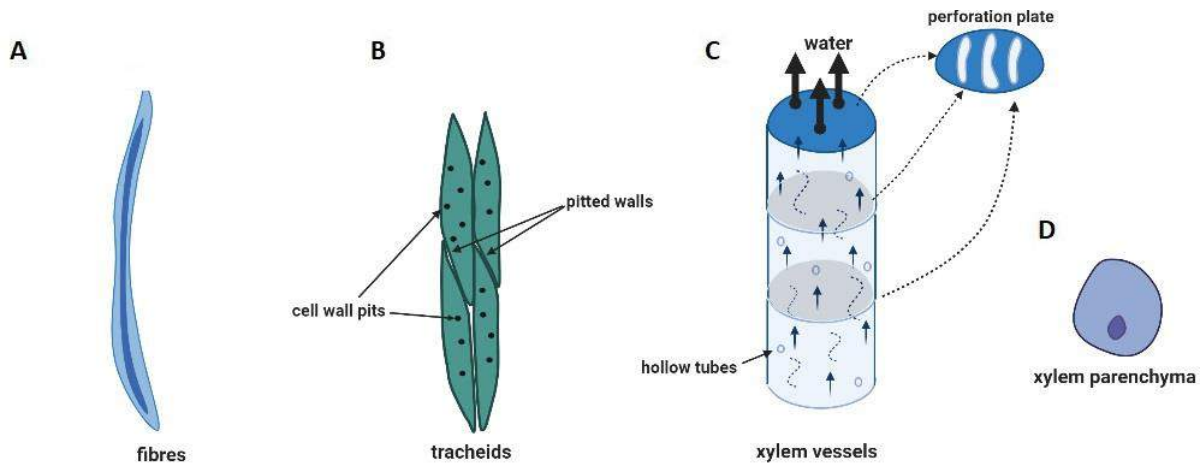

Figure 3: Diagram of xylem cell types. Longtiudinal section of xylem fibres(A), tracheids (B), xylem vessels organised in channels for water transport(C) and transverse section of xylem parenchyma cells.

1.1.3.2 Phloem

Unlike xylem, phloem cells are still alive and function primarily as conductors of sap (water-based solution of sugars, hormones and minerals) throughout the plant[43-45]. This transport is multi-directional, whereas xylem carries water only from root upwards. Broadly, the phloem is composed of sieve-tube elements, companion cells, parenchyma and fibres (Figure 4 A, B) [43-45]. Nutrient storage and some transport is performed by the parenchyma, while fibres provide support. The main conductors of nutrients, however, are the sieve elements[43-45]. They lack nuclei and most organelles, which makes them metabolically dependent on adjacent companion cells (major component of the parenchyma) (Figure 4 A,B) [43-45]. In fact, a single meristematic mother-cell gives rise to both the seive-tube and its companions [44]. This mother-cell produces several daughter-cells, among which typically the largest one differentiates into a seive-tube [44]. One or more of the remaining cells become companion cells which reside in close proximity to one or more of the seive-tube's cell walls. Phloem's ability to transport nutrients and hormones from sites of production (sources) to sinks, has been attributed to a pressure flow mechanism hypothesized by Ernst Munch in 1930. This pressure flow mechanism uses osmotic pressure gradients from regions with high nutrient concentration to draw water from adjacent cells. The resulting hydrostatic (turgor) pressure then facilitates the transporting function [44].

1.1.3.3 Parenchyma

In the above discussion, I briefly mentioned parenchyma cells and their roles as a subcategory of the xylem and phloem tissues. Part of the ground tissue, parenchyma cells generally constitute wide-spread differentiated cells that serve a range of functions[43-45]. They are largely unspecialized living cells, produced from different meristematic regions, with overall thin walls, vacuoles, protoplasts and a variety of contents depending on the cells' purpose. In the previous context, parenchyma cells were correspondents to activity of transport tissues, but they also provide photosynthetic, secretive, respiratory function, serve as a 'filler' between other structural units or even divide to perform meristematic role upon occurrences such as injury [43-45]. Usually large in size, parenchyma are often polyhedral, but this may change under external influences and proximity to other cells (Figure 4 C) [43, 44].

Similarly, they can alter their composition and lignify to provide better support, develop pits for transport or lesions to allow flexibility and oxygen-retention for aquatic plants [43, 44]. The versatility of parenchyma alongside its meristematic potential make it an important attribute to plant growth and development [68].

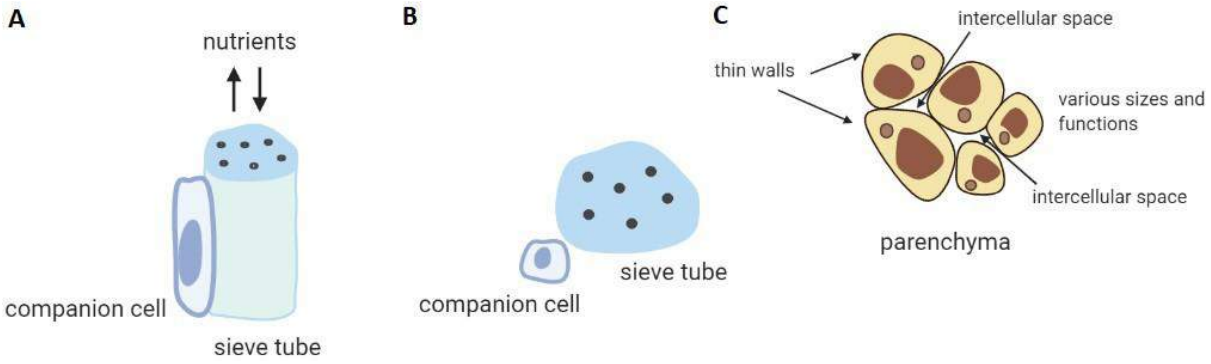

Figure 4*:* Diagram of a longitudinal cross-section of phloem seive tube and companion cell pair (A) vs a transverse cross section of the same. A cluster of general parenchyma cells are given by (C).

1.1.3.4 Cambium

At the centre of vascular development and secondary growth is the generation of tissues from the vascular cambium. This lateral meristem generates files of cells on either of its sides via periclinal divisions [44, 69]. A schematic of the orientation of cell divisions from the perspective of longitudinal and transverse section is given in Figure 5 A and B, respectively. The cambium consists of small, undifferentiated cells that show exceptional polarity [60], preserving the direction of original cell division and differentiation, even during grafting experiments where tissue sections were cut out and replaced at a 180° orientation [70, 71].

Notably, this bidirectional property of the cambium was seen to be true even at the pre-formation stage. In an experiment by Siebers (1971), incised sections were chosen from hypocotyls in locations where the cambium was expected to emerge. Inversion of these pieces did not alter the pre-cutting layout of the vasculature, suggesting polarity of the vascular ring formation was determined prior to the experiment and that the cambium

operates using short-term signals [70]. As discussed later, cambium bidirectionality has been more thoroughly investigated in recent publications by Smetana *et al*., (2019) [72] and Shi *et al*., (2019) [73].

In terms of structure, the cambium can be distinguished into two cell types: fusiform and ray initials [43, 44, 68, 74] (Figure 5 C). The fusiform cells are thin and more elongated, with wider tangential walls and wedge-shaped ends; they form the axial system of the cambium. Ray initials are somewhat elongated, close to isodiametric, and form the radial system of the vascular cambium. Both types differentiate into xylem and phloem according to the vascular patterning (Figure 5). The ray initials correspond to the production of the more radial transport system, such as the xylem parenchyma and the phloem parenchyma, whereas fusiform cells generate axial transport cells (TEs, sieve tubes, fibres) [43, 44, 68, 74].

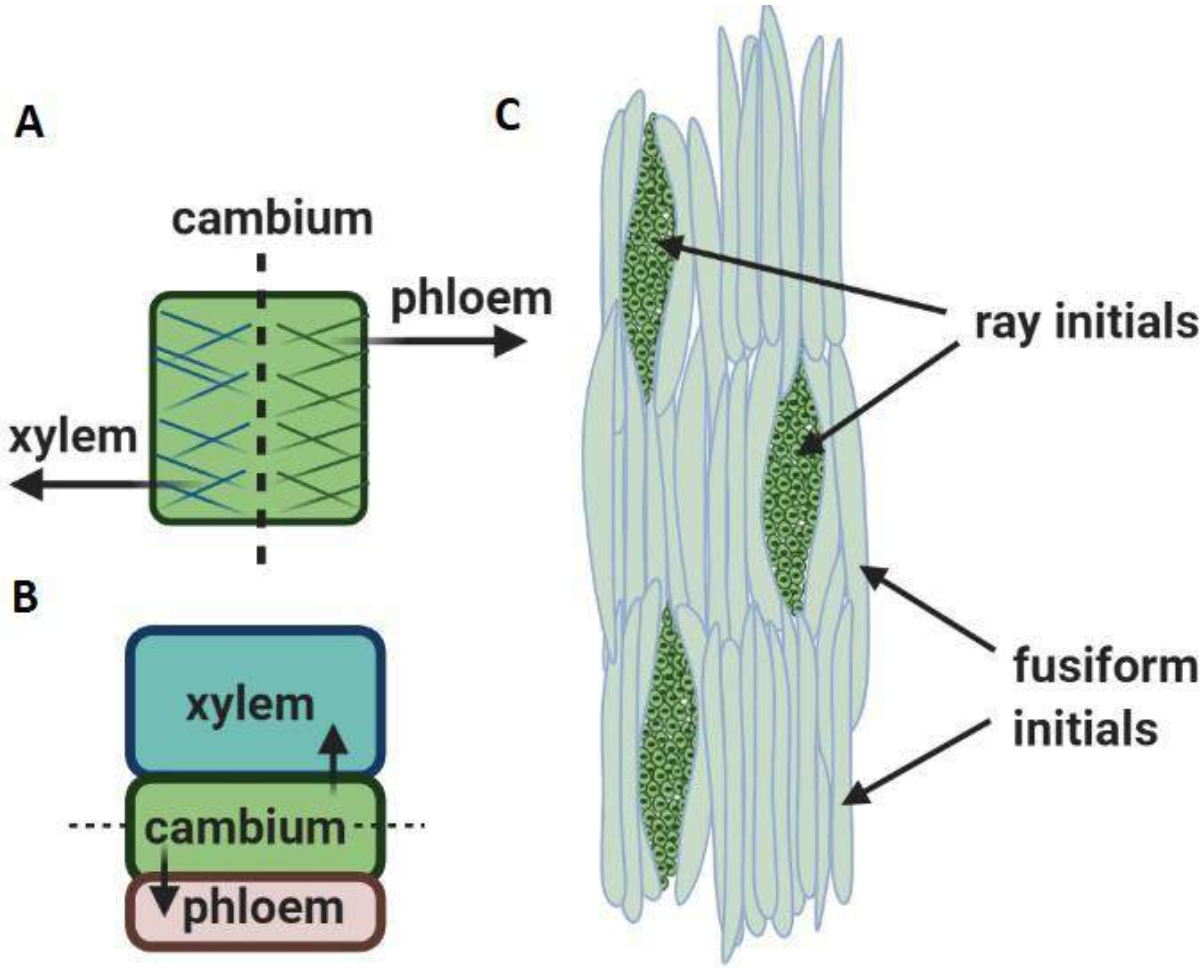

Figure 5: Longitudinal section of cambium, phloem and xylem sections with the correct orientation of division plane (A). Transverse cross section of the same organisation is given in (B). The two main types of cambium initials are in longitudinal direction in (C).

1.1.4 Summary

The role of the different cells in the vasculature contributes to the health, resilience and growth of the plant. Structural distinction of these cells provides better understanding how tissues perform their function and highlights the significant level of organisation required to maintain processes within the plant. The ability of the plant to produce spatially separated specialised cells in the required numbers and with the required properties for tissue formation is under the governance of a single cell type - the vascular cambium. Nevetherless, much is still poorly understood about the components that control cambial activity (divisions in the cambium).

Here, I aim to investigate the regulatory mechanisms that control cambium activity through short and long-distance signals, including hormones and peptide ligands. Of particular interest for this research are root, hypocotyl and stem vascular organisation in *Arabidopsis*. In the next section I will review the signalling mechanisms which impact the cambium and coordinate the correct establishment and expansion of the vasculature.

1.2 Review of major signalling mechanisms regulating cambial activity during secondary growth

Having examined the vascular tissue structure and function, I will now discuss how it is regulated. The work done for this section has been published as 'Connections in the cambium, receptors in the ring' in *Current Opinion in Plant Biology* [75]. It represents a review of the up-to-date literature of the signaling mechanisms that govern the vascular development and maintenance. The review discusses major hormone contributors, receptor-ligand interactions and their downstream components, as well as present progress in the scientific understanding of the cambium role in establishing and sustaining the correct tissue patterning during secondary growth. In addition, the review outlines several unanswered questions and directions for future research, thus building a overall picture of the field. The full publication can be found in Appendix A.

1.2.1 Review introduction

As previously discussed, in the vascular tissue, xylem provides mechanical strength to support the plant body, whilst also faciliatating the movement of water and solutes from roots to shoots. Meanwhile, the phloem distributes photosynthates and conducts the bulk flow of phytohormones (reviewed in Refs. [76, 77]) including auxin [78], cytokinin [79-82], gibberellin [83-85] and abscisic acid (ABA) [86-89], to drive physiological responses and regulate plant development. Both cell types are derived from the cambium, with the specification of their cell type identity and function summarised in recent reviews [90-97]. Here, I will discuss the signalling mechanisms that regulate the homeostasis of the cambium to allow it to generate tissues in the vasculatures.

1.2.2 Hormone harmonies

Most plant hormones play a role in the regulation of cambial activity [85, 98-100], but the most prominent and well-studied are auxin and cytokinin. Auxin is involved in numerous developmental processes, operating through a signalling pathway that includes auxin/indole-3-acetic acid inducible Aux/IAA proteins, TRANSPORT INHIBITOR RESPONSE 1 (TIR1) receptor, and the AUXIN RESPONSE FACTOR (ARF) family of genes [101-106]. ARFs act as transcriptional

regulators [58, 59].

Auxin's interaction with ARFs is established via a de-repression mechanism modulated by auxin. In the absence of auxin, ARFs are blocked by heterodimerization by auxin/indole-3-acetic acid inducible Aux/IAA proteins [101-109] and are thus unable to facilitate subsequent signalling responses. Auxin's role to offset downstream activity involves TIR1 protein which forms a ubiquitin-ligase complex $\mathrm{SCF}^{\mathrm{TIR1}}$ with SKIP-CULLIN-FBOX (SCF) and acts as an auxin receptor [110-113]. As it is introduced into the cell, auxin directly binds to $\mathrm{SCF}^{\mathrm{TIR1}}$'s Leucine Rich Repeats (LRR) domain and promotes interaction with Aux/IAA proteins. This triggers the degradation of these Aux/IAA proteins and releases ARFs to perform their function [102, 112]. Of the ARFs, ARF5/MONOPTEROS (MP) regulates proliferation in the vascular stem cell niche, as well as performing distinct roles in early and late stages of vascular development. During embryogenesis, *mp* mutants fail to establish a central axis in the provascular cylinder [114, 115]. Weak *mp* alleles also demonstrate disrupted auxin transport [114, 116, 117] due to MP directly activating transcription of several PIN-FORMED (PIN) auxin efflux transporters [118, 119]. Thus, in early development, MP promotes vascular proliferation. Late in development, during secondary growth, *mp* mutants demonstrate increased cambial divisions, suggesting that in this context MP suppresses vascular expansion [120, 121]. Conversely, other auxin response factors, ARF3 and ARF4, have been shown to operate in concert to upregulate cambium activity [121].

Cytokinin also contributes to cambium development, with loss of cytokinin-synthesizing genes deterring cambium formation and thus radial vascular expansion [122, 123]. Cytokinin signalling occurs via a phosphorelay, which begins with cytokinin perception by its family of receptors CYTOKININ RESPONSE 1 (CRE1)/WOODEN LEG (WOL)/ *Arabidopsis* HISTIDINE KINASE4 (AHK4), AHK2 and AHK3 [123-127]. Following perception, *ARABIDOPSIS* PHOSPHOTRANSFER PROTEINS (AHPs) AHP1- AHP6 are activated [128-130], with AHP1-AHP5 promoting cytokinin signalling, and AHP6, acting as a pseudo-AHP and thus as a negative regulator of the signal [128-131]. In the final steps of the signalling cascade, AHPs phosphorylate type-B *ARABIDOPSIS THALIANA RESPONSE REGULATORS (ARRs)*, transcription factors that promote cytokinin responses including vascular proliferation. AHPs also trigger the transcription of type-A ARRs, which in turn suppress cytokinin responses, thus buffering the system [132-137].

Auxin and cytokinin ratios influence the balance between cell division and

differentiation during plant development [138-142]. Their concentration gradients span the vascular tissue with a cytokinin maxima in the phloem, and an auxin maxima on the xylem side of the cambium (Figure 7) [120, 121, 143]. Cross-talk between these hormones is likely important in establishing the auxin/cytokinin ratios. Auxin stimulates the expression of cytokinin oxidase (CKX), a major cytokinin deactivating enzyme [144], and suppresses the transcription of *isopentenyl tranferase (IPT)* genes that encode cytokinin-promoting enzymes [145, 146]. Auxin also increases expression of AHP6 which, as described above, dampens cytokinin signalling [80, 129, 131]. In the root xylem axis, MP/ARF5 promotes the transcription of TARGET OF MONOPTEROS 5 (TMO5), a bHLH transcription factor that forms a heterodimer with LONESOME HIGHWAY (LHW). In turn, the TMO5/LHW heterodimer upregulates cytokinin biosynthesis genes *LONELY GUY3/4 (LOG3/4)* [52, 147]. Cytokinin notoriously acts on auxin by controlling distribution and levels of auxin transport's main conductors, the PIN proteins [80, 140, 142, 148, 149]. Cytokinin application strongly affects PIN transcription levels, downregulating PIN1-PIN4 and upregulating PIN7 [142]. In developing roots and shoots, transcription levels of auxin biosynthesis genes were stimulated by cytokinin, thus promoting auxin production[150]. Cytokinin also induces expression of a group of related DOF-family transcription factors, DOF2.1, DOF6, TMO6, PHLOEM EARLY DOF 1 (PEAR1), PEAR2, OBF BINDING PROTEIN 2 (OBP2) and HIGH CAMBIAL ACTIVITY 2 (HCA2) which promote procambial cell divisions [151-154].

1.2.3 Peptides and proliferation

Peptide ligands and their cognate receptors contribute substantially to secondary growth and patterning. The cambium-expressed, leucine-rich repeat receptor-like protein kinase (LRR-RLK) PXY, also known as TDIF-RECEPTOR (TDR) [154, 155] and its phloem-expressed ligand TRACHEARY ELEMENT DIFFERENTIATION INHIBITORY FACTOR (TDIF) are essential for cell proliferation and division plane specification (Figure 7 and 8a) [155-159]. TDIF, encoded by *CLAVATA3/ENDOSPERM SURROUNDING REGION 41 (CLE41)*, *CLE42* and *CLE44*, was identified as a repressor of xylem differentiation and is structurally similar to CLAVATA3 (CLV3) [156] a peptide ligand that regulates meristem maintenance in shoots and signals to receptor CLV1 [160, 161]. *pxy* mutants were first described as lacking separation between cambium-derived phloem and xylem tissues and as having disrupted orientation of cambial cell divisions [154]. Hirakawa *et al.* independently identified PXY by testing loss-of-

function mutants in relatives of CLV1, for TDIF insensitivity [155].

Since CLV signalling acts to repress expression of homeodomain transcription factor WUSCHEL (WUS) [162, 163], potential transcript targets of TDIF/PXY signalling were hypothesised to be members of the WUSCHEL-RELATED HOMEOBOX (WOX) family [164, 165]. WOX4 exhibited a rise in expression levels following TDIF treatment, and WOX14 was identified as being down-regulated in *pxy* mutants. Both WOX4 and WOX14 were seen to stimulate cambial cell proliferation [158, 159], with WOX14 cooperatively controlling expression of LOB DOMAIN-CONTAINING PROTEIN (LBD4) transcription factor with a DOF transcription factor, TMO6 (7 and 8a) [166].

The PXY/TDIF signalling module influences outputs of auxin signalling. For instance, PXY acts to repress one glycogensynthase kinase-3 (GSK3), BIN2-LIKE 1 (BIL1). In the absence of PXY, BIL1 phosphorylates MP (Figure 8a), which is thought to loosen MP's interaction with an IAA suppressor, thus releasing it to control gene expression [120]. Recently, Smetana et al. have reported a positive influence of auxin/MP on PXY expression in the initial stages of cambium formation in roots [72]. Since the PXY-BIL1-MP negative interactions were shown to function in the stem [120], an interesting question is whether a negative feedback loop might exist between MP and PXY, wherein MP attenuates its own activity by boosting PXY expression or whether the regulation is organ-specific. While PXY represses BIL1, it activates other GSK3s and most notably, BRASSINOSTEROID INSENSITIVE 2 (BIN2) in the presence of TDIF. Active BIN2, in turn, phosphorylates a transcription factor BRI1 EMS SUPPRESSOR 1 (BES1), marking it for degradation. BES1 promotes xylem differentiation (Figure 7 and 8a), thus its removal protects the cambium from differentiation [91].

1.2.4 Ring of receptors

LRR-RLKs of the SOMATIC EMBRYOGENESIS RECEPTOR-LIKE KINASE (SERK) family, including BRI1-ASSOCIATED RECEPTOR KINASE 1 (BAK1), are thought to form complexes with PXY at the plasma membrane in the presence of TDIF (Figure 8a) [167]. BAK1 also functions as a co-receptor for brassinolide with BRAS-SINOSTEROID INSENSITIVE 1 (BRI1), and as a co-receptor for bacterial flagellin peptide (flg22) with FLAGELLIN SENSING 2 (FLS2), and in these interactions the ligands act as molecular glue for the BAK1-BRI1 and BAK1-FLS2 interaction [168-170]. The PXY-SERK interactions likely differ from those described for other receptors. PXY LRR domains are shorter, and the receptor domain lacks the curvature of BRI1 and FLS2.

TDIF binds PXY further from the membrane, clear of the BAK1-PXY interaction site and thus its function, in this respect, is distinct in that it is unlikely to mediate a SERK-RLK interaction [171].

In pursuit of other vascular regulators, Yang *et al*. analysed gain-of-function activation-tagging lines, one of which, *xvp-d*, demonstrated *pxy*-like morphology [172] (Figure 8). XVP encodes a cambium-expressed transcription factor of the NAC family which surprisingly localised to the plasma membrane. Bimolecular fluorescence complementation (BiFC), a split ubiquitin yeast-two-hybrid system(mbSUS) and a Fluorescence Resonance Energy Transfer (FRET) assay support the notion that XVP binds to the PXY-BAK1 complex (Figures 71 and 8a, d, e). Removal of *XVP* enhanced TDIF activity, suggesting that XVP represses vascular proliferation by allowing xylem differentiation to occur. *xvp-d* gain-of-function lines demonstrated increased *CLE44* expression, while *CLE41* and *CLE44* overexpression lines demonstrated reduced XVP expression. Thus, XVP promotes the expression of TDIF-encoding genes, but suppresses the TDIF signal and is itself repressed by TDIF (Figure 8a) [172].

In the hypocotyl, *ERECTA(ER)* and its paralogues *ERECTA-LIKE (ERL1)* and *ERECTA-LIKE (ERL2)* (abbreviated the *ER*f gene family) have been reported to promote auxin biosynthesis [173]. Of these, *ER* and *ERL1*, have been shown to prevent premature xylem fibre formation, as *er erl1* lines exhibit precocious fibre differentiation [55]. *er* enhances the loss-of-function phenotype for another LRR-RLK, SUPPRESSOR OF BIR-1 (SOBIR1)/EVERSHED (EVR) [174], which is also responsible for preventing early xylem fibre formation in *Arabidopsis* hypocotyls. ER and SOBIR1 physically interact at the plasma membrane to perform this function. ER family members regulate not only the xylem, but also the cambium. ER and ERL1 are thought to restrict radial expansion of hypocotyls as *er erl1* lines exhibit increases in xylem area (Figures 7 and 8a) [55]. Moreover, *ER* family regulation of vascular development occurs via a genetic interaction with members of the *PXY* gene family (*PXY*, *PXY-LIKE 1 (PXL1)* and *PXL2*, together the *PX*f), with *er* mutation worsening the *px*f phenotype [158] (Figure 6). Thus, ER is involved in several pathways regulating cell division and organisation in the vascular tissue (Figures 7 and 8b, c) [3].

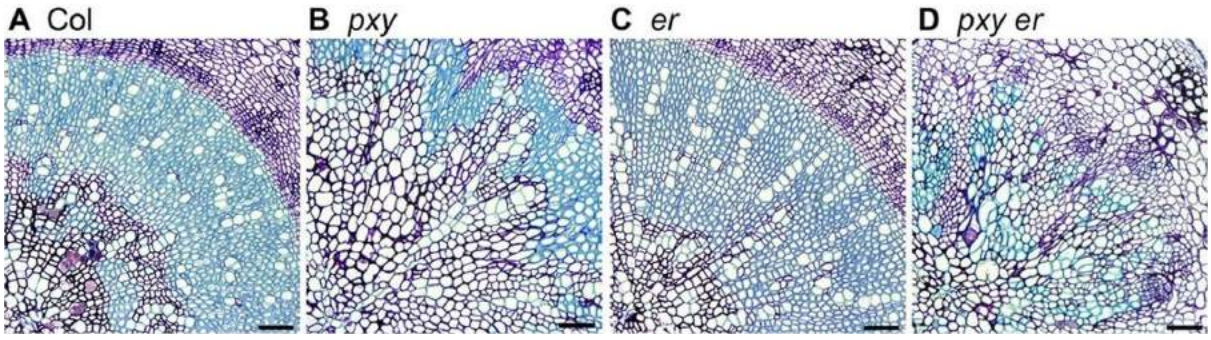

Figure 6: Adapted from Etchells et al. (2013) [158], Figure 10. er mutations enhance pxy defects in vascular tissue. Transverse sections of Arabidopsis (A)wild type, (B)pxy, (C) er, (D) pxy er. Scale bars: 50 μm.

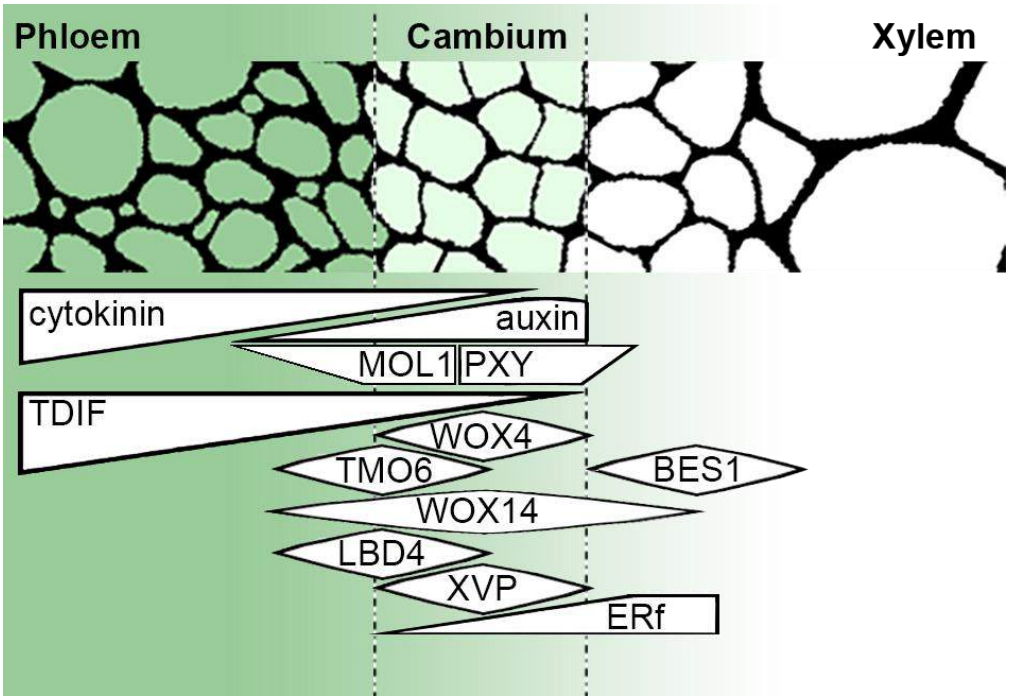

Figure 7: Source: Bagdassarian et al (2020)[2], Figure 1. Stylised depiction of *Arabidopsis* stem protein distribution and auxin and cytokinin accumulation across the vascular cambium in wild type plants. Cytokinin has a concentration maxima in the phloem; auxin on xylem-adjacent cambium. RLK's MOL1 and PXY are expressed on phloem facing and xylem facing cambium, respectively; ERf receptor expression spans the cambium. TDIF ligand is expressed in the phloem and perceived by PXY. Transcription factors WOX4, WOX14, and XVP exhibit maxima in the cambium. BES1 is present in the xylem; TMO6 and LBD4 expression as at the edge of the cambium on the phloem side.

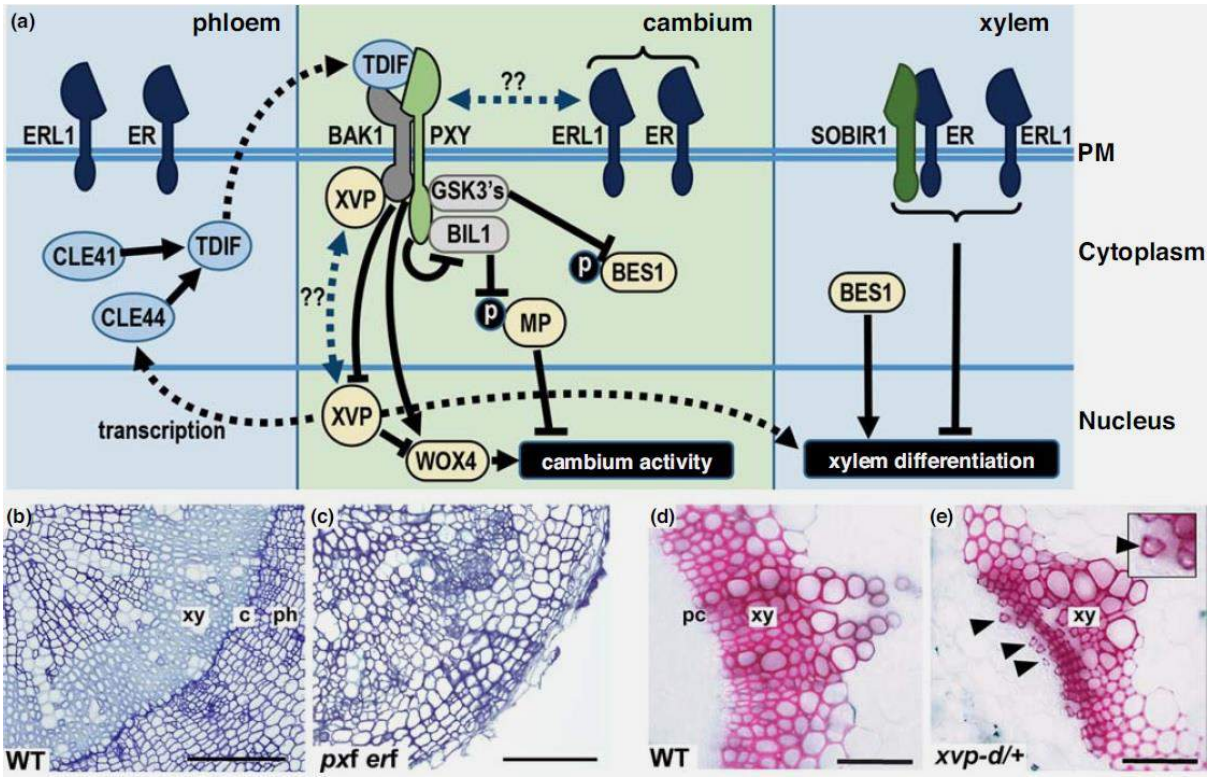

Figure 8: Signals that regulate cambium activity in Arabidopsis. (a) Schematic representation of phloem, cambium and xylem with signal components shown in the plasma membrane (PM), cytoplasm, and nucleus. RLK's are shown in the PM. PXY ligand components are light blue, transcription factors are pale yellow, and GSK3's are light grey. '??' on blue dashed arrows indicates limited understanding (signals promoting XVP translocation to the nucleus are not known; partial evidence for a physical interaction between PXY and ER family receptors has been reported). 'P' indicates phosphorylation. (b- c) Hypocotyl transverse sections, with wild type (WT; (b)) showing distinct phloem (ph), xylem (xy) and cambial (ca) domains. (c) Loss of both PXY and ER family of genes results in loss of distinct tissue domains. Plants also fail to make the transition to true secondary growth. (d-e) Stem sections stained for lignin, adapted from Yang et al. [94], with the permission from the publisher. (d) WT shows lignin deposition and thus xylem differentiation in a single arc (d). xvp-d/+ lines demonstrate premature xylem differentiation in the regions marked by arrowheads.

Like *ER* and *ERL1*, a LRR-RLK, MORE LATERAL GROWTH (MOL1), also suppresses cambial activity as *mol1* mutants demonstrated larger cambium-derived domains compared to wild type [100, 175]. MOL1 was identified in a set of experiments where *Arabidopsis* inflorescence stem explants were subjected to auxin (NAA) treatments. These treatments initiated cambium formation in the explants which were then subjected to transcriptome analysis. REDUCED IN LATERAL GROWTH (RUL1), a receptor with a positive effect on cambium activity, was additionally identified in these experiments [100]. While ER's signal peptides have been determined to belong to the *EPIDERMAL PATTERNING FACTOR LIKE (EPFL)* family [147-154], exactly which of them control cell division in the cambium is yet to be determined. Ligands for MOL1, RUL1 and SOBIR1 are also to be discovered.

1.2.5 Ontogeny of the organiser

The cambium represents a group of mostly periclinally dividing cells with the ability to generate xylem and phloem, on its two opposite sides [73, 151, 176]. A vascular organizer in xylem cells adjacent to the initiating cambium that is characterized by high auxin levels, imposes stem-cell function on its neighbour to initiate cambial divisions [151]. Since at the secondary growth stage xylem cells have already undergone programmed cell death, thus stripping them from signalling ability, Smetana *et al*. proposed that cell identity information must be passed on earlier, during xylem formation [72]. Auxin, acting through MP, ARF7 and ARF19, promotes the expression of HD-ZIP III genes, which have been previously reported as regulators of xylem identity [177-180] downstream of auxin [181, 182]. Here, they were linked to the correct establishment of the vascular organizer [72]. *WOX4* and *PXY*, which are needed for auxin responses in the cambium [183], were also required in the stem-cell organizer [72].

While Smetana *et al*. characterised the ability of the xylem to specify the position of the initiating cambium in adjacent cells in the *Arabidopsis* root [72], Shi *et al*. aimed to explore pattern in the established hypocotyl vasculature [73]. The cambium was found to be separated into three distinct sub-domains in each cell file along the radial axis' proximal, central, and distal. Independently, both Smetana *et al*. and Shi *et al*. defined PXY and WOX4 as part of the xylem-facing side of the cambium, that is the organizer side of the cambium, verifying the importance of these components for the cambium activity [72, 73]. They also confirmed a long-standing hypothesis in which the cambium stem cells (central) are flanked

by mother cells of the xylem (proximal) and phloem (distal) within each vascular cell file [1].

1.2.6 Summary

Interactions between LRR-RLKs, their ligands, cytoplasmic signalling intermediates, and their targets are increasingly well-defined in our understanding of cambium regulation [184, 185]. A recent study has proposed a transcriptional network that may explain many of the relationships between these components [166]. Identification of further signalling elements, such as ligands for MOL1 and RUL1, will help refine this picture. Remaining challenges surround hormones such as gibberellic acid and jasmonic acid, known to contribute to radial growth [99, 186], but whose role in the existing networks is largely unexplored. Much of what is known has also been characterised in a single tissue type, but differences in cambium regulation occur along the apical-basal axis of the plant [144] and how those differences underpin variations in morphology remains unclear. Finally, this review has focussed mostly on *Arabidopsis*, and entirely on dicot species. A recent analysis of cambium-regulating genes identified a small number of genes that were absent in the monocot clade [187]. Thus, an important question concerns how these networks may have been modified to give rise to the significantly different scattered vascular morphology of grass species.

As discussed above, cambium activity is in the centre of secondary growth regulation and establishment. In the previous two sections, I looked at vascular structure and function as well as the current understanding of how the cambium interacts with other signalling components to coordinate the formation and maintenance of the vascular tissue. Questions into the contemporary unknowns in this field were also highlighted. Below, I will discuss some of the interdisciplinary approaches, particularly mathematical modelling and analysis, that can be used to unveil such questions.

1.3 Review of mathematical models

While most of the studies in the previous section use genetics and molecular biology to explore signalling components and their pathways, there are aspects of these genetic networks that are not intuitively explained with genetics alone. This is where multi-disciplinary approaches can be of assistance.

Using mathematical tools to analyse biological systems has become an increasingly widespread approach in recent years, with many researchers employing a combination of experimental and mathematical methods. There are a number of reasons for this. As more information becomes available on the mechanisms controlling plant growth and development, it becomes more challenging to study individual, coupled and chain-triggered events in the grander context of the existing knowledge.

For example, in plant biology, plant hormones and their downstream components are involved in a complex system of interactions such that gaining a comprehensive understanding of small and large-scale effects and consequences is a challenging and resource-expensive process[188-190]. Such questions can be answered by manipulating mathematical frameworks built through comparison to real-life data. Once calibrated to produce results that match experiments, such models allow for an interactive relationship with the hypothesis, reorientation of perspective during testing and ability to alter the basic framework to address new questions[191]. Moreover, it is often the case that small, abstract models, which are easy to test and design, are built upon over time as more information is acquired. Such endeavours follow the emergence of novel tools, collaboration between models which exhibit different properties and the identification of fresh questions [191, 192].

Here, I will discuss several illustrative examples of mathematical modelling from the literature to show the various contexts in which such frameworks have provided valuable insight in plant biology. I will trace how such models undergo developments over time as they are expanded to accommodate more features, asses different hypotheses or are fed new data. I show that by iteratively expanding on models and challenging perspectives, the biological knowledge base is enriched to explain phenomena and secure future directions. Moreover, I argue that when used alongside experimental results, mathematical models provide flexibility in research and can be used as a powerful tool to supplement data-based science.

Since the model described in Chapter 4 centres around auxin distribution across the vascular tissues and the influence of its response factor MP, PIN transport and PXY, I will focus on models investigating hormonal interactions, downstream pathways and auxin active transport in *Arabidopsis thaliana*.

1.3.1 Modelling the auxin signalling loop

Since auxin is involved in most developmental and growth processes [146, 193-207], particularly through accumulating concentration maximas to produce a response, understanding how its distribution is controlled is particularly helpful. Auxin behavior, however, is not intuitive. Hormone cross-talk, interaction with signalling components and responses to the environment are among the many variables that impact auxin dynamics. A number of models have been dedicated to unravelling auxin's distribution and regulation, typically with an increase in complexity of formulation over time due to building on previous work.

Auxin interaction, with its downstream response factors, lays in the centre of auxin's relationship with other molecular and genetic components in the plant.Thus, understanding the dynamics of this interplay is essential for the unravelling of further biological problems. In this section, I will discuss an example of a modelling effort commenced with a single network that captures auxin's molecular dynamics but is then developed through the years to reach a more comprehensive and realistic framework that includes multiple cells, various transport mechanisms, and other hormones.

Middleton et al. (2010) [208] translated the central link between auxin, Aux/IAA proteins and ARFs in mathematical terms. On sub-cellular level, their study focused on the negative feedback loops at the core of auxin action within plant systems, using a Michaelis-Menten kinetics approach to describe the dynamics of *Aux/IAA* signalling. By combining the model with data from the literature, Middleton et al. (2010) [208] were able to assert that the ratio of Aux/IAA protein and mRNA is essential for modulating the behavior of the system. Moreover, for a small such ratio, the simulations identified a stable limit cycle illustrating a biologically sound oscillation in *Aux/IAA* expression, such as the one previously documented by Smet et al. (2007) [209] for the two protoxylem cells in the basal root meristem region. Alternative dynamic regimes caused by auxin treatment versus auxin pulse exhibited stable

node or stable spiral steady state, both of which had also been experimentally observed in members of the Aux/IAA family [210]. Thus, this model provided an efficient tool in testing and examining auxin signalling.

A later model by Muraro et al. (2011) [211] expanded Middleton et al. (2010)'s work [208] into a larger root cell model, which incorporated elements of the cytokinin signalling. Specifically, the model included the member of the Aux/IAA family, IAA3/SHORT HYPOCOTYL2 (SHY2), known to be promoted by cytokinin-activated type-B ARRs, and seen to repress PINs [139]. The model aimed to define the relationship between auxin and cytokinin for the establishment and maintenance of lateral roots and meristem size, thereby introducing elements of active transport and regulation to investigate this hormonal cross-talk [211].

In particular, the model [211] explored the hypothesis that cell division and differentiation are governed by the concentration ratio between auxin and cytokinin [144]. The model was matched to experimentally obtained results from the literature [212] and compared to data on hormone concentration derived from *shy2* loss-of-function and gain-of-function mutants. Importantly, finding disagreements between the model output and the experimental data conveyed the possibility of missing components in the system. In this way, Muraro et al. (2011)[211] utilized mathematical frameworks to suggest directions for further experimental testing to be explored.

A further expansion to Middleton et al. (2010) [208] and Muraro et al. (2011) [211] was presented in Muraro et al. (2013) [213]. Here, re-evaluation of the previously proposed models at sub-cellular and multi-cellular level was used to investigate aspects of primary root composition and lateral root initiation. More specifically, the authors discussed how hormonal cross-talk can influence division domain localisation and scope, as well as how related periodicity of hormone levels might trigger the emergence of lateral roots [213].

Unlike the earlier versions of the model, aspects of tissue identity and root zonation were incorporated. The model suggested *PIN* over-expression may result in a longer root relative to wild type, with a larger elongation zone and smaller division zone. In order to address the question of how efflux carriers may alter root composition, a three-part modelling design was employed, highlighting the flexibility of mathematical analysis to re-align a functional framework to answer newly raised questions [213].

First, a sub-cellular model intended to match experimental data on oscillatory behavior was designed using delayed Hill kinetics. This was compiled as a basis for the

subsequent analysis. Next, several domains (cells) were introduced and linked by diffusion to deploy cell-to-cell communication to the model. An independent model, described in Griensen et al. (2007) [214], (discussed in section 1.3.3 of this chapter) was used as a source for PIN localisation parameters. The solutions were compared to outputs of Muraro et al. (2011) [211] for validity.

Differences in cytokinin distribution yielded changes in the behavior of the Aux/IAA in different zones, which was interpreted as a possible explanation for tissue specification. For instance, where cytokinin was high in the basal tissues, the oscillatory solutions for Aux/IAA were suppressed, whereas low cytokinin levels in the apical domains allowed for Aux/IAA periodicity [208, 211] to dominate [213].

Finally, Muraro et al. (2013) [213] addressed the question of how cell proliferation and elongation are managed under the influence of hormonal crosstalk. A one-dimensional model construct was designed from the previous models, with different root zones specified through literature-informed auxin-cytokinin distributions. Introducing growth rates and regions, Muraro et al. (2013) [213] proposed an analysis of zone size and hormone dependence. The final continuum model, calibrated to wild type experimental results that linked growth and elongation to specific auxin-cytokinin relationships, could be used for simulation of hypothetical scenarios to direct experimental testing [213].

The investigation of hormone cross-talk for the regulation of root growth was continued in a later model by Muraro et al. (2016) [215], wherein the effects of gibberellin in the hormonal regulation of the root meristem size was included. The two-dimensional multiscale model allowed for passive and active transport and auxin flux effect between cells. Experimentally-obtained segmented image data of longitudinal root sections was used for callibration. Set at the stage of root meristem specification, the model explored cell-to-cell communication and zone characterisation using differential equations embedded in each cell structure[215].

Initially, the model suggested that in roots grown at reduced gibberellin levels, *ARR1* would accumulate more in the meristem than in the elongation zone during root growth. The staining image data generated by the group, however, showed the opposite. The required pattern could only be reproduced with an additional, ARR1-inhibiting component X. In pursuit of the unknown component, suitable genetic candidates were identified from existing microarray data. From the mutant lines that were grown, two exhibited the required

phenotype of an enlarged elongation zone and reduced meristem size. However, neither could individually account for the restricted expression of ARR1 in meristems, suggesting either that the required gene X was absent from the original sample, or that multiple regulators were responsible for X's effects [215]. In this way, the Muraro et al. (2016) [215] proposed a model which could be used to examine impact of hormonal perturbations, provide hypotheses for molecular genetic experimentation, and point to future scientific projects.

The above models are an example of model correspondence, evolution of technique, scientific hypothesis and conclusion. Together, they argue in favour of the various contributions to research offered by mathematical analysis. In addition to informing each other, these models can guide experimental research by identifying gaps in the existing data. In the next part of this thesis, I will discuss how highly dynamic processes, such as active transport though the plant, can be explained by mathematical tools, and how such models propose hypotheses to explain complex processes from biology.

1.3.2 Models of auxin active transport

A challenging aspect of understanding auxin behavior is its movement via PIN proteins. In efforts to elucidate how such dynamics define auxin patterning, mathematical models have proven essential for visualisation and interactive testing. In this section, I will discuss hypotheses related to auxin movement in root, describing how different studies culminated in explanations for emergence and maintenance of auxin distribution, and how these studies complement each other to offer, together, a much fuller picture of auxin flow through *Arabidopsis* root.

Auxin is known to flow rapidly from shoots down the phloem, accumulating in the root cap [77]. However, the molecular processes behind this accumulation are not easily understood. Two notable early studies, dating back to 1969 and 1980, attempted to eludicate how such local maxima may be achieved, each proposing a possible mechanism of action. The first, known as the *source-decay mechanism*, described by Wolpert (1969)[216] conceptualised the generation of a morphogen gradient (such as auxin in the context of the root cap) as the result of local production, diffusion and decay. The second, the *uni-directional transport mechanism*, suggested transport of morphogen as a constrained space phenomena where the end limit of the domain allows morphogen to accumulate [217]. That is, the first

source-decay mechanism was reaction-driven [216], whereas the *uni-directional transport mechanism* [217] involved flow and a geometric limit.

More recently, another mechanism by Grieneisen et al. (2007) [214] was proposed to model auxin's shoot-root dynamics. Here, using modern computational techniques, the authors showed that, crucially, PIN active transport is sufficient to achieve the required auxin peak in the root apex.

Grieneisen et al. (2007)'s [214] investigation of hormone gradients utilised several novel ideas in a multi-cellular 2D model. Within their model, a longitudinal root section was represented as a rectangular lattice of cells, consisted of an internal 'vascular' domain surrounded by 'epidermis'. To investigate hormone gradient effect on growth and development, auxin was driven through the structure using flux and active transport processes. The result was a robust, realistic distribution of auxin, with auxin moving down the root (from the shoots) through the central vascular region, accumulating in the distal regions of the root apex and then pushing up and out through the periphery (epidermis).

In simulating the model, auxin maxima localisation was shown to be unaffected by growth or abrupt halt of the auxin supply, supporting the idea that hormone distribution may operate independently of the shoot (the source) to collect auxin in the root tip. This was validated experimentally by cutting off the shoot and taking measurements of auxin reporter genes [214]. Despite the limitation of a pre-prescribed PIN positioning, the model was able to integrate several aspects of auxin-driven growth as well as illustrate that morphogenesis can be established and maintained by directional permeability and diffusion. This model was subsequently referred to as the *reverse fountain* model [214]. In the following years, the pattern output in the study was experimentally tested in Petersson et al. (2009) [218] who combined data from 14 green fluorescent protein (GFP)-expressing lines to map endogenous IAA with fluorescence-activated cell sorting (FACS) and mass spectrometry. This confirmed the computational framework's validity, and a number of subsequent mathematical investigations of auxin dynamics in the root followed, using rectangular templates representing a schematic illustration of longitudinal root section in *Arabidopsis thaliana*.

While Grieneisen et al.(2007) [214] was able to explain how the auxin distribution is maintained (even in the absence of the supply point), the requirement for prescribed PIN expression levels left the question as to how those PIN levels can be achieved in young root. This problem was addressed by a later model by Mironova et al. (2010) [219], who used a

similar two-dimensional template consisting of vascular and non-vascular cells and targeting the emergence of auxin behavior prior to the growth stages described in the Grieneisen et al.(2007) [214] framework [219].

In the initial stages of model development, Mironova et al. (2010) [219] prescribed PIN positioning to a file of cells to mirror auxin flow along the central axis of the vascular cylinder. To allow PIN levels to be calibrated to real-life data, a self-regulatory mechanism was introduced for auxin wherein PINs were positively influenced by low levels of auxin and inhibited by high levels of auxin. With this adjustment, the single-file construct successfully generated the correct hormone distribution, motivating the introduction of a more realistic, two-dimensional template of a root, with added diffusion between the cells. Testing the model showed that a wide range of parameters yielded the correct PIN and auxin dynamics, making it a fitting supplementary mechanism to the *reverse fountain* setup. This model by Mironova et al. (2010) [219] was thus referred to as the *reflected flow* model.

The limitations of the models developed in Grieneisen et al. (2007)[214] and Mironova et al. (2010)[219] motivated a combined approach wherein the virtues of each mathematical design could explain a different part of the root development process. A two-phase system was introduced, able to link root gradient emergence [219] and maintenance [214]. In Mironova et al. (2012) [220] early root was governed by the mechanisms described in Mironova et al. (2010) [219] and as the prescribed PIN expression levels emerged, the Grieneisen et al. (2007) [214, 221] setup was triggered, allowing a robust maintenance of the correct auxin pattern. Notably, the *reflected flow* model acquired the additional role of a 'recovery' mechanism, meaning it was activated following damage or disruption to the plant root system to restore auxin flow pattern.

As the above examples indicate, alongside the ability to determine connections between different setups and enriching pre-existing frameworks to fill in knowledge gaps, mathematical approaches are also an excellent tool for critically evaluating hypotheses and establishing the limits of their validity. For instance, following the publication of the model by Grieneisen et al. (2007) [214], a later discussion (by Grieneisen et al. (2012) [221]) assessed it against the previously mentioned older theories postulating means for morphogen gradient generation [216, 217, 221].

Within Grieneisen et al. (2012) [221], the three mechanisms, the *source-decay mechanism*, described by Wolpert (1969)[216], the *uni-directional transport mechanism*

[217], and the *'reverse fountain model'* by Griensen et al. (2007)[214] (here named *reflux-loop* instead), were compared to investigate how they could or could not be implemented to the establishment of auxin gradient in *Arabidopsis root*.

From a mathematical perspective, the *source-decay* model was represented using partial differential equations and solved analytically. With the introduction of particular parameter values corresponding to auxin, however, the Wolpert (1969) [216] hypothesis yielded a gradient that was too shallow to distinguish between domains and communicate positional information. Working backwards to establish what combination of parameters may yield the necessary slope, Grieneisen et al. (2012) [221] confirmed that such modified parameters would require an unrealistically slow process or a morphorgen that did not travel the distance necessary for auxin to supply sufficiently large portion of the plant.

The *unidirectional transport* mechanism was described using a framework consisting of a file of cells where auxin was driven downwards by active transport [221]. A system of ODEs was deployed. However, upon implementing the PIN permeability parameter derived from the literature, Griensen et al. (2012) [221] determined that the resulting gradient was too steep, due to a rapid 20-fold concentration decrease with every cell. A large increase in the background permeability was seen to give the correct behavior. However, such large background permeability contradicted experimental data in three ways: it overrode the contribution of PIN proteins for increasing the plasma membrane permeability, substantially decreased the active transport rate, and failed to attribute the correct high auxin-maxima pattern to PIN-expressing cells.

Finally, Grieneisen et al. (2012) [221] discussed the ability of the *reflux-loop* model to recreate the correct auxin pattern in root using experimentally justified parameters. The output of the model, its spatial and temporal scales were compared to the other two hypotheses, concluding that it was the only one out of the three to establish a stable, realistic gradient in reasonable time and space.

In a different modelling approach inspired by Grieneisen et al. (2012) [221], Band et al. (2014) [222] used the auxin signalling reporter DII-VENUS as part of the modelling setup to examine the auxin distribution in root. The authors incorporated realistic cell geometry, auxin influx and efflux carriers into their framework. The model setup was aligned with the *reverse fountain* framework of Griensen et al. (2007; 2012) [214, 221] and investigated the role of cellular regulation and auxin transporters for emergence and maintenance of auxin response

and patterning.

A novelty of the model was the use of a new tool for generating experimental data with high accuracy. A common approch to validating models against biological data, is the use of confocal images which provide not only realistic cell geometries, but can map relative hormone response and protein levels through assessment of the portrayed pixel intensity. Such data, however, can be characterized by imperfections and unclear regions. Thus, to overcome the lack of focus in the different areas of the images, the authors also developed a software *SurfaceProject* able to extrapolate a higher resolution image from a stack of images. Next, the model capabilities were assessed by comparing the resulting patterning of the DII-VENUS component in the model with the experimentally collected data manipulated by *SurfaceProject*. The model outcomes could not be matched to reality when efflux carriers were used alone. Thus, a non-polar AUXIN1/LIKE-AUX1 (AUX1/LAX) influx carrier was introduced into the framework, correcting the behavior [222] .

To test the model for validity, the efflux carriers were removed and the DII-VENUS distribution was compared to the one of a loss-of-function *aux1* mutant [222]. The results of the model matched experimental data, thus confirming the model's conclusions that influx carriers are required for correct patterning. Moreover, AUX1 was seen to direct the upflow of the reverse fountain by driving shootward auxin movement through the lateral root cap. Further analysis suggested that while PIN carriers may be necessary to establish the direction of auxin transport, efflux carriers limit high auxin levels to specific tissues [222].

The above Band et al. (2014) [222] model framework was employed as a foundation for investigation of lateral root formation in Xuan et al. (2016) [223]. Xuan et al. (2016) [223] hypothesized that programmed cell death in the root cap releases auxin and allows lateral root induction further up the primary root. Along with confirming the idea, the model showed that the appropriate auxin oscillations from the root cap necessary to trigger lateral roots, were linked to the presence of AUX1 in the root cap [223].

Conversely, the multicellular model developed by Band et al. (2014) [222] was used as an expansion to a compartment ODE homeostasis framework in Mellor et al. (2017) [224] to discuss the spatial aspect of auxin oxidation and conjugation in roots. In later models, such as Mellor et al. (2020) [225], the ideas and conclusions of Band et al. (2014) [222] were expanded to encompass other means of auxin active transport, such as transport through the plasmodesmata (a narrow channel through the cell walls of adjacent cells that allows cell

communication).

In a different branch out of the Griensen et al. (2007) [214] *reverse fountain* model, concerned with physical perturbation, Laskowski *et al.* (2008) [226] examined root architecture and sites of lateral root emergence [166]. The study combined experimental observations, imaging and mathematical modelling to discuss the effect of auxin distribution pattern on lateral root formation. The focus of the model were auxin transporters and root geometry, with Laskowski *et al.* (2008) [226] hypothesizing a tendency in lateral roots to form when the primary root was subjected to bending [226].

By inverting seedlings for a different amount of time prior to recovering their correct position, Laskwoski et al. (2008) [226] determined that the longer the seedlings were inverted, the larger the root curve angle and hence the probability of a lateral root forming. When bending roots in a **J** shape, lateral roots were seen to form preferentially on the outer side of the full curve length, where cells were more elongated. Thus, Laskwoski et al. (2008) [226] argued that cell geometry may trigger developmental changes such as determining the sites of lateral root formation.

To address this question, Laskwoski et al. (2008) [226] developed a mathematical model, wherein active transport and auxin dynamics were embedded in a realistic cell geometry. As in Grieneisen et al. (2007) [214], transporter location and polarisation was determined experimentally and the overall root structure behaved according to the *reverse fountain* mechanism published previously. The model root was then subjected to bending, which triggered rapid auxin accumulation in the bent region, with higher levels seen in the outer, more elongated cells. This result was seen to be particularly strong when cell volume was maintained during deformation, and also proved incredibly robust to parameter changes, different widths of cell walls and switch to mature cell sizes, hence confirming the Laskwoski et al. (2008) [226] hypothesis.

Previously, AUX1 importer had been shown to be positively regulated by auxin [226] while loss of *AUX1* reduced the number of lateral roots [227]. Experimental results in Laskwoski et al. (2008) [226] also indicated an overlap between auxin response and AUX1. Model simulations, on the other hand, revealed that AUX1 was accumulating in the pericycle cells exclusively during bending, drawing auxin in the region to create an auxin maxima while draining neighbouring cells of the hormone. Thus, Laskowski et al. (2008) [226] reasoned that the bias in auxin accumulation imposed by the bend and cell shape geometry, was magnified

by AUX1 activity, driving lateral root formation. Altogether, the study illustrated an excellent collaboration between experiments and computational techniques, proposing a convincing mechanisms for lateral root initiation [226].

1.3.3 Hormone interactions from a modelling perspective

Hormone cross-talk is a complex set of processes moderated by a variety of factors. Even though hormones play a crucial role in all aspects of growth and development, investigating the particulars of their effects remains challenging. To aid such research efforts, mathematical tools provide a highly informative way to study interactions at different levels of intricacy.

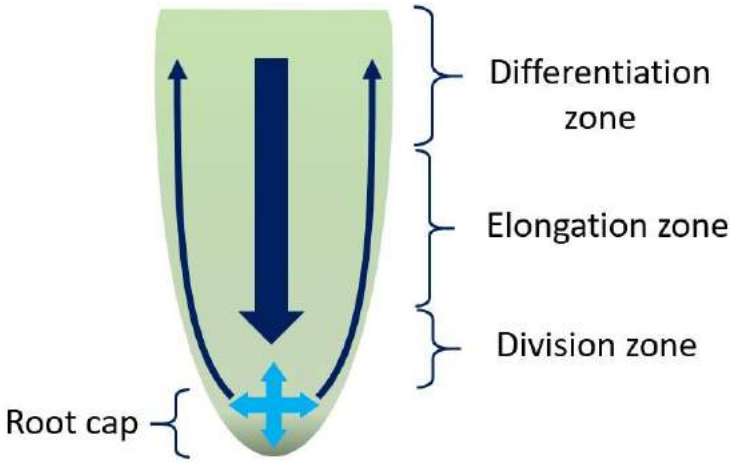

Figure 9: Root zonation and auxin flow. Arrows indicate active transport direction. Dark blue arrows indicate flow to and from the shoots. Light blue arrows indicate auxin accumulation in the root tip and movement out of the accumulation zone.

In this review, I have already mentioned two examples of modelling the synergy of hormones for root growth. Indeed, previously I discussed the work of Muraro et al. (2016) [215] and Muraro et al. (2013) [213] who built upon Middleton et al. (2010)'s [208] model of simple auxin signalling, by including other hormones - cytokinin, and cytokinin and gibberelin, respectively. In this section, I will discuss further examples of using computational techniques to elucidate hormonal interactions and how such studies pointed towards absent components in the knowledge base and possible directions for experimental work. Notably, PIN active transport, which was the focus of the previous section, is also subject to hormone regulation. The models discussed here will thus include hormone interaction with particular

reference to those that regulate PIN activity.

In an expansion of the Grieneisen et al. (2007) [214] framework, Di Mambro et al. (2017) [228] modelled the switch between cell division and differentiation under the influence of auxin-cytokinin interactions in root. In order to integrate the effect of cytokin on its hormone counterpart, the authors used realistic root geometry, supplied with experimentally valid cell sizes and shapes. In addition, PIN expression patterns were measured and embedded into the model such that the added inhibitory effect of cytokinin on them would be illustrated reliably. This refinement altered the earlier patterning achieved in the *reverse fountain* framework, introducing now an auxin maximum in the quiescent centre, followed by reduction towards the shoot and another increase in the differentiation zone (Figure 9) of all tissues [229, 230]. Model simulations proposed that the existence of the auxin dip was attributed to two cytokinin-dependent mechanisms: cytokinin's suppression of auxin transporters and the introduction of auxin degradation rate linked to cytokinin. This auxin minimum was specified at the site of emergence of differentiating cells, with increase in cytokinin supply shifting the dip downward along with reducing meristem size (enhanced differentiation), while increasing auxin supply by reducing degradation was seen to propel the opposed (rise in cell divisions). These tendencies were observed both theoretically and experimentally.

Another example, this time of a single-cell model, was reported by Liu et al. (2010) [231], examining the correspondence between auxin, cytokinin and ethylene for root growth, specifically through the *POLARIS(PLS)* gene whose loss had been reported to produce shorter roots and defective vasculature in leaves [232]. *PLS* had been previously examined by the group and linked to auxin-cytokinin homeostasis, as it was shown to be auxin-inducible and exhibited a sensitivity to exogenous cytokinin [232], whereas ethylene was seen to suppress *PLS* [233]. The exact mechanisms of interaction between these hormones and *PLS*, however, had not been identified, motivating the introduction of a mathematical framework.

Mass action and Michaelis-Menten kinetics were used to describe auxin induction of *PLS* [232], *PLS* downregulation by ethylene [233]and cytokinin ihibition by auxin [145]. For auxin-ethylene cross-talk, an additional species *X* inhibiting auxin active transport was added to callibrate the model to experimental data obtained by the group. With this component in place, the model outputs were able to match previous results of the sensitivity of *PLS* to exogenous cytokinin as well as of the link between auxin and ethylene function in root

growth[232, 233]. Thus, PLS-centered predictions could be made.

For example, disagreement between model output and experimental measurements of auxin levels after application of the ethylene precursor 1-aminocyclopropane-1-carboxylic acid (ACC) suggested adjustments to the model to incorporate PLS regulation of auxin biosynthesis. Another proposed outcome was that root length was shown to be connected to auxin concentration - an agreement with the earlier Griensen et al. (2007) [214] model. Liu et al. (2010)'s [231] single-cell model was subsequently expanded in space in Moore et al. (2015) [234].

To better understand how hormone interactions coordinate root growth through *PLS* mediation, PIN activity and localisation, Moore et al. (2015) [234] utilised the ideas of Liu et al. (2010) [231] and a similar spatio-temporal structure to the one described by Griensen et al. (2007) [214]. The cells were represented by a grid, with individual points having prescribed cell wall and cytosol properties. Many of this model's scientific approaches and conclusions were in line with the previously discussed Band et al. (2014) [222] model. For example, Moore et al. (2015) [234]'s framework was similarly validated against confocal images and also proposed that both PINs and auxin influx carriers AUXIN1/LIKE-AUX1 (AUX1/LAX) (modelled as a singular, collective AUX1 component) were needed to generate pattern. Furthermore, to fit the model, cytokinin needed to be synthesized in vascular and pericycle cells only. The authors argued that this latter adjustment suggested either a restriction of this sort existing in plants or that the model required this particular simplification, due to cytokinin and cytokinin response not being modelled separately.

The subsequent auxin pattern matched data from IAA2::GUS staining and the auxin signalling reporter DII-VENUS in wild type and mutants. Expression patterns of *PLS*, efflux and influx transporters and ethylene were correctly predicted by the model, suggesting that such network could explain these components' distribution and concentration. Furthermore, while previous models had suggested either PIN [214] or AUX1 ([222] to be discussed later) sufficiency in generating root chemical profile, Moore et al. (2015) [234] proposed that a correspondence between the two was necessary.

While discussion so far has been concerned primarily with models of *Arabidopsis thaliana* genetic networks and phenotype, an interesting model by Mellor et al. (2019) [235] discussed vascular development as dynamic structure across different species. I provide this example to illustrate once more the variety of contexts in which mathematical models can be

used to address biological queries.

Mellor et al. (2019) [235] designed a simple, three-component framework concerned only with auxin, cytokinin and a generalised PIN protein, to explain the effect of external factors on predisposing flowering plants to developing different number of xylem poles in the post-embryonic stage. By simulating a ring template of 8 to 26 cells, Mellor et al. (2019) [235] created a Hill-kinetics based predictive model which upon perturbation correlated a tendency for a large number of xylem poles with the increase in template size. Thus, a relationship between root size (as a form of spacial constraint) and structural properties (number of xylem poles) was observed.

Introducing a bias of higher auxin concentration in the xylem poles according to preiviously published data [51], the model produced a diarch vascular pattern in all subsequent template sizes, demonstrating that auxin supply can override random effects and enforce pattern [235]. To simulate growth, the model was run to steady state with inactive division and expansion, then, to mimic post-embryonic development, the template was allowed to grow until it reached a certain number of cells. Growth was seen to reduce the range of xylem pole numbers for the different templates, thus stabilising the pattern. The same results were confirmed 'in reverse', with a starting template of 40 or 20 cells and continuous reduction of number of cells.

Investigating mutant lines similarly confirmed the validity of the model. For example, mutant lines, such as a loss-of-function *lhw* mutant, were simulated, wherein the mutated gene was represented by halving the production of cytokinin. Single-pole pattern was produced both mathematically and experimentally. Thus, a simple model of hormone interactions and transport could account for morphological changes and tendencies in different cell templates and thus, in different plant species.

1.3.4 Vascular development in mathematical frameworks

In the previous sections, I focused specifically on hormone transport, distribution and regulation, from sub-cellular to organ level. Of the above examples, a single study, by Mellor et al. (2019) [235] examined vascular dynamics, by questioning how external factors coordinate the number of xylem poles developed in a plant post-embryonically. Here, I will discuss further models with relevance to vascular organisation and secondary growth.

Three models on root vascular patterning stand out in the literature – Muraro et al. (2014) [82], el-Showk et al. (2015) [236] and De Rybel et al. (2014) [52]. I will briefly summarise their setup and conclusions before examining a single publication by Mellor et al. (2017) [224] which incorporates a collaborative effort between the three groups to test the consensus between the three frameworks computationally.

Muraro et al. (2014) [82] was the first published study that used computational approaches to describe the primary root vasculature. The project aimed to identify a minimal network to stabilise radial patterning and explain the impact of auxin-cytokinin interactions on spatial organization. The study concluded that along with hormone activity, tissue arrangement is dependent on the signalling of several other key components: the SHORT ROOT (SHR) transcription factor, mobile microRNA 165/6 and the member of the HD-ZIP III family transcription factor PHABULOSA (PHB), all of which were previously shown to interact in controlling xylem patterning [177, 237]. To construct the model, a vascular tissue template was used, utilising realistic cell geometries with PIN proteins embedded in the cell membranes and Hill kinetics governing the network dynamics in each cell. The model output was cross checked with data on *IAA2* patterning in plants, while the ability of the model to recreate phenotypes was validated against experimentally obtained *shr* mutants. The model proposed an unidentified cytokinin suppressor to be experimentally sought, as well as a requirement for a mutually inhibitory PHB-microRNA 165/6 relationship [82].

De Rybel et al. (2014)'s [52] model also centred on auxin-cytokinin interaction and PIN active transport, but this time in the context of vascular development at the early embryonic stage. Of particular interest to the study were the relationships between initial structural geometry, auxin concentration bias and subsequent emergence of a correct vascular pattern. By encoding a system of ordinary differential equations into a cell template mimicking the heart-shaped stage of embryonic development, the authors simulated a growing model in the software *VirtualLeaf* [238]. Two auxin 'source' cells were defined in the centre of the template and prescribed higher auxin concentration. Auxin was modelled to promote cytokinin production but to inhibit its response, while cytokinin suppressed PIN localization at the cell membranes and activated periclinal cell divisions. The final outputs of the model were compared to the real life vascular phenotype. This computational approach allowed De Rybel et al. (2014) [52] to make a surprising discovery - geometric constraints were seen to be essential for the normal development of the plant vasculature. Indeed, stable patterns were

found only in the presence of a bridge connecting the two source cells at the centre of the template, although varying the size of the bridge and its involvement in cellular signalling dynamics proved irrelevant to the model output. The model furthermore found that local cytokinin activation in the xylem axis was central for development. Since cytokinin is not experimentally observable, this hypothesis was tested otherwise, by tracking cytokinin response markers in root instead. Experimental work supported the modelling hypothesis by finding a gradient of cytokinin response from the xylem axis that diffused outward. In this way, De Rybel et al. (2014) [52] proposed a uniquely dynamic tool for investigating growth and hormonal link to cell division and tissue organisation[52].

The third model by El-Showk et al. (2015) [236] examined auxin profile in the root tip to unravel how auxin interaction with its counterpart cytokinin allowed vascular cell identities to be specified during development. The Grieneisen et al. (2007) [214] framework was utilised as a starting point for the study. El-Showk et al. (2015)'s [236] model included hormone responses, PIN transport and diffusion in an interactive, geometrically sound template. The outputs of the model showed that, surprisingly, the auxin profile was independent of cytokinin concentration pattern, but that to achieve accurate distribution, auxin instead was required to mediate cytokinin response. Moreover, the model suggested that, just as Moore et al. (2015) [234] and Band et al. (2014) [222] had proposed earlier, both influx and efflux carriers were necessary for auxin patterning, with AUX1 and LAX1/2 playing an important role. This hypothesis was verified experimentally by the group by comparing the results from the computational simulations again loss-of-functio *aux1* and *lax1/2* mutants.

The three models above were later discussed in Mellor et al. (2017) [224]. Here, a series of computational tests were carried out to evaluate the extent of agreement between the frameworks.

Although the three publications discussed root, embryonic root and root tip vasculatures (Muraro et al. (2014) [82], De Rybel et al. (2014) [52] and El-Showk et al. (2015) [236], respectively), there were a number of similarities between the models. PIN transport, for instance, was included in all three. However, due to the complexity of the auxin transport system, each model focused on a specific aspect of the PIN function and regulation. Both De Rybel et al. (2014) [52] and Muraro et al. (2014) [82] chose a summarily defined PIN protein (dubbed PIN7 in Muraro et al. (2014) [82]'s case), while El-Showk et al (2015) [236] permitted several explicitly described PINs (PIN1, 2, 3 and 7) and a summative auxin importer. Cytokinin-

dependent regulation of PINs differed between models, with De Rybel et al. (2014) [52] choosing to focus on the inhibitory effect of cytokinin on PIN localisation, whereas Muraro et al. (2014) [82] was interested in the ability of cytokinin to induce PIN7.

To explore how asymmetry in the model setup relates to pattern formation, the works of De Rybel et al. (2014) [52] and Muraro et al. (2014) [82] were examined more closely. In Muraro et al. (2014) [82], a temporary auxin bias is needed at the initial stages of the model establishment, while De Rybel et al. (2014)'s [52] model operates with a continuously higher auxin input in the two 'source' initials. Upon swapping these conditions for the two models, adopting De Reybel et al. (2014)'s [52] initial bias onto Muraro et al. (2014) [82]'s model, and providing only a transient bias for De Reybel et al. (2014)'s [52] growing template, the experiment showed that the Muraro et al. (2014) [82] model retained reliability of output, while the De Reybel et al. (2014)'s [52] one did not. Notably, these results indicated a necessity in auxin asymmetry at initial stages of vascular establishment, but only a transient skew at the later stages of development [82, 236].

Next, cytokinin behaviour was analysed. De Rybel et al. (2014) [52] had proposed the xylem axis as a principal source of cytokinin. As mentioned previously, while cytokinin response markers are measurable, cytokinin itself cannot be examined experimentally and thus many cytokinin-related parameters, such as degradation and diffusion, are unknown. Thus, to explore the hypothesis of cytokinin distribution stated in De Rybel et al. (2014) [52], several tests were run. First, the question was asked as to whether the De Rybel et al. (2014) [52] model could create accurate patterns in the absence of a cytokinin gradient from the xylem axis. Upon increasing diffusion rates, it was revealed that the De Rybel et al. (2014) [52] framework was capable of realistic outputs at a much shallower gradient than previously suggested, although the need of a maxima in the xylem axis remained. The authors speculated that cytokinin's inhibition of PIN localization may be imposing the need for such a gradient. To test this, the cytokinin-PIN relationship was flipped, with cytokinin now promoting PIN localisation. The results confirmed that under this change a gradient for cytokinin was no longer needed, suggesting that further work was required on how the hormone interacts with active transport at different stages and in different tissues.

Next, the two remaining models were examined to test the cytokinin distribution hypothesis. Under appropriate parameter choices, the El-Showk et al (2015) [236] model was able to recreate a cytokinin gradient to match De Rybel et al. (2014) [52]'s results. The same

held for Muraro et al. (2014) [82]. However, the parameter set able to achieve this was distinctly small, suggesting that regulation of cytokinin production by other sources is likely necessary to recreate wild type behaviour more robustly. Thus, through examining the already constructed models and introducing various conditions and novel questions, Mellor et al. (2017)[224] proposed a valuable discussion on the ability of mathematical frameworks to offer insights.

Shortly after the publication of Muraro et al. (2014) [82], a different model exploring primary root patterns emerged, this time aimed at unravelling the mechanisms which drive stele pattern in plant species as a whole. In Carteni et al. (2014) [239], the goal was to provide proof of concept, namely to show that there is a commonality in the mechanisms which underline plant vascular structures, across taxa. For this, a reaction-diffusion framework was designed in MATLAB, and embedded into a circular structure mimicking the process of differentiation of the procambium, xylem and phloem. Numerical simulations were able to recreate the majority of vascular patterns in plants, with varying degrees of complexity. Thus, the model provided an excellent tool for examining hypotheses of vascular emergence across multiple species[239].

VirtualLeaf was recently used in another exploration of secondary growth. A computationally-based study by Lebovka et al. (2020) [240] built up on the group's previous experimental conclusions (Shi et al., 2019) which found that the hypocotyl cambium was marked by PXY on the proximal side and the phloem-promoting *SUPPRESSOR OF MAX2 1-LIKE PROTEIN 5 (SMLX5)* gene [241] expression on the distal [73]. To unravel the minimal network required for the cambium's ability to dynamically produce distinct vascular tissues on its opposite sides, Lebovka et al. (2020) [240] designed a computational model, in the centre of which was the TDIF-PXY signalling module. Within this model, cells were set to grow to an experimentally verified size, and cambium cells were to divide upon reaching a certain threshold. Since activated PXY (TDIF bound to a PXY receptor) had been shown to suppress xylem differentiation but promote divisions [91, 155], the model was initially set to require low PXY-active levels in order for cells to differentiate into xylem, and high PXY-active levels for divisions to occur. This produced a cell template where proximal cambial cells were hindered from differentiating into xylem due to high active PXY but were able to proliferate, whereas the opposite was true distally. No phloem, however, was yet procured [240].

The distally expressed MOL1 had been seen to repress the cambium [100]. To program

phloem emergence, a local inhibitor with these properties was introduced. Phloem differentiation was coded such that low active PXY levels in a cambial cell of appropriate size would produce a xylem cell, whereas high PXY levels would trigger the opposite. This resulted in a realistic vascular pattern with a dominant division region in the proximal domain. Thus, key vascular proliferation and organization features were embedded under the governance of only few components, allowing for the dynamics of such system to be studied [240].

Despite the ability of the model to reproduce wild type vascular properties, there were disagreements with the *pxy* mutants. First, in experiments, promoter domains of *PXY* and *SMLX5* were seen to be completely separate, suggesting their distinction was not the result of the TDIF-PXY module as originally assumed by the authors through simulations. Secondly, removal of *PXY* in the model halted all divisions, whereas in practice, *pxy* mutants would still be able to produce more cells,s albeit at a lower rate. Finally, upon studying the cell type numbers between wild type and *pxy,* Lebovka et al. (2020) [240] found that unlike the model, no changes in the number of xylem vessels could be noticed, but instead a difference between parenchyma to fibre ratio was in place. Thus, the authors concluded that while *PXY* appeared to positively regulate fibre formation, it could not singularly account for xylem regulation[240].

To account for this new information, a number of modifications were introduced. The model was altered to include a mechanism for cell divisions in the absence of PXY by introducing a phloem-derived component similar to the previously identified DOF transcription factor *PHLOEM EARLY DOF (PEAR)* and able to stimulate cell proliferation [242]. Since evidence suggested xylem vessels were not just PXY-dependent, the formula was changed, with appropriately positioned xylem cells that had reached the required cell size now able to differentiate into xylem. Phloem poles and phloem parenchyma was distinguished, with a self-regulatory mechanism that enforced default phloem poles to be produced unless they were in the vicinity of other phloem pole cells. In this way, a dynamic framework able to reproduce vascular patterning of mature hypocotyl was accomplished, pointing to several candidates with MOL1 and PEAR properties for the missing components to be sought experimentally [240].

1.3.5 Summary

The above modelling examples discuss varying levels of computational complexity, often developing with time into more elaborate models and addressing a range of biological questions. I have discussed how mathematical frameworks can be used to independently answer a question, challenge ideas, or complement each other in order to produce a more fullfilling explanation of phenomena. In addition, I showed how a single model can be the foundation for several subsequent studies which address vastly different developmental aspects. I argued that, in partnership with experimental data, computational tools are a key part of research.

In Chapter 4 of this thesis, I will introduce a small model centered around PXY, auxin and MP's relationship. With the discussion above, I provided evidence that such small models are an essential part of addressing early stage hypotheses. Thus, I will be proposing the model in Chapter 4 as a formative step towards understanding the relationship between PXY and MP for regulating auxin pattern.

1.4 Conclusions and aims

In this introduction, an argument in favour of multi-disciplinary projects that combine biology and mathematics, has been made. In section 1.1, I described vascular patterning during primary and secondary growth in different *Arabidopsis* plant organs. In section 1.2, the underlying mechanisms that regulate the activity of the cambium, the lateral meristem that produces the vasculature [43-45], were described. Section 1.3 argued how mathematical tools can assist experimental work in answering biological questions.

In the chapters that follow, the background described in sections 1.1, 1.2 and 1.3 will be used to explain the relationship between several cambial regulators – PXY, MP and ER. Oftentimes, to understand the role of different genetic components in plant growth and development, images of plants and plant mutants are examined. The goal of Chapter 2 is to present a method to assist in examining phenotypical variation between such images. This method is MATLAB-based, strengthening the argument provided in section 1.3 here about the benefits of computational approaches in biology.

The goal of Chapter 3, is to understand the relationship between the *PXY* and *ER* family

of genes, described in section 1.2. To do this, combination mutants of these families were used and analysed with the help of the method described in Chapter 2. In accordance with section 1.1, I will show that the difference in regulation in stems and hypocotyls is reflected in phenotypical, as well as gene expression disparities, between these two organs.

The aim of Chapter 4 is to examine a hypothesis that the *PXY* and *MP* genes are tied into a negative feedback loop. This hypothesis is explored using a 3-cell mathematical model, as loss of *MP* is lethal to the plant in a directly experimental sense. The result of the mathematical analysis suggests that such negative feedback loop would stabilize the existing biological network.

Overall, the aim of this thesis is to use a combination of mathematical and experimental techniques in order to contribute to the understanding of how the cambium is regulated on a genetic level.

Chapter 2: Versatile method for quantifying and analyzing morphological differences in experimentally obtained images

In the previous chapter, I discussed the research background to this thesis, particularly describing the vascular tissues and the complex regulatory mechanisms that underpin its establishment and maintenance. To study how these mechanisms operate, loss and gain-of-function mutants are often generated and their phenotypes studied to understand gene role. However, such data is not always easy to interpret with subjective observations alone.

Here, I will discuss a bespoke method that I developed to quantify and analyse the morphological differences between images of plant mutants. The method was developed specifically for the investigation I will describe in Chapter 3, but was published independently in *Plant Signalling and Behavior*. The publication itself can be found in Appendix C with the detailed protocol given in Appendix B. Below, I will introduce the rationale for developing this particular scientific approach, the detailed procedure, how it was used for anatomical images of plants and finally, the associated limitations of the method. Later, in Chapter 3, I will present how this method was used in combination with laboratory work to investigate the relationship between the *PXY* and *ER* family of genes.

2.1 Method rationale

In many branches of science, an important step in investigating a mechanism or structure involves obtaining high-resolution images of the observed behaviors and/or morphology. In biology, the incorporation of image analysis tools has been increasing in popularity [243-245]. Several methods to analyze the histology of roots and root architecture were introduced over the past decade [246-248] and more recently, machine-learning-based tools have begun to emerge [57, 249]. Additionally, open-source platforms such as *LithoGraphX*, developed from the former *MorphoGraphX9* [250], have also been established.

In the study of plant vascular tissue, one means of investigating genetic interactions includes the use of microscopy to image transverse or longitudinal sections of plants and plant mutants. By studying the phenotypes generated through genome editing using CRISPR-Cas9, it is possible to characterize the contribution of a specific gene to the plant growth and development. However, while an intuitive understanding of the differences between genotypes is crucial for formulating hypotheses and prompting further tests, it is oftentimes difficult to quantify how significant certain variabilities are. Despite advances in automatic image analysis of plant organs and tissues [57, 246-250], these tools are not suited for analysing highly irregular mutant phenotypes, especially ones that have not been previously identified and recorded. In such mutants, cell size and localization, and tissue patterning does not always match data from wild type, thus hidering computer recognition algorithms. The absence of a methodology for quantifying cell differences across mutant genotypes, limits the rigorous assessment of gene roles beyond what is observable.

Here, I describe a bespoke method for quantifying the vascular mutations between a range of genotypes using a MATLAB algorithm and appropriate statistical tools. This method can be applied to a range of similar research questions in various disciplines but was specifically employed in Wang et al. (2019) [3] to quantify phenotypic variation in Arabidopsis stems and hypocotyls. Discussion of the work done in Wang et al. (2019) [3] will be given in the Chapter 3, where I will review the relevant laboratory work done to motivate my analysis, then present my results.

2.2 Implementation

2.2.1 Preparation

In Wang et al. (2019) [3] the aim was to address the question of how two gene families, the *PXY* family (*PX*f) [154] and the *ER* family (*ER*f) [251], function in concert to coordinate cell division and organization. To achieve this, the phenotypical variation between the different single and combination loss-of-function PXf and ERf mutants had to be meticulously quantified. Due to the defects of these mutants, however, such qauntification was not trivial. To address this problem, I developed a procedure, including manual data preparation and computational tools, aimed at extracting size and shape differences of cell types across

different plant genotypes based on images. Here, I will describe this procedure.

The desired *Arabidopsis* mutant lines to be analyzed were generated through the crossing of the *px*f and *er*f lines. A total of six mutant lines were produced – *px*f, *px*f *er*, *px*f *er erl1, px*f *er erl2* and *px*f *er*f . The mutant lines were grown using standard protocols, and tissue was prepared for light microscopy imaging following fixation with FAA, embedding in JB4 resin, and sectioning [3].

To study the morphological differences, six images obtained through brightfield microscopy from each genotype were selected. The focus of the study was four of the main vascular cell types: xylem vessels, xylem fibres, phloem cells, and parenchyma. From each image, a minimum of 10 cell representatives from each cell type were selected from a wedge of a pre-defined size (60°). In order to account for the naturally occurring size variation from the centre to border, all the cells along the length of the radius were included. The four cell types were assigned a unique color and using the software GIMP, the cell interiors were manually colored as appropriate (see: Appendix B).

Next, a MATLAB code was generated to study the properties of the individual cell types across the genotypes. The MATLAB Image Processing Toolbox was used, with the overall logic of the algorithm described below, but the specific results of the application of this precedure will be presented separately, in Chapter 3.

2.2.2 Algorithm

The manually manipulated images were separated into folders according to genotype. The programme then looped over the images in that folder. For each image in the folder, four entirely black images of the same size were generated (for each of the four cell types under consideration). The original images were scanned, and the pre-defined cell colors were recognized. The entirely black images were then manipulated as follows: whenever a pixel of a 'known' color was identified in a position (i,j), the pixel in position (i,j) in the new black image was colored white. This left the images completely black with the exception of the selected plant cells, which were white (Figure 10; Figure 11). This was performed for each individual color, isolating the different cell types for analysis, with one original cross-section image yielding four (new) binary images corresponding to the four cell types of interest (Figure 10; Figure 11). To optimise the method, connectivity (4 or 8) was chosen individually for each cell

type via examining binary images against original and selecting the superior connectivity level. This was checked for all muntant types under investigation. Since small non-selected pixels or pixel clusters could match the chosen colour, noise removal was necessary. To remove noise, i.e. data obtained from objects that were wrongly classified as connected components within the algorithm (e.g. stray pixels), the code was devised to discard data that yielded unrealistically small values for perimeter and area (perimeter value of $0\ \mu M$, area smaller than $1\ \mu m^2$). The data were converted from pixels to µm using a calibration factor, in order to yield results consistent with laboratory observations. This was done for all mutants.

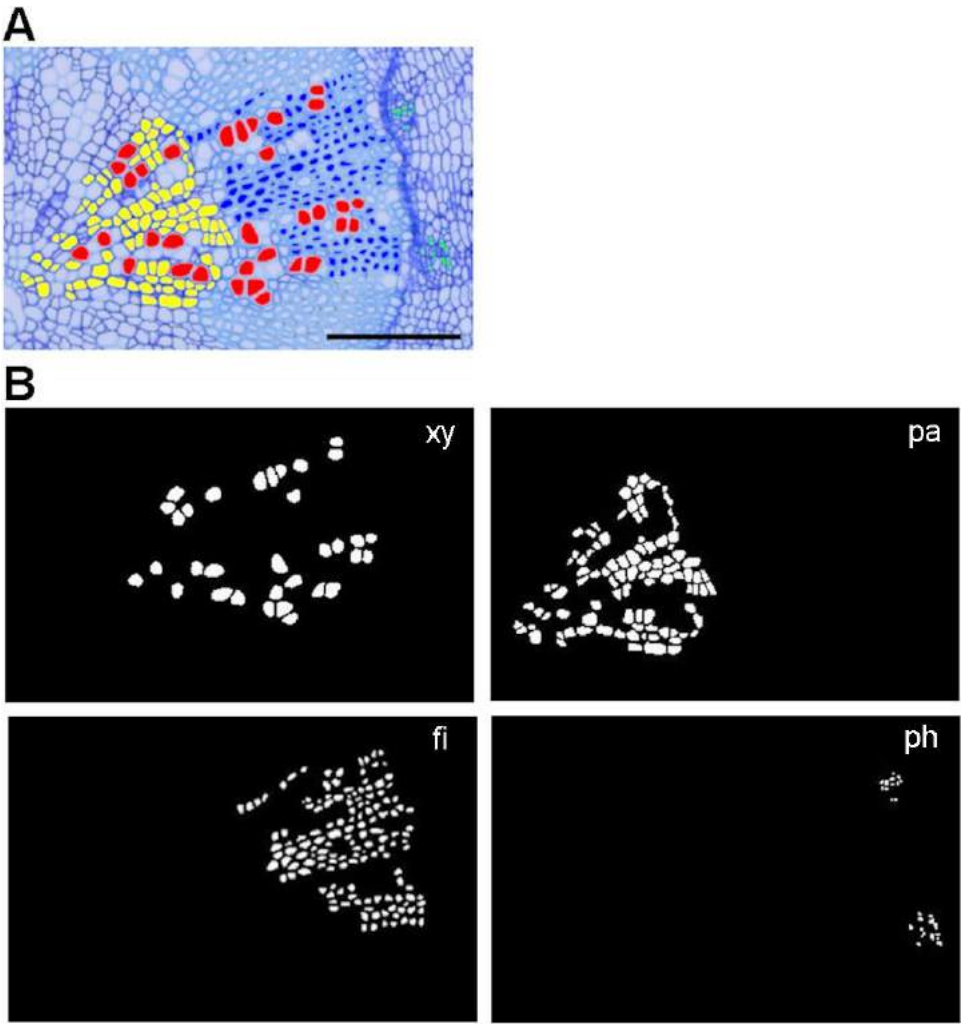

Figure 10: Example of transforming a micrograph (a), into binary images (b) with each image corresponding to four cell types: xylem vessels (xy), xylem parenchyma (pa), fibres (fi) and phloem cells (ph). Scale is $100\mu M$ in the first image (a). Each white object on the binary images (b) can be investigated as a connected component of white pixels and its properties such as area, perimeter and axis, measured.

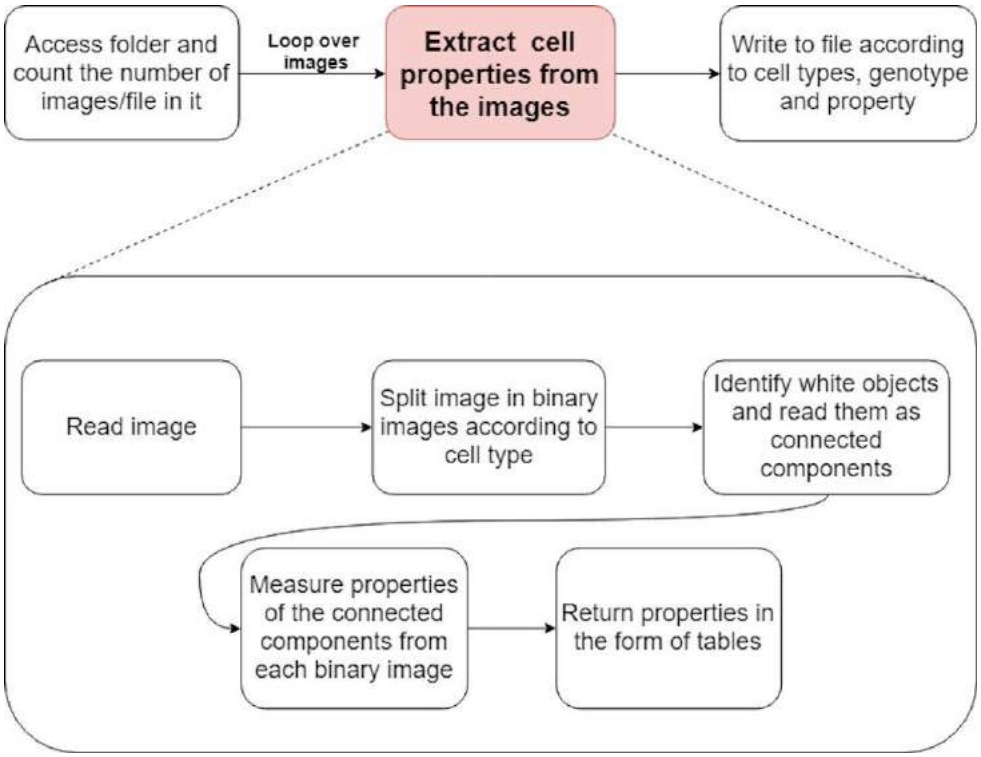

Figure 11 : Block diagram illustrating the main parts of the algorithm. The first row of blocks show the key stages of obtaining the data, with the steps comprising the extraction phase in the bubble below.

The new images were read as binary images in the program. The previously selected cells were now represented as white objects on a black background and their properties (area, perimeter, major and minor axis) could be quantified as follows. Each white object represents a connected component of pixels. Specifically, the binary images are scanned by the program as a matrix of pixels, where each region of adjacent pixels with the same value (here, the color white) is assigned a number identity by the program. The various properties of that region can then be measured in pixels (Figure 10(b)).

The correspondence between pixel size and the actual size can be determined using an image of known size and calculating the micrometer per pixel ratio. Using this method, the data were transformed from pixels to microns/microns squared to calculate the correct perimeter and area of the sampled cells. The ellipticity of the objects (arguably, their geometry) was measured as the ratio of major to the minor axis, which is a dimensionless parameter not requiring conversion.

In Wang et al. (2019) [3] the converted measurements were then saved into an excel spreadsheet where each row corresponded to measurements taken from a different plant. This was done in order to implement a nested ANOVA analysis using R (packages multicomp,

ggplot2, graphics), or other statistical tools as required.

The data from MATLAB was rearranged in an R-readable format of one column of measurements matched to a column of corresponding plant ID's and a column of corresponding plant genotypes. A nested ANOVA analysis and a post hoc Tukey HSD test were performed to identify which genotypes were pairwise significantly different.

The code used in Wang et al. (2019) [3] can be obtained from GitHub (https://bit.ly/2Kht0BI [252]) [177]. A standard operating procedure is available in Appendix B.

2.3 Discussion

The method described above was developed for ease of design compared to other tools and for adjustment and tailoring to a specific research question. For instance, the method can be used to investigate the influence of different factors on organisms through changes in cell deformation and cell size using images of longitudinal and transverse sections. Other questions that can be addressed include: extracting measurements of bubbles or polyhype structures in physics, engineering, and chemistry as well as topological research (especially regarding objects of similar color scheme) and applying statistical analysis.

2.4 Materials and methods

2.4.1 Experimental methods

Plant lines for this section were not generated by the author of this thesis. Full description of all the methods is provided in Appendix D, Materials and Methods[75]. Genome editing was done using the CRISPR/Cas9 methodology [75]. The author of this thesis was involved in embedding, sectioning, staining and imaging. The methods for this will be described bellow.

Images to study vascular morphology were obtained from stems and hypocotyls embedded in JB4 resin. Stem tissues were collected from 0.5 cm above the rossette. The fixative for the tissue was Formaldehyde Alcohol Acetic Acid (FAA). The stem tissues were dehydrated in ethanol, infiltated with JB4 and embedded. For the sections, Thermo Fisher

Scientific Finesse ME 240 microtome was used after 0.02% aqueous Toluidine Blue staining and mounting with histomount. Images of the sections were subsequently taken. Hypocotyl tissues were taken from middle of the hypocotyl and the same procedure was repeated as in stems. Manual sampling of cell representatives was done using GIMP. This involved colouring cells in a specific colour to ensure recognition by the programme. The way the cells were chosen to be sampled for the particular study in Chapter 3 will be outlined there, in section 3.2.2.

2.4.2 Personal contributions

My contributions for this chapter involve the development of the MATLAB-based image analysis method described here. The development of the method was done under the supervision of Dr. Ian H. Jermyn. Sectioning, staining and imagining was done together with Rebecca E. Doherty and Katherine A. Connor. The prerequisite experimental work (such as gene expression analysis) leading to the application of the image analysis tool described here will be provided in the first part of Chapter 3. The results of the image analysis in the results section of Chapter 3 below.

Chapter 3: PXY family of genes - study of genetic interactions and morphology

In section 1.2 of Chapter 1, I summarised key mechanisms that coordinate vascular development during secondary growth. Chapter 2 then offered a method that can be used to analyse anatomical images and complement experimental studies and observations. In this chapter, I will describe the results of applying this procedure in the context of secondary growth.

As discussed in Chapter 2, of interest for my investigation were the *PX*f and *ER*f, previously outlined as major cambial regulators, and seen to interact [158]. As mentioned in Chapter 1, *ER*f and *PX*f each consist of three genes, with *ER* and *PXY* having two paralogues, *ERL1* and *ERL2* [251], and *PXL1* and *PXL2* [167]. Prior to the results outlined in this chapter, exhaustive study of the individual and combined effects of the paralogues had not been conducted, thus aspects of the *ER*f and *PX*f interaction were unknown. To address this knowledge gap, gene expression and phenotypic analysis was carried out in *ER*f and *PX*f loss-of-function mutants [3]. The full work was published in *Development* as 'Organ-specific genetic interactions between paralogues of the PXY and ER receptor kinases enforce radial patterning in Arabidopsis vascular tissue'. Here, I will describe the relevant experiments and background, as well as my contribution as a first co-author, showing that *PX*f and *ER*f collaborate in stem and hypocotyl to regulate secondary growth.

3.1. Background

The cambium is regulated by a variety of components, with mobile signals such as ligand-receptor interactions, governing key aspects of the activity of this meristem (see: Chapter 1, section 1.2).

The ligand TDIF is produced from the phloem-expressed *CLE41* and *CLE44* genes, which undergo translation into 100 amino acid proteins that are later cleaved into a 12 amino acid peptide ligand TDIF [156]. TDIF is perceived by its receptor kinase PXY in the adjacent

cambium cells to produce a signal that regulates vascular organisation and promotes cell divisions. Loss-of-function *pxy* mutants are characterised with disruption of the regular xylem-cambium-phloem arrangement, reduction in cell divisions and early xylem differentiation [154-157, 159] (Figure 6B).

The *ER* gene family interacts with *PXY*, with removal of the *er* gene in a *pxy* background enhancing the *pxy* phenotype [158] (Figure 6). Similarly to PXY, ER is a receptor-kinase. The *EPF/EPFL* family of genes encode the ligands EPFL4 and EPFL6 which signal to ER [253-258]. Functionally, the EPFL-ER ligand-receptor pair has been found to regulate a variety of processes, including cell elongation and division [251, 259], vascular growth in the stem [260] and prevention of precocious xylem differentiation [55]. In contrast to *PXY,* which is a cambial promoter [154, 155, 157, 159], *ER* and *ERL1* were shown to repress hypocotyl expansion as *er erl1* lines resulted in increase in hypocotyl diameter [55, 186].

ER and *EPFL4/6* expression patterns differ between different organs. In stems, *ER* is expressed in the phloem, whereas in hypocotyls the *ER* expression is broader, spanning the phloem, xylem and cambium [55, 254, 261]. Ligands EPFL4 and EPFL6 are endodermis-expressed in stems (endodermis is the area outside the phloem) [254], whereas GUS staining in 5-week-old Arabidopsis hypocotyls demonstrated high expression levels of *EPFL4/6* in xylem parenchyma and cambium-adjacent xylem. Low expression was also found in the cambium [3] and phloem (Figure 12). Thus, both PXY-TDIF and ER-EPFL4/6 are examples of non-cell autonomous signalling mechanisms, making these ligand-receptor pairs particularly important for understanding how information is communicated across different tissues. Together with their paralogues, *PXY* and *ER* had been seen to control secondary growth, though their means of interaction for this process had not been elucidated [55, 154, 155, 157-159, 186, 260]. Here, I describe experimental evidence that suggests how members of the two families interplay in development in both stem and hypocotyl.

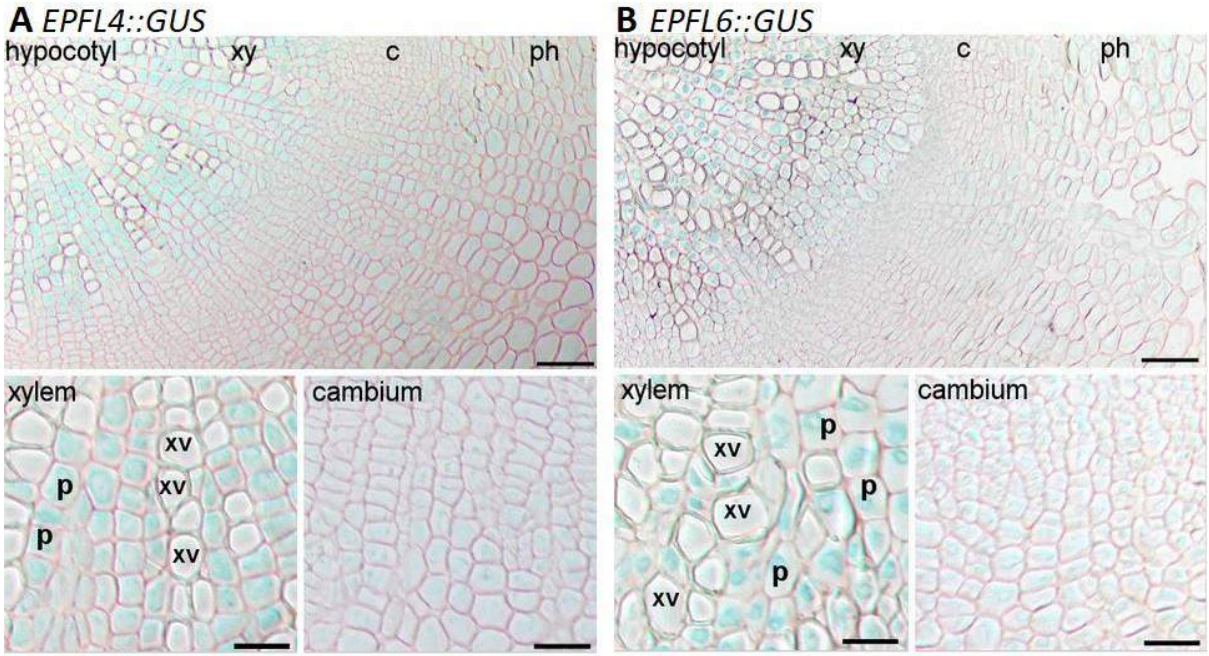

Figure 12: Adapted from Wang et al. (2019) [3], Figure 1. Distribution of gene expression of *EPFL4* (A) and *EPFL6* (B) genes in 5-week-old Arabidopsis hypocotyl transverse sections using GUS staining. Scale bars: 50µm in upper A, B images, 20µm in lower A, B images. xy, xylem; c, cambium; ph, phloem; p, xylem parenchyma; xv, xylem vessels.

3.1.1 *ER* interacts with *PXF* for vascular organization

In addition to *er* mutations, other receptor kinase mutants, notably the *PXY* paralogues, *PXL1* and *PXL2,* have been reported to enhance the *pxy* phenotype [154, 158]. However, transverse sections of standalone *er* and *pxl1 pxl2* stems showed no distinct phenotype relative to wild type [3] (Figure 13; Figure 14 C, D, E; Figure 18 B, D), indicating that both *ER* and *PXL1* and *PXL2* act redundantly with *PXY* [3]. Quadruple mutant lines, however, *er px*f (*er pxy pxl1 pxl2*) demonstrated substantially fewer cells per vascular bundle compared to *px*f, *pxy er* or *er* stems (Figure 14 A) [3], indicating a genetic interaction between *ER*, *PXL1* and *PXL2* that affected stem bundles [3]. For vascular bundle cell counts, cells derived from the procambium were counted. This includes cells within a specific area: those inside the endodermis on the phloem side of the bundles, and those characterised by secondary cell walls on the xylem side of the procambium [3]. In addition to the reduced cell numbers, stem vascular bundle shape was also different in the higher order mutants. Shape was measured by measuring the tangential to radial ratio of the bundles [3]. While in wild type, stem bundles

are expected to have more vascular tissue along the radial axis compared to the tangential (radial:tangential ratio was 0.61 in the Wang et al. (2019)[3]), in *er px*f this ratio changed dramatically to 2.30 (Figure 14 B). Thus, the *ER* gene was seen to coordinate stem vascular growth together with *PXL1* and *PXL2* [3].

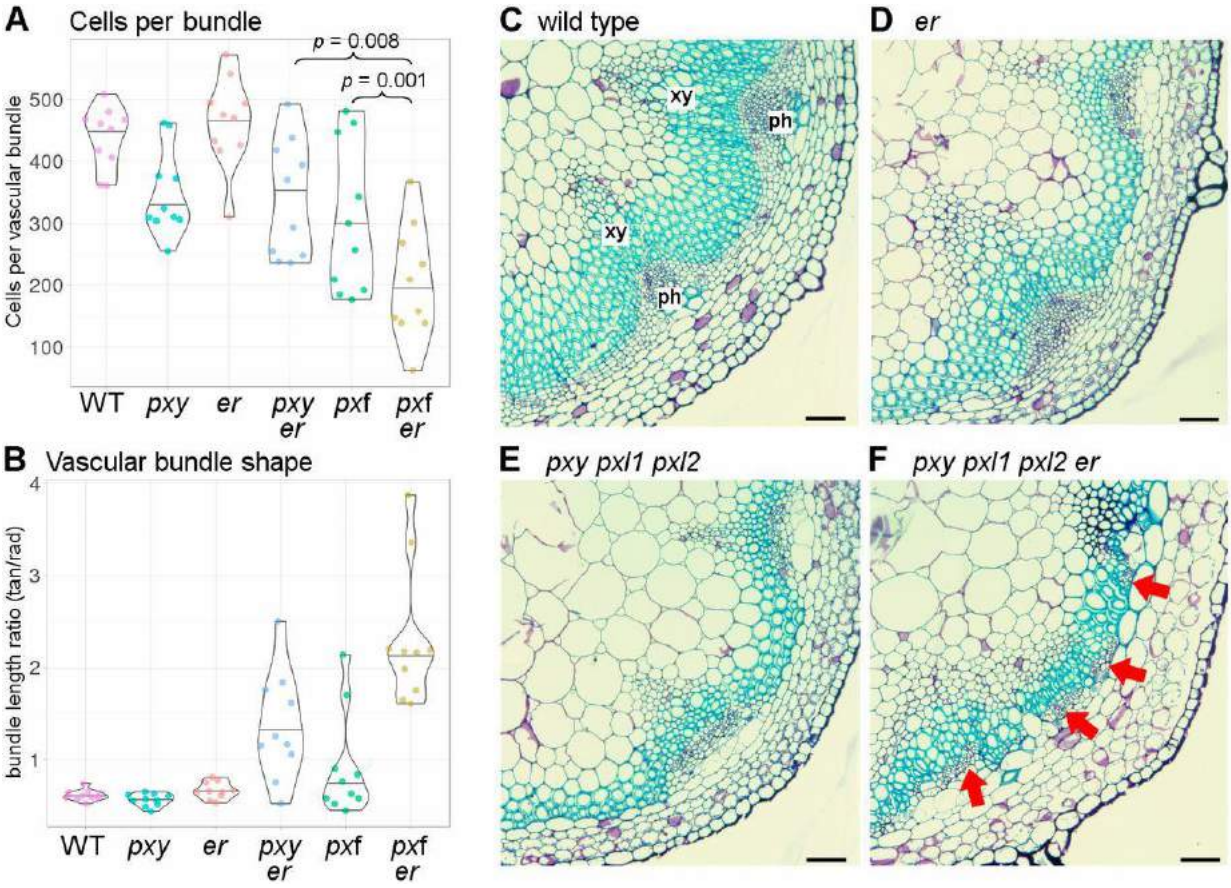

Figure 13: Source: Wang et al. (2019) Figure 2. Violin plots for bundle cell count (A) and bundle shape as tangential to radial axis ratio (B). Transverse section of Arabidopsis wild type (C), *er* (D), *pxf* (E), and *pxf er* (F) stems. Arrows in (F) show uninterrupted phloem distribution that does not form bundles as in the other genotypes (C-E). For (A-B) p-values were calculated with ANOVA and Least Significant Difference (LSD) post-hoc test. Scale bars: 50µm. xy, xylem; ph, phloem

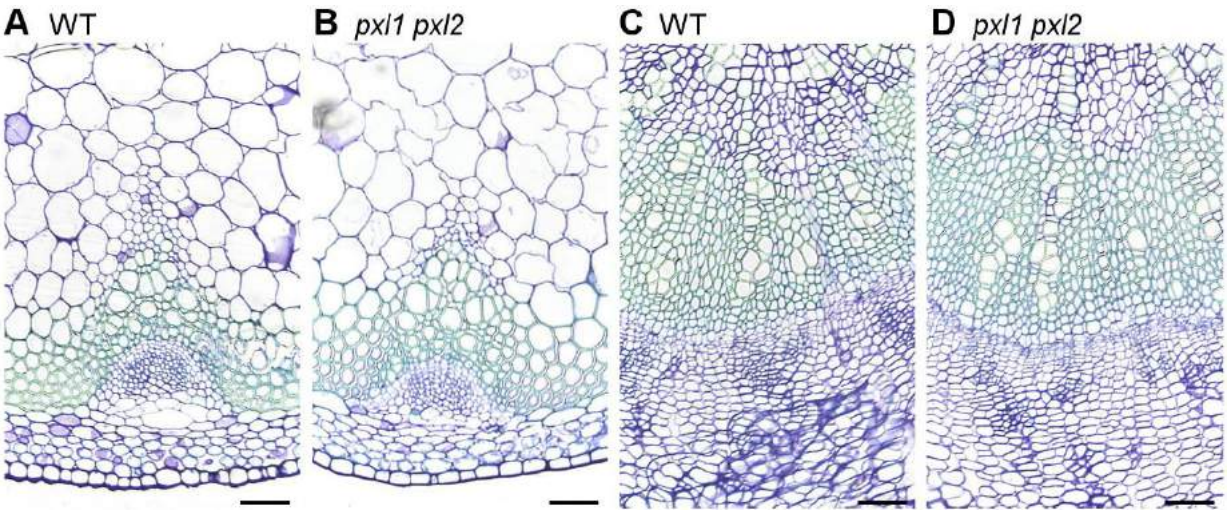

Figure 14*:* Source Wang et al. (2019) [3], Figure S1. Inflorescence stems transverse section for wild type (A) and *pxl1 pxl2* (B). Hypocotyl transverse sections of wild type (C) and *pxl1 pxl2* (B). Scale bars: 50µm.

ER's relationship with the *PXL* genes was further supported by expression data. Indeed, *er* mutants were described with elevated *PXL1* and *PXL2* expression (PXY was unaffected). Interestingly, this was not matched by experiments in hypocotyls where no such

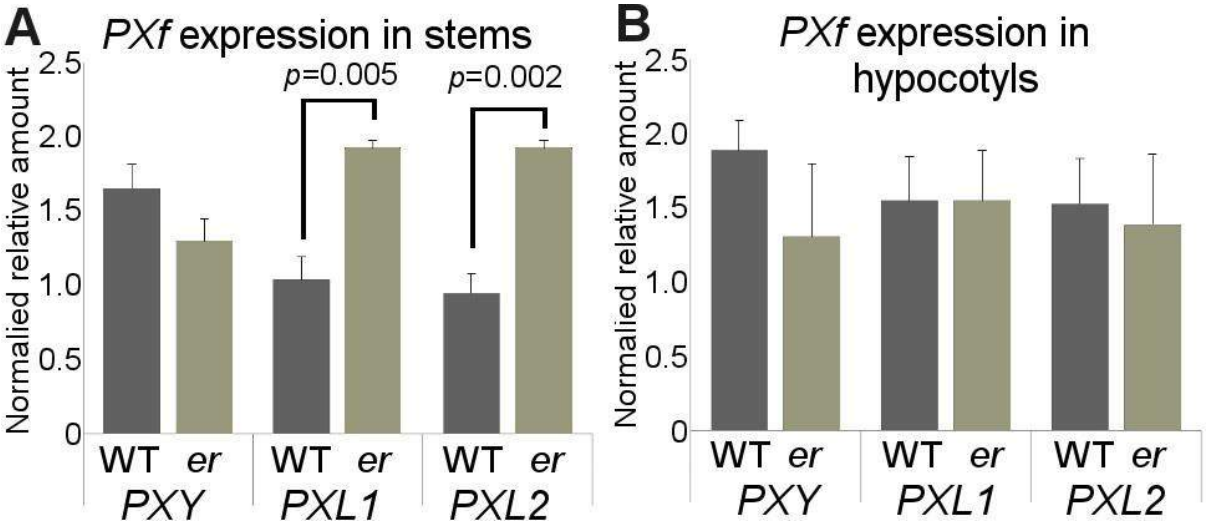

Figure 15: Adapted from Wang et al. (2019) [3], Figure 1. Bar chart of qRT-PCT results for *PXY*, *PXL1* and *PXL2* expression levels in 5-week old wild type and *er* stem (A) and hypocotyl (B). Levels are normalized to ACT2. Error bars represent standard error, $n = 3$.

increase in expression was observed. Thus, only stem levels of *PXL1* and *PXL2* are negatively regulated by *ER* [3] (Figure 15) and the three genes are interlinked in regulating vascular bundle cell count and shape. Together, the data demonstrated a complex relationship between *ER* and *PX*f in vascular development that needs to be explored further.

3.1.2 *px*f *er* mutations result in opposite regulation of ERL1 and ERL2 expression levels in stems and hypocotyl

Previous studies of 3-day old plants and 9-day-old seedlings [55, 260] showed absence of *ERL2* gene expression, even when *ER* and *ERL1* expression was detected and linked to suppression of both hypocotyl growth and precocious xylem fibre differentiation [55, 260]. However, 5-week-old hypocotyls demonstrated *ERL2* gene expression which broadly overlapped with that of the other *ER*f members, suggesting a role for *ERL2* in these older hypocotyls [3]. Moreover, *ER*f transcriptional reporters, *ER::GUS*, *ERL1::GUS*, and *ERL2::GUS* marked most cell types in the mature hypocotyl, with peaks in the cambial and xylem initials, and in the periderm. Interestingly, in *pxy* mutants these maxima were not as clearly distinguished, suggesting *PX*f directs *ER*f maxima in hypocotyl[3].

qRT-PCR tests performed in both stems and hypocotyls, revealed that expression levels of *ER* were not affected by *px*f mutations [3] (Figure 16). *ER*'s paralogues, *ERL1* and *ERL2*, similarly were not significantly changed in *er* and *px*f plants. Loss of both *px*f and *er* genes, however, demonstrated a clear impact. In hypocotyls, *ERL1* and *ERL2* expression was substantially higher in *px*f *er* mutants, whereas in stems with the same mutation, *ERL1* and *ERL2* expression demonstrated a decrease. This indicated organ-specific difference in regulation, with a positive *PX*f influence on *ERL1* and *ERL2* in stem but negative one in hypocotyl (Figure 17) [3].

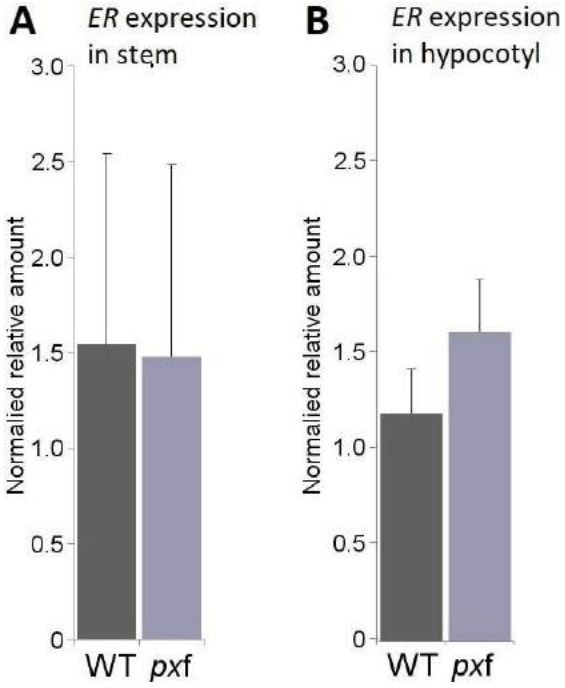

Figure 16: Adapted from Wang et al. (2019) [3] Figure 4, 5. Bar chart of qRT-PCT results for ER levels in stem (A) and hypocotyl (B) for wild type and *px*f. Expression levels are normalized to A18S rRNA. p values were calculated using ANOVA with an LSD post-hoc test.

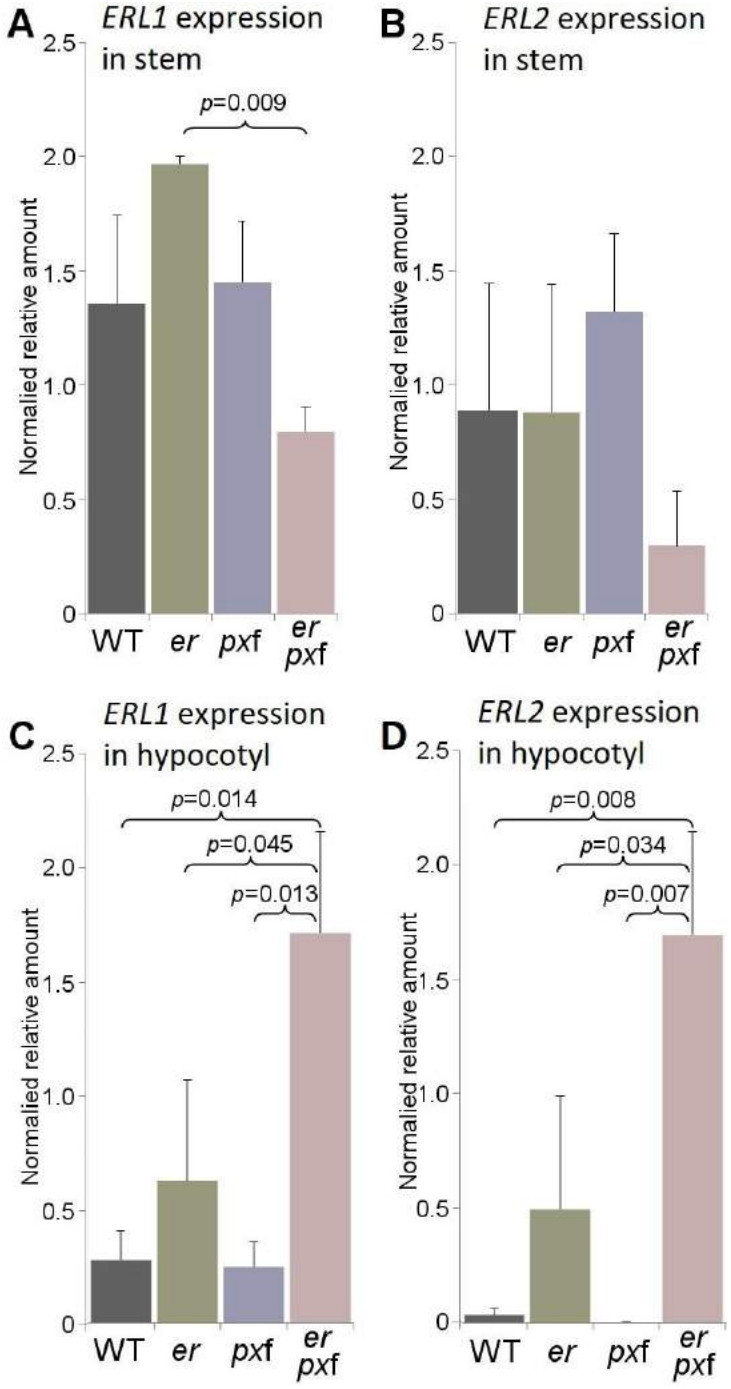

Figure 17: Adapted from Wang et al. (2019), [3] Figure 4, 5. Bar chart of qRT-PCT results for ERL1 levels in stem (A), (B) and hypocotyl (C), (D) for wild type, er, pxf and er pxf. Expression levels are normalized to A18S rRNA. p values were calculated using ANOVA with an LSD post-hoc test

3.1.3 *PX*f and *ER*f regulate rate and orientation of cell division in secondary growth

Cross-sections of 5-week old hypocotyls in wild type and *er*f mutants are characterised by highly oriented cell divisions, perpendicular to the radial axis of the stem (Figure 18B, C). Fisher and Turner (2007) [154] previously demonstrated that division plane orientation changes in plants lacking *px*f (Figure 18D-F), leading to vascular organisation phenotypes

described above (Figure 18 B,D-F). Consistent with this phenotype, images of higher order mutants lacking *ER*f and *PX*f genes are also characterised by loss of vascular organisation (Figure 18 B, D-F).

As will be shown in section 3.2.1 through direct radial measurements taken by me the rate of vascular proliferation decreases with loss of *ER*f in *pxy* mutant backgrounds, with slowest rate observed in *px*f *er*f (Figure 18A). This shows that in addition to regulating vascular organisation, *ER*f and *PX*f also regulate the rate of vascular cell division. Moreover, the *px*f *er*f (*pxy pxl1 pxl2 er erl1 erl2*) sextuple mutant demonstrated two distinctly preserved phloem poles, similar to those found in the embryo (see: Chapter 1, section 1.1). In the same mutant, little expansion of the phloem around the circumference of the hypocotyl could be detected. As this expansion occurs as transition is made between primary and secondary growth, this suggests that in *px*f *er*f such transitions do not commence, i.e. secondary growth was not triggered. Thus, loss of both *ER*f and *PX*f entirely suspended secondary growth (Figure 18F) [3].

Here, the method described in Chapter 2 will be used to determine how members of the *PX*f and *ER*f coordinate cell division and expansion in stems and hypocotyl. Below, I will show using the Chapter 2 image analysis method method that, as *px*f mutations cause reduction in the cell division rates, members of the *ER* family function as a compensatory mechanism to maintain hypocotyl size through cell expansion.

3. 2 Results

3.2.1 ERL2 plays greatest role in hypocotyl radial size

In hypocotyls *ER* and *ERL1* had been previously described as suppressors of radial growth [55]. Wang et al. (2019) demonstrated that *ERL1* and *ERL2* expression in *px*f *er* hypocotyls was elevated (Figure 17 C, D), suggesting that *ER* and the *PX*f suppress *ERL1* and *ERL2* expression [3] (Figure 17 C,D). Given that the *PX*f are promoters of cell division and hypocotyl expansion [154, 155, 158], these results suggest that one mechanism for *PX*f's ability to boost radial size may be related to *ERL1* and *ERL2* suppression [3]. To assess *ERL1/2* function during secondary growth, brightfield microscopy images of hypocotyls of 6-week-old wild type, *px*f, *px*f *er*, *px*f *er erl*1, *px*f *er erl2* and *px*f *er*f mutants were generated. The short

radius of 6 representative hypocotyls from each of these mutants was measured from images using MATLAB. The length of the radii in pixels was subsequently converted to µm. A one-way ANOVA, followed by a post-hoc Tukey HSD test was used to determine pairwise variation between the means (Figure 18A).

Wild type and *px*f mutants showed no difference in hypocotyl radial sizes (Figure 18A). *px*f *er* and *px*f *er erl1* lines similarly were insignificantly different, suggesting that loss of *ERL1* did not substantially change hypocotyl size. By contrast, *px*f *er erl2* and *px*f *er*f radii were significantly smaller than *px*f *er erl1* plants and controls (Figure 18A). This suggested that growth was supported by the presence of *ERL1* and *ERL2* in *px*f *er* hypocotyls. Because *px*f *er erl1* hypocotyls were larger than those of *px*f *er erl2* lines, a greater role was attributed to *ERL2* compared to *ERL1* [3]. How this role was linked to morphology, however, was not clear.

Indeed, since fewer divisions occur in mutants lacking *PXY* genes [154-157, 159], yet the organ size was not substantially changed between wild type and *px*f, one explanation could be a change in cell size or shape to compensate for reduced cell proliferation (Figure 18A). To test this hypothesis and better understand discrepancy in plant morphology across mutants, sections of *px*f, *px*f *er*, *px*f *er erl1*, *px*f *er erl2 Arabidopsis* hypocotyls and stems were analysed using the method described in Chapter 2.

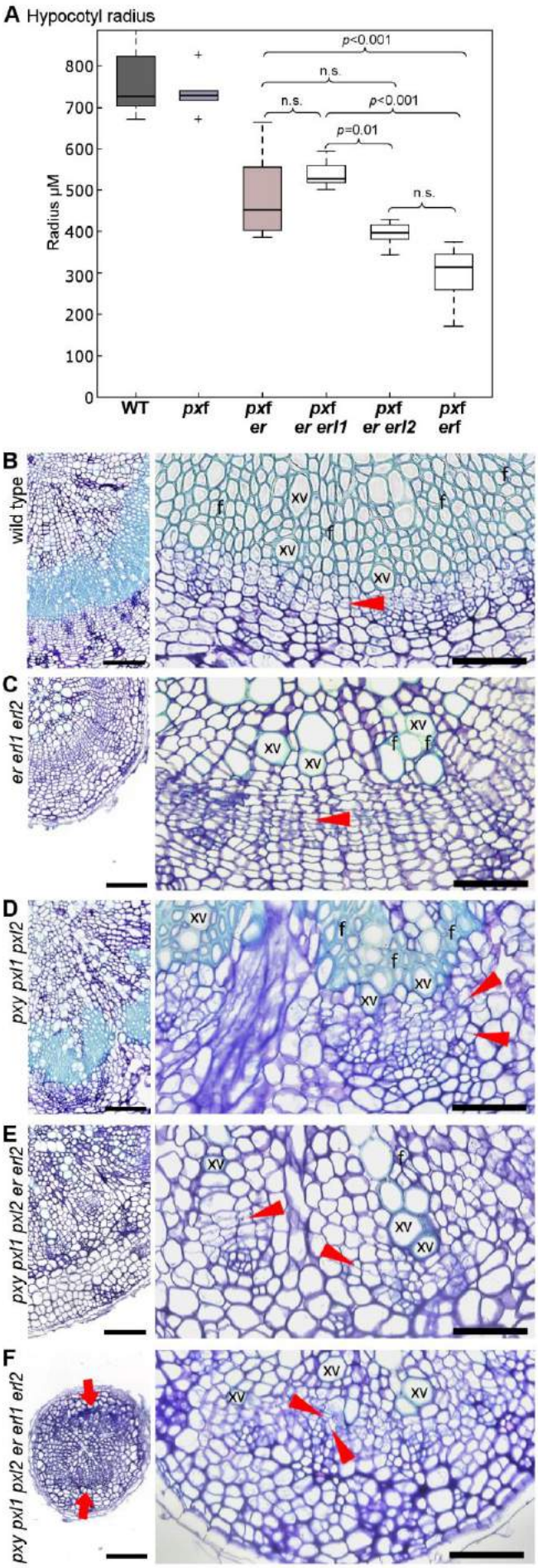

Figure 18: Transverse sections of hypocotyls from *pxf erf* lines. (A) Boxplot showing hypocotyl radii of *pxf* lines with differing numbers of erf mutations. n=6 (B) Wild-type, (C) *erf*, (D) *pxf*, (E) *pxf er erl2* and (F) *pxf erf* vascular tissue. Sites of phloem poles in *pxf erf* are marked with red arrows in the left-hand panel of F (see Fig. S5 for higher magnification). Red arrowheads in B-F align with cell divisions. Scale bars: 100µm (left); 50µm (right); xv, xylem vessel; f, fiber.

3.2.2 Implementation of method for quantifying cell morphology

The four main vascular cell types - xylem vessels, xylem fibres, phloem and parenchyma (not present in stem) – were examined to unravel morphological changes based on gene loss. The MATLAB code described in Chapter 2 and detailed in Appendix D was used to extract the intrinsic properties of each cell type. The area, perimeter and long/short axis length of the cells were then calibrated to real-life accurate sizes and stored in files for analysis.

The only cell type that was not measured across all genotypes was xylem fibre, which in the case of *px*f *er*f plants was present in insufficient numbers and could not be assessed for both stem and hypocotyl.

To test the significance of the variation between cell properties across the different genotypes, a nested ANOVA was performed in R at 5% significance level. This was carried out for all four cell types. To conduct the nested ANOVA, the data were classified according to genotype (treatment) and plant ID (plants within that treatment), with the response variable either the cell area, cell perimeter or cell axis ratio (ratio of major to minor axis). A post-hoc Tukey HSD test was performed to determine the significance of the pairwise differences between the means of the areas, perimeter and axis ratio of the different mutants.

3.2.3 Hypocotyl phenotypic variation

In hypocotyls, consistent across all cell types, the perimeter of *px*f cells were larger than wild type, demonstrating that compensatory cell expansion must indeed occur to allow for similar hypocotyl radial size of both wild type and *px*f mutants (Figure 18A; Figure 19A, left). Between *px*f and *px*f *er* (additional loss of ER gene), no significant difference could be seen in cell sizes, with the only exception of xylem parenchyma where the *px*f *er* mutants showed smaller measurements. Previously, I showed that *px*f hypocotyls were larger than *px*f *er* (Figure 18A). This suggests that the decrease observed in *px*f *er* radii is the consequence of the *er* mutation affecting xylem parenchyma size. The remaining cell types were indistinguishable from those of pxf lines and as such were larger than wild type (Figure 19). This compensatory property was lost with removal of more *ER*f genes in both xylem vessels and parenchyma, bringing those cells back to wild type size. Notably, the largest reductions

in perimeter were observed in genotypes carrying the *erl2* mutation (*px*f *er erl2*, *px*f *er*f). Thus, in hypocotyls *ER*f family members, and especially *ERL2*, promoted cell expansion in the absence of *PX*f. Measurements of cell areas supported the conclusions of the perimeter analysis. Cell areas in xylem vessels and parenchyma in *px*f and *px*f *er* plants were larger than wild type. As with the perimeter, *er erl1* and *er erl2* mutations lost this increase (Figure 19A, right).

Xylem fibres were an exception to the above trends. While *px*f and *px*f *er* still had larger fibres in terms of area and perimeter, *er*f mutations did not rescue this increase.

Ellipticity of the cells was the final property that was measured across the different genotypes. As discussed in Chapter 1, section 1.1, parenchyma cells are adaptable, able to change shape in order to accommodate changes in surrounding cells. Since the increase in cell size (perimeter and area) was most dramatic in xylem vessels, which have rigid secondary cell walls and are therefore unmalleable, it was hypothesized that deformation in parenchyma may have occurred across the different genotypes to accommodate pressure from the xylem vessels. The ratio of major to minor axis was a convenient measure for such change, showing elongation changes across the cells. However, upon examining the data, no significant difference in this ratio was detected among genotypes (Figure 20). Thus, no substantial deformation was observed.

Full table of p-values for hypocotyl differences in perimeter and area between differen genotypes is given in Figure 21 and 22.

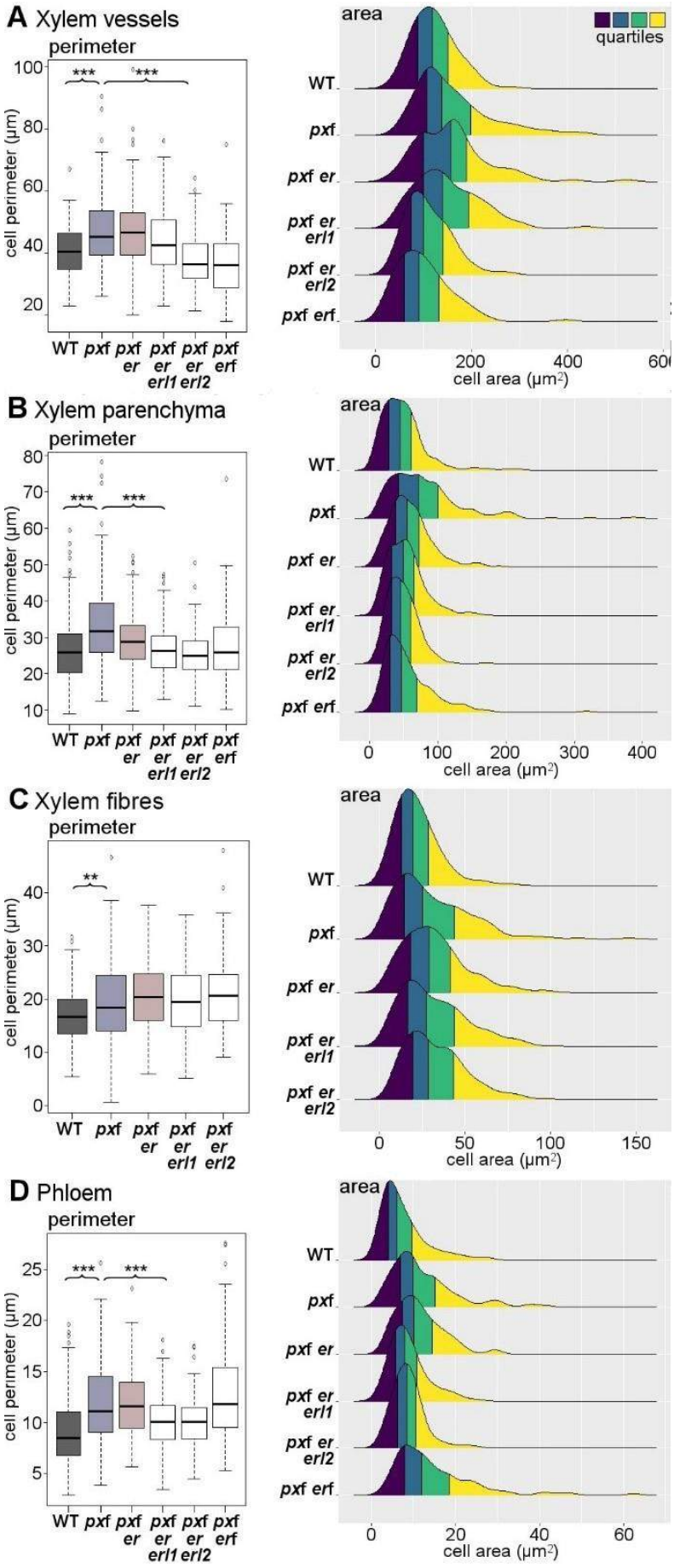

Figure 19: Comparisons of hypocotyl cell morphology. (A-D) Boxplots on left show mean cell perimeter for xylem vessels (A), xylem parenchyma (B), fibres (C) and phloem cells (D). Boxes represent the 25th to 75th percentile, the horizontal line marks the median. Whiskers' endpoints are the min/max points within the interval spanning Q1 − 1.5 × IQR (lower) and Q3 − 1.5 × IQR (upper). IQR = Q3 − Q1 (the length of the box). Asterisks mark significant differences (ANOVA plus Tukey;***P < 0.001, **P < 0.01; see Table S4 for pairwise comparisons of P values). Ridgeline plots on the right show the distributions of cell areas divided into quartiles. Areas of pxf lines were greater than those of pxf er erl2 lines in xylem vessels, phloem and parenchyma (P ≤ 0.001) but not fibres. Differences were calculated with ANOVA and a Tukey post-hoc test.

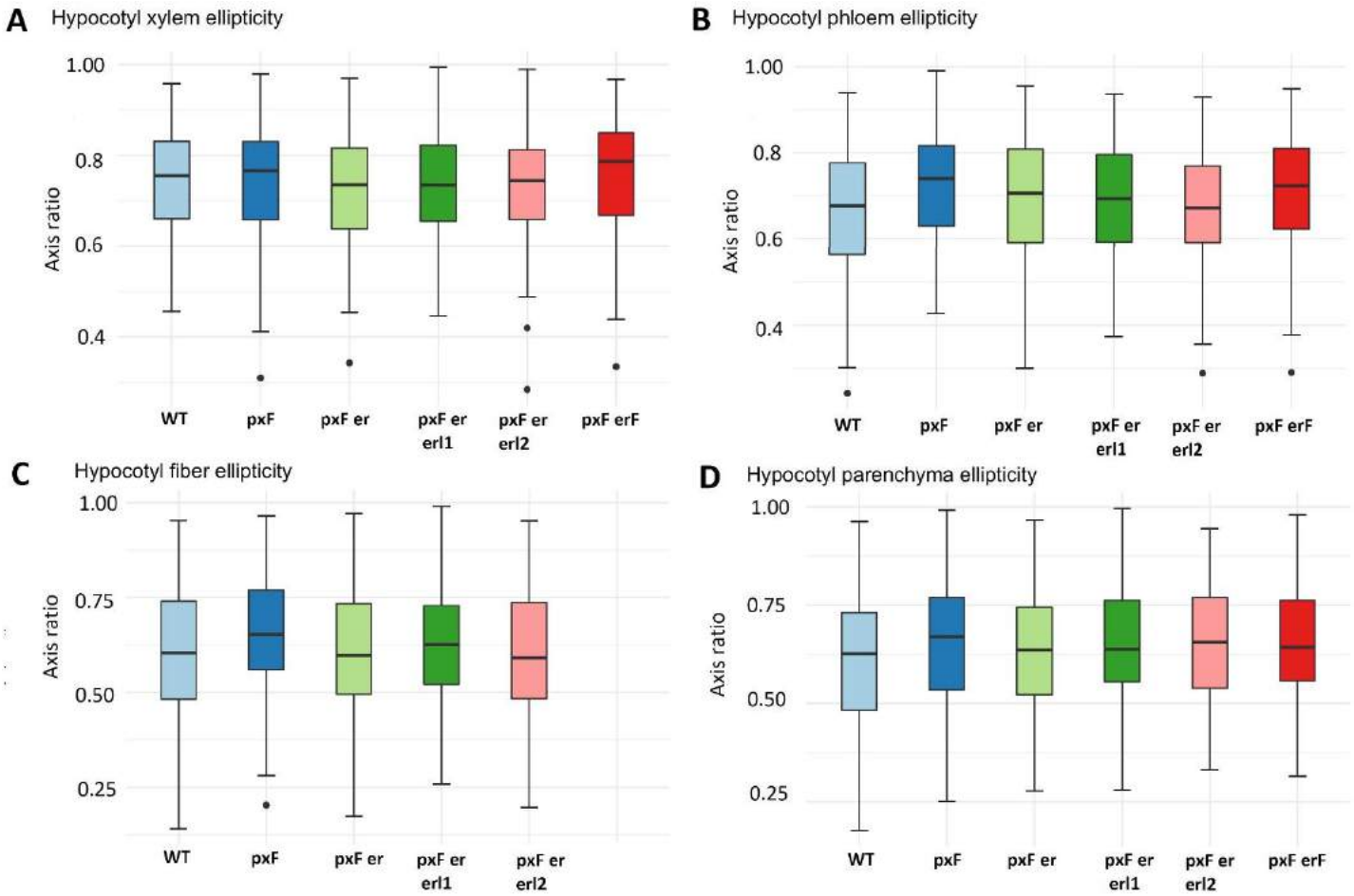

Figure 20: Measurements of the cell axis ratio in hypocotyls. (A-D) Boxplots show mean ellipticity for xylem vessels (A), phloem (B), fibres (C) and parenchyma cells (D).

Statistical differences between hypocotyl cell perimeters

Compared genotypes	xylem			phloem
	vessel	fibres	parenchyma	
WT - *pxf*	0.001	0.007	< 0.0001	< 0.0001
WT - *pxf er*	0.001	< 0.0001	0.014	< 0.0001
WT - *pxf er erl1*	0.515	< 0.0001	1.000	0.374
WT - *pxf er erl2*	0.232	< 0.0001	0.826	0.388
WT - *pxf erf*	0.031	n.d.	0.567	< 0.0001
pxf - pxf er	1.000	0.132	< 0.0001	1.000
pxf - pxf er erl1	0.192	0.652	< 0.0001	0.001
pxf - pxf er erl2	< 0.0001	0.036	< 0.0001	0.001
pxf - pxf erf	< 0.0001	n.d.	< 0.0001	0.204
pxf er - pxf er erl1	0.193	0.863	0.037	0.001
pxf er - pxf er erl2	< 0.0001	0.987	< 0.0001	0.001
pxf er - pxf erf	< 0.0001	n.d.	0.579	0.188
pxf er erl1 - pxf er erl2	0.001	0.570	0.639	1.000
pxf er erl1 - pxf erf	< 0.0001	n.d.	0.769	< 0.0001
pxf er erl2 - pxf erf	0.967	n.d.	0.048	< 0.0001

Figure 21: p values from comparisons of cell perimeters measured from the vascular cells of each genotype tested (ANOVA + Tukey) in hypocotyl. Values in grey boxes were not significantly different at the 95% confidence level.

Compared genotypes	vessel	xylem fiber	parenchyma	phloem
WT - *pxf*	0.001	< 0.0001	< 0.0001	< 0.0001
WT - *pxf er*	0.001	< 0.0001	0.051	< 0.0001
WT - *pxf er erl1*	0.068	< 0.0001	0.908	0.632
WT - *pxf er erl2*	0.787	< 0.0001	1.000	0.732
WT - *pxf erf*	0.231	n.d.	0.333	< 0.0001
pxf - pxf er	1.000	0.973	< 0.0001	0.922
pxf - pxf er erl1	0.819	0.995	< 0.0001	0.001
pxf - pxf er erl2	< 0.0001	0.798	< 0.0001	0.001
pxf - pxf erf	< 0.0001	n.d.	< 0.0001	0.036
pxf er - pxf er erl1	0.833	1.000	0.456	0.033
pxf er - pxf er erl2	< 0.0001	0.987	0.034	0.020
pxf er - pxf erf	< 0.0001	n.d.	0.963	0.001
pxf er erl1 - pxf er erl2	0.001	0.953	0.848	1.000
pxf er erl1 - pxf erf	< 0.0001	n.d.	0.922	< 0.0001
pxf er erl2 - pxf erf	0.941	n.d.	0.255	< 0.0001

Figure 22: p values from comparisons of cell perimeters measured from the vascular cells of each genotype tested (ANOVA + Tukey). Values in grey boxes were not significantly different at the 95% confidence level.

3.2.4 Stem phenotypic variation

Next, the phenotypical variation was examined in stems. Notably, stem morphology of the same genotypes differed from hypocotyl in several regards.

Images of cross-sections of stems revealed a similarity between *px*f *er erl2* and *px*f *er*f, both of which exhibited strongly reduced vascular bundles and very small xylem vessels (Figure 23 D, E; Figure 24A). Tissue layers in *px*f *er erl2* and *px*f *er*f were also substantially different compared to the other mutants. In the sextuple *px*f *er*f no phloem cap was detected, whereas in *px*f *er erl2* the phloem cap could be observed breaching the cortex (Figure 23) [3].

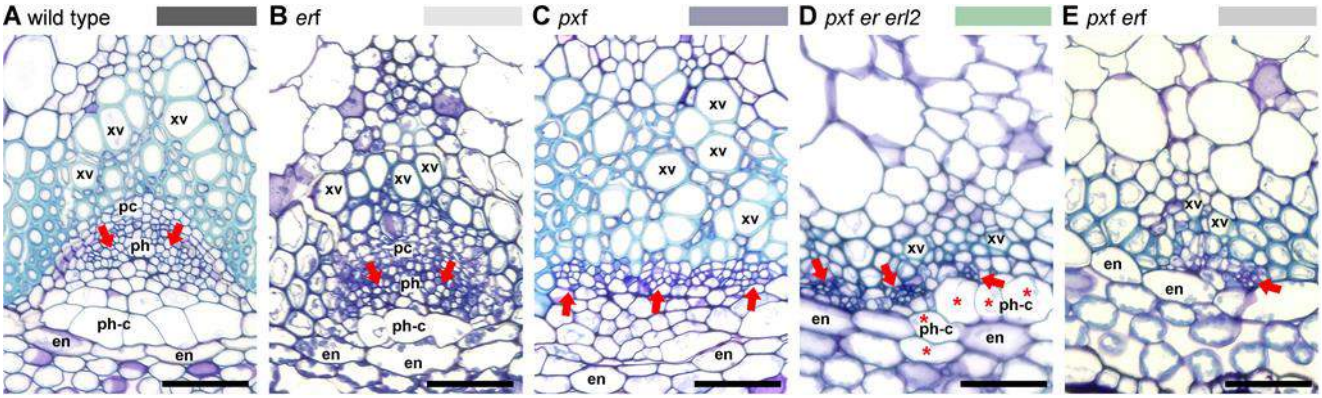

Figure 23: Source: Wang et al. (2019) [3], Figure 8. Vascular tissues in stems of wild type(A), erf(B), pxf (C), pxf er erl2 (D) and pxf erf. Red arrows indicate phloem, while asterisks correspond to phloem cap-like morphology. Scale bar: 50µm; xv, xylem vessel; pc, procambium; ph, phloem; ph-c, phloem cap; en, endodermis

To answer the question of how the phenotypic variation was reflected in cell size and shape, the method described in Chapter 2 was employed, as before. As with hypocotyls, *px*f *er*f fibres could not be assessed due to insufficient numbers. The comparison of cell sizes showed different regulation by *PX*f and *ER*f compared to the hypocotyl results. Unlike the general trend of increased cell sizes observed in hypocotyl upon removal of the *px*f, in stem there was reduction in the area and perimeter of xylem vessels and phloem cells in those mutants, further enhanced as *ERL* genes were lost (Figure 24A, C, left). In particular, though removal of the *PX*f genes resulted in significant decrease between the cell perimeters of wild type vs *px*f and *px*f *er* xylem vessels and phloem, perimeter results for *px*f and *px*f *er* did not differ significantly. However, additional loss of the *ER* paralogues, particularly *erl2*, showed a substantial decrease in perimeter relative to wild type (Figure 24A, C, left). The data for area matched that of perimeter measurements (Figure 24, right). Together, this suggested an interaction between *PX*f and *ER*f in sustaining cell size for stem xylem vessels and phloem.

Interestingly, xylem fibres did not demonstrate the same behaviour. Indeed, *px*f mutants showed a substantial increase in xylem fibre perimeters relative to wild type and *px*f mutants(Figure 24B), suggesting a role for *ER* gene in suppressing xylem fibre growth. Notably, this increase was not seen in *px*f *er erl2* stems, whose perimeters were close to wild type ones. The perimeter data for xylem fibres here also was supported by similar data for cell area (Figure 24).

As with hypocotyls, the third measurement, major to minor axis, revealed no substantial differences across the different genotypes (Figure 25).

Combined, these results indicate a link between the *PX*f and *ER*f for patterning in cell size.

Full table of p-values for stem differences in perimeter and area between differen genotypes is given in Figure 26 and 27.

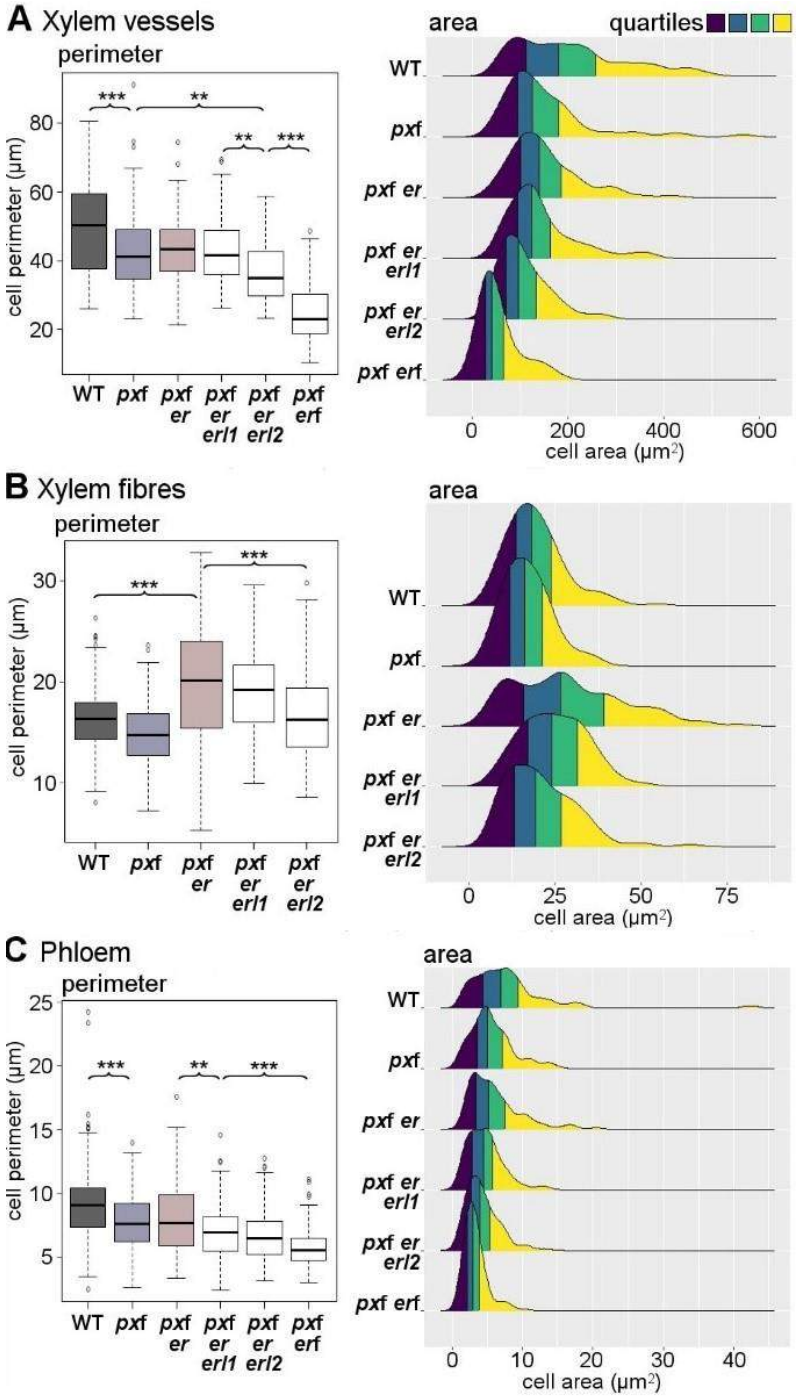

Figure 24: Comparisons of morphology of cells in stem vascular bundles. (A-C) Boxplots on left show mean cell perimeter for xylem vessels (A), xylem fibres (B) and phloem cells (C). Boxes represent the 25th to 75th percentile, the horizontal line marks the median. Whiskers' endpoints are the min/max points within the interval spanning Q1−1.5×IQR (lower) and Q3−1.5×IQR (upper). Asterisks mark significant differences (ANOVA plus Tukey; ∗ ∗ ∗P < 0.001, ∗ ∗ P < 0.01; see Table S6 for pairwise comparisons of P values). Ridgeline plots on the right show the distributions of cell areas divided into quartiles. Areas of pxf er lines were greater than those of pxf er erl2 lines in all three cell types (P ≤ 0.05). Differences were calculated with ANOVA and a Tukey post-hoc test; see Table S7 for pairwise comparisons of P values

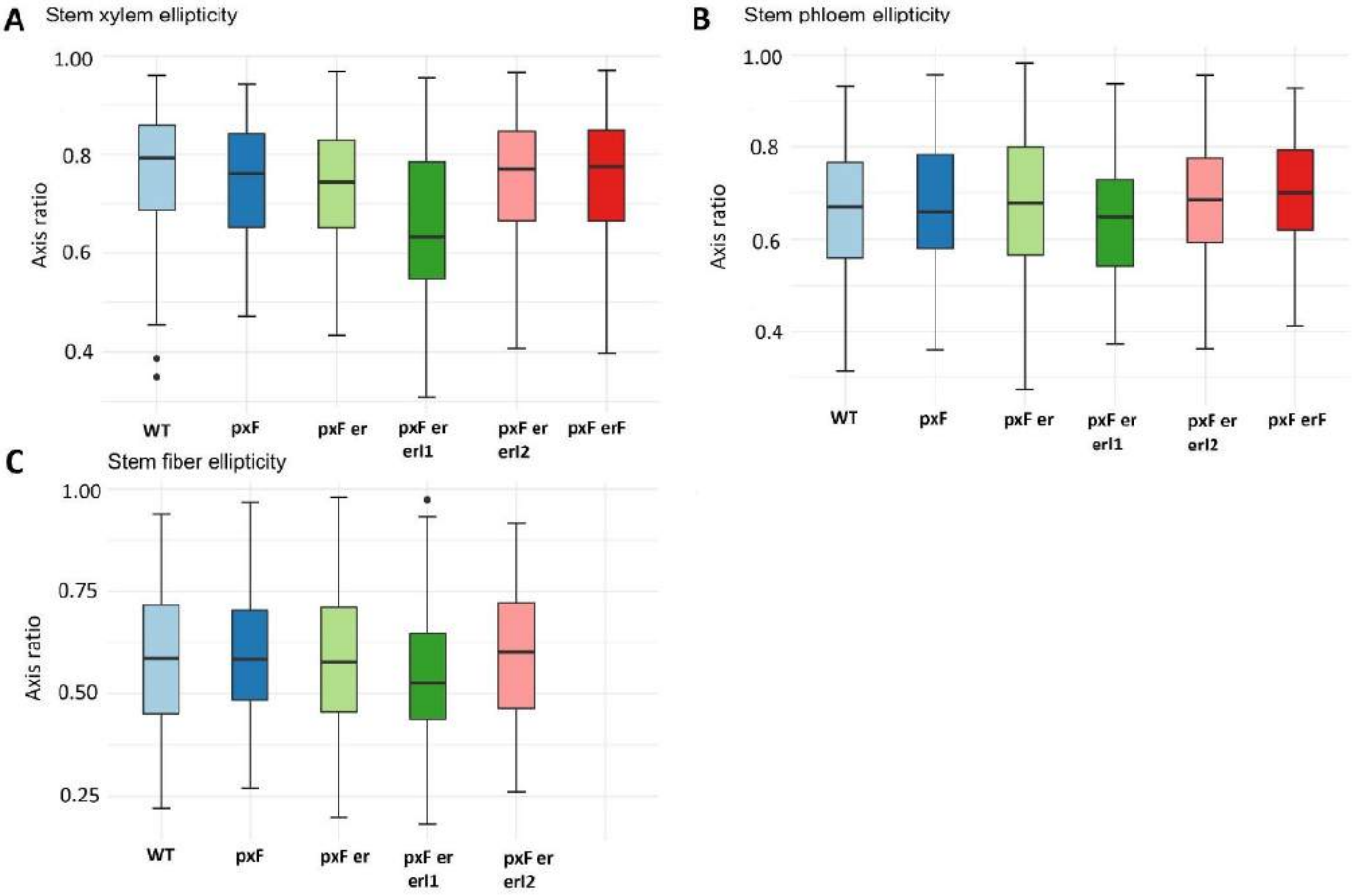

Figure 25: Measurements of the cell axis ratio in hypocotyls. (A-c) Boxplots show mean ellipticity for xylem vessels (A), phloem (B), fibres (C).

Genotypes compared	Xylem		phloem
	vessel	fibres	
WT - *pxf*	0.001	0.136	< 0.0001
WT - *pxf er*	0.004	< 0.0001	0.012
WT - *pxf er erl1*	0.002	< 0.0001	< 0.0001
WT - *pxf er erl2*	< 0.0001	0.996	< 0.0001
WT - *pxf erf*	< 0.0001	n.d.	< 0.0001
pxf - *pxf er*	0.999	< 0.0001	0.773
pxf - *pxf er erl1*	1.000	< 0.0001	0.227
pxf - *pxf er erl2*	0.008	0.055	0.009
pxf - *pxf erf*	< 0.0001	n.d.	< 0.0001
pxf er - *pxf er erl1*	1.000	0.528	0.006
pxf er - *pxf er erl2*	0.002	< 0.0001	< 0.0001
pxf er - *pxf erf*	< 0.0001	n.d.	< 0.0001
pxf er erl1 - *pxf er erl2*	0.004	< 0.0001	0.843
pxf er erl1 - *pxf erf*	< 0.0001	n.d.	0.001
pxf er erl2 - *pxf erf*	< 0.0001	n.d.	0.058

Figure 26 *p* values from comparisons of cell perimeters measured from the vascular cells of each genotype tested (ANOVA + Tukey) in stem. Values in grey boxes were not significantly different at the 95% confidence level.

Genotypes compared	Xylem		phloem
	vessel	fibres	
WT - *pxf*	0.0004	0.420	<0.0001
WT - *pxf er*	0.0003	<0.0001	<0.0001
WT - *pxf er erl1*	<0.0001	0.001	0.632
WT - *pxf er erl2*	<0.0001	0.855	0.732
WT - *pxf erf*	<0.0001	n.d.	<0.0001
pxf - pxf er	0.999	<0.0001	0.922
pxf - pxf er erl1	0.993	<0.0001	0.001
pxf - pxf er erl2	0.015	0.052	0.0005
pxf - pxf erf	<0.0001	n.d.	0.036
pxf er - pxf er erl1	0.995	0.021	0.033
pxf er - pxf er erl2	0.016	<0.0001	0.020
pxf er - pxf erf	<0.0001	n.d.	0.001
pxf er erl1 - pxf er erl2	0.076	0.040	0.999
pxf er erl1 - pxf erf	<0.0001	n.d.	<0.0001
pxf er erl2 - pxf erf	0.001	0.855	<0.0001

Figure 27: p values from comparisons of cell perimeters measured from the vascular cells of each genotype tested (ANOVA + Tukey). Values in grey boxes were not significantly different at the 95% confidence level.

3.3 Discussion

The importance of *PX*f and *ER*f for growth and development has been previously established [55, 154-157, 159, 186, 251, 259, 260]. Both gene families encode receptor-kinases which receive signals cross-tissue and have been proposed as essential regulators of vascular organisation and maintenance. This chapter demonstrates the complexity of gene interactions, at different stages of development and in different organs.

As part of the genetic study of *PX*f-*ER*f interactions conducted alongside my quantification of cell morphology, *PXL1* and *PXL2* expression in *er* stems demonstrated a significant increase in expression, which had not been observed in hypocotyls. This suggested a role for *ER* in suppressing *PXL1* and *PXL2* transcript levels in the stem. Likewise, *ERL1* and *ERL2* expressions were contrastingly regulated in stem and hypocotyl. In *er px*f hypocotyls,

ERL1 and *ERL2* expression levels were shown to increase significantly, whereas in stems, a decrease was observed instead [3].

The work described in this chapter demonstrates that *PX*f and *ER*f interact to maintain organ size and vascular morphology [3]. In hypocotyls, which are characterized by substantial radial expansion during secondary growth, *ER* and *ERL1* are expressed early in development [55, 186], but *ERL2* expression is initiated later [3]. The analysis performed here, revealed that *ERL2* function is required to maintain hypocotyl size with other members of the *ER*f, particularly in the absence of *px*f.

*px*f lines were reduced in size as members of the *ER*f families were removed. This was particularly true for plants carrying a loss-of-function *erl2* mutation (Figure 18A). This implies that the elevated *ERL1* and *ERL2* levels in *er px*f hypocotyls may act to support growth rates in *px*f *er*. This is controversial because previous authors have suggested that *ER* and *ERL1* act as hypocotyl growth inhibitors [3, 55, 186].

Next, to better understand how *ERL1* and *ERL2* might be regulating growth, I examined the impact of loss-of-function *er*f mutations on *px*f mutants in the key vascular cell types: xylem vessels, xylem fibres, phloem and parenchyma. *px*f hypocotyls, which have reduced cell divisions, were comparable in size to wild type, while their cells, along with the cells of pxf *er* mutants, were larger than wild type. Losing further members of the *ER*f, and particularly *ERL2*, rescued this phenotype, bringing the cell size to the original wild type parameters. Thus, hypocotyls lost the ability to trigger compensatory cell expansion to oppose *px*f-related reductions in cell divisions, when the *ER*f genes were removed. Even more strikingly, full loss of the *PX*f and *ER*f genes stopped secondary growth in hypocotyls. This suggests that both gene families, *PX*f and *ER*f are required for secondary growth, and that their interactions maintain normal cell sizes.

In stems, and in accordance with the gene expression data [3], an opposing tendency was observed. Loss of *px*f *er* genes was not associated with cell size increase and instead, vascular cells in stems were generally smaller, with the exception of xylem fibres. This could be due to stems undergoing little radial growth and thus requiring alternative regulation of overall size constraint.

In particular, outside the phloem, the stem has endodermis, cortex and epidermis in which the ability to grow is limited. In hypocotyls, the cork cambium, a proliferative tissue, is present outside the phloem allowing for considerable radial expansion. Additional reason for

the difference in regulation could be the difference in gene expression between stems and hypocotyls. *ER* expression in the hypocotyl includes the phloem, xylem and cambium (the proliferation meristem)[55], whereas in stems, *ER* is expressed in the phloem only [261]. This suggests that the reason for the compensatory cell expansion caused by *ER*f in the absence of the *PXY* family could be caused by *ER* presence in the meristematic cambium in hypototyls [55], which is not observed in stems [261].

Together, these data suggest that receptor families which communicate with their ligands cross-tissue, also genetically interact in a manner specific to the plant organ or stage in development. Thus, signalling mechanisms coordinate plant processes on multiple levels of complexity, including by imposing compensatory mechanism when gene function is impaired.

Chapter 4: A model including an MP-PXY negative feedback loop in the cambium stabilises the auxin maxima during secondary growth

In this chapter, a hypothesis to explain the relationship between *PXY* and *MP* in regulating cambial division (i.e. cambial activity) during secondary growth will be derived and tested using a mathematical model.

The PXY-MP interaction has not been well defined in the past. MP was found to promote *PXY* transcription in root [72], whereas PXY was seen to indirectly inhibit MP in stem [120]. Similarly unclear, is MP's role in regulating cambial divisions. MP was shown to promote the activity of the cambium in root [72], yet suppress it in stem base [121]. PXY, on the other hand, has been universally marked as a cambial promoter [154, 155, 157, 159]. A recent publication has also identified PXY and MP as marking the domain of the cambium characterised by an auxin maxima and required for cell divisions in root [72]. The focus of the study described here is the hypothesis that, in root, the two reactions of MP's promotion of PXY [72] and PXY's inhibition of MP [120] coexist and form a negative feedback loop. To test this hypothesis, the currently existing root network was embedded in a three-cell mathematical model. This was then tested for robustness against an alternative network containing the proposed PXY-MP negative feedback loop in the cambium. Three main reasons motivated the development of a bespoke three-cell model. First, a custom-made algorithm for calculating the concentration of components in each cell allowed tight control over the behaviour of the system of equations, the accuracy of results and insight into how calculations are conducted (including ability to map every individual step of the numerical calculations). Secondary, features such as automated MATLAB equation solvers are slower, which becomes time-expensive over a large number of calculations. Finally, three cells were chosen for simplicity of analysisng how the dynamics of the two possible networks, with and without a PXY-MP negative feedback loop, compare in the absence of specific parameters.

To compare the two possible networks on their ability to reproduce auxin maxima in the cambium, numerical tools and closed form analysis were used [143, 262-264]. As the network containing the PXY-MP negative feedback loop was seen to reproduce an auxin maximum more readily, it was concluded that the network with PXY-MP negative feedback loop is more robust in this function. Moreover, in the case of a stable or abundant MP protein, this PXY-MP reaction was shown to be particularly important for generating an auxin maximum in the cambium. Thus, by examining a hypothetical reaction and its effects on auxin accumulation, this model provides a basis for experimental testing and reconciles contradictory elements in the PXY-MP literature.

4.1 Overview of relevant literature

The discussion below will cover the key components identified from the literature to build a model of auxin, PXY and MP interactions for cambial activity (cell division).

4.1.1 Auxin is necessary for cambial activity

The phytohormone auxin has been implicated in multiple developmental and growth processes, with its distribution patterns, local maxima and gradient formation dynamically directing the plant response [146, 193-207]. In vascular development, auxin was also shown to have a profound effect on the activity of the cambium. Removal of the auxin source by severing the shoots of *Pinus sylvestris L.* saplings resulted in suspension of secondary growth [265], while exogenous application of auxin partially rescued this phenotype [100, 266, 267]. In *Arabidopsis* stems, an increase in auxin gave rise to more cambial divisions [100, 121] and similarly, in *Populus* and *Pinus* trees, auxin was reported to accumulate in the vascular cambium to drive radial expansion [143, 262-264]. In *Arabidopsis* root, an auxin maxima was identified on the xylem side of the cambium, in the domain recently revealed to initiate cambial activity [72]. Together, these data suggest a requirement for auxin presence for normal cambial activity, with auxin maxima in the cambium regulating correct radial expansion.

4.1.2 PIN active transport coordinates auxin distribution

In general, auxin moves down the root, then accumulates in the root quiescent centre,

before being transported back up through the lateral cap and into the epidermis [268, 269]. Auxin is transported throughout the plant using two main routes of distribution. The first one is a fast unregulated shoot-to-root flux of auxin from the synthesis sites in the plant (such as leaves and flowers), down through the phloem to sites of sink (the root) using a pressure-flow mechanism [205, 269]. The second means of auxin transport is cell-to-cell active transport, mainly conducted by the PIN auxin efflux carriers [138, 268-273]. This type of transport refines auxin distribution across tissues [274, 275]. The basically-localized auxin importer AUX1 also plays a role in root-ward auxin transport [78, 276]. PIN's contribution to auxin's flow down the root has been previously modelled [214, 219, 220], with some models also incorporating AUX1[222, 234].

Active transport is slower, a more refined short-distance means of distribution, and coordinates multiple developmental processes, including organogenesis [193, 277-279], the establishment of the embryonic axis [280], gravitotropic response [281, 282] and indeed, root patterning [138, 283]. Since auxin is a weak acid, it becomes protonated in the acidic apoplast. This allows it to diffuse into the cell, where it is ionised, thereby becoming unable to leave [275]. Thus, a mechanism is needed for the removal of auxin from the cell. The PIN proteins perform this function. Polarly localized at the plasma-membrane, they export auxin in a particular direction through direct translocation across the plasma membrane, thus coordinating auxin distribution and directing the emergence of auxin gradients and local auxin maximas [138, 270, 284, 285]. PIN1, PIN3, PIN4 and PIN7, were shown to regulate vascular development in root [196, 200, 272, 280, 282, 286, 287]. In order to understand how auxin is distributed across the secondary vascular tissues from the phloem-restricted bulk flow so as to accumulate in the cambium, PIN active transport must be considered [138, 270-273].

4.1.3 Downstream auxin response factor MP activates PIN transport and influences cambial divisions

Aspects of PIN active transport are linked to the activity of auxin itself. Auxin's signalling pathway operates through the *ARF* family of genes (see: Chapter 1, section 1.1.2 for details), whose proteins mediate the auxin downstream response [105, 106, 108, 288, 289]. A particularly well-established member of the *ARF* family is *MP/ARF5*, expressed on the xylem side of the cambium and encoding a transcription factor [72]. Null *mp* alleles were shown to

prevent the establishment of the hypocotyl/root axis and the corresponding organs [115]. In addition, the *mp* phenotype exhibited similarity to plants with PIN1 transport defects, thus MP was linked to PIN activation [114, 116, 117]. At least three PINs, PIN1, PIN3 and PIN7, were subsequently shown to require MP function during secondary growth [121].

Despite its prominence in multiple regulatory processes, *MP*'s role in cambial activity is contradictory. In different organs and at different stages of development, *MP* was seen to regulate cambial activity differently. In a recent publication by Smetana et al., (2019) [72], *MP* was reported to promote cambial activity during root cambial initiation. Contrastingly, in earlier publications by Brackmann et al., (2018)[121] and Han et al. (2018) [120], MP's function was shown to be the opposite in stems and hypocotyls, with MP suppressing cell divisions in the cambium. Studying *MP* function in detail, however, is particularly challenging, as loss of *MP* is lethal to the plant [114].

4.1.4 Cytokinin negatively regulates auxin transport via downregulation of PIN proteins

A second hormone that interacts with auxin and plays an important role in development and PIN regulation is cytokinin [122, 123]. Loss of cytokinin-synthesizing genes results in a striking root vascular phenotype, characterized by absence of cambium, substantially smaller radial size, and a single layer of vasculature, cortex, epidermis and pericycle [122]. Like auxin, cytokinin is distributed by fast phloem-constrained rootward transport and xylem-constrained transport from root to shoot [79]. Auxin and cytokinin have been implicated in several mutually-reliant feedback mechanisms (reviewed in [149, 290-292]). The auxin-cytokinin cross-talk is key to balancing cell differentiation and division processes[62, 139, 141, 142, 262]. The gradients of auxin and cytokinin, through the vascular tissues, display different patterns. Auxin has a maximum in the cambium while cytokinin's maximum is in the phloem (Figure 24) [72, 143, 262-264] . Negative regulation between auxin and cytokinin has been previously established, post embryonically. For example, auxin was seen to stimulate the expression of the cytokinin-deactivating enzyme CKX [144]. Auxin suppresses the transcription of the *IPT* genes, which encode cytokinin-promoting enzymes [145, 146]. Auxin also promotes the histidine phosphotransfer domain (HPt) protein AHP6, known to negatively regulate cytokinin signalling [129-131]. In turn, cytokinin suppresses

auxin active transport through decreasing the PIN levels at the post-transcriptional stage [140, 148, 293-296]. Together, auxin and cytokinin are interconnected in vascular regulation, with PIN active transport comprising a key node of correspondence between the hormones.

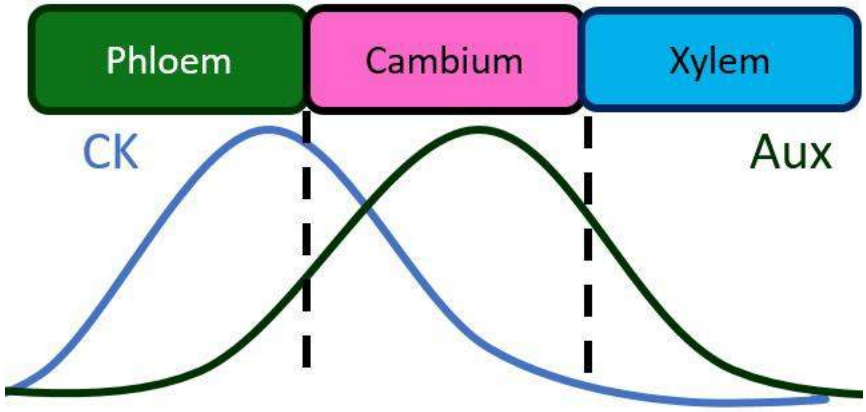

Figure 28: Adapted from Fischer et al. (2019) [62], Figure 2b. A schematic of the distribution of auxin and cytokinin across the vascular tissue. Auxin and cytokinin are transported down the phloem, with auxin then peaking in the cambium, while cytokinin is highest in the phloem.

4.1.5 The PXY receptor kinase promotes cambial activity

The cambium-expressed PXY and its downstream target, the WOX4 transcription factor are promoters of cambial activity [154, 155, 157, 159]. PXY's ligand, TDIF, signals to PXY from the phloem, activating the PXY pathway [154, 155, 157-159]. PXY's interaction with auxin and auxin signalling has been demonstrated in several studies, with WOX4 also shown to be required for auxin response in the cambium [183].

In the vascular cambium, *PXY* expression was described to overlap with auxin and areas of cambial activity. In root, *PXY* was seen to accumulate on the xylem side of the cambium. This is the same region where auxin was shown to reach a maxima in order to promote cell divisions [72, 175]. Similar observations were made in stems, where markers of auxin response were seen to overlap with both the *PXY* domain and the area of cambial activity [121]. Subsequent experiments of increased endogenous auxin concentration in cells containing *PXY* resulted in a boost of cambial divisions [121]. Together these studies support the idea that *PXY* and auxin co-expression and interaction drive cambial activity [72, 121, 175]. Moreover, the auxin response factor *MP* was also found in cells marked by *PXY* expression and characterised by an auxin maximum [72, 121]. This shows a further link between the auxin

signalling pathway, the auxin maxima in the cambium and *PXY* signaling for regulating cambial activity.

The PXY-MP interaction, however, is complex. To study *MP*, whose loss terminates the plant [114], a gain-of-function, dominant form of *MP* (*MPΔ*) was developed [297]. This represents a truncated artificial *MP* allele, able to resist inhibition by AUX/IAA proteins [297]. In root, *MPΔ* was seen to induce *PXY* and its downstream component *WOX4*, thus promoting divisions in the cambium [72].

A contrasting relationship between PXY and MP was identified, however, in stem [120]. PXY had been previously shown to interact with the GSK3 family of genes [91], among which is *BIL1*, a recently established activator of MP phosphorylation [120]. Secondary growth in stems saw PXY restriction of BIL1 [120]. By suppressing BIL1, PXY inhibits the loosening of MP's bonds with its IAA suppressor, effectively hindering the MP downstream response [120]. In this way, PXY was shown to boost cambial activity in hypocotyls and stems, where MP was seen to counteract cambial divisions [120, 121].

4.2 Hypothesis

In the above, *PXY* and *MP* were described to coexist in the same region of the cambium, where auxin accumulates in order to perform its function of promoting cell divisions [72, 121, 175]. This indicates that *PXY*, auxin and auxin's downstream response factor *MP* could interact for regulating cambial activity. Notably, *PXY* is a known cambial promoter [154, 155, 157, 159], whereas *MP* promotes cambial divisions in root [72] but not in stem and hypocotyl [120, 121]. Moreover, *PXY* and *MP* were shown to interact in two distinctly different ways in different plant organs. In root, MP was shown to promote PXY, whereas in stem, PXY was seen to suppress MP [72, 120]. Thus, the question emerges as to how these data can be reconciled to explain the PXY-MP-auxin relationship for regulating cell divisions.

The main hypothesis of this chapter is that MP's promotion of PXY [72] in root and the inhibition of MP by PXY [120], are both present in root and form a negative feedback loop on MP regulation (Figure 29). Within this study, mathematical modelling is used to explore this hypothesis. Specifically, the aim is to investigate the emergence of an auxin maxima in the cambium in the context of the PXY-MP interaction.

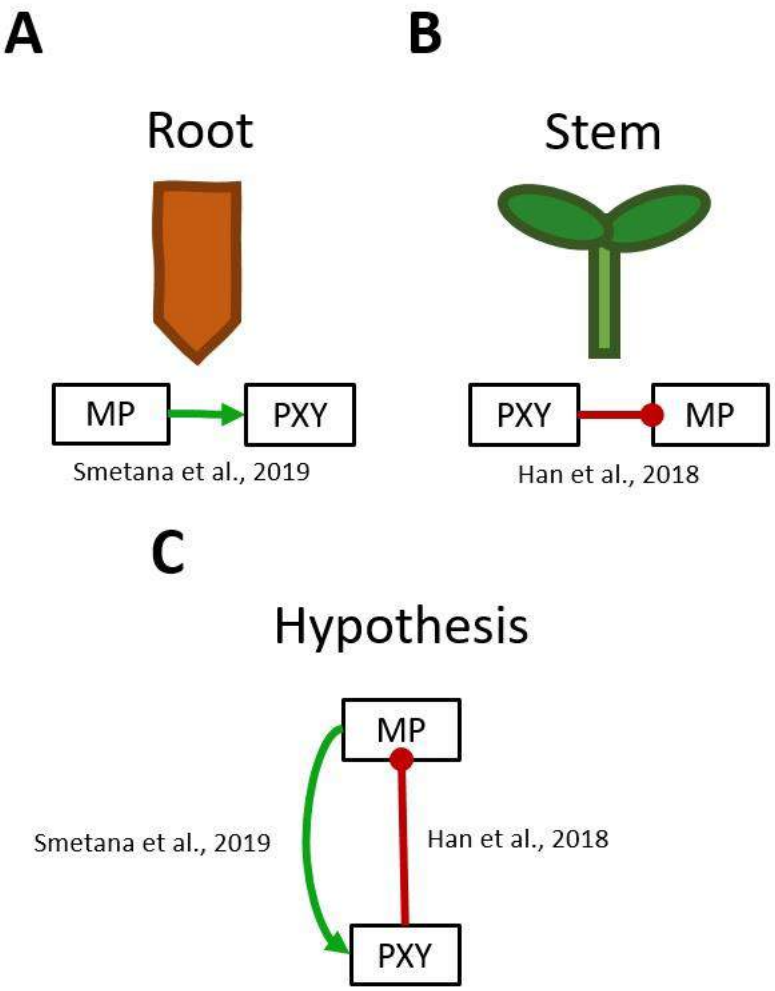

Figure 22: Diagram of the main hypothesis of this chapter. A schematic of the PXY-MP relationship in root (A) and stem (B). The hypothesis proposed in this thesis combines both and is provided in (C).

4.3 Model formulation

As discussed above, auxin and cytokinin play an important role in vascular development, but differ in their distribution patterns – auxin maximum is in the cambium, whereas cytokinin's maximum is in the phloem [72, 143, 262-264] (Figure 28). In order to study how these auxin and cytokinin patterns are obtained, a model was constructed corresponding to a simplified vascular structure and consisting of three domains to represent the main vascular cells - phloem, cambium and xylem. The components embedded in the model have been implicated in cambial activity and auxin patterning, i.e. the hormone auxin itself [100, 143, 262-267], the hormone cytokinin [122], auxin's efflux transporters, the PIN proteins PIN1, PIN3 and PIN7 [196, 200, 272, 280, 282, 286, 287], and their activator MP/ARF5

[72, 119, 121] together with the receptor-kinase PXY and its ligand TDIF [72, 120, 154, 155, 157, 159] (see section 4.1 for details).

4.3.1 Model simplifications

To efficiently address the hypothesis described above, several simplifications were introduced. In the case of this model, only total concentration of auxin and cytokinin in each cell was required to resolve if the auxin and cytokinin patterns match the patterns from Figure 28. Thus, the specific location of the auxin and cytokinin concentration maxima within the cells was not of interest (Figure 28). Each cell was therefore assumed to be well-mixed. Similarly, and as a result of the well-mixed assumption, the PIN proteins included in this study, namely PIN1, PIN3 and PIN7, were collectively described as a singular PIN, functioning to export auxin, as their localization in the cells was not considered. The dynamics of auxin flow down the phloem using PIN proteins [138, 268-273] and basally-located AUX1 importers [78, 276] is not modelled explicitly (see: section 4.3.4). This is the case as auxin is considered to be continuously replenished by sources in the shoots [78, 138, 270, 282, 286] and only the auxin that enters the cambium is required for comparison between homeostasis of the cambium in the networks with and without the PXY-MP negative feedback loop. Translation and transcription were not modelled as individual steps, since only the final product of these processes was of relevance. The model equations, parameters and dynamics will be discussed next.

4.3.2 Reaction-diffusion network

The model's dynamics were described, using reaction-diffusion equations (1)-(10) below. Square brackets correspond to concentration values of the components within them.

$$\frac{d[Aux_c]}{dt} = F_a[Aux_p] + r_8\left(\frac{1}{2}[PIN_x]\right)[Aux_x] - r_8[Aux_c][PIN_c] - d_{Aux}[Aux_c] \quad (1)$$

$$\frac{d[Aux_x]}{dt} = r_8\left(\frac{1}{2}[PIN_c]\right)[Aux_c] - r_8[Aux_x][PIN_x] - d_{Aux}[Aux_x] \quad (2)$$

$$\frac{d[PIN_c]}{dt} = r_6[MP_c] - r_7[CK_c][PIN_c] - d_{PIN}[PIN_c] \quad (3)$$

$$\frac{d[PIN_x]}{dt} = r_6[MP_x] - r_7[CK_x][PIN_x] - d_{PIN}[PIN_x] \quad (4)$$

$$\frac{d[MP_c]}{dt} = r_5[Aux_c] - r_3[PXY_a][MP_c] - d_{MP}[MP_c] \quad (5)$$

$$\frac{d[MP_x]}{dt} = r_5[Aux_x] - d_{MP}[MP_x] \quad (6)$$

$$\frac{d[PXY_{in}]}{dt} = r_4[MP_c] - r_2[PXY_{in}][TDIF] - d_{PXY_{in}}[PXY_{in}] \quad (7)$$

$$\frac{d[PXY_a]}{dt} = r_2[PXY_{in}][TDIF_p] - d_{PXY_a}[PXY_a] \quad (8)$$

$$\frac{d[CK_c]}{dt} = D_{ck}\frac{\partial^2}{\partial x^2}[CK] - r_1[Aux_c][CK_c] - d_{CK}[CK_c] \quad (9)$$

$$\frac{d[CK_x]}{dt} = D_{ck}\frac{\partial^2}{\partial x^2}[CK] - r_1[Aux_x][CK_x] - d_{CK}[CK_x] \quad (10)$$

In the equations (1)-(10), cell association for each component in the network (auxin, cytokinin, MP, PINs, PXY, TDIF) is marked by a subscript related to the correct tissue type ('c' for the cambium, 'p' for the phloem and 'x' for the xylem). For example auxin in the phloem, cambium and xylem is given by $[Aux_p]$, $[Aux_c]$ and $[Aux_x]$, respectively, and each of these concentrations is governed by a separate equation. Parameters r_* where '*' is a number, denote reaction rates. $d_\dagger$ are basal degradation rates where † corresponds to the component the degradation belongs to (e.g. d_{Aux} is the degradation of auxin). F_a is the rate of influx of auxin, D_{ck} is the diffusion coefficient of cytokinin. In the phloem, the concentrations $[Aux_p], [CK_p]$ and $[TDIF_p]$ are constant, with reasoning for this given in section 4.3.4. Together, $[Aux_p]$, $[CK_p]$, $[TDIF_p]$, F_a, D_{ck}, r_1, r_2, r_3, r_4, r_5, r_6, r_7, r_8, d_{Aux}, d_{CK}, d_{PIN}, d_{MP}, $d_{PXY_{in}}$, d_{PXY_a} are the network's parameters. Their units are given in Table 1. Full description of the network dynamics will be given in sections 4.3.3-4.3.6.

Equations (1)-(10) represent both networks to be investigated, the network with the PXY-MP negative feedback loop (hypothesized in section 4.2 above) and the network without it. In the case where the PXY-MP negative feedback loop is included (section 4.2), all reaction rates are non-zero. Conversely, in the absence of a PXY-MP feedback loop (this is the currently existing network in the literature), all of the related reaction rates $r_2, r_3, r_4, d_{PXY_{in}}, d_{PXY_a}$ are set to zero and the concentration of TDIF in the phloem $[TDIF_p]$ is also set to zero.

Auxin concentration in the phloem	Units
$[Aux_p]$	μM
Auxin flux	Units
F_a	s^{-1}
Cytokinin concentration in the phloem	Units
$[CK_p]$	μM
Concentration of TDIF in the phloem	Units
$[TDIF_p]$	μM
Diffusion coefficient	Units
D_{ck}	$\mu m^2/s$
Reaction rates	Units
r_1	$\mu^{-1}s^{-1}$
r_2	$\mu^{-1}s^{-1}$
r_3	$\mu^{-1}s^{-1}$
r_4	s^{-1}
r_5	s^{-1}
r_6	s^{-1}
r_7	$\mu^{-1}s^{-1}$
r_8	$\mu^{-1}s^{-1}$
d_{Aux}	s^{-1}
d_{CK}	s^{-1}
d_{PIN}	s^{-1}
d_{MP}	s^{-1}
$d_{PXY_{in}}$	s^{-1}
d_{PXY_a}	s^{-1}

Table 1: Table of all the parameters in the model and their corresponding units

The network is schematically represented in Figure 30. Basal degradations are omitted from Figure 30 for clarity of illustration. The reactions and references are provided in Table 2 (compare with Figure 30). Each of the reactions seen in Figure 30 (equations (1)-(10) and Table 2) are discussed in detail below.

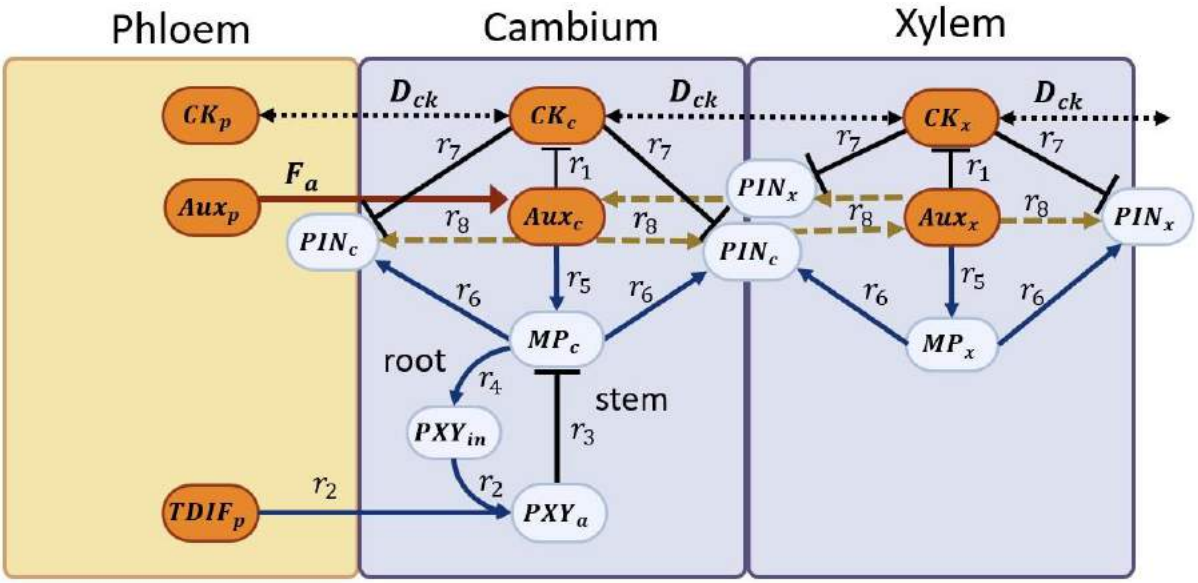

Figure 30: A schematic of the reaction-diffusion network domains and interactions. Three main cells are illustrated. The phloem (pale orange) is viewed as an inexhaustible hormone source and a source of TDIF. All orange components are mobile (cytokinin, auxin, TDIF). Blue arrows indicate promotion/activation. Blunted arrows indicate suppression. Brown solid arrows represent the influx of auxin from the phloem. Pale yellow dashed arrows indicate interaction between PINs and auxin for auxin export from the cell in a given direction. Black dotted lines correspond to cytokinin diffusion. Reaction rates are shown next to arrows in italics. Basal degradation is not shown for clarity of diagram. The hypothesis being tested is represented by the reactions with reaction rates r_2, r_3 and r_4 (compare to Figure 25 C).

Network Interactions		
Reaction rate	Interaction summary	Reference
r_1	Aux ⊣CK	[80, 129, 131, 141, 144, 145]
r_2	TDIF binds to PXY	[154-157]
r_3	PXY ⊣MP/ARF5	[120]
r_4	MP →PXY	[72]
r_5	Aux →MP	[105, 106, 111, 288, 289, 298]
r_6	MP → PINs	[114, 115, 117, 119, 147]
r_7	CK ⊣PINs	[140-142, 148, 293, 295]
r_8	PIN transports auxin	[138, 270-272]

Table 2: A table of the model reactions, where column 1 provides the name given to the reaction inside the model, column 2 gives a schematic description of the reaction. Blunted arrows correspond to suppression, arrows correspond to promotion/activation. Column 3 contains the references for each reaction.

4.3.3 Hormone movement

Auxin enters the cambium as a flux from the phloem (F_a, Figure 30). Subsequent movement of auxin out of the cambium and xylem is governed by PIN proteins (r_8, Figure 30) [275]. Since cytokinin does not require protein carriers to exit the cell, cytokinin was modelled as diffusing freely through the system from the phloem (D_{ck}, Figure 30), as done in previous models [214, 234]. However, the cytokinin diffusion coefficient has not been measured. Thus, here, the diffusion constant from the Moore et al. (2015) [234] model (which also studied hormone patterning in root; see: Chapter 1, section 1.3), was used i.e. $D_{CK} = 220\ \mu m^2/s$. For the cell radial distances travelled by diffusion, mean realistic cell sizes were used (see: Figure 30). Full description of diffusion dynamics is given in section Methods 4.6 below.

4.3.4 Phloem source

Within the model, the phloem is viewed as an inexhaustible source of auxin, cytokinin and TDIF. Cytokinin [79] and auxin [78, 138, 270, 282, 286] are rapidly transported down the phloem from shoot to root. Similarly, PXY's peptide ligand, TDIF, undergoes translation and transcription in the phloem from where it signals to PXY in the cambium [155-157].Thus, the concentrations of auxin, cytokinin and TDIF ($[Aux_p]$, $[CK_p]$, $[TDIF_p]$, Figure 30) in the phloem remain constant as any movement of auxin and cytokinin out of the phloem is instantly replenished by the flow. Loss of TDIF is replenished by its production in the phloem.

4.3.5 Cambium reactions

The hormones cytokinin and auxin both move from the phloem towards the cambium. Upon entering the cambium, auxin can only exit with the assistance of PIN proteins, either by moving back towards the phloem or by being transported into the xylem [275, 299, 300]. Any auxin which is transported by PINs back into the phloem is thought to instantly drain down the phloem and is disregarded. In the cambium, auxin and cytokinin interact, with auxin deactivating cytokinin [80, 129, 131, 141, 144, 145] (r_1 , Figure 30) and cytokinin suppressing PIN proteins [140-142, 148, 293, 295] (r_7, Figure 30). Auxin promotes the release of its

downstream response factor MP/ARF5 from inhibition (r_5, Figure 30), while MP/ARF5 activates PIN proteins [114, 116, 117, 119, 298] (r_6, Figure 30). In the root cambium, MP was seen to induce the transcription of *PXY* (r_4, Figure 30) to produce an inactive form of PXY ($\mathrm{PXY_{in}}$, Figure 30). Inactive PXY interacts with TDIF (r_2, Figure 30), activating the PXY protein ($\mathrm{PXY_a}$, Figure 30) [154, 155, 157-159].

The hypothesised PXY-MP negative feedback loop is also in the cambium. This loop consists of active PXY's repression of MP (r_3, Figure 30) [120] and MP's promotion of inactive PXY. Note, MP inhibition by active PXY is not direct, and is in fact facilitated through an intermediate component, BIL1 [120], which is suppressed by active PXY and thereby stopped from promoting MP [120]. However, as BIL1's role here is only to promote MP phosphorylation, BIL1's behaviour is not of individual interest.

4.3.6 Xylem reactions

The final cell in the model is the xylem. Auxin is transported from the cambium into the xylem using PIN-regulated active transport [138, 270-273]. As in the cambium, in the xylem auxin suppresses cytokinin [129-131, 144], cytokinin inhibits PINs [140-142, 148, 293, 295] and auxin de-represses its downstream target MP [52, 108, 147]. PIN proteins in the xylem transport auxin back towards the cambium, exiting the xylem. Any auxin that exits the xylem is disregarded as it leaves the system.

4.4 Results

For the hormone concentration patterns in the model to match the patterns from the literature, cytokinin is to be highest in the phloem and gradually reduce towards the xylem [143, 262], whereas auxin needs to peak in the cambium [72, 143, 262-264] (Figure 30). Thus, in order for the correct hormone pattern to be reproduced by the model, the following inequalities must be satisfied,

$$[CK_p] > [CK_c] > [CK_x] \tag{11}$$

$$[Aux_c] > [Aux_p] \tag{12}$$

$$[Aux_c] > [Aux_x] \quad (13)$$

Inequality (11) describes the required cytokinin pattern, while inequalities (12) & (13) correspond to the required auxin pattern.

4.4.1 The cytokinin pattern in the model always matches the literature

Consider first condition (11). In both networks under investigation (with and without PXY-MP negative feedback), cytokinin diffuses from its source in the phloem and moves towards the xylem [79]. Diffusion is the product of random particle movement. The net result of diffusion is the movement of particles from a space with higher concentration, to a space with lower concentration. Thus, particles diffusing away from a source obtain a concentration pattern that is highest at the source and decreases as the distance from the source is increased. Since the phloem is the sole source of cytokinin in the network, a diffusion-only regulated cytokinin would have the following pattern: $[CK_p] > [CK_c] > [CK_x]$. In the model, cytokinin concentration is also influenced by auxin. Auxin deactivates cytokinin in the cambium and xylem [80, 129, 131, 141, 144, 145], thereby further reducing the concentration of active cytokinin in those cells (reaction r_1). Thus, the following dynamics occur. As cytokinin diffuses into the cambium, the concentration of cytokinin in the cambium (given by $[CK_c]$) becomes lower than in the phloem. In the cambium, auxin deactivates cytokinin (reaction r_1), further reducing the concentration of cytokinin in the cambium. Similarly, cytokinin diffuses from the cambium into the xylem. Thus, the concentration of cytokinin in the xylem (given by $[CK_x]$) is lower than in the cambium. In the xylem, the concentration of cytokinin is again reduced by auxin deactivation, becoming even lower. The inequality $[CK_p] > [CK_c] > [CK_x]$ holds, satisfying (11). All simulations conducted in sections 4.3.2-4.3.5 support this conclusion.

4.4.2 The network with the PXY-MP negative feedback loop is more robust at reproducing the hormone patterns than the network without the PXY-MP negative feedback loop

First, the question was asked whether the networks with and without the PXY-MP negative feedback loop were capable of generating an auxin maximum in the cambium. To address this question, equations (1)-(10) were solved numerically, using the Euler method (see: section 4.6.1 and 4.6.2 Methods). The steady state solutions were evaluated for fulfilling conditions (11)-(13). As the majority of parameter values were not known (namely, all the reaction rates r_1 - r_8, the auxin flux from the phloem F_a, and the phloem-sourced concentrations of auxin $[Aux_p]$, cytokinin $[CK_p]$, and TDIF $[TDIF_p]$), parameter values for the equations were sampled from a uniform interval [0,20]. As will be shown in section 4.4.6, where the results of a closed form analysis of equations (1)-(10) will be discussed, the conclusions made throughout this study hold irrespective of the particular sampling interval.

2, 500 parameter sets were generated independently for each network. The individual parameters were sampled using the sampling strategy for the global sensitivity technique, the Morris method (results of the Morris method application are given in 4.4.4), which involves perturbing parameters with a step Δ (see section 4.6.3: Methods). The Morris sampling strategy relies on discretising the parameter intervals into equally spaced points to be chosen from, with level of partitioning p (p Morris level) related to the perturbation step Δ. Here, the Morris level p was chosen as $p = 41$, as it corresponds to a perturbation step $\Delta = 0.5$ (see section 4.6: Methods for full details). To ensure that all reactions were present unless otherwise specified, the value 0.001 was added post-sampling to all parameters in the case where the PXY-MP loop was present, and to all parameters except r_2, r_3, r_4, $[TDIF_p]$, d_{PXY_a}, $d_{PXY_{in}}$ in the case where it was not.

Term parameter sets that satisfy conditions (11)-(13) as 'successful' and those that do not pattern as 'unsuccessful'. Running the simulations revealed three key findings.

First, all simulations (for both the network with and without the PXY-MP loop) confirmed the previously discussed assessment of the cytokinin pattern (see section 4.4.1),

with final steady state concentrations of cytokinin across the cells always satisfying condition (11), i.e. $[CK_p] > [CK_c] > [CK_x]$.

Second, in all parameter sets condition (13), i.e. $[Aux_c] > [Aux_x]$, held. This result agrees with the closed form analysis which will be discussed in section 4.4.6 and Appendix E3, showing that $[Aux_c] > [Aux_x]$ holds regardless of parameter choices.

Third, as conditions (11) and (13) are always satisfied, successful parameter sets are those that satisfy condition (12). Of the 2,500 parameter sets ran in the network without the PXY-MP negative feedback loop, a total of 467 parameter sets (18.68%) were successful. Of the 2,500 parameter sets ran in the network with the PXY-MP negative feedback loop was present, 725 parameters (29%) were successful (Figure 31). This data shows that the network with the PXY-MP negative feedback loop can achieve an auxin maximum in the cambium for a larger number of parameters under the same parameter sampling strategy. Thus, adding PXY inhibition of MP to the root makes the network more robust for generating an auxin maximum in the cambium.

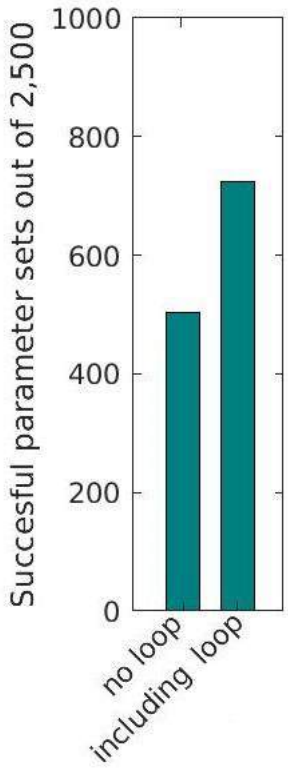

Figure 31: A bar chart of number of successful parameters in both networks: and without PXY-MP negative feedback loop.

4.4.3 The network with the PXY-MP negative feedback loop expands the conditions under which an auxin maximum in the cambium can be achieved

Having established that the network containing the PXY-MP negative feedback loop is more robust at satisfying conditions (11)-(13), the question was asked if the additional successful parameter sets were truly a result of the added PXY-MP negative feedback loop. To answer this question, two experiments were conducted.

The first experiment examined if there were successful parameter sets in the network with the PXY-MP negative feedback loop, for which the negative feedback loop was required for a successful pattern. To this end, from the 725 successful parameter sets obtained from the network with the PXY-MP negative feedback loop, the parameters related to the loop were removed (Figure 31). That is, the values of $r_2, r_3, r_4, [TDIF_p], d_{PXY_a}, d_{PXY_{in}}$ were set to zero and the new (adjusted) parameter sets were run to steady state in the model.

Of the 725 parameter sets that had previously patterned in the presence of the PXY-

MP negative feedback loop, 248 (34.21%) could no longer achieve a pattern when the negative feedback loop was removed. Thus, there were parameter sets for which the PXY-MP negative feedback loop was required.

The second experiment tested to see if in the parameter sets that were able to successfully pattern in the absence of the PXY-MP negative feedback loop, there existed parameter sets for which the introduction of the PXY-MP negative feedback loop would result in an unsuccessful pattern. Similarly to the first experiment above, the 467 successful parameter sets for the network without the PXY-MP negative feedback loop (Figure 31) were adjusted for the network with the PXY-MP negative feedback loop. Instead of having the parameters r_2, r_3, r_4, $[TDIF_p]$, d_{PXY_a}, $d_{PXY_{in}}$ in the 467 parameter sets equal to zero (as is the case with all parameter sets for the network without the PXY-MP negative feedback loop), values for of r_2, r_3, r_4, $TDIF$, d_{PXY_a}, $d_{PXY_{in}}$ were randomly sampled from a continuous interval $[0.001, 20]$. For each of the 467 parameter sets, 10 sets of r_2, r_3, r_4, $TDIF$, d_{PXY_a}, $d_{PXY_{in}}$ were generated at random, resulting in a total of 4670 new parameter sets. Each parameter set was solved to steady state and assessed for successful patterning.

All 4670 parameter sets produced a successful pattern. To test if this could be the result of the interval choice $[0.001, 20]$, the experiment was repeated twice for larger intervals, with values for $r_2, r_3, r_4, TDIF, d_{PXY_a}, d_{PXY_{in}}$ randomly sampled from the continuous intervals $[20.001,100]$ and $[100.001,1000]$. As before, for each of the 467 parameter sets, 10 sets of r_2, r_3, r_4, $[TDIF_p]$, d_{PXY_a}, $d_{PXY_{in}}$ were generated, resulting in another 4670 new parameter sets in each of the two cases. In each iteration of the experiment, all 4670 parameter sets produced a successful pattern. Thus, there were no occasions where adding the PXY-MP negative feedback loop to a parameter set that was successful in the network without the PXY-MP negative feedback loop, resulted in the successful patterning being lost. In section 4.4.6.2, it will be further discussed that the conclusions of this section always hold.

Taken together, the above two experiments suggest that a negative feedback mechanism between PXY and MP in the root network improves the ability of the network to retain an auxin maxima in the cambium.

4.4.4 Sensitivity analysis shows that both networks are

insensitive to perturbations

In this section, the aim was to investigate the networks' sensitivity to parameter perturbations for satisfying inequality (11)-(13) at steady state. The Morris method (fully described in section 4.6.3) is a computationally inexpensive method for calculating measures of sensitivity for parameters. Thus, the Morris method was chosen to be used.

For the questions addressed within this thesis, successful or unsuccessful pattern is considered, not the numerical values of concentrations. Thus, of interest were the instances when a parameter perturbation resulted in changing the network's steady state pattern from successful to unsuccessful, or vice versa. The Morris method was modified to fit this requirement (see: section 4.6.3). A parameter perturbation that resulted in a change in the network's steady state pattern from successful to unsuccessful, or vice versa, was attributed sensitivity value 1. For example, if in a parameter set the parameter r_1 was perturbed and the network's patterning state changed from successful to unsuccessful, then r_1 obtained sensitivity value 1. If perturbation of r_1 in the next parameter set also changed the network's patterning state from successful to unsuccessful, or vice versa, r_1's sensitivity value increases to 2, and so on. Upon the completion of the Morris method, the parameters were ranked in order of sensitivity values. The parameter with the highest sensitivity value has Morris rank 1.

For the Morris method sensitivity analysis, 50 parameter sets were selected from the 2,500 parameter sets used to generate Figure 31, such that they were maximally distant from all other remaining parameter sets. That is, 50 parameter sets were chosen whose sum of Euclidean distances to the remaining parameter sets was largest. Parameters were chosen in this way to maximise the spread of parameter sets within the parameter space.

The Morris method creates new parameter sets from old ones by randomly perturbing each network parameter exactly once (see section 4.6.3 for full description). The network with the PXY-MP negative feedback loop has a total of 18 parameters. Thus, from one parameter set in the network with the PXY-MP negative feedback loop, 18 additional parameter sets were created through Morris perturbations. It follows that a total of $18 \times 50 = 900$ Morris perturbations occur for the network with the PXY-MP negative feedback loop. The network without the PXY-MP negative feedback loop has 12 parameters as the

parameters making up the negative feedback loop, i.e. $r_2, r_3, r_4, [TDIF_p], d_{PXY_a}, d_{PXY_{in}}$, are absent. In the case when no PXY-MP negative feedback loop is present, a total of $12 \times 50 = 600$ Morris perturbations occur.

First, the resulting Morris ranking for each individual parameter for the network with the PXY-MP negative feedback loop was recorded and depicted in a bar graph found in Appendix E1.1. For $p = 41$ this is Figure 1S (C). As each component in the network is linked to several parameters, these individual Morris rankings do not explain how components impact the biological system. For example, for the network with the PXY-MP negative feedback loop, the two parameters with the highest Morris ranking , rank 1, were d_{Aux} and d_{PXY_a}. The three rank 2 parameters (r_2, r_4, $[TDIF_p]$) were all linked to PXY concentration. No lower ranks were recorded. This suggests that parameter sets for the network with the PXY-MP loop negative feedback loop experience most changes in pattern from successful to unsuccessful or vice versa when the concentration of PXY is changed. Thus, looking at the Morris ranking of parameter groupings rather than the Morris ranking of individual parameters would give insight into the effects of components on the ability of the network to satisfy conditions (11)-(13).

To look into the effects of components on the ability of the model to satisfy conditions (11)-(13), individual parameters were grouped into component-related categories to provide a mean sensitivity value for each component. The mean sensitivity value was calculated by averaging the sensitivity values of the parameters within the component group. The five major component groups were as follows: auxin-related parameters, cytokinin-related parameters, PIN-related parameters, MP-related parameters and PXY-related parameters. A parameter was considered a member of a component group if it directly affected the concentration of the component after which the group was named. Under this schema, the group of auxin-related parameters had 3 members ($[Aux_p]$, F_a, d_{Aux}), the group of cytokinin-related parameters had 3 members ($[CK_p]$, r_1, d_{CK}), the group of MP-related parameters had 3 members (r_3, r_5, d_{MP}), the group of PIN-related parameters had 4 members (r_6, r_7, r_8, d_{PIN}) and the group of PXY-related parameters had 5 (r_2, r_4, $[TDIF_p]$, $d_{PXY_{in}}$, d_{PXY_a}). That is, of the 900 perturbations in total, $50 \times 3 = 150$ perturbations directly impact auxin, cytokinin and MP concentrations, while $50 \times 4 = 200$ perturbations impact PIN concentration and $50 \times 5 = 250$ impact PXY concentration. An example of a mean sensitivity value calculation: if a

total of 10 changes from successful to unsuccessful state, or vice versa were recorded for MP-related parameters (a component group which has 3 members), the statistic for that component group would be $\frac{10}{3} = 3.33$ (2 d.p.). The component groups were then ranked, with the component group with the highest mean sensitivity value obtaining Morris rank 1.

Mean sensitivity value results are given in Figure 32 below. Different parameter categories are marked by different colours (e.g. PXY-related parameters are blue; see legend in Figure 32).

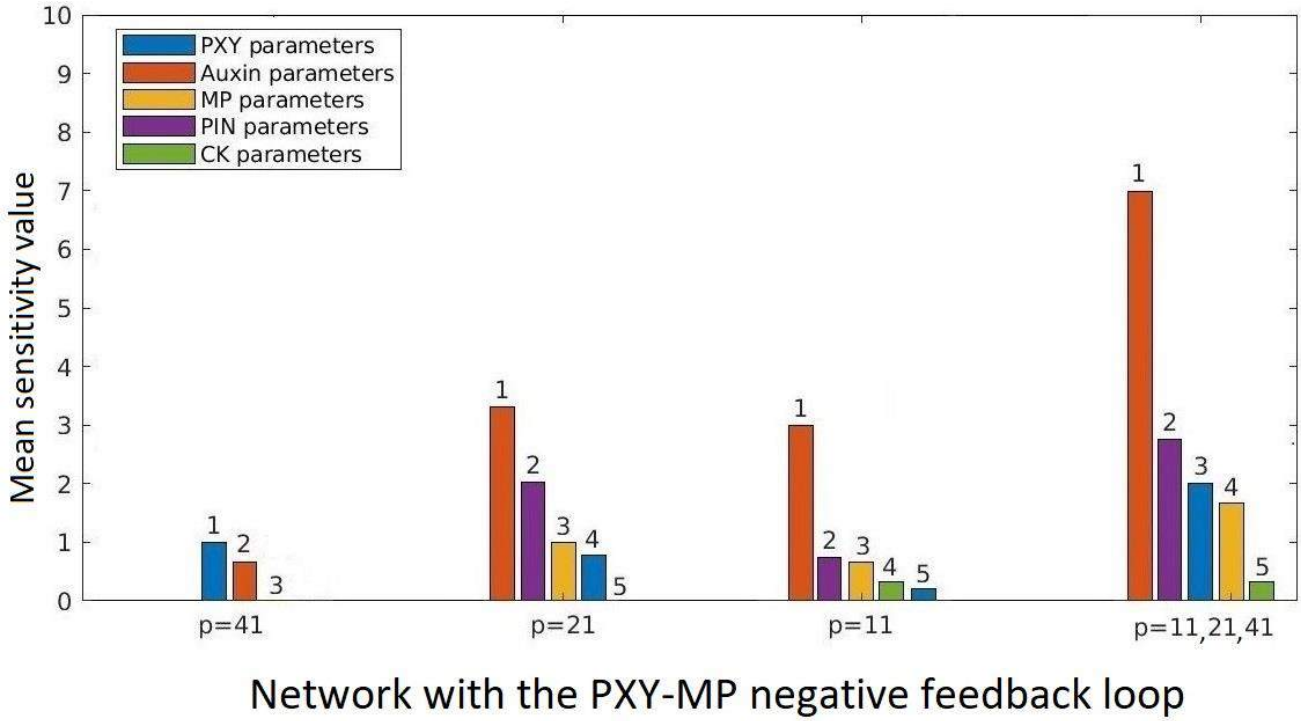

Figure 32: Mean sensitivity value results for Morris levels p=41, 21, 11 (corresponding to step size change $\Delta = 0.5, 1, 2$) and all three combined for the network with the PXY-MP negative feedback loop. Numbers on top of each bar are rankings Rank 1 corresponds to the parameter group that the model is most sensitive to, while 5 corresponds to the parameter group that the network is least sensitive to.

The results of $p = 41$ indicated highest sensitivity to PXY-related parameters, rank 1, and lower sensitivity to auxin-related parameters at rank 2. However, out of the 900 perturbations in the network with the PXY-MP negative feedback loop, a total of only 7 instances (0.78%) of changes (from successful to unsuccessful or vice versa) were detected and distributed across the different parameter groups, with no changes at all detected for the

group of cytokinin, MP or PIN-related parameters. 5 changes were caused by perturbing PXY-related parameters (2 % of the 250 changes related to PXY) and 2 by auxin-related parameters (1.33% of the 150 changes linked to auxin). Overall, this indicated that for $p = 41$ with a step-size $\Delta = 0.5$, the network with the PXY-MP negative feedback loop was insensitive to perturbations and the initial state of successful or unsuccessful is retained under almost all single-step perturbations. A summary of the number of group-related and total changes is given in Table 3 below.

Network with PXY-MP loop	All groups	Auxin-related parameters	CK-related parameters	MP-related parameters	PIN-related parameters	PXY-related parameters
Total number of changes	900	150	150	150	200	250
Number of changes for p=41	7 (0.78%)	2 (1.33%)	0	0	0	5 (2 %)
Number of changes for p=21	25 (2.78%)	10 (6.67%)	0	3 (2%)	8 (4%)	4 (1.6 %)
Number of changes for p=11	16 (1.78%)	9 (6%)	0	2 (1.33 %)	3 (1.5%)	1 (0.4%)

Table 3: Table of changes under Morris perturbations in the network with the PXY-MP loop. Column 1 is headings. Row 1 gives the total number of observed changes across all parameters (Column 2) and the number of changes observed in different parameter groups (Auxin, CK, MP, PIN and PXY-related parameters). Remaining rows correspond to Morris levels $p = 41, p = 21, p = 11$. Each cell from rows 2-4 provide a net number and proportion. All percentages are reported to 2 d.p.

To address the question of whether higher sensitivity may be detected at larger step size (i.e. lower Morris levels p; see section 4.6.3 for full details), the above experiment was replicated for Morris levels $p = 21$ and $p = 11$. This corresponded to perturbation step sizes $\Delta = 1$ (5% of the interval size of 20) and $\Delta = 2$ (10% of the interval), respectively. 2, 500 parameter sets were generated independently for the network with the PXY-MP negative feedback loop using the Morris sampling strategy, this time with Morris levels set to $p = 21$ and $p = 11$. Parameter intervals remained $[0, 20]$ (with a subsequent addition of 0.001).

Of each of the 2, 500 independently generated parameter sets for $p = 21$ and $p = 11$, 50 maximally distant parameter sets were selected from each (as done for the $p = 41$ case) and the Morris method was used. The results of the Morris ranking are given in Figure 28, for $p = 21$ and $p = 11$. In both cases, the Morris perturbations at higher step size yielded more changes from successful to unsuccessful pattern, or vice versa. The results indicated that the network was most sensitive to auxin-related parameters and PIN-related parameters (ranks 1 and 2). MP-related parameters were rank 3, while ranks 4 and 5 were either the PXY or CK component group. The results show that for smaller perturbations, at $p = 41$, the network is more sensitive to PXY-related parameters, but at larger perturbations, auxin and PIN transport dominate in ability to produce changes in the parameter sets' state (from successful to unsuccessful or vice versa).

To gain an overview of the sensitivity of the model for all step sizes studied, the results of all the $p = 41, 21$ and 11 were also combined (Figure 32). Here, auxin and PIN-related parameters retained ranks 1 and 2, showing that parameter sets were most likely to change from successful to unsuccessful or vice versa if members of the auxin-related or PIN-related parameter group were perturbed. Ranks 3, 4 and 5 were held by MP-related, PXY-related and cytokinin-related parameters. The breakdown for individual Morris parameter rankings (given in Appendix E1.1, Figure 1S) showed that changes in state (from successful to unsuccessful pattern, or vice versa) were not caused by perturbations in one specific parameter in a group, but generally spread out across the members of the group.

Although more pattern state changes were recorded for $p = 21$ and $p = 11$ compared to $p = 41$, the total number of changes was still low in each case. A total of 25 (2.78% of the total 900) changes occurred for the $p = 21$ case and 16 (1.78%) changes for the $p = 11$ case, spread out across all 5 groups of parameters. This suggests that the network is not particularly sensitive to perturbations (the details of the number of changes are summarized in Table 3). The parameter groups whose perturbation seemed to most consistently generate a state change for parameter sets (from successful to unsuccessful or vice versa) were those of auxin and PIN-related parameters. Thus, even though a single step perturbation is unlikely to cause a change in the network's behaviour, such change is most likely to happen if parameters belonging to the auxin or PIN group are perturbed.

The same sensitivity analysis was performed on the network without a PXY-MP negative feedback loop. The results of the individual parameter sensitivity is given in Appendix E1.2, Figure 2S. As before, parameter groups were identified: the groups of auxin, cytokinin, MP and PIN-related parameters. No PXY-related parameter group is observable in the case of the network with no PXY-MP negative feedback loop. The group of MP-related parameters here contains only 2 parameters, r_5 and d_{MP}. The remaining parameter groups are the same as for the case of the network with the PXY-MP negative feedback loop. Thus, of the 600 perturbations in total, $50 \times 3 = 150$ perturbations directly impact auxin and cytokinin concentration, while $50 \times 4 = 200$ perturbations impact PIN concentration and $2 \times 5 = 100$ impact MP concentration. As before, the mean sensitivity value was calculated for each component group by averaging the sensitivity values of the parameters within the component group.

The results of applying the Morris method to the network with no PXY-MP negative feedback loop are given in Figure 33 below. For $p = 41$, auxin-related parameters obtained rank 1, while PIN-related parameters ranked 2. Perturbations in none of the parameters of the remaining groups caused any changes in state from successful to unsuccessful or vice versa. However, of the 600 perturbations conducted for the network without a PXY-MP negative feedback loop, a total of only 2 state changes from successful to unsuccessful or vice versa (Appendix E1.2 C; Table 4) were recorded for $p = 41$ (0.33% of the total). As with the case of the network with the PXY-MP negative feedback loop, the small step size Δ was assumed to be the reason. Thus, Morris sensitivity analysis was repeated with larger step sizes $\Delta = 1$, or 5% of the sampling interval (this corresponds to Morris levels $p = 21$), and $\Delta = 2$, equivalent to 10% of the sampling interval (or Morris levels $p = 11$). 2, 500 parameter sets were independently generated for the network without the PXY-MP negative feedback loop using the Morris sampling strategy at Morris levels $p = 21$ and $p = 11$. 50 maximally distant parameter sets were selected and the Morris sensitivity analysis was applied to them. The results of the Morris ranking are given in Figure 29, for $p = 21$ and $p = 11$. In both cases, more changes were detected compared to the case of $p = 41$.

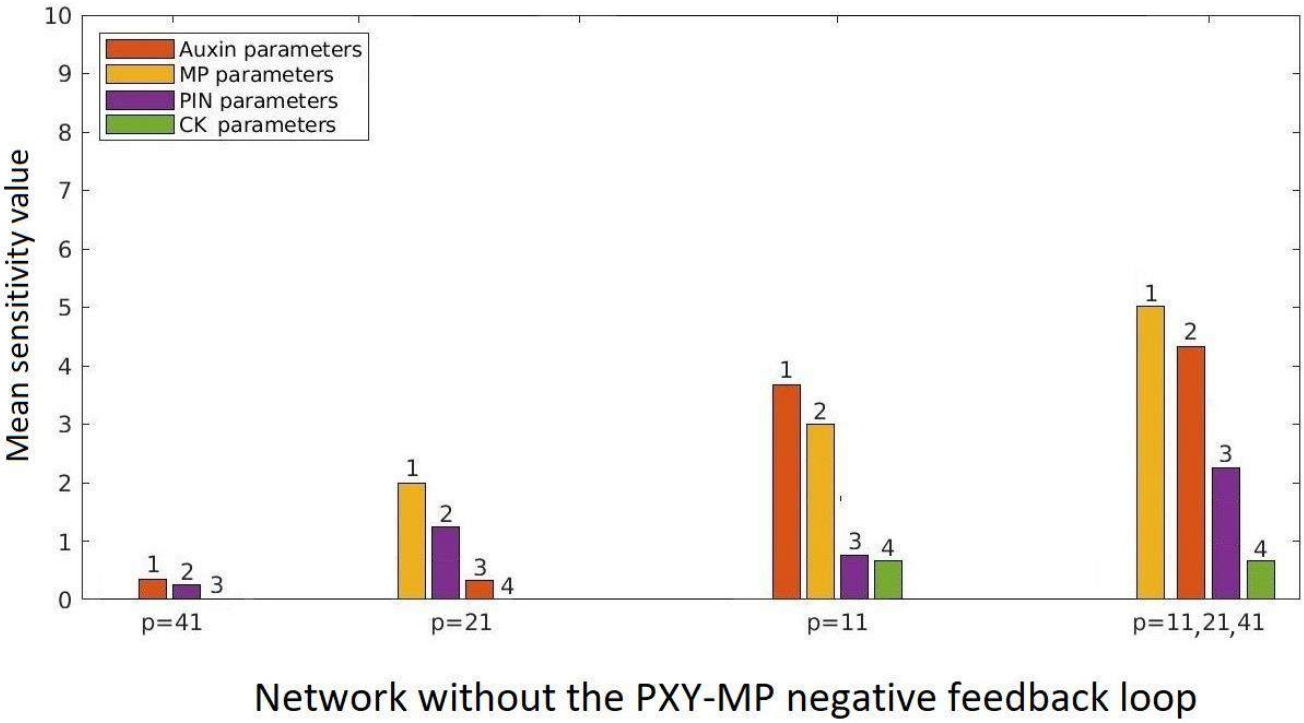

At $p = 21$, a total of 10 changes in state occurred from successful to unsuccessful or vice versa (1.67% of the total of 600 perturbations). The network showed to be most sensitive to MP-related parameters (rank 1), followed closely by PIN-related parameters (rank 2) and finally auxin-related parameters (rank 3) (Table 4; Figure 33). At the largest step-size $\Delta = 2$ at $p = 11$, an overall of 22 instances of changes in state from successful to unsuccessful or vice versa were recorded (3.67% of the 600 perturbations). In this case the network was most sensitive to auxin-related parameters (rank 1), followed by MP-related parameters (rank 2) and PIN-related parameters (rank 3) (Table 4). Sensitivity to CK-related parameters ranked last (rank 4). The combined ranking data from $p = 11, 21, 41$ showed that MP-related parameters overall hold rank 1, auxin-related parameters hold rank 2, PIN-related parameters have rank 3 and CK-related parameters rank 4 (Figure 29). Overall, this data shows that perturbations in MP-related and auxin-related parameters are most likely to cause a change in state in a parameter set, from successful to unsuccessful or vice versa. Higher sensitivity

Figure 33: Mean sensitivity value results for Morris levels p=41, 21, 11 (corresponding to step size change $\Delta = 0.5, 1, 2$) and all three combined for the network without the PXY-MP negative feedback loop. Numbers on top of each bar are rankings Rank 1 corresponds to the parameter group that the network is most sensitive to, while 4 corresponds to the parameter group that the model is least sensitive to.

was attributed to MP-related parameters for the cases of $p = 21$ (rank 1) and $p = 11$ (rank

2) compared to the network with PXY-MP negative feedback loop (where MP-related parameters ranked 3rd or lower), outranking PIN-related parameters in sensitivity measure (Figure 32; Figure 33). MP-related parameters also ranked 1 in the $p = 11, 21, 41$ combined graph (Figure 33) compared to having rank 4 in the network with the PXY-MP negative feedback loop (Figure 32). This suggests that the addition of the PXY-MP negative feedback loop reduces sensitivity of the pattern to MP-related parameters. As in the network with the PXY-MP negative feedback loop, although more changes were detected for $p = 21$ and $p = 11$ compared to the $p = 41$ case (where only 0.33% of the perturbations cased a change), changes overall were still few (1.67% and 3.67% for $p = 11$ and $p = 21$, respectively). This indicates that both with and without the PXY-MP negative feedback loop, the network is insensitive to state change under the influence of a single perturbation.

Network without PXY-MP loop	All groups	Auxin-related parameters	CK-related parameters	MP-related parameters	PIN-related parameters
Total number of changes	600	150	150	100	200
Number of changes for p=41	2 (0.33%)	1 (0.67%)	0	0	1 (0.5%)
Number of changes for p=21	10 (1.67%)	1 (0.67%)	0	4 (4%)	5 (2.5%)
Number of changes for p=11	22(3.67%)	11 (7.33%)	2 (1.33%)	6 (6%)	3 (1.5%)

Table 4: Table of changes under Morris perturbations in the network without the PXY-MP loop. Column 1 is headings. Row 1 gives the total number of observed changes across all parameters (Column 2) and the number of changes observed in different parameter groups (Auxin, CK, MP, PIN and PXY-related parameters). Remaining rows correspond to Morris levels $p = 41, p = 21, p = 11$. Each cell from rows 2-4 provides a net number and proportion. All percentages are reported to 2 d.p.

4.4.5 The PXY-MP feedback loop is required for patterning if MP degradation is small

In section 4.4.2 the network with the PXY-MP negative feedback loop was shown to be more robust at generating an auxin maximum in the cambium, with the PXY-MP negative

feedback loop required for 34.21% of the successful parameter sets in Figure 31 (see section 4.3.3). Here, the question was asked whether there were parameter sampling ranges which maximise the proportion of parameter sets for which the PXY-MP negative feedback loop is required.

In order to find regions for which the network with the PXY-MP negative feedback loop would have more successful parameter sets compared to the network without the PXY-MP negative feedback loop, the data from Figure 31 were considered. Of the 725 successful parameter sets for $p = 41$ in the network with the PXY-MP negative feedback loop, 248 required the PXY-MP negative feedback loop for a successful pattern, while the remaining 477 parameter sets did not. From these two successful parameter sets, two probability density graphs were generated for each parameter shared by both networks (i.e. all of $[Aux_p]$, F_a, $[CK_p]$, r_1, r_5, r_6, r_7, r_8, d_{Aux}, d_{CK}, d_{PIN}, d_{MP}). This was done in order to determine whether there were differences in how parameter values are distributed between the successful parameter sets that required the PXY-MP negative feedback loop and those that did not. Probability density functions were chosen, rather than histograms, to manage the difference in sample sizes (248 vs 477 parameter sets). Of the two probability density graphs generated for each of the shared parameters, one corresponded to a distribution of the values of the parameter from the successful parameter sets for which the PXY-MP negative feedback loop was not required (the collection of 477 parameter sets). The other probability density graph showed the distribution of values of that parameter in the successful parameter sets which required the PXY-MP negative feedback loop to be successful (the collection of 248 parameter sets).

The basal rate of degradation of MP, d_{MP}, showed the most striking contrast between distributions for the successful parameters that required a PXY-MP negative feedback loop and those that did not (Figure 34 A, B). The graphs for the remaining shared parameters can be found in Appendix E2, Figure 3S. In Figure 34 A, the distribution of d_{MP} across the parameter range showed an upward tendency. That is, in the successful parameter sets for which the PXY-MP negative feedback loop was not required, the largest values for d_{MP} most frequently belonged to a successful parameter set. Conversely, a downward trend was observed in d_{MP} in the successful parameter sets that required the PXY-MP negative feedback loop (Figure 34 B), where the majority of the values were close to zero. Thus, d_{MP} values closer to zero are most likely to require the PXY-MP negative feedback loop. It was reasoned

that smaller d_{MP} values require the PXY-MP negative feedback because the degradation rate of $[MP_c]$ in the network without the PXY-MP negative feedback loop is only d_{MP}. However, when the PXY-MP loop is added, $[MP_c]$ is degraded by rate $d_{MP} + r_3[PXY_a]$ in the cambium.

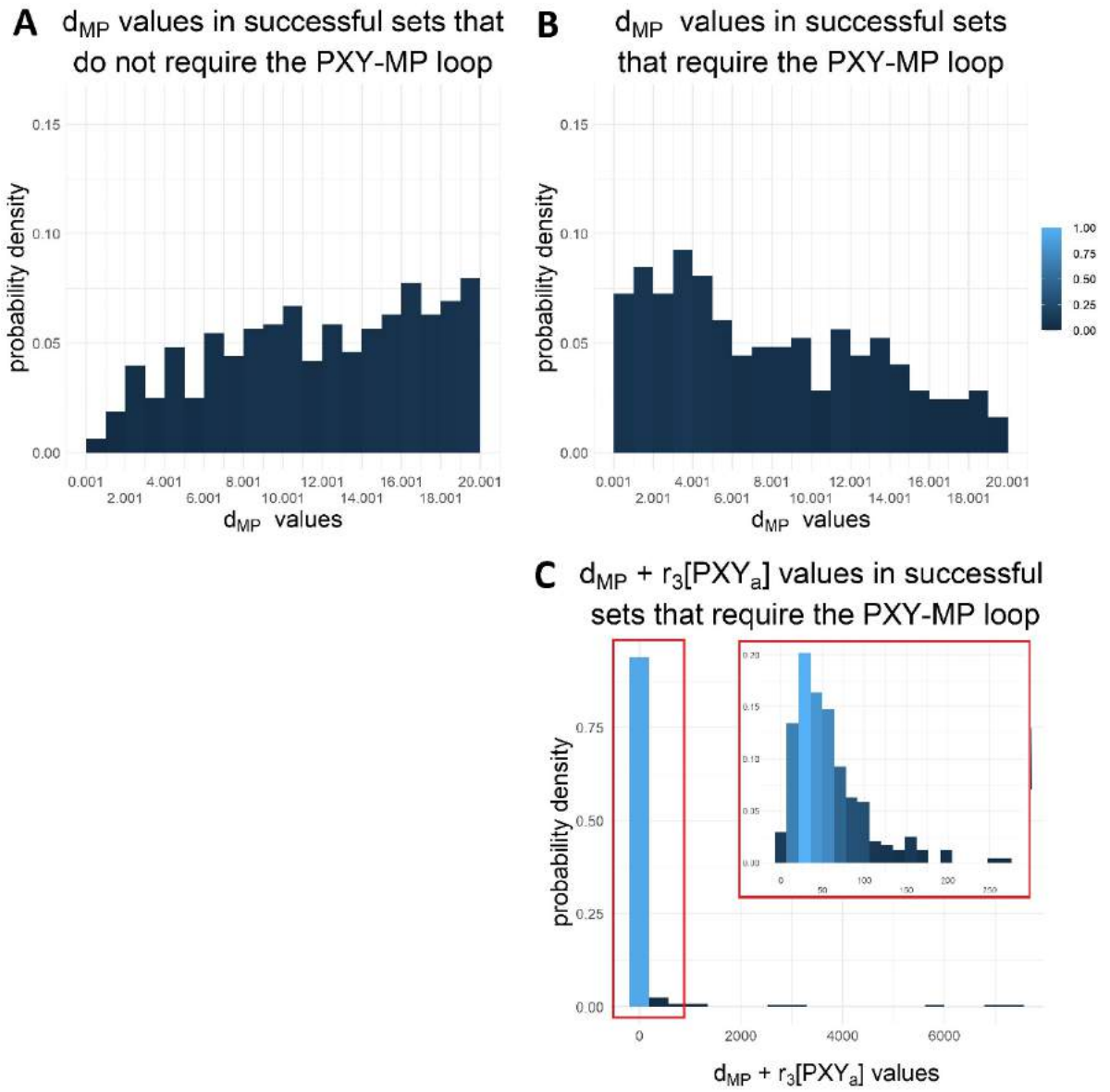

Figure 34: Probability density functions of the distribution of d_{MP} in the successful parameter set that do not require the PXY-MP negative feedback loop (A) and in those that require a PXY-MP negative feedback loop (B). Bin count = 20. Each bin contains 2 possible choices of values, except the last one which contains 3. The distribution of $d_{MP} + r_3[PXY_a]$ is given in (C). The panel in the right upper corner corresponds to a values of $d_{MP} + r_3[PXY_a]$ between 0 and 300 to enable a better view of the data. Red rectangles represent the same regions. Bin count = 20. Darker blue corresponds to smaller probability, lighter is higher probability.

In order to explore if an opposing trend between the two degradation rates d_{MP} and $d_{MP} + r_3[PXY_a]$ existed in the successful parameter sets that required PXY-MP negative

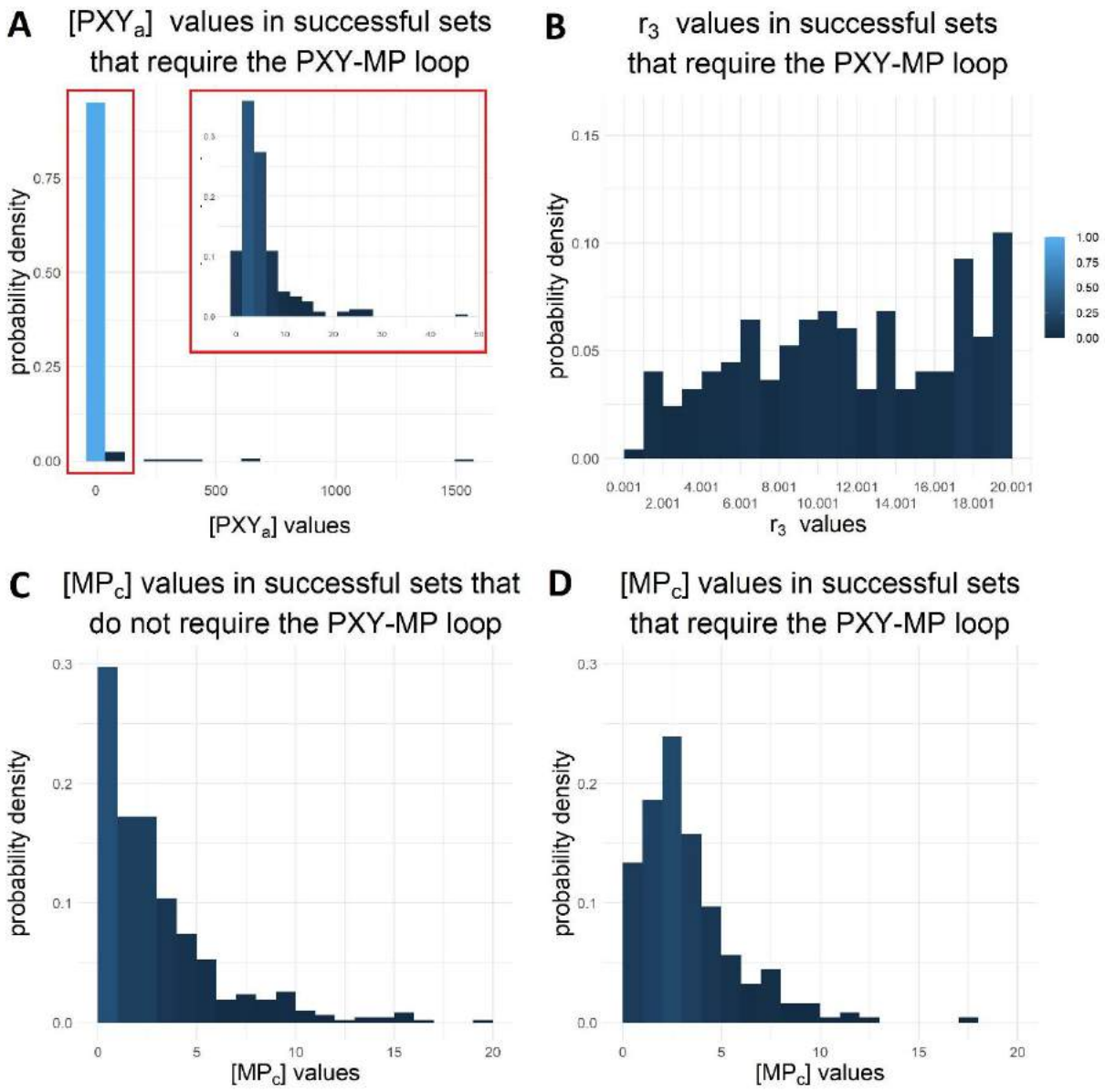

Figure 35: Probability density function of the distributions of $[PXY_a]$ final steady state concentration (A), the reaction r_3 (B) in the successful parameter set that require the PXY-MP negative feedback loop. Probability density function of the final steady state concentration of $[MP_c]$ in the successful parameter sets that do not require a PXY-MP negative feedback loop (C) and in the successful parameter sets that do (D) Bin count = 20. Each bin contains 2 possible choices of values, except the last one which contains 3. In (A), the panel in the right upper corner corresponds to a values of $d_{MP} + r_3[PXY_a]$ between 0 and 50 to enable a better view of the data. Red rectangles represent the same regions. Bin count = 20. Darker blue corresponds to smaller probability, lighter is higher probability.

feedback loop, the probability density function for $d_{MP} + r_3[PXY_a]$ (with $[PXY_a]$ being the PXY_a concentration at steady state) was plotted (Figure 34 C). Several outlier large values were observed in the plot. The majority of values were accumulated closer to the [0, 300] interval. To see the data more clearly, an additional graph was plotted (in the right upper

corner of Figure 34 C) which focused on the interval 0 to 300. In this graph (Figure 34 C), a downward trend could be observed, similar to the one in Figure 34 B. Thus, for the successful parameter sets which require the PXY-MP loop, the d_{MP} and $d_{MP} + r_3[PXY_a]$ trends (Figure 34B, C) were similar.

To understand why d_{MP} and $d_{MP} + r_3[PXY_a]$ have the same trend, the distributions of $[PXY_a]$ and r_3 (Figure 35 A, B), were examined. Note that the probability density functions of the remaining parameters from the PXY-MP negative feedback loop, (r_2, r_3, r_4, $TDIF$, d_{PXY_a}, $d_{PXY_{in}}$) are in Appendix E2, Figure 4S. As with Figure 34 A and the expression $d_{MP} + r_3[PXY_a]$, the distribution of $[PXY_a]$ had several large outlier values. The majority of values were accumulated closer to the [0, 50] interval. As before, a graph was plotted for clarity (in the right upper corner of Figure 35 A) which focused on the interval 0 to 50. In this focused graph depicting the [0, 50] range, $[PXY_a]$ values in the successful parameter sets that required the PXY-MP negative feedback loop, showed a downward trend, with most values accumulating closer to zero (Figure 35 A).

The r_3 distribution in the successful parameter sets in the network with the PXY-MP negative feedback loop, was seen to have an upward trend (Figure 35 B). Thus, a higher degradation of MP via PXY enables successful patterning. As discussed above, however, $[PXY_a]$ values in the successful parameter sets that required the PXY-MP negative feedback loop, had an opposing, downward trend (Figure 35 A). To understand the $[PXY_a]$ trend, the distribution of $[MP_c]$ was considered.

The final steady state concentration of $[MP_c]$ in the successful parameter sets that required and did not require the PXY-MP negative feedback loop, both showed a distribution with a downward trend, with the number of values decreasing away from zero (Figure 35 C, D). This indicated that lower concentrations of $[MP_c]$ at steady state are more likely to produce a successful pattern. It was reasoned that this is the case as lower concentrations of $[MP_c]$ result in less PINs being activated in the cambium via the reaction r_6 (Figure 30). Less availability of PINs reduces auxin transport out of the cambium and thus more auxin is retained to produce a maxima. This hypothesis was supported by the data showing that the r_3 distribution in the successful sets in the network with the PXY-MP negative feedback loop has an upward trend (Figure 35 B). Thus, a higher rate of repression of MP via PXY (reaction r_3) promotes patterning by restricting $[MP_c]$ levels. $[PXY_a]$ corresponds to the final steady state concentration of PXY_a, the resulting product of activating the inactive form of PXY,

PXY_{in}. Within the network, PXY_{in} concentration is promoted by MP via reaction r_4 (Figure 30). Thus, a lower concentration of MP at time t ultimately results in a lower concentration of PXY_a at time t. Since lower $[MP_c]$ concentrations are preferred for a pattern to be achieved, upon reaching steady state, lower concentration levels of MP are observed in the cambium. This results in lower final concentration of $[PXY_a]$, explaining the observations in Figure 35A. The downward trends of d_{MP} and$[PXY_a]$, in turn, influence the expression $d_{MP} + r_3[PXY_a]$. Therefore, in the successful parameter sets that require the PXY-MP loop for a successful pattern, both the new degradation rate $d_{MP} + r_3[PXY_a]$ and the base degradation d_{MP} (which appears in that expression), share a similar trend (Figure 34C).

The data in Figure 30 indicate that a parameter range of d_{MP} closer to zero is less likely to pattern without the PXY-MP negative feedback loop. To test whether a choice of d_{MP} closer to zero will maximise the number of successful parameter sets that require a PXY-MP negative feedback loop, two new experiments were performed.

Previously, all parameters were sampled from the interval [0,20] before the value 0.001 was added to shift all parameters away from zero. Here (and similarly to section 4.4.2), 2, 500 parameters were generated independently for each of the networks with and without the PXY-MP negative feedback loop, for two d_{MP} ranges: d_{MP} sampled from the interval [0,5] and d_{MP} sampled from the interval [0,1]. The 0.001 shift was added in both cases. The resulting parameter sets were then run to steady state and evaluated for number of the successful parameter sets within them.

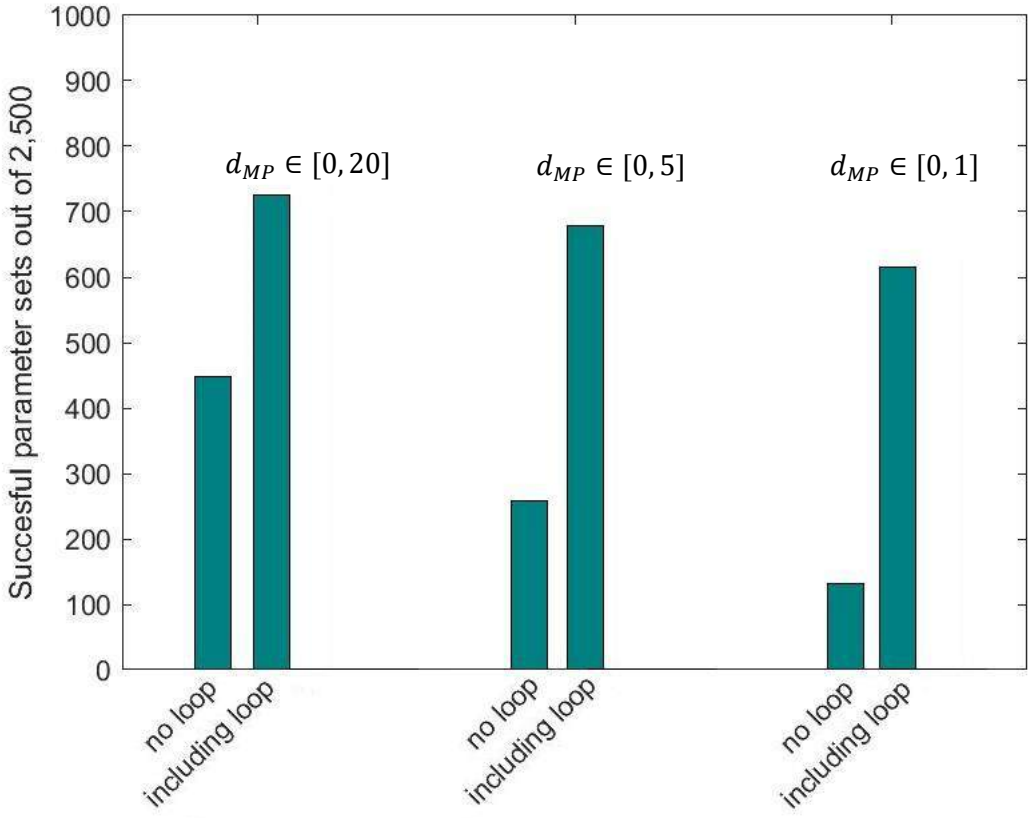

Figure 36: Bar graphs of the number of parameter sets of the 2,500 sampled independently for the network with and without a PXY-MP loop. Leftmost bar graph matches the results of Figure 24. The second bar graph shows the results of d_{MP} sampled in the interval $[0,5]$ and the third bar shows the results of d_{MP} sampled in the interval $[0,1]$.

The results of the experiment are provided in Figure 36. To visualize the impact of gradually moving the d_{MP} sampling closer to zero, the data from the original experiment (d_{MP} chosen in the interval [0,20] as all other parameters), from Figure 31 was included in Figure 36 on the leftmost side of the graph. When d_{MP} was chosen from the interval [0,20], 467 (18.68%) parameter sets were successful in the network without the PXY-MP negative feedback loop (of the 2,500 generated ones), versus 725 (or 29%) in the presence of a PXY-MP negative feedback loop (Figure 36, leftmost bar graph). As discussed previously, of these 725 parameter sets that succeeded in the network with the PXY-MP negative feedback loop, 248 (34.21%) were no longer successful when the loop was removed (Table 5, column 2; section 4.4.3).

	$d_{MP} \in [0, 20]$	$d_{MP} \in [0, 5]$	$d_{MP} \in [0, 1]$
Number of parameters (out of 2, 500) that succeed in network without the PXY-MP loop	467 (18.68%)	279 (10.36%)	132 (5.28 %)
Number of parameters (out of 2, 500) that succeed in network with the PXY-MP loop	725 (29%)	679 (27.16%)	615 (24.6%).
Number of parameters of the above that only succeed in the presence of the PXY-MP loop	248 (34.21%)	425 (62.59%)	494 (80.33%)

Table 5: Table showing the number of successful parameter sets for different d_{MP} ranges in the network with a PXY-MP loop vs the network without a loop. The first column corresponds to $d_{MP} \in [0, 20]$, the second column corresponds to $d_{MP} \in [0, 5]$, and the third one – to $d_{MP} \in [0, 1]$. Row one gives the number of successful parameter sets in the network without the PXY-MP loop from the independently generated 2, 500 parameter for each of the ranges. Row two gives the number of successful parameter sets from the independently generated 2, 500 ones for the network without the PXY-MP loop. Row 3 gives the proportion of parameters from the ones given in row 2, which cannot produce an auxin pattern when the PXY-MP loop is removed. All percentages are reported to 2 d.p.

The two subsequent experiments where d_{MP} was sampled from the interval [0,5] and [0,1] are shown in the second and third bar graph (Figure 36). Of the 2,500 parameter sets where d_{MP} was sampled from the interval [0,5], 279 (10.36%) were successful without the PXY-MP negative feedback loop. In the network with the PXY-MP negative feedback loop, 679 (27.16%) of the 2, 500 parameters were successful. Of those, 425 (62.59% of the 679 parameters) required the PXY-MP negative feedback loop to be successful (Table 5, column 3). In the case where d_{MP} was chosen from the interval [0, 1], only 132 of the 2,500 parameters (5.28%) succeeded in the network without the PXY-MP negative feedback loop. 615 (24.6%) of the parameters generated for the network with the PXY-MP negative feedback loop, were successful. Of those, 494 (80.33%) required the PXY-MP negative feedback loop to succeed (Table 5, column 4).

Thus, as the d_{MP} sampling interval is moved closer to zero, a decreasing proportion of the 2, 500 parameter sets sampled are successful in the network without the PXY-MP negative feedback loop (18.68%, 10.36% and 5.28% for each of the 3 cases $d_{MP} \in [0,20], [0,5]$ and $[0,1]$, respectively; Table 5). The network with the PXY-MP negative feedback loop demonstrates only a small decrease in the proportion of successful parameter sets when $d_{MP} \in [0,20]$, $[0,5]$ and $[0,1]$ (29%, 27.16% and 24.6%; Table 5). Thus, the difference between the proportion of successful parameter sets in network with the PXY-MP negative feedback loop and the network without, increases as the chosen d_{MP} range moves closer to zero. The proportion of successful parameter sets that required the PXY-MP negative feedback loop, also increased as the d_{MP} interval was chosen closer to zero (34.21%, 62.59% and 80.33% for $d_{MP} \in [0,20], [0,5]$ and $[0,1]$, respectively; Table 5). This suggests that if d_{MP} is small, then the presence of a PXY-MP negative feedback loop makes the network much more robust for generating an auxin maxima in the cambium.

Interestingly, the results of this section that smaller d_{MP} values require the PXY-MP negative feedback loop, are supported by the individual Morris rankings from section 4.4.4. In the network with the PXY-MP negative feedback loop, no changes at all from successful to unsuccessful, or vice versa, were recorded for perturbations in the parameter d_{MP}. However, in the network without the PXY-MP negative feedback loop, for the cases for $p = 11$ and $p = 21$, perturbations in d_{MP} caused changes in state and had rank 3 and 1, respectively (Appendix E1.2). This indicates that the presence of a PXY-MP negative feedback loop reduced sensitivity towards the MP basal degradation rate d_{MP}. Together with the analysis conducted in this section, this suggests that the PXY-MP negative feedback loop makes the network more robust against d_{MP} perturbations by expanding the possible values d_{MP} can take and allowing d_{MP} to be sampled closer to zero.

4.4.6 Closed form analysis confirms numerical results

4.4.6.1 Analysis conditions

In section 4.4.1 above, the cytokinin concentration pattern across the network was shown to always satisfy inequality (11), which was confirmed numerically in section 4.4.2. So,

in the following closed form analysis, inequality (11) is assumed to hold, i.e. $\left[CK_p\right] > [CK_c] > [CK_x]$ holds.

In this section, closed form analysis was used to address the question: are there analytical conditions for which successful patterning with an auxin maxima in the cambium is achieved (i.e. inequalities (12) and (13) hold)? These successful patterning conditions would be derived in such a way as to minimise their dependence on final steady state concentrations of the components in the network (exceptions are the phloem-based concentrations $\left[Aux_p\right]$, $[CK_p]$ and $[TDIF_p]$ which are constant and are part of the parameter set for the networks). Once derived, the successful patterning conditions would: one, provide a better understanding of patterning behaviour as a product of parameter interactions and two, make the model more predictable during numerical simulations, wherein the final outcome could be foreseeable at the parameter-specifying step. Together, this would allow the two networks, with and without the PXY-MP negative feedback loop, to be analysed at steady state and compared in a generalised way, independently of specific parameter values or components concentrations. In order to derive successful patterning conditions for network with and without the PXY-MP negative feedback loop, equations (1)-(10) were separately solved at steady state for the two networks.

For the case of the network without a PXY-MP negative feedback loop, no PXY-related reactions feedback into the system (i.e. $r_2, r_3, r_4, [TDIF_p], d_{PXY_a}, d_{PXY_{in}}$ were all equal to zero). As the analysis was conducted at steady state, no change in concentration occurs, and thus the diffusion term is equal to zero. The system to be analysed was given by

$$F_a[Aux_p] + \frac{1}{2}r_8[Aux_x][PIN_x] - r_8[Aux_c][PIN_c] - d_{Aux}[Aux_c] = 0$$
$$\frac{1}{2}r_8[Aux_c][PIN_c] - r_8[Aux_x][PIN_x] - d_{Aux}[Aux_x] = 0$$
$$r_6[MP_c] - r_7[CK_c][PIN_c] - d_{PIN}[PIN_c] = 0$$
$$r_6[MP_x] - r_7[CK_x][PIN_x] - d_{PIN}\,[PIN_x] = 0$$
$$r_5[Aux_c] - d_{MP}\,[MP_c] = 0$$
$$r_5[Aux_x] - d_{MP}\,[MP_x] = 0$$

Taking into account the relationship $\left[CK_p\right] > [CK_c] > [CK_x]$, the equations were solved for each of the conditions (12) and (13), $[Aux_c] > \left[Aux_p\right]$ and $[Aux_c] > [Aux_x]$, respectively.

First, proof by contradiction was used to show that $[Aux_c] > [Aux_x]$ always holds at steady state. This matched the numerical results obtained in section 4.4.2, confirming inequality (13) would always hold, regardless of parameter sampling. The condition for $[Aux_c] > \left[Aux_p\right]$ is shown in Table 6. The full analysis is given in Appendix E3.1.

Closed form analysis was conducted for the network containing the PXY-MP negative feedback loop. The equations for this case are,

$$F_a[Aux_p] + \frac{1}{2} r_8[Aux_x][PIN_x] - r_8[Aux_c][PIN_c] - d_{Aux}[Aux_c] = 0$$
$$\frac{1}{2} r_8[Aux_c][PIN_c] - r_8[Aux_x][PIN_x] - d_{Aux}[Aux_x] = 0$$
$$r_6[MP_c] - r_7[CK_c][PIN_c] - d_{PIN}[PIN_c] = 0$$
$$r_6[MP_x] - r_7[CK_x][PIN_x] - d_{PIN}\,[PIN_x] = 0$$
$$r_5[Aux_c] - r_3[PXY_a][MP_c] - d_{MP}\,[MP_c] = 0$$
$$r_5[Aux_x] - d_{MP}\,[MP_x] = 0$$
$$r_4[MP_c] - d_{PXY_{in}}[PXY_{in}] - r_2[PXY_{in}][TDIF] = 0$$
$$r_2[PXY_{in}]\left[TDIF_p\right] - d_{PXY_a}\,[PXY_a] = 0$$

Taking into account the relationship $\left[CK_p\right] > [CK_c] > [CK_x]$, the equations were solved for $[Aux_c] > \left[Aux_p\right]$ and $[Aux_c] > [Aux_x]$. As before, proof by contradiction was used to show that $[Aux_c] > [Aux_x]$ always holds at steady state for the network with the PXY-MP negative feedback loop, confirming the numerical results from section 4.4.2. The successful patterning condition for $[Aux_c] > \left[Aux_p\right]$ is shown in Table 6. The full analysis is provided in Appendix E3.2. As seen in Table 6, the successful patterning condition derived for the network with the PXY-MP negative feedback loop is not independent of final steady state concentrations; it depends on the final steady state concentration of $[PXY_a]$. This is the case due to the additional $r_3[PXY_a][MP_c]$ term in equation (5) in the network with the PXY-MP negative feedback loop. This term increases the complexity of the analysis, removing the ability to form an expression for $[MP_c]$ that depends only on final steady state concentration of auxin. Without this ability to rewrite $[MP_c]$ in terms of auxin, the $[Aux_c] > \left[Aux_p\right]$ relationship cannot be used to yield successful patterning condition that are independent of final steady state concentrations. Other attempts at the analysis were performed, however all of them resulted in dependence on more final steady state concentrations for one or both networks,

with and without the PXY-MP negative feedback loop. Moreover, the conditions in Table 6 showed similarity, making them easy to compare as will be done in section 4.4.6.2 below. Thus, at the point of writing, the analysis given in Appendix E3.2 and the resulting successful patterning conditions (Table 6) were deemed most satisfactory.

Conditions for auxin pattern in both networks		
Conditions for cambial auxin maxima	$[Aux_c] > [Aux_p]$	$[Aux_c] > [Aux_x]$
No PXY-MP loop	**Condition 1:** $F_a - \frac{1}{2} r_8 \frac{r_5 r_6 [Aux_p]}{(r_7[CK_p]+d_{PIN})}\left(\frac{1}{d_{MP}}\right) - d_{Aux} > 0$	Always true
With PXY-MP loop	**Condition 2:** $F_a - \frac{1}{2} r_8 \frac{r_6 r_5 [Aux_p]}{(r_7[CK_p]+d_{PIN})}\left(\frac{1}{r_3[PXY_a]+d_{MP}}\right) - d_{Aux} > 0$ with $PXY_a > -\frac{d_{MP}}{2r_3} + \frac{1}{2}\sqrt{\left(\frac{d_{MP}}{r_3}\right)^2 + \frac{r_2 TDIF_p}{d_{PXY_a} r_3} \frac{r_4 r_5 Aux_p}{\left(d_{PXY_{in}} + r_2 TDIF\right)}}$	Always true

Table 6: A summary table for the successful patterning conditions in both possible networks: with and without the PXY-MP negative feedback loop. Column 1 shows headings. Column 2 shows the conditions for auxin accumulation in the cambium over the phloem. Column 3 shows that the auxin concentration in the cambium in both system exceeds the auxin concentration in the xylem.

4.4.6.2 The network in which PXY downregulates MP is more robust at satisfying the condition $[Aux_c] > [Aux_p]$

In sections 4.4.1-4.4.5, it was shown numerically that the network containing the PXY-MP negative feedback loop is more robust for obtaining an auxin maxima in the cambium than the network without the PXY-MP negative feedback. In section 4.4.6 above, conditions were derived for successful patterning of the two networks (Table 6). Here, these conditions will be compared.

Since in both networks the condition $[Aux_c] > [Aux_x]$ was seen to hold (Table 6), it remained to test which network's condition satisfied $[Aux_c] > [Aux_p]$ for a larger parameter

space. Note that the conditions in both networks were similar, differing in the term $\frac{1}{d_{MP}}$ for the network without the PXY-MP negative feedback loop (condition 1, Table 6), versus the term $\frac{1}{r_3[PXY_a]+d_{MP}}$ for the network with the PXY-MP negative feedback loop (condition 2, Table 6). Thus, conditions 1 and 2 differed in the terms associated with the degradation rate of MP in the cambium, $[MP_c]$. This confirms that the PXY-MP negative feedback loop impacts the patterning ability of the network by altering the $[MP_c]$ degradation rate from d_{MP} to the expression $r_3[PXY_a] + d_{MP}$ (see: Figure 30; section 4.4.5).

Here, conditions 1 and 2 were used to confirm the numerical results shown in section 4.4.3. To conduct the analysis, two notation simplifications were made as follows.

Conditions 1 and 2 (Table 6) are given by

$$F_a - \frac{1}{2} r_8 \frac{r_5 r_6 [Aux_p]}{d_{MP}(r_7[CK_p]+d_{PIN})} - d_{Aux} > 0 \qquad \text{(condition 1)}$$

$$F_a - \frac{1}{2} r_8 \frac{r_5 r_6 [Aux_p]}{(r_7[CK_p]+d_{PIN})} \left(\frac{1}{r_3[PXY_a]+d_{MP}}\right) - d_{Aux} > 0 \qquad \text{(condition 2)}$$

Denote $X = F_a - d_{Aux}$ and $Y = \frac{1}{2} r_8 \frac{r_5 r_6 [Aux_p]}{r_7[CK_p]+d_{PIN}}$. Thus, the above conditions 1 and 2 are rewritten as

$$X - \frac{Y}{d_{MP}} > 0 \qquad \text{(condition 1.1)}$$

$$X - \frac{Y}{r_3[PXY_a]+d_{MP}} > 0. \qquad \text{(condition 2.1)}$$

Firstly, it was asked if conditions 1 and 2 could be used to confirm the results in section 4.4.2: all successful parameter sets in the network without the PXY-MP negative feedback loop are also successful once the PXY-MP negative feedback loop is added. The analysis for this is given below.

Consider condition 1.1. If condition 1.1 holds and patterning is successful, then

$$X - \frac{Y}{d_{MP}} > 0 \qquad \text{(condition 1.1)}$$

$$X > \frac{Y}{d_{MP}} \qquad \text{(condition 1.2)}$$

Note that here $d_{MP} \neq 0$. Since d_{MP} is a non-negative parameter, $d_{MP} > 0$. Next, consider condition 2.1 and rearrange.

The rearranged condition 2.1 gives

$$X - \frac{Y}{r_3[PXY_a]+d_{MP}} > 0 \qquad \text{(condition 2.1)}$$

$X > \frac{Y}{r_3[PXY_a]+d_{MP}}$. (condition 2.2)

For condition 2.2, $r_3 > 0$ because of the presence of the PXY-MP negative feedback loop. $[PXY_a] > 0$ is also true as only the cases where $[PXY_a]$ is present are considered, thus the term $r_3[PXY_a] > 0$. As $r_3[PXY_a] > 0$ and $d_{MP} > 0$, $d_{MP} + r_3[PXY_a] > d_{MP}$. Therefore, the following inequality can be derived

$d_{MP} + r_3[PXY_a] > d_{MP}$

$1 > \frac{d_{MP}}{d_{MP} + r_3[PXY_a]}$

$\frac{1}{d_{MP}} > \frac{1}{d_{MP}+r_3[PXY_a]}$ (inequality 1)

Now consider Y. The case with $Y = 0$ is trivial as it leads to the same inequality $X > 0$ for both conditions 1.1 and 2.1, showing that when condition 1 holds, so does condition 2 for $Y = 0$. For the case when $Y > 0$ inequality 1 becomes

$\frac{1}{d_{MP}} > \frac{1}{d_{MP}+r_3[PXY_a]}$ (inequality 1)

$\frac{Y}{d_{MP}} > \frac{Y}{d_{MP}+r_3[PXY_a]}$ (inequality 2)

Thus, the right-hand side of condition 1.2 is greater than or equal to the right-hand side of condition 2.2. Merging condition 1.2 and inequality 2 obtains the following,

$X > \frac{Y}{d_{MP}} > \frac{Y}{r_3[PXY_a] + d_{MP}}$,

which gives condition 2.2

$X > \frac{Y}{r_3[PXY_a]+d_{MP}}$. (condition 2.2)

Thus, if condition 1.1 holds, then condition 2.1 holds. It then follows that if condition 1 holds, so does condition 2. This result agrees with the numerical results from section 4.4.3.

Next, the second result of section 4.4.3 was tested: that there exist parameter sets which require the PXY-MP negative feedback loop to be successful. The analysis below will show that if condition 1 is broken condition 2 still holds.

Suppose that condition 1 is broken. This is the equivalent of condition 1.1 being broken, or

$\frac{Y}{d_{MP}} > X$ (condition 1.3)

being satisfied.

Let condition 2 hold. Condition 2 is equivalent to condition 2.2

$X > \frac{Y}{r_3[PXY_a]+d_{MP}}$. (condition 2.2)

Merge conditions 1.3 and 2.2 to get

$\frac{Y}{d_{MP}} > X$ (condition 1.3)

$X > \frac{Y}{r_3[PXY_a]+d_{MP}}$ (condition 2.2)

$\frac{Y}{d_{MP}} > X > \frac{Y}{r_3[PXY_a]+d_{MP}}$ (condition 2.3)

Furthermore, for $Y > 0$ it was shown that

$\frac{Y}{d_{MP}} > \frac{Y}{d_{MP}+r_3[PXY_a]}$ (inequality 2)

Inequality 2 holds independently of whether condition 1.1 (equivalent to condition 1) is satisfied (provided $Y, d_{MP},\ d_{MP} + r_3[PXY_a] > 0$, as is the case here). Since inequality 2 holds, there exists parameter space where the value of $X = F_a - d_{Aux}$ is such that condition 1 is broken and condition 2 is satisfied (condition 2.3).

The analysis in this section supports the previous numerical results, that the addition of the PXY-MP negative feedback loop to the root system results in a more robust network.

4.4.6.3 Numerical test confirms that the analytical conditions are necessary but not sufficient

Conditions 1 and 2 were checked numerically using the parameter sets generated in section 4.4.2. For the 2,500 parameter sets in the network without the PXY-MP negative feedback loop, all successful parameter sets satisfied condition 1 (Table 6). However, 225 unsuccessful parameter sets also satisfied condition 1. Similarly for the network with the PXY-MP negative feedback loop, all successful parameter sets satisfied condition 2, but 206 unsuccessful parameter sets also satisfied condition 2. Thus, while all successful parameter sets satisfy condition 1 and 2 for their respective networks, some unsuccessful parameters also satisfy condition 1 and 2, suggesting that conditions 1 and 2 are necessary but not sufficient for generating a successful auxin pattern. Thus, while no pattern can be obtained without satisfying conditions 1 and 2, it is not possible to predict if a pattern will be successful by ensuring conditions 1 and 2 are satisfied.

To identify at what stage of the analysis sufficiency is lost, the analysis in Appendix E3 was tested numerically, using the parameter sets generated in section 4.4.2 and their corresponding steady state component concentrations. At each step of the analysis, starting

from equation 1, unsuccessful parameter sets were sought that satisfied condition 1 and 2 at that step of derivation. It was found that sufficiency loss occurred when directly using the relationships $[Aux_c] > [Aux_p]$, likely due to the fact that this is not always a close inequality. Thus, a different relationship N in addition to $[Aux_c] > [Aux_p]$ will be needed to provide sufficiency for both networks. However, the requirement for the two networks to satisfy condition 1 and condition 2 will remain, where condition 2 is still stronger than condition 1. Thus, the fact that the conditions 1 and 2 are necessary but not sufficient does not impact the conclusions made in this section or in sections 4.4.3.

4.5 Discussion

MP and PXY were previously shown to function with auxin in directing cambial activity [72, 73, 120, 154, 155, 157, 159, 175, 183]. However, MP was seen to promote the activity of the cambium in root [72], yet suppress it in stem base [121]. PXY is a cambial promoter [154, 155, 157, 159]. Different relationships between MP and PXY were observed in different plant organs, with MP promoting PXY in root [72] and PXY suppressing MP in stem[120]. Here, it was proposed that the two reactions may coexist in a single tissue, with the balance of interacting factors explaining the contradictory relationship between PXY and MP. Mathematical modelling was used to compare the currently existing network in root with a network which contained a PXY-MP negative feedback loop.

By independently sampling a large number of parameter sets using the Morris method sampling strategy and inputting them into the two networks, it was concluded that the additional feedback loop allows a larger proportion of the sampled parameter sets to produce the auxin pattern observed in nature (an auxin maximum in the cambium) [72]. Moreover, while all parameter sets which produced a successful pattern without a PXY-MP loop, continued to do so when the loop was added, the opposite was not true. There were some parameter sets which, while successful at producing an auxin pattern in the presence of the PXY-MP loop, were no longer able to do so without it. Thus, the network which contained a PXY-MP loop was more robust at producing a correct auxin pattern than its counterpart. This is likely to be the case due to MP's activation of PIN transport. As PXY suppresses MP in the cambium, PIN transport is restricted, allowing more auxin to accumulate in the cambium and produce the correct hormone pattern for cambial division. It can be argued that because the

vascular organizer in roots is marked by both PXY and MP, their presence is not coincidental. Instead, it might be the case that the presence of both MP and PXY is required to assist in auxin accumulation in the cambium [72].

Closed form analysis confirmed that the addition of a PXY-MP loop is *always* beneficial, regardless of the intervals chosen to sample parameters. This suggests a greater flexibility in a biologically-based system which does contain a PXY-MP loop, and thus a biologically preferential mechanism.

Sensitivity analysis of the two networks further revealed a higher influence of the basal degradation rate d_{MP} for auxin accumulation when the loop was absent, but an ability of the PXY-MP loop to abolish d_{MP} sensitivity. Comparing the distributions of the model parameters in the successful parameter sets which did not require the PXY-MP loop, and those that did, d_{MP} was seen to show the most striking trend. In the parameter sets that did not require the PXY-MP negative feedback loop, most d_{MP} values were large. The opposite was true in the parameter sets that required the PXY-MP loop. This suggested that the network without the PXY-MP loop may struggle to produce a pattern when the value for d_{MP} is small. By contrast, the PXY-MP loop loosens this constraint as it provides an additional mechanism for degrading MP (Figure 30 A, B) and overall makes the network more robust. This aligns with earlier observation that the PXY-MP loop appears to desensitize the network to d_{MP} perturbations and that the ability of the network with the PXY-MP loop to more readily generate a pattern is linked to indirectly suppressing PIN active transport.

Upon restricting the d_{MP} range gradually closer to zero, the network with the PXY-MP loop was seen to allow an increasingly higher proportion of parameter sets to produce a pattern compared to its counterpart. Thus, in the case when MP has a low degradation rate, i.e. is particularly stable or particularly abundant, a PXY-MP loop or a similar mechanism is needed to make the network more robust.

These results are meaningful in helping to resolve some of the conflicting data around the PXY-MP relationship (Smetana et al. (2019) [72] and Han et al. (2018) [120]). In particular, the investigation conducted here helps to identify a potential schema within the vascular tissue, wherein one branch of the PXY-MP relationship dominates at different stages to create a balanced system. High auxin maxima in the cambium results in increased MP concentration. Overabundance of MP, however, activates auxin transport out of the cambium, thus exporting auxin out of the cambium and lowering the auxin availability in the cambium. The

lowered availability of auxin does not necessarily resolve MP overabundance, especially if the basal degradation of MP is low. The reduction in auxin in the cambium, caused by MP, reduces divisions in the cambium. The overabundance of MP also boosts *PXY* transcription, *PXY* being a cambial promoter. PXY, in turn, inhibits MP phosphorylation, curbing MP's overabundance and restricting auxin maxima in the cambium.

The hypothesis that a PXY-MP negative feedback loop exists in both stem and root remains to be tested experimentally. To investigate whether a negative feedback loop exists between the *MP* and *PXY* gene, the following experimental designs could be employed. First, *pxy* roots could be grown and tested on their *MP* expression levels relative to wild type. If the hypothesis is true, *MP* expression should be elevated in these tissues. Similarly, roots with *PXY* overexpression should trigger the opposite, reducing *MP* expression levels in root. The presence of a negative feedback loop should also be tested in stem. Thus, to examine whether *MP* is a *PXY* promoter in stem, *PXY* expression levels should be measured in mutants with overexpressed *MP* gene. Provided that *PXY* expression levels are increased, the negative feedback loop will be shown to hold in stem.

Several potential directions for testing loss-of-function *mp* mutants can also be deployed to test whether *mp* mutants show reduced *PXY* expression levels in stems and roots. One option is the loss of the weak *mp-S319* described by Cole et al. (2009) [301]. Silencing of small RNAs is one means of overcoming loss-of-gene lethality [302, 303], however this can be unreliable as only partial reduction in transcription is observed. More sophisticated methods also exist, but they can be complex and difficult to execute (Cre/lox-based clonal deletion system[304-306]; zinc finger nuclease [307]; transcription activator-like effector nuclease-based gene editing systems [308]). More recently developed methodologies include inducible genome editing (IGE) [309], a cross between CRISPR/Cas9 technology [310] and an XVE-based, cell-type-specific inducible system [311, 312].

The model described here is small and answers a predominantly theoretical question. However, as argued in Chapter 1, part 3, there have been many examples of mathematical models in biology that have started from small initial frameworks and expanded through multiple iterations and data collection. Chapter 4 is therefore proposed as first step in modelling PXY-MP interactions and suggests that with more data, it will be possible to explain multiple aspects of this relationship.

4.6 Methods

To understand the behaviour of the system, equations (1)-(10) were solved numerically to steady state in MATLAB. The original numerical solver was written by N. Savage and edited by K. Bagdassarian [313] (GitHub link: https://bit.ly/3g8tFWe [313]). The model is a reaction-diffusion system, the reaction and diffusion part of the model were solved separately. The reaction part of the model was solved using a simple Euler method. The diffusion part of the model is only relevant to cytokinin behaviour and is calculated using a modification of the Euler method where the cytokinin concentration is updated with a diffusion matrix at each time-step. The Euler method and the diffusion matrix derivation are detailed below.

4.6.1 Euler method

4.6.1.1 Overview

The explicit Euler method for solving differential equations was used in this study. For simplicity, the explicit Euler method will be discussed in one dimension. Consider an initial value problem of the form

$$\frac{\mathrm{d}y(t)}{\mathrm{d}t} = f(t, y(t))$$
$$y(t_0) = y_0,$$

where y is a function of t, f is a function of $y(t)$ and t, and y_0 is the value of y at the point t_0.To solve the implicit Euler equation (above) over the time interval $I = [a, b]$, where a, b are real numbers, I is discretized into smaller time sections of size h [314]. Then from time $t = a$ to $t = b$, the method approximates the value of the function $y(t)$ for each of the time points $t = a, t = a + h, t = a + 2h, \ldots . t = b$ as will be detailed below. The smaller the size of h, the more accurate the final approximation. Smaller h results in a larger number of calculations to reach the end of the interval, which increases the required computational power. In this study, $h = 1 \times 10^{-7}$ was used, which, for computational efficiency, is the highest value that can be chosen to ensure accuracy for this model [314].

Let y_n denote the value of the function at time step n, where $n = 0,1,2 \ldots$ is a

sequence in time. Let t_0 be the initial time point at which the function is calculated. Then t_n is such that $t_n = t_0 + nh$. Thus, at time-step t_{n+1} the explicit Euler method is,

$$y_{n+1} = y_n + hf(t_n, y_n).$$

The above formula is applied iteratively until the end of the interval I is reached such that the final time-point is given by $t_{n+1} = b$. An illustrative example is given below. For the initial value problem

$$\frac{\mathrm{d}y(t)}{\mathrm{d}t} = f(t, y(t))$$
$$y(t_0) = y_0,$$

three steps of the explicit Euler will be shown. The first step is given by

$$y_1 = y_0 + hf(t_0, y_0)$$

Next, y_2 is approximated from the above

$$y_2 = y_1 + hf(t_1, y_1)$$

Finally,

$$y_3 = y_2 + hf(t_2, y_2)$$

Thus, after calculating the value of the function at the initial timestep, $y(t_0) = y_0$, the values of the function are approximated at three subsequent time points as y_1, y_2 and y_3.

4.6.2 Diffusion matrix

This section will describe the derivation of the diffusion matrix used to solve the diffusion part of the system (1)-(10). Cytokinin is the only component in the network whose movement is governed by diffusion. The equations describing how the concentration of cytokinin changes over time are given by

$$\frac{\mathrm{d}[CK_c]}{\mathrm{d}t} = D_{ck}\frac{\partial^2[CK_c]}{\partial x^2} - r_1[Aux_c][CK_c] - d_{CK}[CK_c]$$

$$\frac{\mathrm{d}[CK_x]}{\mathrm{d}t} = D_{ck}\frac{\partial^2[CK_x]}{\partial x^2} - r_1[Aux_x][CK_x] - d_{CK}[CK_x]$$

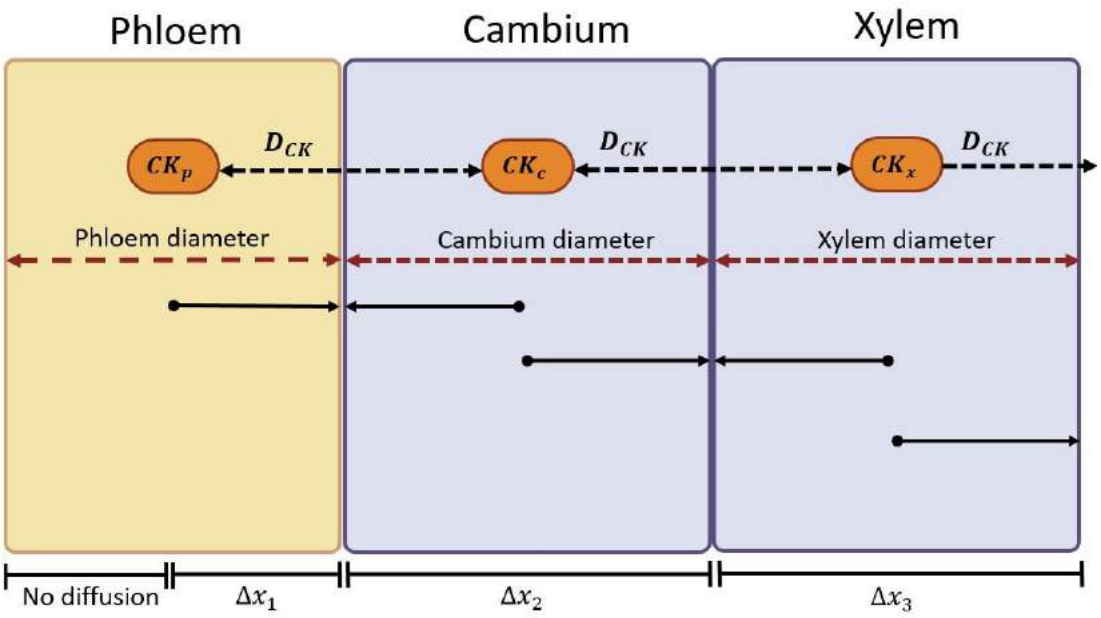

Figure 37: Diagram of distance travelled by diffusion. Red dashed lines indicate diameters of cells. Black arrows indicate directions of diffusion. Distances travelled are denoted by Δx_1, Δx_2 and Δx_3.

Let Δt be the diffusion time increment, while Δx_1, Δx_2 and Δx_3 denote the distances between the centre of the phloem and the centre of the cambium cell, between the centre of the cambium and the xylem cell, and between the centre of the xylem cell and the edge of the system (Figure 37). Distances Δx_1, Δx_2 and Δx_3 are travelled by cytokinin and will be used below in describing how cytokinin concentration is influenced by diffusive movement within each time increment. Diffusion depends on time and space ($D_{CK} = 220\ \mu m^2/s$, the units are area over time). In order to solve the diffusion equation within the model, the diffusion coefficient ($D_{CK} = 220\ \mu m^2/s$) is scaled using Δt and Δx_i such that the resulting new term is dimensionless and the diffusion equation can be solved in each cell

$$Diff_{pc} = D_{ck}\frac{\Delta t}{(\Delta x_1)\text{^}2}$$

$$Diff_{cx} = D_{ck}\frac{\Delta t}{(\Delta x_2)\text{^}2}$$

$$Diff_{x} = D_{ck}\frac{\Delta t}{(\Delta x_3)\text{^}2}.$$

To derive the numerical solution to the diffusion equation within the model, consider each cell individually, accounting for the contributions of cytokinin concentration from neighbouring cells as well as the loss of cytokinin towards neighbouring cells. Recall that, in the model, cytokinin does not diffuse left outside of the phloem (Figure 30; Figure 37) and that the supply of cytokinin in the phloem remains constant, i.e.

$$CK_p^{t+1} = CK_p^t,$$

where the superscript t describes the concentration of cytokinin at time-step t. Consider each cell individually. The concentration of cytokinin in the cambium at time $t+1$ depends on the diffusion of cytokinin at time t out towards the xylem and phloem as well as the input of cytokinin from the same phloem and xylem. This is represented by the following equation:

$$CK_c^{t+1} = CK_c^t + Diff_{pc}CK_p^t - Diff_{pc}CK_c^t + Diff_{cx}CK_x^t - Diff_{cx}CK_c^t.$$

Similarly, as cytokinin from the cambium diffuses towards the xylem, cytokinin in the xylem diffuses out of the three cell structure. Thus, for the change of concentration of cytokinin in the xylem we have

$$CK_x^{t+1} = CK_x^t + Diff_{cx}CK_c^t - Diff_{cx}CK_x^t - Diff_xCK_x^t.$$

Grouping terms and rearranging gives us the following system,

$$CK_p^{t+1} = CK_p^t$$

$$CK_c^{t+1} = Diff_{pc}CK_p^t + (1 - Diff_{pc} - Diff_{cx})CK_c^t + Diff_{cx}CK_x^t$$

$$CK_x^{t+1} = Diff_{cx}CK_c^t + (1 - Diff_{cx} - Diff_x)CK_x^t,$$

which is in matrix form

$$\begin{bmatrix} CK_p(t+1) \\ CK_c(t+1) \\ CK_x(t+1) \end{bmatrix} = \begin{bmatrix} 1 & 0 & 0 \\ Diff_{pc} & 1 - Diff_{pc} - Diff_{cx} & Diff_{cx} \\ 0 & Diff_{cx} & 1 - Diff_{cx} - Diff_x \end{bmatrix} \begin{bmatrix} CK_p(t) \\ CK_c(t) \\ CK_x(t) \end{bmatrix}.$$

Thus, in order to obtain the concentration of cytokinin in all three cells at the next time step $t+1$, the right-hand-side of the above matrix is applied, using the concentration of cytokinin at time t in all three cells.

4.6.3 The Morris method

The code for the Morris method for this study was written by K. Bagdassarian (GitHub https://bit.ly/3g8tFWe [315])

4.6.3.1 Overview

The Morris method consists of individually randomised univariate sensitivity analysis experiments [316-318]. Refer to the total number of model parameters as k. Thus, a vector $\mathbf{x}$ of model parameters has k dimensions, i.e. $\mathbf{x}$ can be represented as $\mathbf{x} = [x_1, x_2, \ldots, x_k]$, where x_i are the individual parameters, for $i = 1, .., k$.

At step 1, the Morris method selects an initial (base) vector of model parameters denoted $\mathbf{x}^* = [x_1^*, x_2^*, \ldots, x_k^*]$. The method by which the base vector is chosen will be described in section 4.6.3.2. Step 2, a parameter from $\mathbf{x}^*$, is selected at random, x_i^*, and its value is changed by an increment $\pm\Delta$, ($\pm\Delta$ is described in section 4.6.3.2) where the sign of Δ is chosen at random with equal probability. The new vector of parameters denoted $\mathbf{x^1}$, is identical to $\mathbf{x}^*$ apart from the parameter in the i-th position, $x_i^* = x_i^* \pm \Delta$. Thus, $\mathbf{x^1} = [x_1^*, x_2^*, \ldots, x_i^* \pm \Delta, \ldots, x_k^*]$. Step 3, a parameter from $\mathbf{x^1}$ is selected at random, x_j^* where $i \neq j$. The value of x_j^* is changed incrementally to give the new parameter vector $\mathbf{x^2} = [x_1^*, x_2^*, \ldots, x_j^* \pm \Delta, \ldots, x_i^* \pm \Delta, \ldots, x_k^*]$. This process continues until all k parameters are incrementally changed exactly once. Thus, the Morris method draws a *trajectory* through the parameter space, where the coordinates of each point differ by exactly 1 parameter from the subsequent point [316-318]. To illustrate, let $k = 3$. Below is one possible trajectory through three dimensional parameter space, in matrix form. Note that each of the rows in the matrix on the right-hand side is a parameter set, representing a point in the parameter space.

$$\begin{bmatrix} \mathbf{x}^* \\ \mathbf{x^1} \\ \mathbf{x^2} \\ \mathbf{x^3} \end{bmatrix} = \begin{pmatrix} x_1 & x_2 & x_3 \\ x_1 & x_2 & x_3 \pm \Delta \\ x_1 \pm \Delta & x_2 & x_3 \pm \Delta \\ x_1 \pm \Delta & x_2 \pm \Delta & x_3 \pm \Delta \end{pmatrix}$$

In this study, the Morris method was applied in section 4.4.4, generating trajectories from a sample of 50 parameter sets for each of the networks with and without the PXY-MP negative feedback loop. Each of the parameter sets generated through these trajectories were used within the model, with the equations solved to steady state and the final corresponding hormone pattern marked as successful or unsuccessful. In what follows, the method for measuring sensitivity employed in this study will be described. Note that this is a modification of the classic Morris method (see: [121, 316-318]) as here total concentration value of the components was not considered, only successful or unsuccessful pattern.

Let $\mathbf{Y}$ denote the output of the model at steady state, i.e. successful or unsuccessful pattern (see: section 4.4.2). $\mathbf{Y}(\mathbf{x^m})$ is the steady state solution of the model using parameter set $\mathbf{x^m} = [x_1, x_2, \dots, x_k]$. In this model, a successful $\mathbf{Y}(\mathbf{x^m}) = \mathbf{1}$, while unsuccessful is $\mathbf{Y}(\mathbf{x^m}) = \mathbf{0}$.

Denote YY the difference in output resulting from a parameter perturbation. In particular, suppose vectors $\mathbf{x^m}$and $\mathbf{x^{m+1}}$ differ in their l-th parameters, with $l \subset [1,2,\dots,k]$. That is, $\mathbf{x^m} = [\dots x_l \dots]$ and $\mathbf{x^m} = [\dots x_l \pm \Delta \dots]$. The outputs of the two simulations would be given by $\mathbf{Y}(\mathbf{x^m})$ and $\mathbf{Y}(\mathbf{x^{m+1}})$. Then YY_l for parameter x_l for this trajectory is defined as

$$YY_l = |\mathbf{Y}(\mathbf{x^{m+1}}) - \mathbf{Y}(\mathbf{x^m})|$$

The straight brackets, on the right-hand side, refer to the positive value of the expression inside them. Here, an illustrative example will be given to show how measurements of sensitivity are taken. Consider a perturbation $\pm\Delta$ in the parameter set $\mathbf{x^m}$ which results in a new parameter set $\mathbf{x^{m+1}}$. The two outcomes of the parameter sets $\mathbf{x^m}$ and $\mathbf{x^{m+1}}$ are given by $\mathbf{Y}(\mathbf{x^m})$ and $\mathbf{Y}(\mathbf{x^{m+1}})$. If the parameter set $\mathbf{x^m}$ was successful, then $\mathbf{Y}(\mathbf{x^m}) = 1$. If $\mathbf{x^{m+1}}$, the parameter set resulting from the perturbation $\pm\Delta$ in the parameter set $\mathbf{x^m}$, is unsuccessful, then $\mathbf{Y}(\mathbf{x^{m+1}}) = 0$. The difference in output between the two parameter sets

$\mathbf{x^m}$ and $\mathbf{x^{m+1}}$ would be given by $YY_l = \left|\mathbf{Y}(\mathbf{x^{m+1}}) - \mathbf{Y}(\mathbf{x^m})\right| = |\mathbf{0} - \mathbf{1}| = 1$. Thus, the resulting measurement of sensitivity has value 1.

By generating r trajectories ($r = 50$ in this study, see section 4.4.4), the measures of sensitivity for parameter are then summed. That is, for the above parameter x_l, and for trajectories $n = 1,2,\ldots r$, the measure of sensitivity for parameter $x_l$would be given by

$$\mu_l = \sum_{n=1}^{r} YY_l^n$$

The larger the μ of a parameter, the larger the impact of that parameter on the network, the more sensitive the network is to perturbations in that parameter. By arranging μ of all parameters by size, a ranking of the parameters in terms of importance for the output is obtained, with rank 1 (largest value) indicating the parameter that the model is most sensitive to, and rank k corresponding to the parameter that the model is least sensitive to.

4.6.3.2 Sampling for Morris

Here, the method for choosing the base parameter set, x^*, will be described. The user must define the intervals within which parameter values will be chosen. Define a general interval $[a, b]$ where a, b are real numbers ($a, b \subseteq \mathbb{R}$). The Morris method samples parameter values from a finite set of numbers within the defined parameter intervals. The finite sets of parameters are generated by dividing the intervals into equal sections, creating p equally spaces parameter values within the intervals and $p - 1$ number of intervals. Thus, the user must also define p (termed the number of Morris levels), where p is a natural number ($p \subseteq \mathbb{N}$). Hence, the base vector is sampled from the set $\left\{a,\ a + \frac{(b-a)}{(p-1)}, a + \frac{2(b-a)}{(p-1)}, \ldots, a + \frac{(p-2)(b-a)}{(p-1)},\ b\right\}$. Denote the space between parameter values as Δ, $\Delta = \frac{(b-a)}{(p-1)}$. The larger the value of p (number of possible points to be sampled), the smaller Δ , and the closer parameter values will be within each interval. In one run of the Morris method, each parameter value is changed, in turn, by $\pm\,\Delta$. This means that for large p a smaller amount of parameter space will be explored during one Morris run .

To generate the base vector, the probability of choosing any of the interior values from the finite set of parameter values, $\left\{ a + \frac{(b-a)}{(p-1)}, a + \frac{2(b-a)}{(p-1)}, \ldots, a + \frac{(p-2)(b-a)}{(p-1)} \right\}$, is set to $(b - a)/(p - 1)$, whereas the probability of choosing the end-values (a and b) is set to $(b - a)/2(p - 1)$. This is the case as the end-points a and b have only 1 neighbour in their interval, forcing the sign of the perturbation to be $+\Delta$ and $-\Delta$, respectively. Interior points have 2 neighbouring points that can be reached with equal probability with perturbations $\pm\Delta$. Thus, to avoid over-exploring the neighbours of a and b, the probability choosing a and b is halved [316-318].

Chapter 5: Discussion

Plant development is a complex process, whose understanding is of growing importance for biodiversity, sustainability and agriculture. However, the mechanisms underlying the highly coordinated process of radial thickening and thereby the production of the majority of the plant biomass, are still not well understood. In this thesis, I employed a cross-disciplinary approach to studying the receptor-kinase PXY, one of the key actors in cell proliferation and vascular tissue organisation during secondary growth.

The goal of this thesis was to understand how PXY organizes the vascular tissue layers and drives cell division together with other components and hormone signals. To address this, two distinct approaches were used. First, a bespoke method was developed to quantify cell variation across different genotypes. This method was used to examine the relationship between the *PXY* and *ER* family of genes in the context of morphological changes caused by mutations. Second, a mathematical framework was designed to test PXY's interaction with MP in the context of hormone patterning. Both of these investigations were able to tackle different aspects of PXY's role for secondary growth.

The method described in Chapter 2 represents a purpose-built tool chosen to allow the study of highly irregular mutant phenotypes. Outside the field of biology, the protocol can be easily adapted to other questions by introducing small changes in the code. The use of such techniques alongside subjective phenotypical assessment of anatomical and other images enhances our understanding of morphological changes and visualizes trends much more clearly. As shown in Chapter 3, using this method on sampled cells from different mutants allowed to unravel subtle differences in how the individual genes from the *ER* and *PXY* families regulate morphology. For example, cell size data distinctly showed that in hypocotyl, the larger cell size of *px*F and *px*F *er* mutants was not maintained with additional *erl* mutations (Figure 19), implicating *ERL1* and *ERL2* as the genes behind the increase. Using the same technique, I was able to rule out cell deformation as a morphological property of any of the mutants, through measuring ellipticity of the cells and finding no differences across the genotypes (Figure 20). Together with the data of hypocotyl radial size, I demonstrated that *ERL2* was the gene critical to maintaining hypocotyl size.

Another interesting result of the study was the distinction between *PX*f-*ER*f interaction in regulating different plant organs during secondary growth. In particular, while *ER*f was seen to promote cell size expansion in hypocotyl, the opposite was observed in stem (Figure 19; Figure 22). One explanation is that an underlying network that is activated under different developmental regimes, and determining the components of such network and the corresponding developmental regimes could be addressed in future study. Indeed, further look into components linked to *PX*f and *ER*f could provide essential insight into what allows plants to enlarge and produce xylem/woody tissues. For example, as the MOL1 pathway is broadly unexplored but points to an opposing function to that of *PXY* (i.e. MOL1 being a cambial inhibitor), it would be interesting to examine how the *ER*f may interact with MOL1 and its yet undiscovered ligand [175]. The final result of the study, that loss of *PX*f and *ER*f genes wholly suspends secondary growth, points to an interruption in the key genetic networks responsible for radial expansion, and thus the process of plant body growth. This discovery is truly striking and poses the question: do the two genetic pathways balance the process of secondary growth induction, with *ER*f stabilizing growth in the absence of *PX*f but repressing it otherwise? More research will be needed to answer such questions.

The method described in Chapter 2, has some limitations. While the selection of objects with identical or close in range colour scheme can be done automatically within the code, this is not possible when such requirements are not fulfilled. As a result, the sampling of cells described in this thesis was performed manually, which can be time consuming. To overcome this limitation, changes beyond the timescale allowed for this PhD thesis would have to be conducted. To be able to direct the programme in selecting objects, a number of details would need to be known a priori, such as conditions of proximity or probability of emergence in certain locations in the plant. One possible direction for further development of the code could then be the possibility of employing a detailed conditions schema to be adjusted as required at the start of the programme. A number of sliders could be made available corresponding to features of plant mutants. Using experimentally obtained images as input, the user would be able to perform trial and error adjustments to the images in real time in order to identify when the sampling is optimal. Another possibility would be building a coherent and well-organized database of images of known mutants and imposing a probabilistic machine learning algorithm to automate sampling for related genes. The latter

option requires a substantial initial time investment and the collection of high quality experimental images. Nevertheless, obtaining a dataset of this type would be invaluable to unravelling complex genetic interactions in future studies.

In addition to ER, auxin has also been reported to cross-talk with PXY signalling. One point of convergence between these two signalling mechanisms is represented by a potential PXY-MP feedback loop to robustify auxin pattern. It was argued that such mechanism could explain the contradictory findings of PXY and MP's relationship (MP is reported to be both promoter and repressor of cambial cell division [72, 120, 121]). It is possible that overabundance of MP caused by auxin accumulation drives auxin out of the cambium, thus inhibiting cell divisions. Overabundance of MP, however, results in MP-driven increase in *PXY* transcription. Once activated by TDIF, PXY then inhibits additional MP phosphorylation through BIL1, slowing down the accumulation of MP and allowing it to degrade. Auxin accumulation is thus restored and cambial activity is promoted. The fact PXY and MP expression overlaps with auxin maxima in the cambium [72] to promote cell division points to other future possibilities that impinge on the results from Chapter 3 in this thesis. It would be interesting to establish whether an auxin peak in the cambium is lacking, limited or displaced in *pxy* mutants and thus loss of vascular organisation in such plants is the result of reduced ability to retain auxin in the cambium. If this is indeed the case, worsening of the *pxy* phenotype under the additional loss of the paralogues *PXL1* and *PXL2* could be related to a further decrease in the ability of auxin to accumulate, such that perhaps when removed alone, *pxl1 pxl2* mutants do not produce a noticeable change, but elimination of all 3 genes generates an augmented effect. It would therefore be even more beneficial to examine auxin patterning in a range of *px*F mutants, and indeed *px*F *er*F mutants, to unravel whether auxin levels may lie in the core of the extremely drastic *px*F *er*F phenotype.

Two types of follow-up research can be outlined for the work conducted in Chapter 4: experimental, and mathematical. The model proposed in Chapter 4 still remains to be tested experimentally. Due to time constraints, this was not possible during the course of my PhD. As discussed in section 4.5, one set of experiments involves examining the presence of a PXY-MP negative feedback loop in stem and hypocotyl by testing for the reaction from the loop not found in each organ. This would involve, firstly, to study the effects of *pxy* mutation on *MP* expression in roots – expecting *MP* levels to be elevated. Secondly, overexpressing *PXY* to

check if *MP* expression is reduced in root. Third, studying *MP* overexpression in stems for an increase in *PXY* expression. More complex techniques [301-312] can allow for testing loss-of-function *mp* roots and stems for decreased *PXY* expression.

Another set of possible experimental directions should involve testing hypocotyls for the existence of a PXY-MP negative feedback loop. *PXY* expression was shown to mark the xylem side of the cambium in hypocotyls, and to be responsible for the bidirectional property of the cambium in hypocotyl in Shi et al. (2019) [73]. In Han et al. (2018), *MP* was shown to be promoted by BIL1 in both stem and hypocotyl [120]. PXY was shown to directly interact with BIL1 on the plasma membrane [91] and to inhibit BIL1 in stem [120]. PXY's interaction with BIL1 in hypocotyl, however, has not been tested. Investigating PXY and BIL1's interaction in hypocotyl could suggest a possible expansion of the PXY-MP negative feedback loop hypothesis to incorporate all three of stem, hypocotyl and root. In particular, *BIL1* expression levels should be tested in *pxy* hypocotyls and PXY overexpression hypocotyls, expecting them to respectively increase in the former and decrease in the latter.

The second direction for improving the work done in Chapter 4 involves mathematical investigations. As mentioned in Chapter 4, while it was possible to analytically derive necessary conditions for the two networks to pattern, conditions that were sufficient were not found. Resolving this issue will allow to understand what relationships between parameters are required to ensure accurate hormone pattern.

A second mathematical experiment that could not be conducted due to time limitations involved expanding on the use of the Morris method. As discussed in Chapter 4, both the network with the PXY-MP loop and the one without the loop showed to be relatively robust to single perturbations. Parameter sets that were shown to produce a pattern or not to produce a pattern, generally remained in that state under single perturbations. This posed the question as to how many random perturbations would be needed to force a parameter set to cease to produce a successful pattern. Since the network with the PXY-MP loop was seen to be more robust at generating pattern, it was suggested that this network may be more stable under long-term perturbations. To conduct this experiment, both networks will need to be examined. A sample of parameter sets with maximal spread will be chosen from the successful parameter sets obtained for the network with and without the PXY-MP negative feedback loop. Perturbations are then to be ran for each of these parameter sets

until the parameter set became unsuccessful. The number of perturbation steps required would be recorded for both networks, and compared.

One limitation of the model includes the well-mixed assumption. PIN localization, specifically, was not considered in the theoretical model discussed in this thesis. The summative PIN which lacked positioning somewhat restricted the ability to observe the details of auxin transport under the influence of PXY and MP interactions. This limitation could be addressed in later iterations of the model and in a larger cell template to provide better comprehension of auxin distribution. For instance, if the PXY-MP loop is shown to exist in nature, it will be interesting to specify how auxin distribution, particularly an auxin peak, could be influenced by manipulating the MP-PXY relationship. A tool for achieving this could involve the incorporation of the software *VirtualLeaf* [238] (discussed in Chapter 1). *VirtualLeaf* is capable of simulating a growing cell template. This could be an excellent way to overcome the lack of definitive parameters in the model by calibrating the output to experimentally obtained wild type and mutant phenotypes. Once this is achieved, such a model could be used to examine the cambium-localised auxin maxima and PXY-MP interactions, as well as point to the discovery of other possible components to the network. Furthermore, the use of *VirtualLeaf* [238] with the data acquired from Chapter 2 and 3 on *px*F *er*F phenotypical data can be collated into a uniform investigation of cross-tissue communication and hormone pattern. In particular, the components described in this thesis – the members of the PXY and ER family, MP and auxin can be incorporated into a singular special structure. Experimental data on auxin distribution across *px*F, *px*F *er*, *px*F *er erl*1, *px*F *er erl*2 and *px*F *er*F mutats can be studied in combination with the data described in this thesis (Chapter 2 and 3) of these mutant's morphology. A *VirtualLeaf*-based [238] model calibrated in this way could allow the study of the regulators of auxin distribution. By callibrating the data to real life phenotypes and component expression, it could be possible to identify additional components whose role may provide a sufficiency condition for the correct auxin pattern.

Concluding remarks

In this thesis, I have engaged with understanding the underlying components that govern the establishment and maintenance of vascular tissue during secondary growth. The

focus of my investigation was the receptor-kinase PXY and its interaction with other regulators to define the division plane and boost cambial activity. I used a multi-disciplinary approach to conduct my research, including the development of a bespoke method for analysing cell morphology. Using this method, I showed that the *PXY* family of genes interacts with the *ER* family of genes for vascular development in an organ-distinct manner, and loss of both suspends transition into secondary growth. In the final part of my thesis, another role for PXY was investigated – in boosting the accumulation of the hormone auxin in the cambium in order to promote cell divisions. This was tested through defining a three cell reaction-diffusion model and evaluating its ability to produce hormone pattern through the template, concluding a PXY-MP negative feedback loop could promote auxin maxima in the cambium. Much yet remains to be unravelled. Through the work conducted here I have proposed several ideas for addressing knowledge gaps in our understanding of the field, and future theoretical and methodological development of these ideas should give a much fuller insight into the mechanisms controlling secondary growth.

1. Ragni, L. and T. Greb. *Secondary growth as a determinant of plant shape and form*. in *Seminars in Cell & Developmental Biology*. 2018. Elsevier.
2. Bagdassarian, K.S., et al., *Connections in the cambium, receptors in the ring.* Current Opinion in Plant Biology, 2020. **57**: p. 96-103.
3. Wang, N., et al., *Organ-specific genetic interactions between paralogues of the PXY and ER receptor kinases enforce radial patterning in Arabidopsis vascular tissue.* Development, 2019. **146**(10): p. dev177105.
4. Turner-Skoff, J.B. and N. Cavender, *The benefits of trees for livable and sustainable communities.* Plants, People, Planet, 2019. **1**(4): p. 323-335.
5. Fargione, J.E. and D. Tilman, *Diversity decreases invasion via both sampling and complementarity effects.* Ecology Letters, 2005. **8**(6): p. 604-611.
6. Tilman, D., *The ecological consequences of changes in biodiversity: a search for general principles.* Ecology, 1999. **80**(5): p. 1455-1474.
7. Clark, K.H. and K.A. Nicholas, *Introducing urban food forestry: a multifunctional approach to increase food security and provide ecosystem services.* Landscape Ecology, 2013. **28**(9): p. 1649-1669.
8. Wall, E. and B. Smit, *Climate change adaptation in light of sustainable agriculture.* Journal of sustainable agriculture, 2005. **27**(1): p. 113-123.
9. Stanton, R.A., *A plant-based diet—good for us and for the planet.* Medical Journal of Australia, 2012. **9**: p. 5.

10. Cervantes-Godoy, D. and J. Dewbre, *Economic importance of agriculture for poverty reduction.* 2010.
11. Jones, A.D. and G. Ejeta, *A new global agenda for nutrition and health: the importance of agriculture and food systems.* Bulletin of the World Health Organization, 2016. **94**(3): p. 228.
12. Kennedy, T.A., et al., *Biodiversity as a barrier to ecological invasion.* Nature, 2002. **417**(6889): p. 636-638.
13. Yuan, J.S., et al., *Plants to power: bioenergy to fuel the future.* Trends in plant science, 2008. **13**(8): p. 421-429.
14. Vogel, K.P. and H.-J.G. Jung, *Genetic modification of herbaceous plants for feed and fuel.* Critical Reviews in Plant Sciences, 2001. **20**(1): p. 15-49.
15. Ballard-Tremeer, G. and H. Jawurek, *Comparison of five rural, wood-burning cooking devices: efficiencies and emissions.* Biomass and Bioenergy, 1996. **11**(5): p. 419-430.
16. Garrity, D.P., *Agroforestry and the achievement of the Millennium Development Goals.* Agroforestry systems, 2004. **61**(1): p. 5-17.
17. Jamnadass, R., et al., *Agroforestry, food and nutritional security.* 2013.
18. Fowler, M.W., *Plants, medicines and man.* Journal of the Science of Food and Agriculture, 2006. **86**(12): p. 1797-1804.
19. Farnsworth, N.R., *Screening plants for new medicines.* Biodiversity, 1988. **15**(3): p. 81-99.
20. Gossell-Williams, M., R. Simon, and M. West, *The past and present use of plants for medicines.* West Indian Med J, 2006. **55**(4): p. 217-218.
21. Verpoorte, R., H. Kim, and Y. Choi, *Plants as source for medicines: New perspectives.* Frontis, 2006: p. 261-273.
22. Agosta, W.C., *Medicines and drugs from plants.* Journal of chemical education, 1997. **74**(7): p. 857.
23. Keenan, T.J., *How trees are converted into paper.* Scientific American, 1913. **109**(14): p. 256-258.
24. Stockwell, P. and F. Richter, *Hybrid forest trees.* Yearb. Agr, 1943.
25. Campinhos, E., *Sustainable plantations of high-yield shape Eucalyptus trees for production of fiber: the Aracruz case.* New Forests, 1999. **17**(1): p. 129-143.
26. Gordon, S. and Y.-l. Hsieh, *Cotton: Science and technology*. 2006: Woodhead Publishing.
27. Bullard, S.H., *Furniture Production and the Forest Resources of Southwest Mississippi.* 1989.
28. Ratanawilai, T., T. Chumthong, and S. Kirdkong, *An investigation on the mechanical properties of trunks of palm oil trees for the furniture industry.* Journal of Oil Palm Research, 2006. **18**: p. 114-121.
29. Xing, Y. and P. Brimblecombe, *Trees and parks as "the lungs of cities".* Urban Forestry & Urban Greening, 2020. **48**: p. 126552.
30. Howell, A.J., H.-A. Passmore, and K. Buro, *Meaning in nature: Meaning in life as a mediator of the relationship between nature connectedness and well-being.* Journal of Happiness Studies, 2013. **14**(6): p. 1681-1696.
31. Houlden, V., et al., *The relationship between greenspace and the mental wellbeing of adults: A systematic review.* PloS one, 2018. **13**(9): p. e0203000.
32. Akbari, H., *Shade trees reduce building energy use and CO2 emissions from power plants.* Environmental pollution, 2002. **116**: p. S119-S126.

33. Pan, Y., et al., *A large and persistent carbon sink in the world's forests.* Science, 2011. **333**(6045): p. 988-993.
34. Luyssaert, S., et al., *Old-growth forests as global carbon sinks.* Nature, 2008. **455**(7210): p. 213-215.
35. Reichstein, M., et al., *Climate extremes and the carbon cycle.* Nature, 2013. **500**(7462): p. 287-295.
36. Verduin, J. and W. Loomis, *Absorption of carbon dioxide by maize.* Plant physiology, 1944. **19**(2): p. 278.
37. Siah, W., A. Aminah, and A. Ishak, *Edible films from seaweed (Kappaphycus alvarezii).* International Food Research Journal, 2015. **22**(6): p. 2230.
38. Mooney, B.P., *The second green revolution? Production of plant-based biodegradable plastics.* Biochemical Journal, 2009. **418**(2): p. 219-232.
39. Tadesse, A., *Increasing crop production through improved plant protection*. 2008, Plant Protection Society Of Ethiopia (PPSE).
40. Bassham, J.A., *Increasing crop production through more controlled photosynthesis.* Science, 1977. **197**(4304): p. 630-638.
41. Gómez, C. and L.G. Izzo, *Increasing efficiency of crop production with LEDs.* AIMS Agriculture and Food, 2018. **3**(2): p. 135-153.
42. Cakmak, I., *Potassium for better crop production and quality*. 2010, Springer.
43. Esau, K., *Anatomy of seed plants.* Soil Science, 1960. **90**(2): p. 149.
44. Evert, R.F., *Esau's plant anatomy: meristems, cells, and tissues of the plant body: their structure, function, and development*. 2006: John Wiley & Sons.
45. Esau, K., *Vascular differentiation in plants*. 1965.
46. De Rybel, B., et al., *A bHLH complex controls embryonic vascular tissue establishment and indeterminate growth in Arabidopsis.* Developmental cell, 2013. **24**(4): p. 426-437.
47. Scheres, B., et al., *Embryonic origin of the Arabidopsis primary root and root meristem initials.* Development, 1994. **120**(9): p. 2475-2487.
48. Dolan, L. and K. Roberts, *Secondary thickening in roots of Arabidopsis thaliana: anatomy and cell surface changes.* New Phytologist, 1995. **131**(1): p. 121-128.
49. Chaffey, N., et al., *Secondary xylem development in Arabidopsis: a model for wood formation.* Physiologia plantarum, 2002. **114**(4): p. 594-600.
50. Dolan, L., et al., *Cellular organisation of the Arabidopsis thaliana root.* Development, 1993. **119**(1): p. 71-84.
51. Bauby, H., et al., *Protophloem differentiation in early Arabidopsis thaliana development.* Plant and cell physiology, 2007. **48**(1): p. 97-109.
52. De Rybel, B., et al., *Integration of growth and patterning during vascular tissue formation in Arabidopsis.* Science, 2014. **345**(6197): p. 1255215.
53. Miyashima, S., et al., *Stem cell function during plant vascular development.* The EMBO journal, 2013. **32**(2): p. 178-193.
54. Jouannet, V., K. Brackmann, and T. Greb, *(Pro) cambium formation and proliferation: two sides of the same coin?* Current opinion in plant biology, 2015. **23**: p. 54-60.
55. Ikematsu, S., et al., *ERECTA-family receptor kinase genes redundantly prevent premature progression of secondary growth in the Arabidopsis hypocotyl.* New Phytologist, 2017. **213**(4): p. 1697-1709.

56. Lehmann, F. and C.S. Hardtke, *Secondary growth of the Arabidopsis hypocotyl—vascular development in dimensions.* Current opinion in plant biology, 2016. **29**: p. 9-15.
57. Sankar, M., et al., *Automated quantitative histology reveals vascular morphodynamics during Arabidopsis hypocotyl secondary growth.* Elife, 2014. **3**: p. e01567.
58. Ragni, L. and C.S. Hardtke, *Small but thick enough–the Arabidopsis hypocotyl as a model to study secondary growth.* Physiologia plantarum, 2014. **151**(2): p. 164-171.
59. Altamura, M.M., et al., *Development of the vascular system in the inflorescence stem of Arabidopsis.* New Phytologist, 2001. **151**(2): p. 381-389.
60. Nieminen, K., et al., *Vascular cambium development.* The Arabidopsis book/American Society of Plant Biologists, 2015. **13**.
61. Campbell, L. and S. Turner, *Regulation of vascular cell division.* Journal of experimental botany, 2017. **68**(1): p. 27-43.
62. Fischer, U., et al., *The dynamics of cambial stem cell activity.* Annual review of plant biology, 2019. **70**: p. 293-319.
63. Hellmann, E., et al., *Plant vascular tissues—Connecting tissue comes in all shapes.* Plants, 2018. **7**(4): p. 109.
64. Ruonala, R., D. Ko, and Y. Helariutta, *Genetic networks in plant vascular development.* Annual review of genetics, 2017. **51**: p. 335-359.
65. De Rybel, B., et al., *Plant vascular development: from early specification to differentiation.* Nature reviews Molecular cell biology, 2016. **17**(1): p. 30.
66. Bailey, I.W., *Evolution of the tracheary tissue of land plants.* American Journal of Botany, 1953. **40**(1): p. 4-8.
67. Jung, J.-H., et al., *Molecular mechanisms underlying vascular development.* Advances in Botanical Research, 2008. **48**: p. 1-68.
68. Cutter, E.G., *Plant anatomy. Part I. Cells and tissues*. 1978: Edward Arnold London.
69. Cutler, D., *Plant Anatomy: Experiment and Interpretation. Part 2. Organs*. 1972, JSTOR.
70. Siebers, A., *Initiation of radial polarity in the interfascicular cambium of Ricinus communis L.* Acta Botanica Neerlandica, 1971. **20**(2): p. 211-220.
71. Thair, B.W. and T. Steeves, *Response of the vascular cambium to reorientation in patch grafts.* Canadian Journal of Botany, 1976. **54**(3-4): p. 361-373.
72. Smetana, O., et al., *High levels of auxin signalling define the stem-cell organizer of the vascular cambium.* Nature, 2019. **565**(7740): p. 485-489.
73. Shi, D., et al., *Bifacial cambium stem cells generate xylem and phloem during radial plant growth.* Development, 2019. **146**(1).
74. Crang, R., S. Lyons-Sobaski, and R. Wise, *Plant anatomy: a concept-based approach to the structure of seed plants*. 2018: Springer.
75. Wang, N., et al., *Organ-specific genetic interactions between paralogues of the PXY and ER receptor kinases enforce radial patterning in Arabidopsis vascular tissue.* Development, 2019. **146**(10).
76. Robert, H.S. and J. Friml, *Auxin and other signals on the move in plants.* Nature chemical biology, 2009. **5**(5): p. 325-332.
77. Hoad, G., *Transport of hormones in the phloem of higher plants.* Plant Growth Regulation, 1995. **16**(2): p. 173-182.

78. Swarup, R., et al., *Localization of the auxin permease AUX1 suggests two functionally distinct hormone transport pathways operate in the Arabidopsis root apex.* Genes & development, 2001. **15**(20): p. 2648-2653.
79. Hirose, N., et al., *Regulation of cytokinin biosynthesis, compartmentalization and translocation.* Journal of experimental botany, 2008. **59**(1): p. 75-83.
80. Bishopp, A., et al., *A mutually inhibitory interaction between auxin and cytokinin specifies vascular pattern in roots.* Current Biology, 2011. **21**(11): p. 917-926.
81. Kudo, T., T. Kiba, and H. Sakakibara, *Metabolism and long-distance translocation of cytokinins.* Journal of Integrative Plant Biology, 2010. **52**(1): p. 53-60.
82. Muraro, D., et al., *Integration of hormonal signaling networks and mobile microRNAs is required for vascular patterning in Arabidopsis roots.* Proceedings of the National Academy of Sciences, 2014. **111**(2): p. 857-862.
83. Lavender, D., et al., *Spring shoot growth in Douglas-fir may be initiated by gibberellins exported from the roots.* Science, 1973. **182**(4114): p. 838-839.
84. Hoad, G. and M. Bowen, *Evidence for gibberellin-like substances in phloem exudate of higher plants.* Planta, 1968. **82**(1): p. 22-32.
85. Israelsson, M., B. Sundberg, and T. Moritz, *Tissue-specific localization of gibberellins and expression of gibberellin-biosynthetic and signaling genes in wood-forming tissues in aspen.* The Plant Journal, 2005. **44**(3): p. 494-504.
86. Everant-Bourbouloux, A., *Transport and metabolism of labelled abscisic acid in broad-bean plants (Vicia faba L.).* Physiologia Plantarum, 1982. **54**(4): p. 431-439.
87. Ikegami, K., et al., *Activation of abscisic acid biosynthesis in the leaves of Arabidopsis thaliana in response to water deficit.* Journal of plant research, 2009. **122**(2): p. 235.
88. Jiang, F. and W. Hartung, *Long-distance signalling of abscisic acid (ABA): the factors regulating the intensity of the ABA signal.* Journal of experimental botany, 2008. **59**(1): p. 37-43.
89. Zeevaart, J.A. and G.L. Boyer, *Accumulation and transport of abscisic acid and its metabolites in Ricinus and Xanthium.* Plant Physiology, 1984. **74**(4): p. 934-939.
90. Brodersen, C.R., et al., *Functional status of xylem through time.* Annual review of plant biology, 2019. **70**: p. 407-433.
91. Kondo, Y., et al., *Plant GSK3 proteins regulate xylem cell differentiation downstream of TDIF–TDR signalling.* Nature communications, 2014. **5**(1): p. 1-11.
92. Růžička, K., et al., *Xylem development–from the cradle to the grave.* New Phytologist, 2015. **207**(3): p. 519-535.
93. Anne, P. and C.S. Hardtke, *Phloem function and development—biophysics meets genetics.* Current opinion in plant biology, 2018. **43**: p. 22-28.
94. Blob, B., J.-o. Heo, and Y. Helariutta, *Phloem differentiation: an integrative model for cell specification.* Journal of plant research, 2018. **131**(1): p. 31-36.
95. Heo, J.o., et al., *Phloem development: current knowledge and future perspectives.* American journal of botany, 2014. **101**(9): p. 1393-1402.
96. López-Salmerón, V., et al., *The phloem as a mediator of plant growth plasticity.* Current Biology, 2019. **29**(5): p. R173-R181.
97. Otero, S. and Y. Helariutta, *Companion cells: a diamond in the rough.* Journal of experimental botany, 2016: p. erw392.
98. Love, J., et al., *Ethylene is an endogenous stimulator of cell division in the cambial meristem of Populus.* Proceedings of the National Academy of Sciences, 2009. **106**(14): p. 5984-5989.

99. Sehr, E.M., et al., *Analysis of secondary growth in the Arabidopsis shoot reveals a positive role of jasmonate signalling in cambium formation.* The Plant Journal, 2010. **63**(5): p. 811-822.
100. Agusti, J., et al., *Characterization of transcriptome remodeling during cambium formation identifies MOL1 and RUL1 as opposing regulators of secondary growth.* PLoS genetics, 2011. **7**(2).
101. Gray, W.M., et al., *Identification of an SCF ubiquitin–ligase complex required for auxin response in Arabidopsis thaliana.* Genes & development, 1999. **13**(13): p. 1678-1691.
102. Gray, W.M., et al., *Auxin regulates SCF TIR1-dependent degradation of AUX/IAA proteins.* Nature, 2001. **414**(6861): p. 271-276.
103. Kieffer, M., J. Neve, and S. Kepinski, *Defining auxin response contexts in plant development.* Current opinion in plant biology, 2010. **13**(1): p. 12-20.
104. Mockaitis, K. and M. Estelle, *Auxin receptors and plant development: a new signaling paradigm.* Annual review of cell and developmental biology, 2008. **24**.
105. Ulmasov, T., G. Hagen, and T.J. Guilfoyle, *ARF1, a transcription factor that binds to auxin response elements.* Science, 1997. **276**(5320): p. 1865-1868.
106. Ulmasov, T., G. Hagen, and T.J. Guilfoyle, *Activation and repression of transcription by auxin-response factors.* Proceedings of the National Academy of Sciences, 1999. **96**(10): p. 5844-5849.
107. Benjamins, R. and B. Scheres, *Auxin: the looping star in plant development.* Annu. Rev. Plant Biol., 2008. **59**: p. 443-465.
108. Guilfoyle, T.J. and G. Hagen, *Auxin response factors.* Current opinion in plant biology, 2007. **10**(5): p. 453-460.
109. Weijers, D., et al., *Auxin triggers transient local signaling for cell specification in Arabidopsis embryogenesis.* Developmental cell, 2006. **10**(2): p. 265-270.
110. Calderon-Villalobos, L.I., et al., *Auxin perception—structural insights.* Cold Spring Harbor perspectives in biology, 2010. **2**(7): p. a005546.
111. Dharmasiri, N., S. Dharmasiri, and M. Estelle, *The F-box protein TIR1 is an auxin receptor.* Nature, 2005. **435**(7041): p. 441-445.
112. Villalobos, L.I.A.C., et al., *A combinatorial TIR1/AFB–Aux/IAA co-receptor system for differential sensing of auxin.* Nature chemical biology, 2012. **8**(5): p. 477-485.
113. Kepinski, S. and O. Leyser, *The Arabidopsis F-box protein TIR1 is an auxin receptor.* Nature, 2005. **435**(7041): p. 446-451.
114. Hardtke, C.S. and T. Berleth, *The Arabidopsis gene MONOPTEROS encodes a transcription factor mediating embryo axis formation and vascular development.* The EMBO journal, 1998. **17**(5): p. 1405-1411.
115. Berleth, T. and G. Jurgens, *The role of the monopteros gene in organising the basal body region of the Arabidopsis embryo.* Development, 1993. **118**(2): p. 575-587.
116. Bhatia, N., et al., *Auxin acts through MONOPTEROS to regulate plant cell polarity and pattern phyllotaxis.* Current Biology, 2016. **26**(23): p. 3202-3208.
117. Przemeck, G.K., et al., *Studies on the role of the Arabidopsis gene MONOPTEROS in vascular development and plant cell axialization.* Planta, 1996. **200**(2): p. 229-237.
118. Wenzel, C.L., et al., *Dynamics of MONOPTEROS and PIN-FORMED1 expression during leaf vein pattern formation in Arabidopsis thaliana.* The Plant Journal, 2007. **49**(3): p. 387-398.

119. Krogan, N.T., et al., *The auxin response factor MONOPTEROS controls meristem function and organogenesis in both the shoot and root through the direct regulation of PIN genes.* New Phytologist, 2016. **212**(1): p. 42-50.
120. Han, S., et al., *BIL1-mediated MP phosphorylation integrates PXY and cytokinin signalling in secondary growth.* Nature plants, 2018. **4**(8): p. 605-614.
121. Brackmann, K., et al., *Spatial specificity of auxin responses coordinates wood formation.* Nature communications, 2018. **9**(1): p. 1-15.
122. Matsumoto-Kitano, M., et al., *Cytokinins are central regulators of cambial activity.* Proceedings of the National Academy of Sciences, 2008. **105**(50): p. 20027-20031.
123. Hejátko, J., et al., *The Histidine Kinases CYTOKININ-INDEPENDENT1 and ARABIDOPSIS HISTIDINE KINASE2 and 3 Regulate Vascular Tissue Development in Arabidopsis Shoots.* The Plant Cell, 2009. **21**(7): p. 2008-2021.
124. Kieber, J.J. and G.E. Schaller, *The perception of cytokinin: a story 50 years in the making.* Plant physiology, 2010. **154**(2): p. 487-492.
125. Inoue, T., et al., *Identification of CRE1 as a cytokinin receptor from Arabidopsis.* Nature, 2001. **409**(6823): p. 1060-1063.
126. Nishimura, C., et al., *Histidine kinase homologs that act as cytokinin receptors possess overlapping functions in the regulation of shoot and root growth in Arabidopsis.* The Plant Cell, 2004. **16**(6): p. 1365-1377.
127. Ueguchi, C., et al., *The AHK4 gene involved in the cytokinin-signaling pathway as a direct receptor molecule in Arabidopsis thaliana.* Plant and Cell Physiology, 2001. **42**(7): p. 751-755.
128. Hutchison, C.E., et al., *The Arabidopsis histidine phosphotransfer proteins are redundant positive regulators of cytokinin signaling.* The Plant Cell, 2006. **18**(11): p. 3073-3087.
129. Mähönen, A.P., et al., *Cytokinin signaling and its inhibitor AHP6 regulate cell fate during vascular development.* Science, 2006. **311**(5757): p. 94-98.
130. Suzuki, T., et al., *Histidine-containing phosphotransfer (HPt) signal transducers implicated in His-to-Asp phosphorelay in Arabidopsis.* Plant and cell physiology, 1998. **39**(12): p. 1258-1268.
131. Moreira, S., et al., *AHP6 inhibits cytokinin signaling to regulate the orientation of pericycle cell division during lateral root initiation.* PLoS One, 2013. **8**(2).
132. D'Agostino, I.B., J. Deruere, and J.J. Kieber, *Characterization of the response of the Arabidopsis response regulator gene family to cytokinin.* Plant physiology, 2000. **124**(4): p. 1706-1717.
133. Hwang, I. and J. Sheen, *Two-component circuitry in Arabidopsis cytokinin signal transduction.* nature, 2001. **413**(6854): p. 383-389.
134. Mason, M.G., et al., *Type-B response regulators display overlapping expression patterns in Arabidopsis.* Plant physiology, 2004. **135**(2): p. 927-937.
135. Tajima, Y., et al., *Comparative studies on the type-B response regulators revealing their distinctive properties in the His-to-Asp phosphorelay signal transduction of Arabidopsis thaliana.* Plant and Cell Physiology, 2004. **45**(1): p. 28-39.
136. Sakai, H., et al., *ARR1, a transcription factor for genes immediately responsive to cytokinins.* Science, 2001. **294**(5546): p. 1519-1521.
137. Mason, M.G., et al., *Multiple type-B response regulators mediate cytokinin signal transduction in Arabidopsis.* The Plant Cell, 2005. **17**(11): p. 3007-3018.

138. Blilou, I., et al., *The PIN auxin efflux facilitator network controls growth and patterning in Arabidopsis roots.* Nature, 2005. **433**(7021): p. 39-44.
139. Ioio, R.D., et al., *Cytokinins determine Arabidopsis root-meristem size by controlling cell differentiation.* Current Biology, 2007. **17**(8): p. 678-682.
140. Ioio, R.D., et al., *A genetic framework for the control of cell division and differentiation in the root meristem.* Science, 2008. **322**(5906): p. 1380-1384.
141. Müller, B. and J. Sheen, *Cytokinin and auxin interaction in root stem-cell specification during early embryogenesis.* Nature, 2008. **453**(7198): p. 1094-1097.
142. Růžička, K., et al., *Cytokinin regulates root meristem activity via modulation of the polar auxin transport.* Proceedings of the National Academy of Sciences, 2009. **106**(11): p. 4284-4289.
143. Tuominen, H., et al., *A radial concentration gradient of indole-3-acetic acid is related to secondary xylem development in hybrid aspen.* Plant Physiology, 1997. **115**(2): p. 577-585.
144. Werner, T., et al., *New insights into the biology of cytokinin degradation.* Plant Biology, 2006. **8**(03): p. 371-381.
145. Nordström, A., et al., *Auxin regulation of cytokinin biosynthesis in Arabidopsis thaliana: a factor of potential importance for auxin–cytokinin-regulated development.* Proceedings of the National Academy of Sciences, 2004. **101**(21): p. 8039-8044.
146. Tanaka, M., et al., *Auxin controls local cytokinin biosynthesis in the nodal stem in apical dominance.* The Plant Journal, 2006. **45**(6): p. 1028-1036.
147. Schlereth, A., et al., *MONOPTEROS controls embryonic root initiation by regulating a mobile transcription factor.* Nature, 2010. **464**(7290): p. 913-916.
148. Šimášková, M., et al., *Cytokinin response factors regulate PIN-FORMED auxin transporters.* Nature communications, 2015. **6**: p. 8717.
149. Pernisová, M., A. Kuderová, and J. Hejátko, *Cytokinin and auxin interactions in plant development: metabolism, signalling, transport and gene expression.* Current Protein and Peptide Science, 2011. **12**(2): p. 137-147.
150. Jones, B., et al., *Cytokinin regulation of auxin synthesis in Arabidopsis involves a homeostatic feedback loop regulated via auxin and cytokinin signal transduction.* The Plant Cell, 2010. **22**(9): p. 2956-2969.
151. Smet, W., et al., *DOF2. 1 controls cytokinin-dependent vascular cell proliferation downstream of TMO5/LHW.* Current Biology, 2019. **29**(3): p. 520-529. e6.
152. Miyashima, S., et al., *Mobile PEAR transcription factors integrate positional cues to prime cambial growth.* Nature, 2019. **565**(7740): p. 490-494.
153. Guo, Y., et al., *Dof5. 6/HCA2, a Dof transcription factor gene, regulates interfascicular cambium formation and vascular tissue development in Arabidopsis.* The Plant Cell, 2009. **21**(11): p. 3518-3534.
154. Fisher, K. and S. Turner, *PXY, a receptor-like kinase essential for maintaining polarity during plant vascular-tissue development.* Current Biology, 2007. **17**(12): p. 1061-1066.
155. Hirakawa, Y., et al., *Non-cell-autonomous control of vascular stem cell fate by a CLE peptide/receptor system.* Proceedings of the National Academy of Sciences, 2008. **105**(39): p. 15208-15213.
156. Ito, Y., et al., *Dodeca-CLE peptides as suppressors of plant stem cell differentiation.* Science, 2006. **313**(5788): p. 842-845.

157. Etchells, J.P. and S.R. Turner, *The PXY-CLE41 receptor ligand pair defines a multifunctional pathway that controls the rate and orientation of vascular cell division.* Development, 2010. **137**(5): p. 767-774.
158. Etchells, J.P., et al., *WOX4 and WOX14 act downstream of the PXY receptor kinase to regulate plant vascular proliferation independently of any role in vascular organisation.* Development, 2013. **140**(10): p. 2224-2234.
159. Hirakawa, Y., Y. Kondo, and H. Fukuda, *TDIF peptide signaling regulates vascular stem cell proliferation via the WOX4 homeobox gene in Arabidopsis.* The Plant Cell, 2010. **22**(8): p. 2618-2629.
160. Clark, S.E., M.P. Running, and E.M. Meyerowitz, *CLAVATA3 is a specific regulator of shoot and floral meristem development affecting the same processes as CLAVATA1.* Development, 1995. **121**(7): p. 2057-2067.
161. Clark, S.E., R.W. Williams, and E.M. Meyerowitz, *The CLAVATA1gene encodes a putative receptor kinase that controls shoot and floral meristem size in Arabidopsis.* Cell, 1997. **89**(4): p. 575-585.
162. Brand, U., et al., *Dependence of stem cell fate in Arabidopsis on a feedback loop regulated by CLV3 activity.* Science, 2000. **289**(5479): p. 617-619.
163. Schoof, H., et al., *The stem cell population of Arabidopsis shoot meristems is maintained by a regulatory loop between the CLAVATA and WUSCHEL genes.* Cell, 2000. **100**(6): p. 635-644.
164. Haecker, A., et al., *Expression dynamics of WOX genes mark cell fate decisions during early embryonic patterning in Arabidopsis thaliana.* Development, 2004. **131**(3): p. 657-668.
165. Sarkar, A.K., et al., *Conserved factors regulate signalling in Arabidopsis thaliana shoot and root stem cell organizers.* Nature, 2007. **446**(7137): p. 811-814.
166. Smit, M.E., et al., *A PXY-Mediated Transcriptional Network Integrates Signaling Mechanisms to Control Vascular Development in Arabidopsis.* The Plant Cell, 2020. **32**(2): p. 319-335.
167. Zhang, H., et al., *SERK family receptor-like kinases function as co-receptors with PXY for plant vascular development.* Molecular plant, 2016. **9**(10): p. 1406-1414.
168. Sun, Y., et al., *Structural basis for flg22-induced activation of the Arabidopsis FLS2-BAK1 immune complex.* Science, 2013. **342**(6158): p. 624-628.
169. Hothorn, M., et al., *Structural basis of steroid hormone perception by the receptor kinase BRI1.* Nature, 2011. **474**(7352): p. 467-471.
170. She, J., et al., *Structural insight into brassinosteroid perception by BRI1.* Nature, 2011. **474**(7352): p. 472-476.
171. Morita, J., et al., *Crystal structure of the plant receptor-like kinase TDR in complex with the TDIF peptide.* Nature communications, 2016. **7**: p. 12383.
172. Yang, J.H., et al., *A membrane-associated NAC domain transcription factor XVP interacts with TDIF co-receptor and regulates vascular meristem activity.* New Phytologist, 2019.
173. Qu, X., Z. Zhao, and Z. Tian, *ERECTA regulates cell elongation by activating auxin biosynthesis in Arabidopsis thaliana.* Frontiers in plant science, 2017. **8**: p. 1688.
174. Milhinhos, A., et al., *SOBIR1/EVR prevents precocious initiation of fiber differentiation during wood development through a mechanism involving BP and ERECTA.* Proceedings of the National Academy of Sciences, 2019. **116**(37): p. 18710-18716.

175. Gursanscky, N.R., et al., *MOL 1 is required for cambium homeostasis in Arabidopsis.* The Plant Journal, 2016. **86**(3): p. 210-220.
176. Bossinger, G. and A.V. Spokevicius, *Sector analysis reveals patterns of cambium differentiation in poplar stems.* Journal of experimental botany, 2018. **69**(18): p. 4339-4348.
177. Carlsbecker, A., et al., *Cell signalling by microRNA165/6 directs gene dose-dependent root cell fate.* Nature, 2010. **465**(7296): p. 316-321.
178. Izhaki, A. and J.L. Bowman, *KANADI and class III HD-Zip gene families regulate embryo patterning and modulate auxin flow during embryogenesis in Arabidopsis.* The Plant Cell, 2007. **19**(2): p. 495-508.
179. Ohashi-Ito, K. and H. Fukuda, *HD-Zip III homeobox genes that include a novel member, ZeHB-13 (Zinnia)/ATHB-15 (Arabidopsis), are involved in procambium and xylem cell differentiation.* Plant and Cell Physiology, 2003. **44**(12): p. 1350-1358.
180. Ursache, R., et al., *Tryptophan-dependent auxin biosynthesis is required for HD-ZIP III-mediated xylem patterning.* Development, 2014. **141**(6): p. 1250-1259.
181. Zhou, G.-K., et al., *Overexpression of miR165 affects apical meristem formation, organ polarity establishment and vascular development in Arabidopsis.* Plant and Cell Physiology, 2007. **48**(3): p. 391-404.
182. Baima, S., et al., *The expression of the Athb-8 homeobox gene is restricted to provascular cells in Arabidopsis thaliana.* Development, 1995. **121**(12): p. 4171-4182.
183. Suer, S., et al., *WOX4 imparts auxin responsiveness to cambium cells in Arabidopsis.* The Plant Cell, 2011. **23**(9): p. 3247-3259.
184. Olsson, V., et al., *Look closely, the beautiful may be small: Precursor-derived peptides in plants.* Annual review of plant biology, 2019. **70**: p. 153-186.
185. Fukuda, H. and C.S. Hardtke, *Peptide signaling pathways in vascular differentiation.* Plant Physiology, 2020.
186. Ragni, L., et al., *Mobile Gibberellin Directly Stimulates Arabidopsis Hypocotyl Xylem Expansion.* The Plant Cell, 2011. **23**(4): p. 1322-1336.
187. Roodt, D., et al., *Loss of wood formation genes in monocot genomes.* Genome biology and evolution, 2019. **11**(7): p. 1986-1996.
188. Van den Broeck, L., et al., *Gene regulatory network inference: connecting plant biology and mathematical modeling.* Frontiers in genetics, 2020. **11**: p. 457.
189. Prusinkiewicz, P. and A. Runions, *Computational models of plant development and form.* New Phytologist, 2012. **193**(3): p. 549-569.
190. Prusinkiewicz, P. and A.-G. Rolland-Lagan, *Modeling plant morphogenesis.* Current opinion in plant biology, 2006. **9**(1): p. 83-88.
191. Morris, R.J., *Mathematical modelling in plant biology*. 2018: Springer.
192. Edelstein-Keshet, L., *Mathematical models in biology*. 2005: SIAM.
193. Benková, E., et al., *Local, efflux-dependent auxin gradients as a common module for plant organ formation.* Cell, 2003. **115**(5): p. 591-602.
194. Cassab, G.I., D. Eapen, and M.E. Campos, *Root hydrotropism: an update.* American journal of botany, 2013. **100**(1): p. 14-24.
195. Enders, T.A. and L.C. Strader, *Auxin activity: Past, present, and future.* American journal of botany, 2015. **102**(2): p. 180-196.
196. Gälweiler, L., et al., *Regulation of polar auxin transport by AtPIN1 in Arabidopsis vascular tissue.* Science, 1998. **282**(5397): p. 2226-2230.

197. Ibañes, M., et al., *Brassinosteroid signaling and auxin transport are required to establish the periodic pattern of Arabidopsis shoot vascular bundles.* Proceedings of the National Academy of Sciences, 2009. **106**(32): p. 13630-13635.
198. Kaneyasu, T., et al., *Auxin response, but not its polar transport, plays a role in hydrotropism of Arabidopsis roots.* Journal of experimental botany, 2007. **58**(5): p. 1143-1150.
199. Lavenus, J., S. Guyomarc'h, and L. Laplaze, *PIN transcriptional regulation shapes root system architecture.* Trends in plant science, 2016. **21**(3): p. 175-177.
200. Mattsson, J., Z.R. Sung, and T. Berleth, *Responses of plant vascular systems to auxin transport inhibition.* Development, 1999. **126**(13): p. 2979-2991.
201. Mroue, S., A. Simeunovic, and H.S. Robert, *Auxin production as an integrator of environmental cues for developmental growth regulation.* Journal of experimental botany, 2018. **69**(2): p. 201-212.
202. Rahman, A., *Auxin: a regulator of cold stress response.* Physiologia plantarum, 2013. **147**(1): p. 28-35.
203. Taniguchi, Y.Y., et al., *Involvement of Arabidopsis thaliana phospholipase Dζ2 in root hydrotropism through the suppression of root gravitropism.* Planta, 2010. **231**(2): p. 491-497.
204. Taylor-Teeples, M., A. Lanctot, and J.L. Nemhauser, *As above, so below: Auxin's role in lateral organ development.* Developmental biology, 2016. **419**(1): p. 156-164.
205. Vanneste, S. and J. Friml, *Auxin: a trigger for change in plant development.* Cell, 2009. **136**(6): p. 1005-1016.
206. Wang, Y., K. Li, and X. Li, *Auxin redistribution modulates plastic development of root system architecture under salt stress in Arabidopsis thaliana.* Journal of plant physiology, 2009. **166**(15): p. 1637-1645.
207. Zhao, Y., *Auxin biosynthesis and its role in plant development.* Annual review of plant biology, 2010. **61**: p. 49-64.
208. Middleton, A.M., et al., *Mathematical modelling of the Aux/IAA negative feedback loop.* Bulletin of mathematical biology, 2010. **72**(6): p. 1383-1407.
209. De Smet, I., et al., *Auxin-dependent regulation of lateral root positioning in the basal meristem of Arabidopsis.* Development, 2007. **134**(4): p. 681-690.
210. Abel, S., M.D. Nguyen, and A. Theologis, *ThePS-IAA4/5-like Family of Early Auxin-inducible mRNAs inArabidopsis thaliana.* Journal of molecular biology, 1995. **251**(4): p. 533-549.
211. Muraro, D., et al., *The influence of cytokinin–auxin cross-regulation on cell-fate determination in Arabidopsis thaliana root development.* Journal of theoretical biology, 2011. **283**(1): p. 152-167.
212. Laplaze, L., et al., *Cytokinins act directly on lateral root founder cells to inhibit root initiation.* The Plant Cell, 2007. **19**(12): p. 3889-3900.
213. Muraro, D., et al., *The role of auxin and cytokinin signalling in specifying the root architecture of Arabidopsis thaliana.* Journal of theoretical biology, 2013. **317**: p. 71-86.
214. Grieneisen, V.A., et al., *Auxin transport is sufficient to generate a maximum and gradient guiding root growth.* Nature, 2007. **449**(7165): p. 1008-1013.
215. Muraro, D., et al., *A multi-scale model of the interplay between cell signalling and hormone transport in specifying the root meristem of Arabidopsis thaliana.* Journal of theoretical biology, 2016. **404**: p. 182-205.

216. Wolpert, L., *Positional information and the spatial pattern of cellular differentiation.* Journal of theoretical biology, 1969. **25**(1): p. 1-47.
217. Mitchison, G., *The dynamics of auxin transport.* Proceedings of the Royal Society of London. Series B. Biological Sciences, 1980. **209**(1177): p. 489-511.
218. Petersson, S.V., et al., *An auxin gradient and maximum in the Arabidopsis root apex shown by high-resolution cell-specific analysis of IAA distribution and synthesis.* The Plant Cell, 2009. **21**(6): p. 1659-1668.
219. Mironova, V.V., et al., *A plausible mechanism for auxin patterning along the developing root.* BMC systems biology, 2010. **4**(1): p. 1-19.
220. Mironova, V., et al., *Combined in silico/in vivo analysis of mechanisms providing for root apical meristem self-organization and maintenance.* Annals of botany, 2012. **110**(2): p. 349-360.
221. Grieneisen, V.A., et al., *Morphogengineering roots: comparing mechanisms of morphogen gradient formation.* BMC systems biology, 2012. **6**(1): p. 1-20.
222. Band, L.R., et al., *Systems analysis of auxin transport in the Arabidopsis root apex.* The Plant Cell, 2014. **26**(3): p. 862-875.
223. Xuan, W., et al., *Cyclic programmed cell death stimulates hormone signaling and root development in Arabidopsis.* Science, 2016. **351**(6271): p. 384-387.
224. Mellor, N., et al., *Theoretical approaches to understanding root vascular patterning: a consensus between recent models.* Journal of Experimental Botany, 2017. **68**(1): p. 5-16.
225. Mellor, N.L., et al., *Auxin fluxes through plasmodesmata modify root-tip auxin distribution.* Development, 2020. **147**(6).
226. Laskowski, M., et al., *Root system architecture from coupling cell shape to auxin transport.* PLoS Biol, 2008. **6**(12): p. e307.
227. Hobbie, L. and M. Estelle, *The axr4 auxin-resistant mutants of Arabidopsis thaliana define a gene important for root gravitropism and lateral root initiation.* The Plant Journal, 1995. **7**(2): p. 211-220.
228. Di Mambro, R., et al., *Auxin minimum triggers the developmental switch from cell division to cell differentiation in the Arabidopsis root.* Proceedings of the National Academy of Sciences, 2017. **114**(36): p. E7641-E7649.
229. Brunoud, G., et al., *A novel sensor to map auxin response and distribution at high spatio-temporal resolution.* Nature, 2012. **482**(7383): p. 103-106.
230. Santuari, L., et al., *Positional information by differential endocytosis splits auxin response to drive Arabidopsis root meristem growth.* Current Biology, 2011. **21**(22): p. 1918-1923.
231. Liu, J., et al., *Modelling and experimental analysis of hormonal crosstalk in Arabidopsis.* Molecular Systems Biology, 2010. **6**(1): p. 373.
232. Casson, S.A., et al., *The POLARIS gene of Arabidopsis encodes a predicted peptide required for correct root growth and leaf vascular patterning.* The Plant Cell, 2002. **14**(8): p. 1705-1721.
233. Chilley, P.M., et al., *The POLARIS peptide of Arabidopsis regulates auxin transport and root growth via effects on ethylene signaling.* The Plant Cell, 2006. **18**(11): p. 3058-3072.
234. Moore, S., et al., *Spatiotemporal modelling of hormonal crosstalk explains the level and patterning of hormones and gene expression in Arabidopsis thaliana wild-type and mutant roots.* New Phytologist, 2015. **207**(4): p. 1110-1122.

235. Mellor, N., et al., *A core mechanism for specifying root vascular patterning can replicate the anatomical variation seen in diverse plant species.* Development, 2019. **146**(6).
236. el-Showk, S., et al., *Parsimonious model of vascular patterning links transverse hormone fluxes to lateral root initiation: auxin leads the way, while cytokinin levels out.* PLoS Comput Biol, 2015. **11**(10): p. e1004450.
237. Miyashima, S., et al., *Non-cell-autonomous microRNA165 acts in a dose-dependent manner to regulate multiple differentiation status in the Arabidopsis root.* Development, 2011. **138**(11): p. 2303-2313.
238. Merks, R.M., et al., *VirtualLeaf: an open-source framework for cell-based modeling of plant tissue growth and development.* Plant physiology, 2011. **155**(2): p. 656-666.
239. Cartenì, F., et al., *Modelling the development and arrangement of the primary vascular structure in plants.* Annals of botany, 2014. **114**(4): p. 619-627.
240. Lebovka, I., et al., *Computational modelling of cambium activity provides a regulatory framework for simulating radial plant growth.* bioRxiv, 2020.
241. Wallner, E.-S., et al., *Strigolactone-and karrikin-independent SMXL proteins are central regulators of phloem formation.* Current Biology, 2017. **27**(8): p. 1241-1247.
242. Miyashima, S., et al., *Mobile PEAR transcription factors integrate positional cues to prime cambial growth.* Nature, 2019. **565**(7740): p. 490-494.
243. Gehan, M.A., et al., *PlantCV v2: Image analysis software for high-throughput plant phenotyping.* PeerJ, 2017. **5**: p. e4088.
244. Wunderling, A., et al., *Novel tools for quantifying secondary growth.* Journal of experimental botany, 2017. **68**(1): p. 89-95.
245. Roeder, A.H., et al., *A computational image analysis glossary for biologists.* Development, 2012. **139**(17): p. 3071-3080.
246. Burton, A.L., et al., *RootScan: software for high-throughput analysis of root anatomical traits.* Plant and Soil, 2012. **357**(1): p. 189-203.
247. Lartaud, M., et al., *PHIV-RootCell: a supervised image analysis tool for rice root anatomical parameter quantification.* Frontiers in plant science, 2015. **5**: p. 790.
248. Chopin, J., et al., *Rootanalyzer: a cross-section image analysis tool for automated characterization of root cells and tissues.* PloS one, 2015. **10**(9): p. e0137655.
249. Hall, H.C., et al., *Precision automation of cell type classification and sub-cellular fluorescence quantification from laser scanning confocal images.* Frontiers in plant science, 2016. **7**: p. 119.
250. de Reuille, P.B., et al., *MorphoGraphX: A platform for quantifying morphogenesis in 4D.* Elife, 2015. **4**: p. e05864.
251. Shpak, E.D., et al., *Synergistic interaction of three ERECTA-family receptor-like kinases controls Arabidopsis organ growth and flower development by promoting cell proliferation.* Development, 2004. **131**(7): p. 1491-1501.
252. Bagdassarian, K.S. *GitHub Content*. 2019 [cited 2019 August 5]; Available from: https://github.com/KristineBagdassarian/PXY-ER_enforce_radial_growth.
253. Abrash, E.B. and D.C. Bergmann, *Regional specification of stomatal production by the putative ligand CHALLAH.* Development, 2010. **137**(3): p. 447-455.
254. Abrash, E.B., K.A. Davies, and D.C. Bergmann, *Generation of signaling specificity in Arabidopsis by spatially restricted buffering of ligand–receptor interactions.* The Plant Cell, 2011. **23**(8): p. 2864-2879.

255. Hara, K., et al., *The secretory peptide gene EPF1 enforces the stomatal one-cell-spacing rule.* Genes & development, 2007. **21**(14): p. 1720-1725.
256. Hara, K., et al., *Epidermal cell density is autoregulated via a secretory peptide, EPIDERMAL PATTERNING FACTOR 2 in Arabidopsis leaves.* Plant and Cell Physiology, 2009. **50**(6): p. 1019-1031.
257. Hunt, L., K.J. Bailey, and J.E. Gray, *The signalling peptide EPFL9 is a positive regulator of stomatal development.* New Phytologist, 2010. **186**(3): p. 609-614.
258. Hunt, L. and J.E. Gray, *The Signaling Peptide EPF2 Controls Asymmetric Cell Divisions during Stomatal Development.* Current Biology, 2009. **19**(10): p. 864-869.
259. Torii, K.U., et al., *The Arabidopsis ERECTA gene encodes a putative receptor protein kinase with extracellular leucine-rich repeats.* The Plant Cell, 1996. **8**(4): p. 735-746.
260. Uchida, N. and M. Tasaka, *Regulation of plant vascular stem cells by endodermis-derived EPFL-family peptide hormones and phloem-expressed ERECTA-family receptor kinases.* Journal of experimental botany, 2013. **64**(17): p. 5335-5343.
261. Uchida, N., et al., *Regulation of inflorescence architecture by intertissue layer ligand–receptor communication between endodermis and phloem.* Proceedings of the National Academy of Sciences, 2012. **109**(16): p. 6337-6342.
262. Immanen, J., et al., *Cytokinin and auxin display distinct but interconnected distribution and signaling profiles to stimulate cambial activity.* Current Biology, 2016. **26**(15): p. 1990-1997.
263. Uggla, C., et al., *Auxin as a positional signal in pattern formation in plants.* Proceedings of the national academy of sciences, 1996. **93**(17): p. 9282-9286.
264. Uggla, C., E.J. Mellerowicz, and B. Sundberg, *Indole-3-acetic acid controls cambial growth in Scots pine by positional signaling.* Plant Physiology, 1998. **117**(1): p. 113-121.
265. Sundberg, B. and C. Uggla, *Origin and dynamics of indoleacetic acid under polar transport in Pinus sylvestris.* Physiologia Plantarum, 1998. **104**(1): p. 22-29.
266. Björklund, S., et al., *Cross-talk between gibberellin and auxin in development of Populus wood: gibberellin stimulates polar auxin transport and has a common transcriptome with auxin.* The Plant Journal, 2007. **52**(3): p. 499-511.
267. Johnsson, C., et al., *The plant hormone auxin directs timing of xylem development by inhibition of secondary cell wall deposition through repression of secondary wall NAC-domain transcription factors.* Physiologia plantarum, 2019. **165**(4): p. 673-689.
268. Adamowski, M. and J. Friml, *PIN-dependent auxin transport: action, regulation, and evolution.* The Plant Cell, 2015. **27**(1): p. 20-32.
269. Michniewicz, M., P.B. Brewer, and J. Friml, *Polar auxin transport and asymmetric auxin distribution.* The Arabidopsis Book/American Society of Plant Biologists, 2007. **5**.
270. Blakeslee, J.J., W.A. Peer, and A.S. Murphy, *Auxin transport.* Current opinion in plant biology, 2005. **8**(5): p. 494-500.
271. Goldsmith, M., *The polar transport of auxin.* Annual Review of Plant Physiology, 1977. **28**(1): p. 439-478.
272. Vieten, A., et al., *Functional redundancy of PIN proteins is accompanied by auxin-dependent cross-regulation of PIN expression.* Development, 2005. **132**(20): p. 4521-4531.
273. Zhou, J.-J. and J. Luo, *The PIN-FORMED auxin efflux carriers in plants.* International journal of molecular sciences, 2018. **19**(9): p. 2759.

274. Grunewald, W. and J. Friml, *The march of the PINs: developmental plasticity by dynamic polar targeting in plant cells.* The EMBO journal, 2010. **29**(16): p. 2700-2714.
275. Zažímalová, E., et al., *Auxin transporters—why so many?* Cold Spring Harbor perspectives in biology, 2010. **2**(3): p. a001552.
276. Ljung, K., et al., *Sites and regulation of auxin biosynthesis in Arabidopsis roots.* The Plant Cell, 2005. **17**(4): p. 1090-1104.
277. Reinhardt, D., T. Mandel, and C. Kuhlemeier, *Auxin regulates the initiation and radial position of plant lateral organs.* The Plant Cell, 2000. **12**(4): p. 507-518.
278. Reinhardt, D., et al., *Regulation of phyllotaxis by polar auxin transport.* Nature, 2003. **426**(6964): p. 255-260.
279. Heisler, M.G., et al., *Patterns of auxin transport and gene expression during primordium development revealed by live imaging of the Arabidopsis inflorescence meristem.* Current biology, 2005. **15**(21): p. 1899-1911.
280. Friml, J., et al., *Efflux-dependent auxin gradients establish the apical–basal axis of Arabidopsis.* Nature, 2003. **426**(6963): p. 147-153.
281. Rakusová, H., et al., *Polarization of PIN3-dependent auxin transport for hypocotyl gravitropic response in Arabidopsis thaliana.* The Plant Journal, 2011. **67**(5): p. 817-826.
282. Friml, J., et al., *Lateral relocation of auxin efflux regulator PIN3 mediates tropism in Arabidopsis.* Nature, 2002. **415**(6873): p. 806-809.
283. Friml, J., et al., *AtPIN4 mediates sink-driven auxin gradients and root patterning in Arabidopsis.* Cell, 2002. **108**(5): p. 661-673.
284. Tanaka, H., et al., *Spatiotemporal asymmetric auxin distribution: a means to coordinate plant development.* Cellular and Molecular Life Sciences CMLS, 2006. **63**(23): p. 2738-2754.
285. Petrášek, J., et al., *PIN proteins perform a rate-limiting function in cellular auxin efflux.* Science, 2006. **312**(5775): p. 914-918.
286. Friml, J., et al., *AtPIN4 mediates sink-driven auxin gradients and root patterning in Arabidopsis.* Cell, 2002. **108**(5): p. 661-673.
287. Scheres, B. and J. Xu, *Polar auxin transport and patterning: grow with the flow.* Genes & development, 2006. **20**(8): p. 922-926.
288. Peer, W.A., *From perception to attenuation: auxin signalling and responses.* Current opinion in plant biology, 2013. **16**(5): p. 561-568.
289. Weijers, D. and D. Wagner, *Transcriptional responses to the auxin hormone.* Annual review of plant biology, 2016. **67**: p. 539-574.
290. El-Showk, S., R. Ruonala, and Y. Helariutta, *Crossing paths: cytokinin signalling and crosstalk.* Development, 2013. **140**(7): p. 1373-1383.
291. Schaller, G.E., A. Bishopp, and J.J. Kieber, *The yin-yang of hormones: cytokinin and auxin interactions in plant development.* The Plant Cell, 2015. **27**(1): p. 44-63.
292. Vanstraelen, M. and E. Benková, *Hormonal interactions in the regulation of plant development.* Annual review of cell and developmental biology, 2012. **28**: p. 463-487.
293. Bishopp, A., et al., *Phloem-transported cytokinin regulates polar auxin transport and maintains vascular pattern in the root meristem.* Current Biology, 2011. **21**(11): p. 927-932.

294. Marhavý, P., et al., *Cytokinin modulates endocytic trafficking of PIN1 auxin efflux carrier to control plant organogenesis.* Developmental cell, 2011. **21**(4): p. 796-804.
295. Pernisová, M., et al., *Cytokinins modulate auxin-induced organogenesis in plants via regulation of the auxin efflux.* Proceedings of the National Academy of Sciences, 2009. **106**(9): p. 3609-3614.
296. Zhang, W., et al., *Type-A response regulators are required for proper root apical meristem function through post-transcriptional regulation of PIN auxin efflux carriers.* The Plant Journal, 2011. **68**(1): p. 1-10.
297. Krogan, N.T., et al., *Deletion of MP/ARF5 domains III and IV reveals a requirement for Aux/IAA regulation in Arabidopsis leaf vascular patterning.* New Phytologist, 2012. **194**(2): p. 391-401.
298. Chen, Q., et al., *A coherent transcriptional feed-forward motif model for mediating auxin-sensitive PIN3 expression during lateral root development.* Nature communications, 2015. **6**(1): p. 1-12.
299. Rubery, P.H. and A.R. Sheldrake, *Carrier-mediated auxin transport.* Planta, 1974. **118**(2): p. 101-121.
300. Raven, J., *Transport of indoleacetic acid in plant cells in relation to pH and electrical potential gradients, and its significance for polar IAA transport.* New Phytologist, 1975. **74**(2): p. 163-172.
301. Cole, M., et al., *DORNROSCHEN is a direct target of the auxin response factor MONOPTEROS in the Arabidopsis embryo.* 2009.
302. Borghi, L., et al., *Arabidopsis RETINOBLASTOMA-RELATED is required for stem cell maintenance, cell differentiation, and lateral organ production.* The Plant Cell, 2010. **22**(6): p. 1792-1811.
303. Guo, J., et al., *Inducible knock-down of GNOM during root formation reveals tissue-specific response to auxin transport and its modulation of local auxin biosynthesis.* Journal of experimental botany, 2014. **65**(4): p. 1165-1179.
304. Heidstra, R., D. Welch, and B. Scheres, *Mosaic analyses using marked activation and deletion clones dissect Arabidopsis SCARECROW action in asymmetric cell division.* Genes & Development, 2004. **18**(16): p. 1964-1969.
305. Wachsman, G., R. Heidstra, and B. Scheres, *Distinct cell-autonomous functions of RETINOBLASTOMA-RELATED in Arabidopsis stem cells revealed by the Brother of Brainbow clonal analysis system.* The Plant Cell, 2011. **23**(7): p. 2581-2591.
306. Wildwater, M., et al., *The RETINOBLASTOMA-RELATED gene regulates stem cell maintenance in Arabidopsis roots.* Cell, 2005. **123**(7): p. 1337-1349.
307. Qi, Y., et al., *Targeted deletion and inversion of tandemly arrayed genes in Arabidopsis thaliana using zinc finger nucleases.* G3: Genes, Genomes, Genetics, 2013. **3**(10): p. 1707-1715.
308. Christian, M., et al., *Targeted mutagenesis of Arabidopsis thaliana using engineered TAL effector nucleases.* G3: Genes, Genomes, Genetics, 2013. **3**(10): p. 1697-1705.
309. Wang, X., et al., *An inducible genome editing system for plants.* Nature plants, 2020. **6**(7): p. 766-772.
310. Ma, X., et al., *A robust CRISPR/Cas9 system for convenient, high-efficiency multiplex genome editing in monocot and dicot plants.* Molecular plant, 2015. **8**(8): p. 1274-1284.
311. Siligato, R., et al., *MultiSite gateway-compatible cell type-specific gene-inducible system for plants.* Plant physiology, 2016. **170**(2): p. 627-641.

312. Zuo, J., Q.W. Niu, and N.H. Chua, *An estrogen receptor-based transactivator XVE mediates highly inducible gene expression in transgenic plants.* The Plant Journal, 2000. **24**(2): p. 265-273.
313. Bagdassarian, K.S. and N. Savage. *GitHub Code - Numerical Solver*. 2021 [cited 2021 09/06]; Available from: https://github.com/KristineBagdassarian/PXY_MP_model_solver.git.
314. Atkinson, K.E., *An introduction to numerical analysis*. 2008: John wiley & sons.
315. Bagdassarian, K.S. *GitHub Content - Morris method*. Available from: https://github.com/KristineBagdassarian/PXY-MP-model_Morris.
316. Campolongo, F., J. Cariboni, and A. Saltelli, *An effective screening design for sensitivity analysis of large models.* Environmental modelling & software, 2007. **22**(10): p. 1509-1518.
317. van Houwelingen, H.C., H.C. Boshuizen, and M. Capannesi, *Sensitivity analysis of state-transition models: How to deal with a large number of inputs.* Computers in Biology and Medicine, 2011. **41**(9): p. 838-842.
318. Likhachev, D., *Parametric sensitivity analysis as an essential ingredient of spectroscopic ellipsometry data modeling: An application of the Morris screening method.* Journal of Applied Physics, 2019. **126**(18): p. 184901.

Appendices

Appendix A

Available online at www.sciencedirect.com

ScienceDirect

Current Opinion in Plant Biology

Connections in the cambium, receptors in the ring

Kristine S Bagdassarian, Catherine M Brown, Ewan T Jones and Peter Etchells

In plants, pluripotent cells in meristems divide to provide cells for the formation of postembryonic tissues. The cambium is the meristem from which the vascular tissue is derived and is the main driver for secondary (radial) growth in dicots. Xylem and phloem are specified on opposing sides of the cambium, and tightly regulated cell divisions ensure their spatial separation. Peptide ligands, phytohormones, and their receptors are central to maintaining this patterning and regulating proliferation. Here, we describe recent advances in our understanding of how these signals are integrated to control vascular development and secondary growth.

Address

Department of Biosciences, Durham University, Durham, DH1 3LE, United Kingdom

Corresponding author: Etchells, Peter (Peter.Etchells@durham.ac.uk)

Current Opinion in Plant Biology 2020, **57**:96–103

This review comes from a themed issue on **Cell signaling and gene regulation**

Edited by **Jaimie M Van Norman**, **Lucia C Strader** and **Rosangela Sozzani**

For a complete overview see the Issue and the Editorial

Available online 28th August 2020

https://doi.org/10.1016/j.pbi.2020.07.001

Introduction

A prerequisite for size is structural support, and the ability to distribute water and nutrients. The vascular tissue performs these functions, with xylem providing mechanical strength and movement of water and solutes from roots, and phloem distributing photosynthates and bulk flow of phytohormones (reviewed in Refs. [1,2]) including auxin [3], cytokinin [4–7], gibberellin [8–10] and abscisic acid (ABA) [11–14], to facilitate physiological responses and regulate plant development. Specification of xylem and phloem cell type identity and function has been summarised in recent reviews [15–22]. Here, we review signalling mechanisms that regulate the homeostasis of the cambium, the meristematic tissue from which the xylem and phloem are derived.

Hormone harmonies

Most plant hormones play a role in the regulation of cambial activity [10,23–25], but the most prominent and well-studied are auxin and cytokinin. Auxin is involved in numerous developmental processes, operating through a signalling pathway that includes auxin/indole-3-acetic acid inducible Aux/IAA proteins, TRANSPORT INHIBITOR RESPONSE 1 (TIR1) receptor, and the AUXIN RESPONSE FACTOR (ARF) family of genes [26–31]. ARFs act as transcriptional regulators [30,31]. Of these, ARF5/MONOPTEROS (MP) regulates proliferation in the vascular stem cell niche, as well as performing distinct roles in early and late stages of vascular development. During embryogenesis, *mp* mutants fail to establish a central axis in the provascular cylinder [32•,33]. Weak *mp* alleles also demonstrate disrupted auxin transport [32•,34,35] due to MP directly activating transcription of several PIN-FORMED (PIN) auxin efflux transporters [36,37]. Thus, in early development, MP promotes vascular proliferation. Late in development, during secondary growth, *mp* mutants demonstrate increased cambial divisions, suggesting that in this context MP suppresses vascular expansion [38••,39]. Conversely, other auxin response factors, ARF3 and ARF4, have been shown to operate in concert to upregulate cambium activity [39].

Cytokinin also contributes to cambium development, with loss of cytokinin-synthesizing genes deterring cambium formation and thus radial vascular expansion [40,41]. Cytokinin signalling occurs via a phosphorelay, which begins with cytokinin perception by its family of receptors CYTOKININ RESPONSE 1 (CRE1)/WOODEN LEG (WOL)/*Arabidopsis* HISTIDINE KINASE4 (AHK4), AHK2 and AHK3 [41–45]. Following perception, *ARABIDOPSIS* PHOSPHOTRANSFER PROTEINS (AHPs) AHP1-AHP6 are activated [46–48], with AHP1-AHP5 promoting cytokinin signalling, and AHP6, acting as a pseudo-AHP and thus as a negative regulator of the signal [46–49]. In the final steps of the signalling cascade, AHPs 1–5 phosphorylate type-B *ARABIDOPSIS THALIANA RESPONSE REGULATORS* (*ARRs*), transcription factors that promote cytokinin responses including vascular proliferation. AHPs also trigger the transcription of type-A ARRs, which in turn suppress cytokinin responses, thus buffering the system [50–55].

Auxin and cytokinin ratios influence the balance between cell division and differentiation during plant development [56–61]. Their concentration gradients span the vascular tissue with a cytokinin maxima in the phloem,

and an auxin maxima on the xylem side of the cambium (Figure 1) [38••,39,62••]. Cross-talk between these hormones is likely important in establishing the auxin/cytokinin ratios. Auxin stimulates the expression of cytokinin oxidase (CKX), a major cytokinin deactivating enzyme [63], and suppresses the transcription of *isopentenyl transferase* (*IPT*) genes that encode cytokinin-promoting enzymes [64,65]. Auxin also increases expression of *AHP6* which as described above dampens cytokinin signalling [5,47,49]. In the root xylem axis, MP/ARF5 promotes the transcription of TARGET OF MONOPTEROS 5 (TMO5), a bHLH transcription factor that forms a heterodimer with LONESOME HIGHWAY (LHW). In turn, the TMO5–LHW heterodimer upregulates cytokinin biosynthesis genes *LONELY GUY3/4 (LOG3/4)* [66,67]. Cytokinin notoriously acts on auxin by controlling distribution and levels of auxin transport's main conductors, the PIN-FORMED (PIN) proteins [5,58,60,68,69]. Cytokinin application strongly affects PIN transcription levels, downregulating PIN1–PIN4 and upregulating PIN7 [60]. In developing roots and shoots, transcription levels of auxin biosynthesis genes were stimulated by cytokinin, thus promoting auxin production [70]. Cytokinin also induces expression of group of related DOF-family transcription factors, DOF2.1, DOF6, TMO6, PHLOEM EARLY DOF 1 (PEAR1), PEAR2, OBF BINDING PROTEIN 2 (OBP2) and HIGH CAMBIAL ACTIVITY 2 (HCA2) which promote procambial cell divisions [71–73].

Figure 1

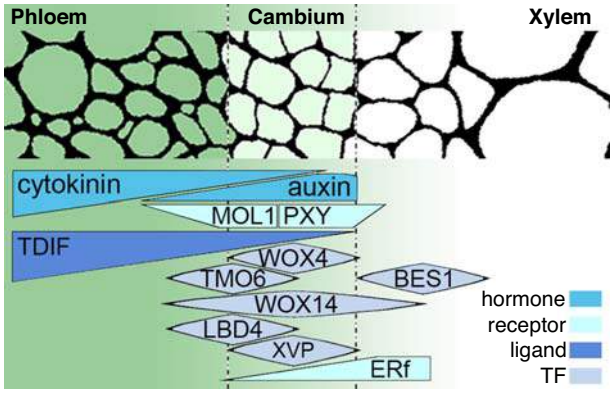

Stylised depiction of protein distribution and auxin and cytokinin accumulation across the vascular cambium in wild type plants. Cytokinin has a concentration maxima in the phloem; auxin on xylem–adjacent cambium. RLK's MOL1 and PXY are expressed on phloem facing and xylem facing cambium, respectively; ERf receptor expression spans the cambium. TDIF ligand is expressed in the phloem and perceived by PXY. Transcription factors WOX4, WOX14, and XVP exhibit maxima in the cambium. BES1 is present in the xylem; TMO6 and LBD4 expression as at the edge of the cambium on the phloem side.

Peptides and proliferation

Peptide ligands and their cognate receptors contribute substantially to secondary growth and patterning. The cambium-expressed leucine-rich repeat receptor-like protein kinase (LRR–RLK) PHLOEM INTERCALATED WITH XYLEM (PXY), also known as TDIF-RECEPTOR (TDR) [74,75•] and its phloem-expressed ligand TRACHEARY ELEMENT DIFFERENTIATION INHIBITORY FACTOR (TDIF) are essential for cell proliferation and division plane specification (Figures 1 and 2a) [75•,76–79]. TDIF, encoded by *CLAVATA3/ENDOSPERM SURROUNDING REGION 41* (*CLE41*), *CLE42* and *CLE44*, was identified as a repressor of xylem differentiation and is structurally similar to CLAVATA3 (CLV3) [76], a peptide ligand that regulates meristem maintenance in shoots and signals to receptor CLV1 [80,81]. *pxy* mutants were first described as lacking separation between cambium-derived phloem and xylem tissues and as having disrupted orientation of cambial cell divisions [74]. Hirakawa *et al.* independently identified PXY by testing loss-of-function mutants in relatives of CLV1, for TDIF insensitivity [75•].

Since CLV signalling acts to repress expression of homeodomain transcription factor WUSCHEL (WUS) [82,83], potential transcript targets of TDIF/PXY signalling were hypothesised to be members of the WUSCHEL-RELATED HOMEOBOX (WOX) family [84,85]. WOX4 exhibited a rise in expression levels following TDIF treatment, and WOX14 was identified as being down-regulated in *pxy* mutants. Both WOX4 and WOX14 were seen to stimulate cambial cell proliferation [78,79], with WOX14 cooperatively controlling expression of LOB DOMAIN-CONTAINING PROTEIN (LBD4) transcription factor with a DOF transcription factor, TMO6 (Figures 1 and 2a) [86•].

The PXY/TDIF signalling module influences outputs of auxin signalling. For instance, PXY acts to represses one glycogen synthase kinase-3 (GSK3), BIN2-LIKE 1 (BIL1). In the absence of PXY, BIL1 phosphorylates MP (Figure 2a), which is thought to loosen MP's interaction with an IAA suppressor, thus releasing it to control gene expression [38••]. Recently, Smetana *et al.* have reported a positive influence of auxin/MP on PXY expression in the initial stages of cambium formation in roots [87••]. Since the PXY–BIL1–MP negative interactions were shown to function in the stem [38••], an interesting question is whether a negative feedback loop might exist between MP and PXY, wherein MP attenuates its own activity by boosting PXY expression — or whether the regulation is organ-specific. While PXY represses BIL1, it activates other GSK3s and most notably, BRASSINOSTEROID INSENSITIVE 2 (BIN2) in the presence of TDIF. Active BIN2, in turn, phosphorylates a transcription factor BRI1 EMS SUPPRESSOR 1 (BES1), marking it for degradation. BES1 promotes xylem differentiation (Figures 1 and 2a),

Figure 2

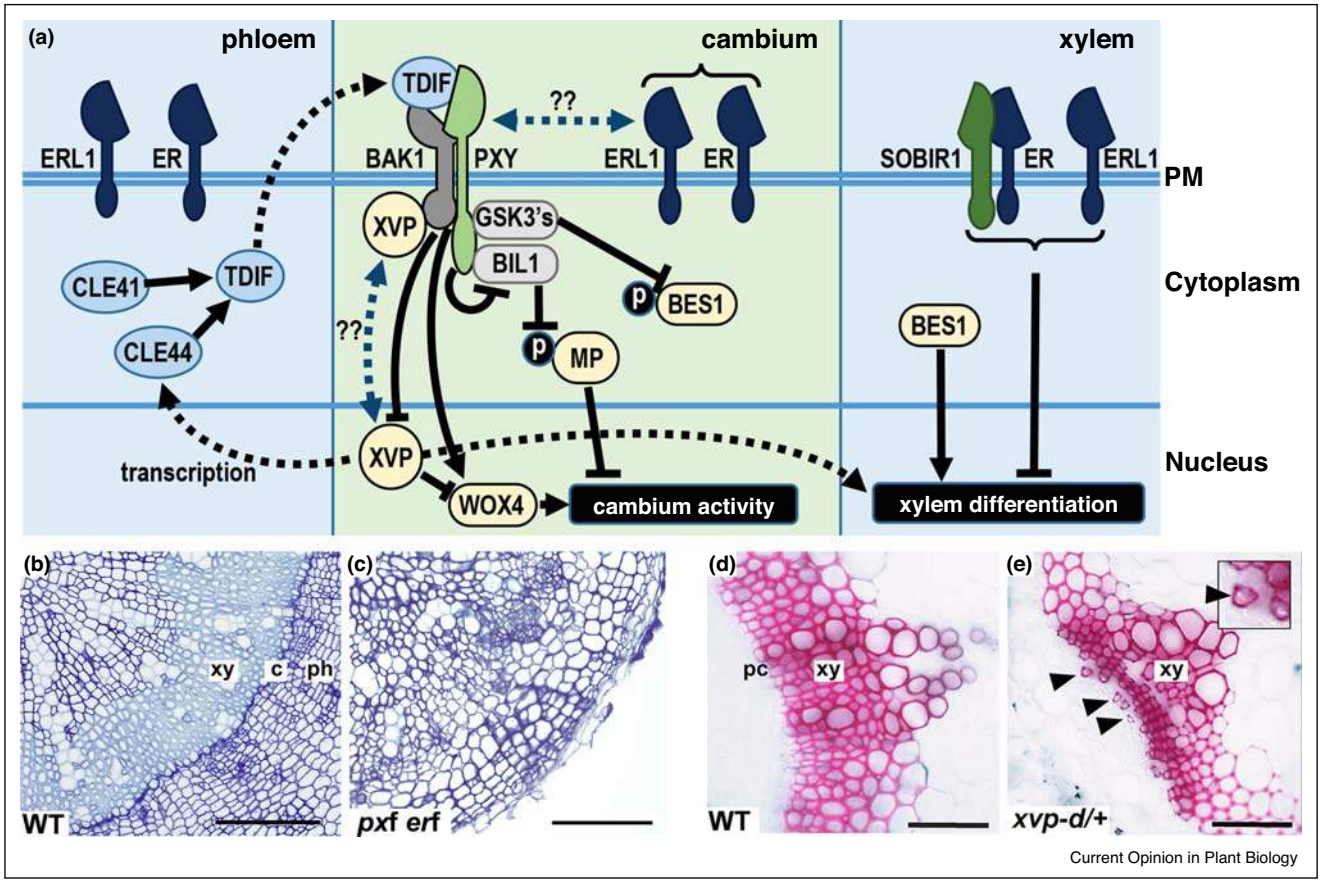

Signals that regulate cambium activity in *Arabidopsis*. **(a)** Schematic representation of phloem, cambium and xylem with signal components shown in the plasma membrane (PM), cytoplasm, and nucleus. RLK's are shown in the PM, PXY ligand components are blue, transcription factors are yellow, and GSK3's are grey. '??' on blue dashed arrows indicates limited understanding (signals promoting XCP translocation to the nucleus are not known; partial evidence for a physical interaction between PXY and ER family receptors has been reported). 'P' indicates phosphorylation. **(b-c)** Hypocotyl transverse sections, with wild type (WT; (b)) showing distinct phloem (ph), xylem (xy) and cambial (ca) domains. **(c)** Loss of both *PXY* and *ER* family of genes results in loss of distinct tissue domains. Plants also fail to make the transition to true secondary growth. **(d–e)** Stem sections stained for lignin, adapted from Yang *et al*. [94], with the permission from the publisher. **(d)** WT shows lignin deposition and thus xylem differentiation in a single arc (d). *xvp-d/+* lines demonstrate premature xylem differentiation in the regions marked by arrowheads.

thus its removal protects the cambium from differentiation [88••].

A ring of receptors

LRR–RLKs of the SOMATIC EMBRYOGENESIS RECEPTOR-LIKE KINASE (SERK) family, including BRI1-ASSOCIATED RECEPTOR KINASE 1 (BAK1), are thought to form complexes with PXY at the plasma membrane in the presence of TDIF (Figure 2a) [89]. BAK1 also functions as a co-receptor for brassinolide with BRASSINOSTEROID INSENSITIVE 1 (BRI1), and as a co-receptor for bacterial flagellin peptide (flg22) with FLAGELLIN SENSING 2 (FLS2), and in these interactions the ligands act as molecular glue for the BAK1–BRI1 and BAK1–FLS2 interaction [90–92]. The PXY–SERK interactions likely differ from those described for other receptors. PXY LRR domains are shorter, and the receptor domain lacks the curvature of BRI1 and FLS2. TDIF binds PXY further from the membrane, clear of the BAK1–PXY interaction site and is thus its function in this respect is distinct in that it is unlikely to mediate a SERK–RLK interaction [93].

In pursuit of other vascular regulators, Yang *et al*. analysed gain-of-function activation-tagging lines, one of which, *xvp-d*, demonstrated *pxy*-like morphology [94] (Figure 2). *XVP* encodes a cambium-expressed transcription factor of the NAC family which surprisingly localised to the plasma membrane. Bimolecular fluorescence complementation (BiFC), a split ubiquitin yeast-two-hybrid system (mbSUS) and a Fluorescence Resonance Energy Transfer (FRET) assay support the notion that XVP binds to the PXY–BAK1

complex (Figures 1 and 2a, d, e). Removal of *XVP* enhanced TDIF activity, suggesting that XVP represses vascular proliferation by allowing xylem differentiation to occur. *xvp-d* gain-of-function lines demonstrated increased *CLE44* expression, while *CLE41* and *CLE44* overexpression lines demonstrated reduced XVP expression. Thus, XVP promotes the expression of TDIF-encoding genes, but suppresses the TDIF signal and is itself repressed by TDIF (Figure 2a) [94].

In the hypocotyl, *ERECTA (ER)* and its paralogues *ERECTA-LIKE (ERL1)* and *ERECTA-LIKE (ERL2)* have been reported to promote auxin biosynthesis [95]. Of these, *ER* and *ERL1*, have been shown to prevent premature xylem fibre formation, as *er erl1* lines exhibited precocious fibre differentiation [96]. *er* enhances the loss-of-function phenotype for another LRR–RLK, SUPPRESSOR OF BIR-1 (SOBIR1)/EVERSHED (EVR) [97], which is also responsible for preventing early xylem fibre formation in *Arabidopsis* hypocotyls. ER and SOBIR1 physically interact at the plasma membrane to perform this function. ER family members regulate not only the xylem, but also the cambium. ER and ERL1 are thought to restrict radial expansion of hypocotyls as *er erl1* lines exhibit increases in xylem area (Figures 1 and 2a) [96]. By contrast, the *er erl1 erl2* triple mutants demonstrate a reduction in secondary growth [98], thus interplay between these three receptors in the context of cambium regulation requires further investigation.

ER family regulation of vascular development occurs via a genetic interaction with members of the *PXY* gene family. In the absence of the *PXY* gene family (*PXY*, *PXY-LIKE 1 (PXL1)* and *PXL2*), vascular cells are larger, however this increase is dependent upon *ER* and *ERL2*, as *pxy pxl1 pxl2 er erl2* lines have cell sizes similar to those of wild type. Removing all members of both families prevented the transition to true secondary growth, as cell division was vastly reduced and phloem was present in poles rather than a continuous ring as is the case in wild type. Thus, interacting PXY and ER families regulate cell division, cell size, and organisation in the vascular tissue (Figures 1 and 2b, c) [98].

Like *ER* and *ERL1*, a LRR–RLK, MORE LATERAL GROWTH (MOL1), also suppresses cambial activity as *mol1* mutants demonstrated larger cambium-derived domains compared to wild type [99,100]. MOL1 was identified in a set of experiments where *Arabidopsis* inflorescence stem explants were subjected to auxin (NAA) treatments. These treatments initiated cambium formation in the explants which were then subjected to transcriptome analysis. REDUCED IN LATERAL GROWTH (RUL1), a receptor with a positive effect on cambium activity was additionally identified in these experiments [99]. While ER's signal peptides have been determined to belong to the *EPIDERMAL PATTERNING FACTOR LIKE* (*EPFL)* family [101–108], exactly which of them control cell division in the cambium is yet to be determined. Ligands for MOL1, RUL1 and SOBIR1 are also to be discovered.

Ontogeny of the organiser

The cambium represents a group of mostly periclinally dividing cells with the ability to generate xylem and phloem, on its two opposite sides [87••,109,110]. A vascular organizer in xylem cells adjacent to the initiating cambium that is characterized by high auxin levels, imposes stem-cell function on its neighbour to initiate cambial divisions [87••]. Since at the secondary growth stage xylem cells have already undergone programmed cell death thus stripping them from signalling ability, Smetana *et al.* proposed that cell identity information must be passed on earlier, during xylem formation [87••]. Auxin, acting through MP, ARF7 and ARF19, promotes the expression of HD-ZIP III genes, which have been previously reported as regulators of xylem identity [111–114] downstream of auxin [115,116]. Here, they were linked to the correct establishment of the vascular organizer [87••]. *WOX4* and *PXY*, which are required for auxin responses in the cambium [117], were also required in the stem-cell organizer [87••].

While Smetana *et al.* characterised the ability of the xylem to specify the position of the initiating cambium in adjacent cells in the *Arabidopsis* root [87••], Shi *et al.* aimed to explore pattern in the established hypocotyl vasculature [109]. The cambium was found to be separated into three distinct sub-domains in each cell file along the radial axis — proximal, central, and distal. Independently, both Smetana *et al.* and Shi *et al.* defined PXY and WOX4 as part of the xylem-facing side of the cambium, that is the organizer side of the cambium, verifying the importance of these components for the cambium activity [87••,109]. They also confirmed a long-standing hypothesis in which the cambium stem cells (central) are flanked by mother cells of the xylem (proximal) and phloem (distal) within each vascular cell file [118].

Sapling similarities

A significant proportion of the molecular mechanisms controlling cambium growth and development comes from studies of *Arabidopsis*, but evidence suggests that much is conserved in forest trees. One such example is ethylene, which promotes cell division in the cambium of both *Arabidopsis* and poplar [23,119]. In poplar, ethylene-induced *ETHYLENE RESPONSE FACTORS (ERFs)* that were overexpressed altered wood formation and stem diameter [120]. Our understanding of the distribution of auxin and cytokinin in the dividing cambia and phloem arose from experiments in poplar. These patterns are supported by transcript profiling showing that cytokinin

and auxin responses coincide with tissue-specific hormonal gradients. Transgenic *Populus* with elevated cytokinin biosynthesis displayed increases in cambial auxin concentration and a dramatic increase in secondary growth, confirming the auxin–cytokinin connection [62••,121].

Alongside the TDIF-PXY-WOX4 signalling module [122,123], further members of the CLE family also regulate the cambium in poplar. *PttCLE47* positively regulates cell division in the vascular cambium, as its repression led to reduced secondary xylem formation. PttCLE47 appears to act in a cell-autonomous fashion in the vascular cambium [124]. By contrast, *PtrCLE20*, expressed specifically in developing xylem, was found to reduce cambial divisions in part by reducing *PtrWOX4* expression [125]. Thus, CLE peptides influence the cambium from opposing sides; *PttCLE41* (from which TDIF is derived) acting from phloem, *PtrCLE20* from the xylem, and *PttCLE47* operating from within the cambium [122–125].

Conclusions

Interactions between LRR–RLKs, their ligands, cytoplasmic signalling intermediates, and their targets are increasingly well-defined in our understanding of cambium regulation [126,127]. A recent study has proposed a transcriptional network that may explain many of the relationships between these components [86•]. Identification of further signalling elements, such as ligands for MOL1 and RUL1 will help refine this picture. Remaining challenges surround hormones such as gibberellic acid and jasmonic acid, known to contribute to radial growth [24,128], but whose role in the existing networks is largely unexplored. Much of what we know has also been characterised in a single tissue type, but differences in cambium regulation occur along the apical–basal axis of the plant [98] and how those differences underpin variations in morphology remains unclear. Finally, this review has focussed mostly on *Arabidopsis*, and entirely on dicot species. A recent analysis of cambium-regulating genes identified a small number of genes that were absent in the monocot clade [129]. Thus, an important question concerns how these networks may have been modified to give rise to the significantly different scattered vascular morphology of grass species.

Conflict of interest statement

Nothing declared.

Acknowledgements

The authors are grateful to BBSRC for funding awarded to KSB and CMB as part of the NLD doctoral training programme.

Declaration of Competing Interest

The authors report no declarations of interest.

References and recommended reading

Papers of particular interest, published within the period of review, have been highlighted as:

- • of special interest
- •• of outstanding interest

1. Robert HS, Friml J: **Auxin and other signals on the move in plants**. *Nat Chem Biol* 2009, **5**:325-332.
2. Hoad G: **Transport of hormones in the phloem of higher plants**. *Plant Growth Regul* 1995, **16**:173-182.
3. Swarup R, Friml J, Marchant A, Ljung K, Sandberg G, Palme K, Bennett M: **Localization of the auxin permease AUX1 suggests two functionally distinct hormone transport pathways operate in the *Arabidopsis* root apex**. *Genes Dev* 2001, **15**:2648-2653.
4. Hirose N, Takei K, Kuroha T, Kamada-Nobusada T, Hayashi H, Sakakibara H: **Regulation of cytokinin biosynthesis, compartmentalization and translocation**. *J Exp Bot* 2008, **59**:75-83.
5. Bishopp A, Help H, El-Showk S, Weijers D, Scheres B, Friml J, Benková E, Mähönen AP, Helariutta Y: **A mutually inhibitory interaction between auxin and cytokinin specifies vascular pattern in roots**. *Curr Biol* 2011, **21**:917-926.
6. Kudo T, Kiba T, Sakakibara H: **Metabolism and long-distance translocation of cytokinins**. *J Integr Plant Biol* 2010, **52**:53-60.
7. Muraro D, Mellor N, Pound MP, Help H, Lucas M, Chopard J, Byrne HM, Godin C, Hodgman TC, King JR *et al.*: **Integration of hormonal signaling networks and mobile microRNAs is required for vascular patterning in *Arabidopsis* roots**. *Proc Natl Acad Sci* 2014, **111**:857-862.
8. Lavender D, Sweet G, Zaerr J, Hermann R: **Spring shoot growth in Douglas-fir may be initiated by gibberellins exported from the roots**. *Science* 1973, **182**:838-839.
9. Hoad G, Bowen M: **Evidence for gibberellin-like substances in phloem exudate of higher plants**. *Planta* 1968, **82**:22-32.
10. Israelsson M, Sundberg B, Moritz T: **Tissue-specific localization of gibberellins and expression of gibberellin-biosynthetic and signaling genes in wood-forming tissues in aspen**. *Plant J* 2005, **44**:494-504.
11. Everant-Bourbouloux A: **Transport and metabolism of labelled abscisic acid in broad-bean plants (*Vicia faba* L.)**. *Physiol Plant* 1982, **54**:431-439.
12. Ikegami K, Okamoto M, Seo M, Koshiba T: **Activation of abscisic acid biosynthesis in the leaves of *Arabidopsis thaliana* in response to water deficit**. *J Plant Res* 2009, **122**:235.
13. Jiang F, Hartung W: **Long-distance signalling of abscisic acid (ABA): the factors regulating the intensity of the ABA signal**. *J Exp Bot* 2008, **59**:37-43.
14. Zeevaart JA, Boyer GL: **Accumulation and transport of abscisic acid and its metabolites in *Ricinus* and *Xanthium***. *Plant Physiol* 1984, **74**:934-939.
15. Brodersen CR, Roddy AB, Wason JW, McElrone AJ: **Functional status of xylem through time**. *Annu Rev Plant Biol* 2019, **70**:407-433.
16. Kondo Y, Tamaki T, Fukuda H: **Regulation of xylem cell fate**. *Front Plant Sci* 2014, **5**:315.
17. Růžička K, Ursache R, Hejátko J, Helariutta Y: **Xylem development–from the cradle to the grave**. *New Phytol* 2015, **207**:519-535.
18. Anne P, Hardtke CS: **Phloem function and development—biophysics meets genetics**. *Curr Opin Plant Biol* 2018, **43**:22-28.
19. Blob B, Heo J-O, Helariutta Y: **Phloem differentiation: an integrative model for cell specification**. *J Plant Res* 2018, **131**:31-36.
20. Heo JO, Roszak P, Furuta KM, Helariutta Y: **Phloem development: current knowledge and future perspectives**. *Am J Bot* 2014, **101**:1393-1402.

21. López-Salmerón V, Cho H, Tonn N, Greb T: **The phloem as a mediator of plant growth plasticity**. *Curr Biol* 2019, **29**:R173-R181.

22. Otero S, Helariutta Y: **Companion cells: a diamond in the rough**. *J Exp Bot* 2017, **68**:71-78.

23. Love J, Björklund S, Vahala J, Hertzberg M, Kangasjärvi J, Sundberg B: **Ethylene is an endogenous stimulator of cell division in the cambial meristem of Populus**. *Proc Natl Acad Sci* 2009, **106**:5984-5989.

24. Sehr EM, Agusti J, Lehner R, Farmer EE, Schwarz M, Greb T: **Analysis of secondary growth in the *Arabidopsis* shoot reveals a positive role of jasmonate signalling in cambium formation**. *Plant J* 2010, **63**:811-822.

25. Agusti J, Herold S, Schwarz M, Sanchez P, Ljung K, Dun EA, Brewer PB, Beveridge CA, Sieberer T, Sehr EM *et al.*: **Strigolactone signaling is required for auxin-dependent stimulation of secondary growth in plants**. *Proc Natl Acad Sci* 2011, **108**:20242-20247.

26. Gray WM, Del Pozo JC, Walker L, Hobbie L, Risseeuw E, Banks T, Crosby WL, Yang M, Ma H, Estelle M: **Identification of an SCF ubiquitin–ligase complex required for auxin response in *Arabidopsis thaliana***. *Genes Dev* 1999, **13**:1678-1691.

27. Gray WM, Kepinski S, Rouse D, Leyser O, Estelle M: **Auxin regulates SCF TIR1-dependent degradation of AUX/IAA proteins**. *Nature* 2001, **414**:271-276.

28. Kieffer M, Neve J, Kepinski S: **Defining auxin response contexts in plant development**. *Curr Opin Plant Biol* 2010, **13**:12-20.

29. Mockaitis K, Estelle M: **Auxin receptors and plant development: a new signaling paradigm**. *Annu Rev Cell Dev Biol* 2008, **24**.

30. Ulmasov T, Hagen G, Guilfoyle TJ: **ARF1, a transcription factor that binds to auxin response elements**. *Science* 1997, **276**:1865-1868.

31. Ulmasov T, Hagen G, Guilfoyle TJ: **Activation and repression of transcription by auxin-response factors**. *Proc Natl Acad Sci* 1999, **96**:5844-5849.

32. • Hardtke CS, Berleth T: **The *Arabidopsis* gene MONOPTEROS encodes a transcription factor mediating embryo axis formation and vascular development**. *EMBO J* 1998, **17**:1405-1411

Role of MP in early vascular development, in establishing the vascular cylinder.

33. Berleth T, Jurgens G: **The role of the monopteros gene in organising the basal body region of the *Arabidopsis* embryo**. *Development* 1993, **118**:575-587.

34. Bhatia N, Bozorg B, Larsson A, Ohno C, Jönsson H, Heisler MG: **Auxin acts through MONOPTEROS to regulate plant cell polarity and pattern phyllotaxis**. *Curr Biol* 2016, **26**:3202-3208.

35. Przemeck GK, Mattsson J, Hardtke CS, Sung ZR, Berleth T: **Studies on the role of the *Arabidopsis* gene MONOPTEROS in vascular development and plant cell axialization**. *Planta* 1996, **200**:229-237.

36. Wenzel CL, Schuetz M, Yu Q, Mattsson J: **Dynamics of MONOPTEROS and PIN-FORMED1 expression during leaf vein pattern formation in *Arabidopsis thaliana***. *Plant J* 2007, **49**:387-398.

37. Krogan NT, Marcos D, Weiner AI, Berleth T: **The auxin response factor MONOPTEROS controls meristem function and organogenesis in both the shoot and root through the direct regulation of PIN genes**. *New Phytol* 2016, **212**:42-50.

38. •• Han S, Cho H, Noh J, Qi J, Jung H-J, Nam H, Lee S, Hwang D, Greb T, Hwang I: **BIL1-mediated MP phosphorylation integrates PXY and cytokinin signalling in secondary growth**. *Nat Plants* 2018, **4**:605-614

Cross-talk between PXY and auxin signalling via GSK3-dependent phosphorylation of MP.

39. Brackmann K, Qi J, Gebert M, Jouannet V, Schlamp T, Grünwald K, Wallner E-S, Novikova DD, Levitsky VG, Agustí J *et al.*: **Spatial specificity of auxin responses coordinates wood formation**. *Nat Commun* 2018, **9**:1-15.

40. Matsumoto-Kitano M, Kusumoto T, Tarkowski P, Kinoshita-Tsujimura K, Václavíková K, Miyawaki K, Kakimoto T: **Cytokinins are central regulators of cambial activity**. *Proc Natl Acad Sci* 2008, **105**:20027-20031.

41. Hejátko J, Ryu H, Kim G-T, Dobešová R, Choi S, Choi SM, Souček P, Horák J, Pekárová B, Palme K *et al.*: **The histidine kinases CYTOKININ-INDEPENDENT1 and *ARABIDOPSIS* HISTIDINE KINASE2 and 3 regulate vascular tissue development in *Arabidopsis* shoots**. *Plant Cell* 2009, **21**:2008-2021.

42. Kieber JJ, Schaller GE: **The perception of cytokinin: a story 50 years in the making**. *Plant Physiol* 2010, **154**:487-492.

43. Inoue T, Higuchi M, Hashimoto Y, Seki M, Kobayashi M, Kato T, Tabata S, Shinozaki K, Kakimoto T: **Identification of CRE1 as a cytokinin receptor from *Arabidopsis***. *Nature* 2001, **409**:1060-1063.

44. Nishimura C, Ohashi Y, Sato S, Kato T, Tabata S, Ueguchi C: **Histidine kinase homologs that act as cytokinin receptors possess overlapping functions in the regulation of shoot and root growth in *Arabidopsis***. *Plant Cell* 2004, **16**:1365-1377.

45. Ueguchi C, Sato S, Kato T, Tabata S: **The AHK4 gene involved in the cytokinin-signaling pathway as a direct receptor molecule in *Arabidopsis thaliana***. *Plant Cell Physiol* 2001, **42**:751-755.

46. Hutchison CE, Li J, Argueso C, Gonzalez M, Lee E, Lewis MW, Maxwell BB, Perdue TD, Schaller GE, Alonso JM *et al.*: **The *Arabidopsis* histidine phosphotransfer proteins are redundant positive regulators of cytokinin signaling**. *Plant Cell* 2006, **18**:3073-3087.

47. Mähönen AP, Bishopp A, Higuchi M, Nieminen KM, Kinoshita K, Törmäkangas K, Ikeda Y, Oka A, Kakimoto T, Helariutta Y: **Cytokinin signaling and its inhibitor AHP6 regulate cell fate during vascular development**. *Science* 2006, **311**:94-98.

48. Suzuki T, Imamura A, Ueguchi C, Mizuno T: **Histidine-containing phosphotransfer (HPt) signal transducers implicated in His-to-Asp phosphorelay in *Arabidopsis***. *Plant Cell Physiol* 1998, **39**:1258-1268.

49. Moreira S, Bishopp A, Carvalho H, Campilho A: **AHP6 inhibits cytokinin signaling to regulate the orientation of pericycle cell division during lateral root initiation**. *PLoS One* 2013, **8**.

50. D'Agostino IB, Deruere J, Kieber JJ: **Characterization of the response of the *Arabidopsis* response regulator gene family to cytokinin**. *Plant Physiol* 2000, **124**:1706-1717.

51. Hwang I, Sheen J: **Two-component circuitry in *Arabidopsis* cytokinin signal transduction**. *Nature* 2001, **413**:383-389.

52. Mason MG, Li J, Mathews DE, Kieber JJ, Schaller GE: **Type-B response regulators display overlapping expression patterns in *Arabidopsis***. *Plant Physiol* 2004, **135**:927-937.

53. Tajima Y, Imamura A, Kiba T, Amano Y, Yamashino T, Mizuno T: **Comparative studies on the type-B response regulators revealing their distinctive properties in the His-to-Asp phosphorelay signal transduction of *Arabidopsis thaliana***. *Plant Cell Physiol* 2004, **45**:28-39.

54. Sakai H, Honma T, Aoyama T, Sato S, Kato T, Tabata S, Oka A: **ARR1, a transcription factor for genes immediately responsive to cytokinins**. *Science* 2001, **294**:1519-1521.

55. Mason MG, Mathews DE, Argyros DA, Maxwell BB, Kieber JJ, Alonso JM, Ecker JR, Schaller GE: **Multiple type-B response regulators mediate cytokinin signal transduction in *Arabidopsis***. *Plant Cell* 2005, **17**:3007-3018.

56. Blilou I, Xu J, Wildwater M, Willemsen V, Paponov I, Friml J, Heidstra R, Aida M, Palme K, Scheres B: **The PIN auxin efflux facilitator network controls growth and patterning in *Arabidopsis* roots**. *Nature* 2005, **433**:39-44.

57. Ioio RD, Linhares FS, Scacchi E, Casamitjana-Martinez E, Heidstra R, Costantino P, Sabatini S: **Cytokinins determine *Arabidopsis* root-meristem size by controlling cell differentiation**. *Curr Biol* 2007, **17**:678-682.

58. Ioio RD, Nakamura K, Moubayidin L, Perilli S, Taniguchi M, Morita MT, Aoyama T, Costantino P, Sabatini S: **A genetic**

framework for the control of cell division and differentiation in the root meristem. *Science* 2008, **322**:1380-1384.

59. Müller B, Sheen J: **Cytokinin and auxin interaction in root stem-cell specification during early embryogenesis**. *Nature* 2008, **453**:1094-1097.

60. Růžička K, Šimášková M, Duclercq J, Petrášek J, Zažímalová E, Simon S, Friml J, Van Montagu MC, Benková E: **Cytokinin regulates root meristem activity via modulation of the polar auxin transport**. *Proc Natl Acad Sci* 2009, **106**:4284-4289.

61. Takahashi N, Kajihara T, Okamura C, Kim Y, Katagiri Y, Okushima Y, Matsunaga S, Hwang I, Umeda M: **Cytokinins control endocycle onset by promoting the expression of an APC/C activator in *Arabidopsis* roots**. *Curr Biol* 2013, **23**:1812-1817.

62. •• Tuominen H, Puech L, Fink S, Sundberg B: **A radial concentration gradient of indole-3-acetic acid is related to secondary xylem development in hybrid aspen**. *Plant Physiol* 1997, **115**:577-585
Auxin–cytokinin patterning and interaction in the cambium.

63. Werner T, Köllmer I, Bartrina I, Holst K, Schmülling T: **New insights into the biology of cytokinin degradation**. *Plant Biol* 2006, **8**:371-381.

64. Nordström A, Tarkowski P, Tarkowska D, Norbaek R, Åstot C, Dolezal K, Sandberg G: **Auxin regulation of cytokinin biosynthesis in *Arabidopsis thaliana*: a factor of potential importance for auxin–cytokinin-regulated development**. *Proc Natl Acad Sci* 2004, **101**:8039-8044.

65. Tanaka M, Takei K, Kojima M, Sakakibara H, Mori H: **Auxin controls local cytokinin biosynthesis in the nodal stem in apical dominance**. *Plant J* 2006, **45**:1028-1036.

66. De Rybel B, Adibi M, Breda AS, Wendrich JR, Smit ME, Novák O, Yamaguchi N, Yoshida S, Van Isterdael G, Palovaara J *et al.*: **Integration of growth and patterning during vascular tissue formation in *Arabidopsis***. *Science* 2014, **345**:1255215.

67. Schlereth A, Möller B, Liu W, Kientz M, Flipse J, Rademacher EH, Schmid M, Jürgens G, Weijers D: **MONOPTEROS controls embryonic root initiation by regulating a mobile transcription factor**. *Nature* 2010, **464**:913-916.

68. Pernisová M, Klíma P, Horák J, Válková M, Malbeck J, Souček P, Reichman P, Hoyerová K, Dubová J, Friml J *et al.*: **Cytokinins modulate auxin-induced organogenesis in plants via regulation of the auxin efflux**. *Proc Natl Acad Sci* 2009, **106**:3609-3614.

69. Šimášková M, O'Brien JA, Khan M, Van Noorden G, Ötvös K, Vieten A, De Clercq I, Van Haperen JMA, Cuesta C, Hoyerová K *et al.*: **Cytokinin response factors regulate PIN-FORMED auxin transporters**. *Nat Commun* 2015, **6**:8717.

70. Jones B, Gunnerås SA, Petersson SV, Tarkowski P, Graham N, May S, Dolezal K, Sandberg G, Ljung K: **Cytokinin regulation of auxin synthesis in *Arabidopsis* involves a homeostatic feedback loop regulated via auxin and cytokinin signal transduction**. *Plant Cell* 2010, **22**:2956-2969.

71. Smet W, Sevilem I, de Luis Balaguer MA, Wybouw B, Mor E, Miyashima S, Blob B, Roszak P, Jacobs TB, Boekschoten M *et al.*: **DOF2. 1 controls cytokinin-dependent vascular cell proliferation downstream of TMO5/LHW**. *Curr Biol* 2019, **29**:520-529 e526.

72. Miyashima S, Roszak P, Sevilem I, Toyokura K, Blob B, Heo J-O, Mellor N, Help-Rinta-Rahko H, Otero S, Smet W *et al.*: **Mobile PEAR transcription factors integrate positional cues to prime cambial growth**. *Nature* 2019, **565**:490-494.

73. Guo Y, Qin G, Gu H, Qu L-J: **Dof5.6/HCA2, a Dof transcription factor gene, regulates interfascicular cambium formation and vascular tissue development in *Arabidopsis***. *Plant Cell* 2009, **21**:3518-3534.

74. Fisher K, Turner S: **PXY, a receptor-like kinase essential for maintaining polarity during plant vascular-tissue development**. *Curr Biol* 2007, **17**:1061-1066.

75. • Hirakawa Y, Shinohara H, Kondo Y, Inoue A, Nakanomyo I, Ogawa M, Sawa S, Ohashi-Ito K, Matsubayashi Y, Fukuda H: **Non-cell-autonomous control of vascular stem cell fate by a CLE peptide/receptor system**. *Proc Natl Acad Sci* 2008, **105**:15208-15213
Identification of the interaction between ligand TDIF and the TDR/PXY receptor.

76. Ito Y, Nakanomyo I, Motose H, Iwamoto K, Sawa S, Dohmae N, Fukuda H: **Dodeca-CLE peptides as suppressors of plant stem cell differentiation**. *Science* 2006, **313**:842-845.

77. Etchells JP, Turner SR: **The PXY-CLE41 receptor ligand pair defines a multifunctional pathway that controls the rate and orientation of vascular cell division**. *Development* 2010, **137**:767-774.

78. Etchells JP, Provost CM, Mishra L, Turner SR: **WOX4 and WOX14 act downstream of the PXY receptor kinase to regulate plant vascular proliferation independently of any role in vascular organisation**. *Development* 2013, **140**:2224-2234.

79. Hirakawa Y, Kondo Y, Fukuda H: **TDIF peptide signaling regulates vascular stem cell proliferation via the WOX4 homeobox gene in *Arabidopsis***. *Plant Cell* 2010, **22**:2618-2629.

80. Clark SE, Running MP, Meyerowitz EM: **CLAVATA3 is a specific regulator of shoot and floral meristem development affecting the same processes as CLAVATA1**. *Development* 1995, **121**:2057-2067.

81. Clark SE, Williams RW, Meyerowitz EM: **The CLAVATA1 gene encodes a putative receptor kinase that controls shoot and floral meristem size in *Arabidopsis***. *Cell* 1997, **89**:575-585.

82. Brand U, Fletcher JC, Hobe M, Meyerowitz EM, Simon R: **Dependence of stem cell fate in *Arabidopsis* on a feedback loop regulated by CLV3 activity**. *Science* 2000, **289**:617-619.

83. Schoof H, Lenhard M, Haecker A, Mayer KF, Jürgens G, Laux T: **The stem cell population of *Arabidopsis* shoot meristems is maintained by a regulatory loop between the CLAVATA and WUSCHEL genes**. *Cell* 2000, **100**:635-644.

84. Haecker A, Gross-Hardt R, Geiges B, Sarkar A, Breuninger H, Herrmann M, Laux T: **Expression dynamics of WOX genes mark cell fate decisions during early embryonic patterning in *Arabidopsis thaliana***. *Development* 2004, **131**:657-668.

85. Sarkar AK, Luijten M, Miyashima S, Lenhard M, Hashimoto T, Nakajima K, Scheres B, Heidstra R, Laux T: **Conserved factors regulate signalling in *Arabidopsis thaliana* shoot and root stem cell organizers**. *Nature* 2007, **446**:811-814.

86. • Smit ME, McGregor SR, Sun H, Gough C, Bågman A-M, Soyars CL, Kroon JT, Gaudinier A, Williams CJ, Yang X *et al.*: **A PXY-mediated transcriptional network integrates signaling mechanisms to control vascular development in *Arabidopsis***. *Plant Cell* 2020, **32**:319-335
Intergration of multiple signalling components into a single network.

87. •• Smetana O, Mäkilä R, Lyu M, Amiryousefi A, Rodriguez FS, Wu M-F, Sole-Gil A, Gavarron ML, Siligato R, Miyashima S *et al.*: **High levels of auxin signalling define the stem-cell organizer of the vascular cambium**. *Nature* 2019, **565**:485-489
Identification of a cambium organiser and a bifacial nature of the cambium through cell lineage tracing and genetic studies.

88. •• Kondo Y, Ito T, Nakagami H, Hirakawa Y, Saito M, Tamaki T, Shirasu K, Fukuda H: **Plant GSK3 proteins regulate xylem cell differentiation downstream of TDIF–TDR signalling**. *Nat Commun* 2014, **5**:1-11
Integration of the GSK3s into the PXY signalling pathway via identification of protein interactions and genetics.

89. Zhang H, Lin X, Han Z, Wang J, Qu L-J, Chai J: **SERK family receptor-like kinases function as co-receptors with PXY for plant vascular development**. *Mol Plant* 2016, **9**:1406-1414.

90. Sun Y, Li L, Macho AP, Han Z, Hu Z, Zipfel C, Zhou J-M, Chai J: **Structural basis for flg22-induced activation of the *Arabidopsis* FLS2-BAK1 immune complex**. *Science* 2013, **342**:624-628.

91. Hothorn M, Belkhadir Y, Dreux M, Dabi T, Noel JP, Wilson IA, Chory J: **Structural basis of steroid hormone perception by the receptor kinase BRI1**. *Nature* 2011, **474**:467-471.

92. She J, Han Z, Kim T-W, Wang J, Cheng W, Chang J, Shi S, Wang J, Yang M, Wang Z-Y *et al.*: **Structural insight into brassinosteroid perception by BRI1**. *Nature* 2011, **474**:472-476.

93. Morita J, Kato K, Nakane T, Kondo Y, Fukuda H, Nishimasu H, Ishitani R, Nureki O: **Crystal structure of the plant receptor-like kinase TDR in complex with the TDIF peptide**. *Nat Commun* 2016, **7**:12383.

94. Yang JH, Lee KH, Du Q, Yang S, Yuan B, Qi L, Wang H: **A membrane-associated NAC domain transcription factor XVP interacts with TDIF co-receptor and regulates vascular meristem activity**. *New Phytol* 2020, **226**:59-74.

95. Qu X, Zhao Z, Tian Z: **ERECTA regulates cell elongation by activating auxin biosynthesis in *Arabidopsis thaliana***. *Front Plant Sci* 2017, **8**:1688.

96. Ikematsu S, Tasaka M, Torii KU, Uchida N: **ERECTA-family receptor kinase genes redundantly prevent premature progression of secondary growth in the *Arabidopsis* hypocotyl**. *New Phytol* 2017, **213**:1697-1709.

97. Milhinhos A, Vera-Sirera F, Blanco-Touriñán N, Mari-Carmona C, Carrió-Seguí À, Forment J, Champion C, Thamm A, Urbez C, Prescott H *et al.*: **SOBIR1/EVR prevents precocious initiation of fiber differentiation during wood development through a mechanism involving BP and ERECTA**. *Proc Natl Acad Sci* 2019, **116**:18710-18716.

98. Wang N, Bagdassarian KS, Doherty RE, Kroon JT, Connor KA, Wang XY, Wang W, Jermyn IH, Turner SR, Etchells JP: **Organ-specific genetic interactions between paralogues of the PXY and ER receptor kinases enforce radial patterning in *Arabidopsis* vascular tissue**. *Development* 2019, **146**:dev177105.

99. Agusti J, Lichtenberger R, Schwarz M, Nehlin L, Greb T: **Characterization of transcriptome remodeling during cambium formation identifies MOL1 and RUL1 as opposing regulators of secondary growth**. *PLoS Genet* 2011, **7**.

100. Gursanscky NR, Jouannet V, Grünwald K, Sanchez P, Laaber-Schwarz M, Greb T: **MOL 1 is required for cambium homeostasis in *Arabidopsis***. *Plant J* 2016, **86**:210-220.

101. Abrash EB, Bergmann DC: **Regional specification of stomatal production by the putative ligand CHALLAH**. *Development* 2010, **137**:447-455.

102. Abrash EB, Davies KA, Bergmann DC: **Generation of signaling specificity in *Arabidopsis* by spatially restricted buffering of ligand–receptor interactions**. *Plant Cell* 2011, **23**:2864-2879.

103. Hara K, Kajita R, Torii KU, Bergmann DC, Kakimoto T: **The secretory peptide gene EPF1 enforces the stomatal one-cell-spacing rule**. *Genes Dev* 2007, **21**:1720-1725.

104. Hara K, Yokoo T, Kajita R, Onishi T, Yahata S, Peterson KM, Torii KU, Kakimoto T: **Epidermal cell density is autoregulated via a secretory peptide, EPIDERMAL PATTERNING FACTOR 2 in *Arabidopsis* leaves**. *Plant Cell Physiol* 2009, **50**:1019-1031.

105. Hunt L, Gray JE: **The signaling peptide EPF2 controls asymmetric cell divisions during stomatal development**. *Curr Biol* 2009, **19**:864-869.

106. Hunt L, Bailey KJ, Gray JE: **The signalling peptide EPFL9 is a positive regulator of stomatal development**. *New Phytol* 2010, **186**:609-614.

107. Uchida N, Lee JS, Horst RJ, Lai H-H, Kajita R, Kakimoto T, Tasaka M, Torii KU: **Regulation of inflorescence architecture by intertissue layer ligand–receptor communication between endodermis and phloem**. *Proc Natl Acad Sci* 2012, **109**:6337-6342.

108. Uchida N, Tasaka M: **Regulation of plant vascular stem cells by endodermis-derived EPFL-family peptide hormones and phloem-expressed ERECTA-family receptor kinases**. *J Exp Bot* 2013, **64**:5335-5343.

109. Shi D, Lebovka I, López-Salmerón V, Sanchez P, Greb T: **Bifacial cambium stem cells generate xylem and phloem during radial plant growth**. *Development* 2019, **146**.

110. Bossinger G, Spokevicius AV: **Sector analysis reveals patterns of cambium differentiation in poplar stems**. *J Exp Bot* 2018, **69**:4339-4348.

111. Carlsbecker A, Lee J-Y, Roberts CJ, Dettmer J, Lehesranta S, Zhou J, Lindgren O, Moreno-Risueno MA, Vatén A, Thitamadee S *et al.*: **Cell signalling by microRNA165/6 directs gene dose-dependent root cell fate**. *Nature* 2010, **465**:316-321.

112. Izhaki A, Bowman JL: **KANADI and class III HD-zip gene families regulate embryo patterning and modulate auxin flow during embryogenesis in *Arabidopsis***. *Plant Cell* 2007, **19**:495-508.

113. Ohashi-Ito K, Fukuda H: **HD-Zip III homeobox genes that include a novel member, ZeHB-13 (*Zinnia*)/ATHB-15 (*Arabidopsis*), are involved in procambium and xylem cell differentiation**. *Plant Cell Physiol* 2003, **44**:1350-1358.

114. Ursache R, Miyashima S, Chen Q, Vatén A, Nakajima K, Carlsbecker A, Zhao Y, Helariutta Y, Dettmer J: **Tryptophan-dependent auxin biosynthesis is required for HD-ZIP III-mediated xylem patterning**. *Development* 2014, **141**:1250-1259.

115. Zhou G-K, Kubo M, Zhong R, Demura T, Ye Z-H: **Overexpression of miR165 affects apical meristem formation, organ polarity establishment and vascular development in *Arabidopsis***. *Plant Cell Physiol* 2007, **48**:391-404.

116. Baima S, Nobili F, Sessa G, Lucchetti S, Ruberti I, Morelli G: **The expression of the Athb-8 homeobox gene is restricted to provascular cells in *Arabidopsis thaliana***. *Development* 1995, **121**:4171-4182.

117. Suer S, Agusti J, Sanchez P, Schwarz M, Greb T: **WOX4 imparts auxin responsiveness to cambium cells in *Arabidopsis***. *Plant Cell* 2011, **23**:3247-3259.

118. Esau K: **Vascular cambium**. *Anatomy of Seed Plants*. New York: John Wiley & Sons Inc; 1960.

119. Etchells JP, Provost CM, Turner SR: **Plant vascular cell division is maintained by an interaction between PXY and ethylene signalling**. *PLoS Genet* 2012, **8**:e1002997.

120. Vahala J, Felten J, Love J, Gorzsás A, Gerber L, Lamminmäki A, Kangasjärvi J, Sundberg B: **A genome-wide screen for ethylene-induced Ethylene Response Factors (ERF s) in hybrid aspen stem identifies ERF genes that modify stem growth and wood properties**. *New Phytol* 2013, **200**:511-522.

121. Immanen J, Nieminen K, Smolander O-P, Kojima M, Serra JA, Koskinen P, Zhang J, Elo A, Mähönen AP, Street N *et al.*: **Cytokinin and auxin display distinct but interconnected distribution and signaling profiles to stimulate cambial activity**. *Curr Biol* 2016, **26**:1990-1997.

122. Kucukoglu M, Nilsson J, Zheng B, Chaabouni S, Nilsson O: **WUSCHEL-RELATED HOMEOBOX 4 (WOX 4)-like genes regulate cambial cell division activity and secondary growth in Populus trees**. *New Phytol* 2017, **215**:642-657.

123. Etchells JP, Mishra LS, Kumar M, Campbell L, Turner SR: **Wood formation in trees is increased by manipulating PXY-regulated cell division**. *Curr Biol* 2015, **25**:1050-1055.

124. Kucukoglu M, Chaabouni S, Zheng B, Mähönen AP, Helariutta Y, Nilsson O: **Peptide encoding *Populus* CLV3/ESR-RELATED 47 (PttCLE47) promotes cambial development and secondary xylem formation in hybrid aspen**. *New Phytol* 2019.

125. Zhu Y, Song D, Zhang R, Luo L, Cao S, Huang C, Sun J, Gui J, Li L: **A xylem-produced peptide PtrCLE20 inhibits vascular cambium activity in *Populus***. *Plant Biotechnol J* 2020, **18**:195-206.

126. Olsson V, Joos L, Zhu S, Gevaert K, Butenko MA, De Smet I: **Look closely, the beautiful may be small: precursor-derived peptides in plants**. *Annu Rev Plant Biol* 2019, **70**:153-186.

127. Fukuda H, Hardtke CS: **Peptide signaling pathways in vascular differentiation**. *Plant Physiol* 2020, **182**:1636-1644.

128. Ragni L, Nieminen K, Pacheco-Villalobos D, Sibout R, Schwechheimer C, Hardtke CS: **Mobile gibberellin directly stimulates *Arabidopsis* hypocotyl xylem expansion**. *Plant Cell* 2011, **23**:1322-1336.

129. Roodt D, Li Z, Van de Peer Y, Mizrachi E: **Loss of wood formation genes in monocot genomes**. *Genome Biol Evol* 2019, **11**:1986-1996.

Appendix B

Standard Operating Procedure for Extracting Cell Morphology Using MATLAB

The guideline below outlines the steps for extracting the intrinsic properties of plant vascular cells using microscope images and MATLAB tools. The example is provided for wild type plants and involves a manual selection step. In the case of simpler or more colour-defined objects, the process of selection could be automated.

I. Cell Selection

In this section, we outline the manual selection process used to prepare the data for analysis.

1. Obtain image of known size/calibration
2. Load it in GIMP or another similar software
3. Identify the 'Fuzzy Select Tool' or an equivalent from the programme Toolbox (Fig. 1).

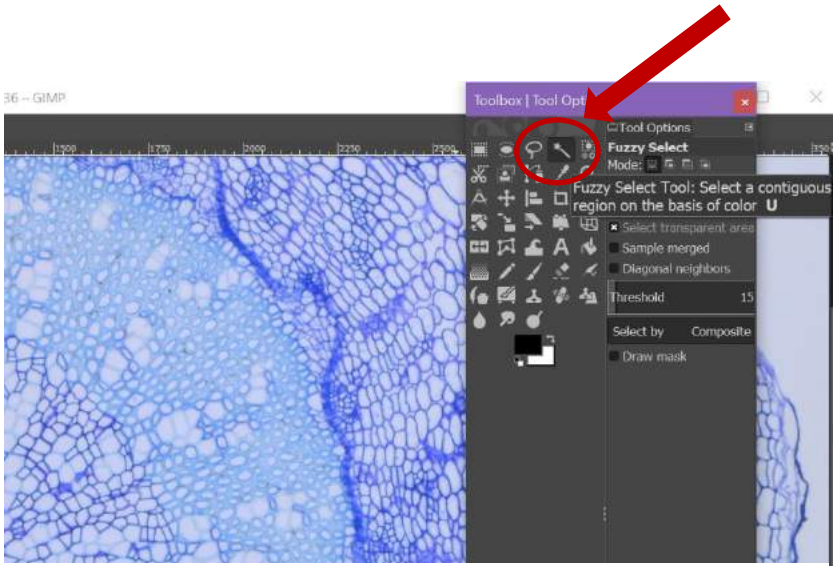

Fig. 1

4. Identify the object (in this case cell) of interest, adjusting the Fuzzy Select Tool threshold as required (Fig. 3).

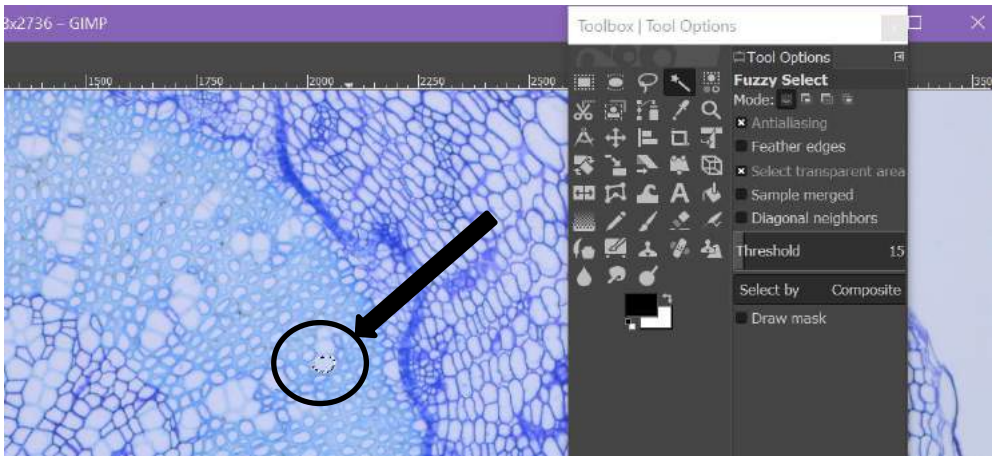

Fig. 2

5. Next, assign your object a colour, with a simple RGB code that can be tracked using MATLAB tools (e.g. ‘red’ (255,0,0)) (Fig. 3).
6. Use Paintbrush or Bucket Fill to colour object (Fig. 3).

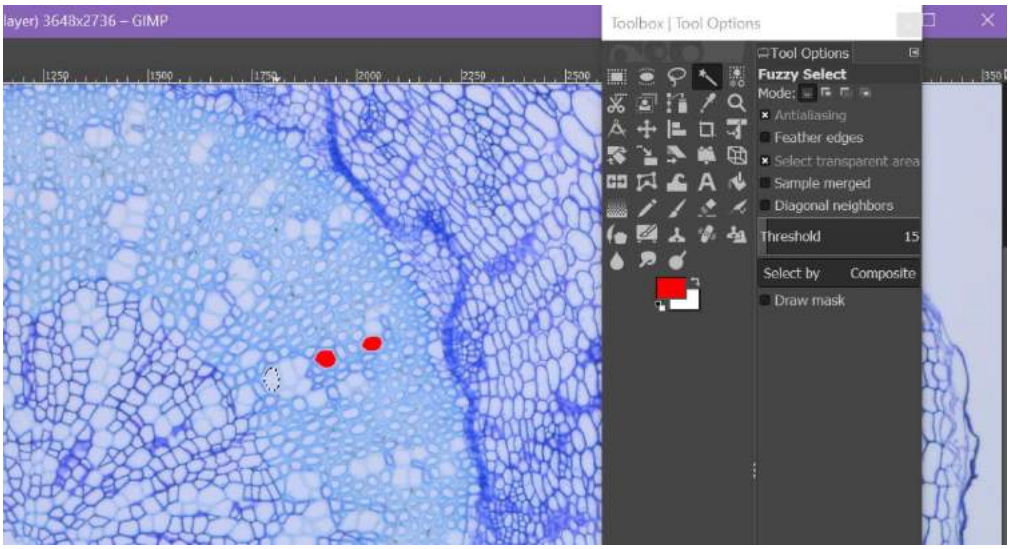

Fig. 3

7. Assign objects of the same type the same colour (Fig. 3).
8. Double-check for defects in colouring/missing areas and correct for those. Note that errors depend on image quality, bias in two-dimensional imaging and accuracy of software should be accounted for. Consistency in choice and method of selection/colouring is imperative for optimal results.

Note: Object colour code can be checked in MATLAB by reading an image X and applying the command ‘impixel(X)’ which allows the user to directly select a pixel and receive as an output its RGB code.

II. MATLAB Procedure

In this section, the MATLAB procedure used to analyse the image data prepared as per the section above is described. The code can be optimised depending on the user requirements. In the section “Main function”, we discuss the part of the programme that is run to obtain results, while the ‘Other functions’ section contains the subfunctions that are responsible for performing operations within the programme.

Main function

The function breaks up a coloured image into binary images corresponding to the different cell types / object types that had been colour-coded. There are different ways to organise and export the data, depending on the analysis requirements. Here, we describe one possible way of organisation.

1. Once you have colour-coded your images, deposit them in a folder (in this case, the folder is called ‘WT’ and the variable ‘sourceWT’ is assigned this folder’s address.)
2. The main function uses the function ‘extractCellProperties’ which acquires the properties of the objects. The function will be described later in this document, in the ‘Other functions’ section.

```
sourceWT = 'C:\Users\NBuser\Documents\MATLAB\Images Paper\Coloured Images\WT';
[propertiesXylem_WT,propertiesFiber_WT,propertiesPhloem_WT,propertiesParynchema_WT]=extractCellProperties(sourceWT);
```

3. The next part of the main function organises your output. It creates a vector of column names, then use the function 'AssignSpecies' to add 'WT' as the corresponding name to all rows that contain data for cells from 'WT' images. Use the function 'assignCellType' to give cell type names to the corresponding data from those cell types (assign row name 'xylem' for a data row with data for an object of type 'xylem').

```
CellProperties={'Species' 'CellType' 'CellArea' 'Ratio' 'Perimeter'};

%name species for each matrix
SpeciesWT='WT';
[Species_WT_Xy,Species_WT_Fi,Species_WT_Ph,Species_WT_Pa]=assignSpecies(propertiesXylem_WT,propertiesFiber_WT,propertiesPhloem_WT,propertiesParynchema_WT,SpeciesWT);

%assign names to the cell types in WT
[cellType_WT_Xy,cellType_WT_Fi,cellType_WT_Ph,cellType_WT_Pa]=assignCellTypes(propertiesXylem_WT,propertiesFiber_WT,propertiesPhloem_WT,propertiesParynchema_WT);
```

4. Next, the main function creates a table with the extracted properties.

```
%create tables with the properties
%add variable names for each
%For WT
WT_Table_Xy = table(Species_WT_Xy, cellType_WT_Xy,
propertiesXylem_WT(:,2),propertiesXylem_WT(:,3),propertiesXylem_WT(:,4)); %the name of the rows come after 'RowNames'
WT_Table_Xy.Properties.VariableNames = CellProperties;

WT_Table_Fi = table(Species_WT_Fi, cellType_WT_Fi,
propertiesFiber_WT(:,2),propertiesFiber_WT(:,3),propertiesFiber_WT(:,4)); %the name of the rows come after 'RowNames'
WT_Table_Fi.Properties.VariableNames = CellProperties;

WT_Table_Ph = table(Species_WT_Ph, cellType_WT_Ph,
propertiesPhloem_WT(:,2),propertiesPhloem_WT(:,3),propertiesPhloem_WT(:,4)); %the name of the rows come after 'RowNames'
WT_Table_Ph.Properties.VariableNames = CellProperties;

WT_Table_Pa = table(Species_WT_Pa, cellType_WT_Pa,
propertiesParynchema_WT(:,2),propertiesParynchema_WT(:,3),propertiesParynchema_WT(:,4)); %the name of the rows come after 'RowNames'
WT_Table_Pa.Properties.VariableNames = CellProperties;
```

5. Finally, spreadsheets with data for each cell type are created.

```
filename_WT_Xy='WT_Table_Xy_tidy.xlsx';
writetable(WT_Table_Xy, filename_WT_Xy);
```

```
filename_WT_Fi='WT_Table_Fi_tidy.xlsx';
writetable(WT_Table_Fi, filename_WT_Fi);

filename_WT_Ph='WT_Table_Ph_tidy.xlsx';
writetable(WT_Table_Ph, filename_WT_Ph);

filename_WT_Pa='WT_Table_Pa_tidy.xlsx';
writetable(WT_Table_Pa, filename_WT_Pa);
```

Other functions

1. The function 'extractCellProperties' take the address of the source folder, loops over the images and outputs the properties of each object type (here, cell types). The sub-functions are described below.

```
function[propertiesXylem,propertiesFiber,propertiesPhloem,propertiesParynchema]=extract
CellProperties(sourceFolder)
images =dir(fullfile(sourceFolder,'*.png'));
numFiles = length(images); %how many images in the folder

%start with a row of zeros to build tables
[propertiesXylem, propertiesFiber, propertiesPhloem, propertiesParynchema] =
deal(zeros(4,1)');

%loop over images
%splitExport splits the images into binary images - white objects on black background
%these can be viewed as connected components of pixels whose properties can
%be extracted (area, perimeter, ellipticity)
%splitExport returns, one image at a time, all the properties for all the
%different cell types for that image.
%the below loops over the images and stacks in a table the properties for
%all images for a specific genotype
for k = length(images):-1:1
[Xylem_Table_Num, Fiber_Table_Num,Phloem_Table_Num,
Parynchema_Table_Num]=splitExport(images(k).name,sourceFolder);
   propertiesXylem=vertcat(propertiesXylem, Xylem_Table_Num);
   propertiesFiber=vertcat(propertiesFiber, Fiber_Table_Num);
   propertiesPhloem=vertcat(propertiesPhloem, Phloem_Table_Num);
   propertiesParynchema=vertcat(propertiesParynchema, Parynchema_Table_Num);
end

%remove zeros and convert pixels to microns
[propertiesXylem, propertiesFiber, propertiesPhloem,
propertiesParynchema]=convert2Microns(propertiesXylem, propertiesFiber,
propertiesPhloem, propertiesParynchema);
```

2. 'splitExport' uses functions 'imagesNew', 'ConnectedComponents' and 'NumberProperties'. It takes the images in the source file and outputs the properties of the cells.

```
function[Xylem_Table_Num_WT, Fiber_Table_Num_WT,Phloem_Table_Num_WT,
Parynchema_Table_Num_WT]=splitExport(baseFileName,source)
```

```
%this function takes the 'name' for a source and the base name for an image
%reads the image and returns table of properties for that image
   fullFileName = fullfile(source, baseFileName); %combine for every filename
   imageRead= imread(fullFileName); %read each image
   [Ix,Ip,Iph,Ipa]=imagesNew(imageRead); %separate the cell images for each
   %for the table of properties
   [Ix_cc,Ip_cc,Iph_cc,Ipa_cc]=ConnectedComponents(Ix,Ip,Iph,Ipa); %connected
components for each cell type
   Xylem_Table_Num_WT=NumberProperties(Ix_cc);
   Fiber_Table_Num_WT=NumberProperties(Ip_cc);
   Phloem_Table_Num_WT=NumberProperties(Iph_cc);
   Parynchema_Table_Num_WT=NumberProperties(Ipa_cc);
```

3. The function 'imagesNew' takes an image and splits it into binary images according to the specified colour-scheme. Note that in 'imagesNew', the RGB codes used must be specific to the data, i.e. the colours chosen in the "Cell Selection" section. The command 'bwareaopen', known as 'area opening', is used to clear noise and removes all connected components with fewer than the specified number of pixels, thus producing another binary image. The specified number of pixels depends on the objects under investigation, and will likely be experiment-specific.

```
function [Ix,Ip,Iph,Ipa]=imagesNew(I)

clc;
[x,y,numberofcolours]=size(I);

%create black images corresponding to each cell type
[Ix,Ip,Iph,Ipa] = deal(0*I);

for i=1:x
   for j=1:y
      if ((I(i,j,1)==254)&&(I(i,j,2)==0)&&(I(i,j,3)==0)) %image for xylem
         Ix(i,j,1)=255;
         Ix(i,j,2)=255;
         Ix(i,j,3)=255;
      elseif ((I(i,j,1)==0)&&(I(i,j,2)==0)&&(I(i,j,3)==254)) %image for fibers
         Ip(i,j,1)=255;
         Ip(i,j,2)=255;
         Ip(i,j,3)=255;
      elseif ((I(i,j,1)==0)&&(I(i,j,2)==255)&&(I(i,j,3)==3))%image for phloem
         Iph(i,j,1)=255;
         Iph(i,j,2)=255;
         Iph(i,j,3)=255;
      elseif ((I(i,j,1)==255)&&(I(i,j,2)==255)&&(I(i,j,3)==0)) %image for parynchema
         Ipa(i,j,1)=255;
         Ipa(i,j,2)=255;
         Ipa(i,j,3)=255;
      end
   end
end
```

```
Ix=im2bw(Ix); %transform into binary image
Ix=bwareaopen(Ix,50);%clear noise


Ip=im2bw(Ip);
Ip=bwareaopen(Ip,20);

Iph=im2bw(Iph);
Iph=bwareaopen(Iph,10);

Ipa=im2bw(Ipa);
Ipa=bwareaopen(Ipa,50);
```

4. The function 'NumerProperties' extracts the area ellipticity and perimeter of the objects.

```
function [NumberPropertiesTable]=NumberProperties(cc) %input connected components,
receive their properties

celldata = regionprops(cc, 'Area','MajorAxisLength','MinorAxisLength', 'Eccentricity',
'Perimeter'); %properties of connected components
cell_number=cc.NumObjects;
cell_areas=[celldata.Area]; %each element is a scalar=actual number of pixels in the region

lambda1=[celldata.MajorAxisLength];
lambda2=[celldata.MinorAxisLength];
ratio=lambda2./lambda1; %create ratio column
cell_perimeter=[celldata.Perimeter];

typeofcellarray = zeros(cell_number, 1);

NumberPropertiesTable(:, 1)= typeofcellarray';
NumberPropertiesTable(:, 2) = cell_areas';
NumberPropertiesTable(:, 3) = ratio';
NumberPropertiesTable(:, 4) = cell_perimeter';
NumberPropertiesTable;
```

5. The function 'ConnectedComponents' extracts the connected components of white pixels in the images. This is done by the command 'bwconncomp' which takes an image and a user-specified connectivity parameter. The connectivity parameter (i.e. how many pixel neighbours of the same colour are required to consider that pixel part of the connected component) are again specified for the particular objects (i.e. the specific cell types). Connectivity can be adjusted according to the requirements of the problem to be solved.

```
function [Ix_cc,Ip_cc,Iph_cc,Ipa_cc]=ConnectedComponents(Ix,Ip,Iph,Ipa)

Ix_cc = bwconncomp(Ix, 8);
Ip_cc = bwconncomp(Ip, 4);
Iph_cc = bwconncomp(Iph, 8);
Ipa_cc = bwconncomp(Ipa, 8);
```

6. The function ‘convert2Microns’, used in ‘extractCellProperties’ converts the data from pixels to microns using a calibration ratio which was measured interactively using a graticule image and the command ‘imtool’ in MATLAB.

```
function[propertiesXylem, propertiesFiber, propertiesPhloem,
propertiesParynchema]=convert2Microns(propertiesXylem, propertiesFiber,
propertiesPhloem, propertiesParynchema)
%the function takes the table of properties of different cell types
%removes first row of zeros
%then uses callibration factors for area and length to convert pixels to
%microns

%calculate spatial and length factors for conversion from pixels to microns
SpatialFactor_Area=[10/33]*[10/33];
SpatialFactor_Length=[10/33];

%remove first row of zeros
propertiesXylem(1,:)=[];
propertiesFiber(1,:)=[];
propertiesPhloem(1,:)=[];
propertiesParynchema(1,:)=[];
%callibrate pixels to microns
propertiesXylem(:,2)=propertiesXylem(:,2)*SpatialFactor_Area;
propertiesXylem(:,4)=propertiesXylem(:,4)*SpatialFactor_Length;

propertiesFiber(:,2)=propertiesFiber(:,2)*SpatialFactor_Area;
propertiesFiber(:,4)=propertiesFiber(:,4)*SpatialFactor_Length;

propertiesPhloem(:,2)=propertiesPhloem(:,2)*SpatialFactor_Area;
propertiesPhloem(:,4)=propertiesPhloem(:,4)*SpatialFactor_Length;

propertiesParynchema(:,2)=propertiesParynchema(:,2)*SpatialFactor_Area;
propertiesParynchema(:,4)=propertiesParynchema(:,4)*SpatialFactor_Length;
```

7. The functions ‘assignSpecies’ and ‘assignCellTypes’ are responsible for organising the data in such a way so as to have each row of data with corresponding genotype (e.g. wild type) and cell type (e.g. xylem, phloem, etc.) information.

```
function[Species_Xy,Species_Fi,Species_Ph,Species_Pa]=assignSpecies(propertiesXylem,
propertiesFiber,propertiesPhloem,propertiesParynchema,speciesName)

Species_Xy=repmat(speciesName,size(propertiesXylem(:,1)),1);
Species_Fi=repmat(speciesName,size(propertiesFiber(:,1)),1);
Species_Ph=repmat(speciesName,size(propertiesPhloem(:,1)),1);
Species_Pa=repmat(speciesName,size(propertiesParynchema(:,1)),1);

function[cellType_Xy,cellType_Fi,cellType_Ph,cellType_Pa]=assignCellTypes(propertiesXyl
em,propertiesFiber,propertiesPhloem,propertiesParynchema)
cellTypes={'Xylem' 'Fiber' 'Phloem' 'Parynchema'};
cellType_Xy=repmat(cellTypes(1),size(propertiesXylem(:,1)),1);
cellType_Fi=repmat(cellTypes(2),size(propertiesFiber(:,1)),1);
cellType_Ph=repmat(cellTypes(3),size(propertiesPhloem(:,1)),1);
cellType_Pa=repmat(cellTypes(4),size(propertiesParynchema(:,1)),1);
```

Appendix C

Plant Signaling & Behavior

ISSN: (Print) 1559-2324 (Online) Journal homepage: https://www.tandfonline.com/loi/kpsb20

Versatile method for quantifying and analyzing morphological differences in experimentally obtained images

Kristine S. Bagdassarian, Katherine A. Connor, Ian H Jermyn & J.Peter Etchells

To cite this article: Kristine S. Bagdassarian, Katherine A. Connor, Ian H Jermyn & J.Peter Etchells (2020) Versatile method for quantifying and analyzing morphological differences in experimentally obtained images, Plant Signaling & Behavior, 15:1, 1693092, DOI: 10.1080/15592324.2019.1693092

To link to this article: https://doi.org/10.1080/15592324.2019.1693092

PLANT SIGNALING & BEHAVIOR
2020, VOL. 15, NO. 1, e1693092 (3 pages)
https://doi.org/10.1080/15592324.2019.1693092

Taylor & Francis
Taylor & Francis Group

ADDENDUM

Versatile method for quantifying and analyzing morphological differences in experimentally obtained images

Kristine S. Bagdassarian [a], Katherine A. Connor [a], Ian H Jermyn [b], and J.Peter Etchells [a]

[a]Department of Biosciences, Durham University, Durham, UK; [b]Department of Mathematical Sciences, Durham University, Durham, UK

ABSTRACT

Analyzing high-resolution images to gain insight into anatomical properties is an essential tool for investigation in many scientific fields. In plant biology, studying plant phenotypes from micrographs is often used to build hypotheses on gene function. In this report, we discuss a bespoke method for inspecting the significance in the differences between the morphologies of several plant mutants at cellular level. By examining a specific example in the literature, we will detail the approach previously used to quantify the effects of two gene families on the vascular development of hypocotyls in *Arabidopsis thaliana*. The method incorporates a MATLAB algorithm and statistical tools which can be modified and enhanced to tailor to different research questions in future studies.

ARTICLE HISTORY
Received 17 September 2019
Revised 8 November 2019
Accepted 11 November 2019

KEYWORDS
Image analysis; xylem; phloem; parenchyma; morphology; method

In many branches of science, an important step in investigating a mechanism or structure involves obtaining high-resolution images of the observed behaviors and/or morphology. In biology, the incorporation of image analysis tools has been increasing in popularity.[1,2,3] Several methods to analyze histology of roots and root architecture were introduced over the past decade[4–6] and more recently, machine-learning-based tools have begun to emerge.[7,8] Additionally, open-source platforms such as LithoGraphX, developed from MorphoGraphX[9] have also been established.

In the study of plant vascular tissue, one means of investigating genetic interactions includes the use of microscopy to image transverse or longitudinal cross-sections of plants and plant mutants. By studying the phenotypes generated through genome editing, it is possible to characterize the contribution of a specific gene to the plant growth and development. However, while an intuitive understanding of the differences between genotypes is crucial for formulating hypotheses and prompting further tests, it is oftentimes difficult to quantify how significant certain variabilities are, especially between mutants with grossly irregular anatomy. Here, we describe a bespoke method for quantifying the vascular mutations between a range of genotypes using a MATLAB algorithm and appropriate statistical tools. This method can be applied for a range of similar research questions in various disciplines but was specifically employed in Wang et al.,[10]to quantify phenotypic variation in *Arabidopsis* stems and hypocotyls. The discussion below may be viewed as an addendum to the Wang et al.,[10] publication, and as an illustrative example to provide clarity of the described approach.

In Wang et al.,[10] we aimed to address the question of how two gene families, the *PHLOEM INTERCALATED WITH XYLEM (PXY)* family of genes (*PX*f)[11] and the *ERECTA (ER)* family of genes (*ER*f)[12] function in concert to coordinate cell division and organization. Here, we will detail the procedure we employed to quantify the morphological discrepancy we observed across different *px*f and *er*f genotypes.

The desired Arabidopsis mutant lines, including those with sextuple mutations across the gene families, were generated through the crossing of previously described lines. A total of six mutant lines were analyzed. The mutant lines were grown using standard protocols, and tissue was prepared for light microscopy imaging following fixation with FAA, embedding in JB4 resin, and sectioning.[10]

To study the morphological differences, six images obtained through brightfield microscopy from each genotype were selected. The focus of our study was four of the main vascular cell types: xylem vessels, xylem fibers, phloem cells, and parenchyma. From each image, a minimum of 10 cell representatives from each cell type were selected from a wedge of a pre-defined size (60°). In order to account for the naturally occurring size variation from the center to border, all the cells along the length of the radius were included. The four cell types were assigned a unique color and using the software GIMP, the cell interiors were manually colored as appropriate (see: Supplemental Data S1).

Next, a MATLAB code was generated to study the properties of the individual cell types across the genotypes. The MATLAB Image Processing Toolbox was used, with the overall logic of the algorithm described below.

The manually manipulated images were separated into folders according to genotype. The programme then looped over the images in that folder. For each image in the folder, four entirely black images of the same size were generated. The original images were scanned, and the pre-defined cell colors were recognized. The entirely black images were then manipulated as follows: whenever a pixel of a 'known' color was identified in a position (i,j), the pixel in position (i,j) in the new black image was colored

CONTACT J. Peter Etchells Peter.Etchells@Durham.ac.uk Department of Biosciences, Durham University, Durham, UK
Supplemental data for this article can be accessed on the publisher's website.

white. This was performed for each individual color, isolating the different cell types for analysis, with one original cross-section image yielding four (new) binary images corresponding to the four cell types of interest (Figure 1; Figure 2).

The new images were read as binary images in the program. The previously selected cells were now represented as white objects on a black background and their properties (area, perimeter, major and minor axis) could be quantified as follows. Each white object represents a connected component of pixels. Specifically, the binary images are scanned by the program as a matrix of pixels, where each region of adjacent pixels with the same value (here, the color white) is assigned a number identity by the program. The various properties of that region can then be measured in pixels (Figure 1(b)).

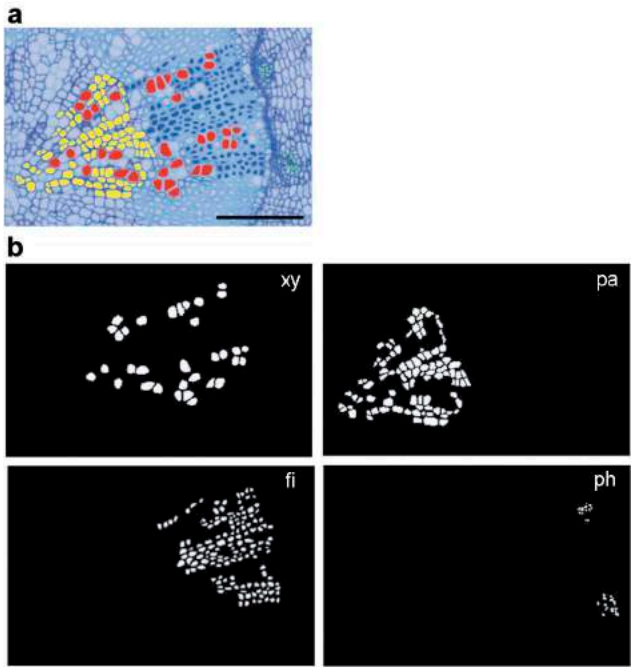

Figure 1. Example of transforming micrograph (a), into binary images (b) with each image corresponding to four cell types: xylem vessels (xy), xylem parenchyma (pa), fibers (fi) and phloem cells (ph). Scale is 100μM in the first image (a). Each white object on the binary images (b) can be investigated as a connected component of white pixels and its properties such as area, perimeter and axis, measured.

The correspondence between pixel size and the actual size can be determined using an image of known size and calculating the micrometer per pixel ratio. Using this method, the data were transformed from pixels to microns/microns squared to calculate the correct perimeter and area of the sampled cells. The ellipticity of the objects (arguably, their level of deformity) were measured as the ratio of major to the minor axis, which is a dimensionless parameter not requiring conversion.

In Wang et al.,[10] the converted measurements were then saved into an excel spreadsheet where each row corresponded to measurements taken from a different plant. This was done in order to implement a nested ANOVA analysis using R (packages multicomp, ggplot2, graphics).

The data from MATLAB was rearranged in an R-readable format of one column of measurements matched to a column of corresponding plant ID's and a column of corresponding plant genotypes. A nested ANOVA analysis and a post hoc Tukey HSD test were performed to identify which genotypes were pairwise significantly different.

The method described above was employed due to its relative ease of design compared to other tools and the ability to be readily adjusted and tailored to a specific research question. For instance, the method can be used to investigate the influence of different factors on organisms through changes in cell deformation and cell size using images of longitudinal and transverse sections. Other questions that

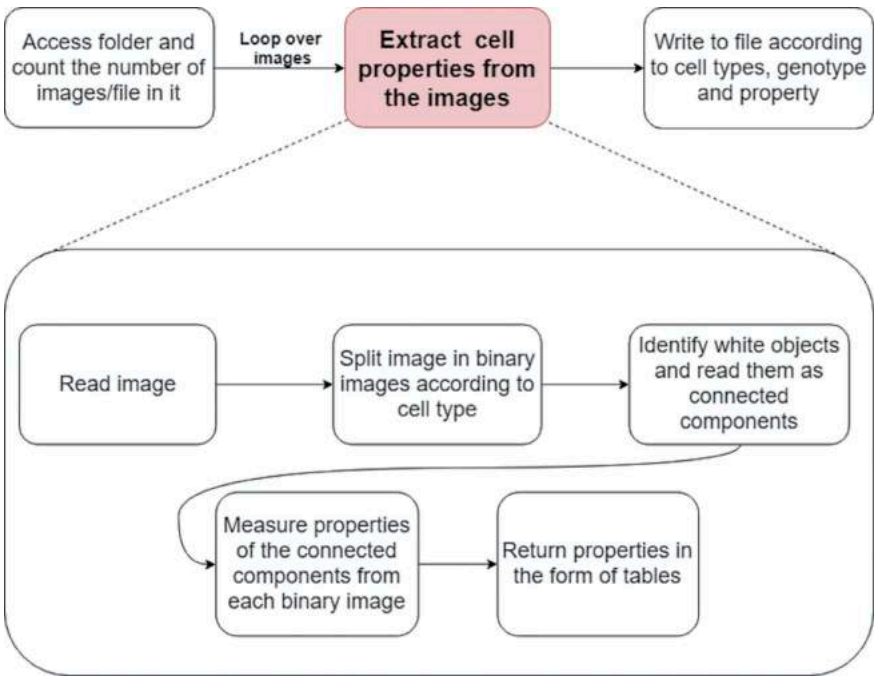

Figure 2. Block diagram illustrating the main parts of the algorithm. The first row of blocks show the key stages of obtaining the data, with the steps comprising the extraction phase in the bubble below.

can be addressed include extracting measurements of bubbles or polyhype structures in physics, engineering, and chemistry as well as topological research (especially regarding objects of similar color scheme) and applying statistical analysis.

The first step of the method represents its largest source of limitations. While in certain instances, where the objects of interest can be defined by a particular color or color range this step can be automated, in cases where the objects are not easily distinguished, the samples must be chosen manually which can be rather time-consuming. Notably, using digital tablets which are supplied with a pen, such as Wacom Drawing Tablets, could speed up the process and improve accuracy. In future studies, one might seek to refine the method for more speedy and automated results. The code used in Wang et al.,[10] can be obtained from Github (https://bit.ly/2Kht0BI).[13] A standard operating procedure is available as Supplemental Data S1.

Funding

This work was supported by the Biotechnology and Biological Sciences Research Council [NLD-DTP].

ORCID

Kristine S. Bagdassarian http://orcid.org/0000-0002-4853-3354
Katherine A. Connor http://orcid.org/0000-0002-7322-1387
Ian H Jermyn http://orcid.org/0000-0002-6546-6173
J.Peter Etchells http://orcid.org/0000-0002-8524-4949

References

1. Gehan MA, Fahlgren N, Abbasi A, Berry JC, Callen ST, Chavez L, Doust AN, Feldman MJ, Gilbert KB, Hodge JG, et al. PlantCV v2: image analysis software for high-throughput plant phenotyping. Peer J. 2017;5:e4088. doi:10.7717/peerj.4088.
2. Wunderling A, Ben Targem M, Barbier de Reuille P, Ragni L. Novel tools for quantifying secondary growth. J Exp Bot. 2016;68 (1):89–95. doi:10.1093/jxb/erw450.
3. Roeder AH, Cunha A, Burl MC, Meyerowitz EM. A computational image analysis glossary for biologists. Development. 2012;139 (17):3071–3080. doi:10.1242/dev.076414.
4. Burton AL, Williams M, Lynch JP, Brown KM. RootScan: software for high-throughput analysis of root anatomical traits. Plant Soil. 2012;357(1–2):189–203. doi:10.1007/s11104-012-1138-2.
5. Lartaud M, Perin C, Courtois B, Thomas E, Henry S, Bettembourg M, Divol F, Lanau N, Artus F, Bureau C, et al. PHIV-RootCell: a supervised image analysis tool for rice root anatomical parameter quantification. Front Plant Sci. 2015;5:790. doi:10.3389/fpls.2014.00790.
6. Chopin J, Laga H, Huang CY, Heuer S, Miklavcic SJ. Rootanalyzer: a cross-section image analysis tool for automated characterization of root cells and tissues. PLoS One. 2015;10(9): e0137655. doi:10.1371/journal.pone.0137655.
7. Sankar M, Nieminen K, Ragni L, Xenarios I, Hardtke C. Automated quantitative histology reveals vascular morphodynamics during arabidopsis hypocotyl secondary growth. Elife. 2014;3:e01567. doi: 10.7554/elife.01567.
8. Hall HC, Fakhrzadeh A, Luengo Hendriks CL, Fischer U. Precision automation of cell type classification and sub-cellular fluorescence quantification from laser scanning confocal images. Front Plant Sci. 2016;7:119. doi:10.3389/fpls.2016.00119.
9. Barbier de Reuille P, Routier-Kierzkowska AL, Kierzkowski D, Bassel GW, Schüpbach T, Tauriello G, Bajpai N, Strauss S, Weber A, Kiss A, et al. MorphoGraphX: A platform for quantifying morphogenesis in 4D. Elife. 2015;4:05864. doi: 10.7554/eLife.05864.
10. Wang N, Bagdassarian KS, Doherty RE, Kroon JT, Connor KA, Wang XY, Wang W, Jermyn IH, Turner SR, Etchells JP. Organ-specific genetic interactions between paralogues of the PXY and ER receptor kinases enforce radial patterning in Arabidopsis vascular tissue. Development. 2019;146(10):dev177105. doi:10.1242/dev.177105.
11. Fisher K, Turner S. PXY, a receptor-like kinase essential for maintaining polarity during plant vascular-tissue development. Curr Biol. 2007;17(12):1061–1066. doi:10.1016/j.cub.2007.05.049.
12. Shpak ED, Berthiaume CT, Hill EJ, Torii KU. Synergistic interaction of three ERECTA-family receptor-like kinases controls Arabidopsis organ growth and flower development by promoting cell proliferation. Development. 2004;131(7):1491–1501. doi:10.1242/dev.01028.
13. Githubcom. GitHub. [Online]. 2019. [accessed 2019 Aug 5]. https://github.com/KristineBagdassarian/PXY-ER_enforce_185radial_growth

Appendix D

© 2019. Published by The Company of Biologists Ltd | Development (2019) 146, dev177105. doi:10.1242/dev.177105

RESEARCH ARTICLE

Organ-specific genetic interactions between paralogues of the *PXY* and *ER* receptor kinases enforce radial patterning in *Arabidopsis* vascular tissue

Ning Wang[1,2,*,¶], Kristine S. Bagdassarian[1,¶], Rebecca E. Doherty[1,‡,¶], Johannes T. Kroon[1], Katherine A. Connor[1], Xiao Y. Wang[3,§], Wei Wang[2], Ian H. Jermyn[4], Simon R. Turner[3] and J. Peter Etchells[1,]**

ABSTRACT

In plants, cells do not migrate. Tissues are frequently arranged in concentric rings; thus, expansion of inner layers is coordinated with cell division and/or expansion of cells in outer layers. In *Arabidopsis* stems, receptor kinases, *PXY* and *ER*, genetically interact to coordinate vascular proliferation and organisation via inter-tissue signalling. The contribution of *PXY* and *ER* paralogues to stem patterning is not known, nor is their function understood in hypocotyls, which undergo considerable radial expansion. Here, we show that removal of all *PXY* and *ER* gene-family members results in profound cell division and organisation defects. In hypocotyls, these plants failed to transition to true radial growth. Gene expression analysis suggested that *PXY* and *ER* cross- and inter-family transcriptional regulation occurs, but it differs between stem and hypocotyl. Thus, *PXY* and *ER* signalling interact to coordinate development in a distinct manner in different organs. We anticipate that such specialised local regulatory relationships, where tissue growth is controlled via signals moving across tissue layers, may coordinate tissue layer expansion throughout the plant body.

KEY WORDS: *Arabidopsis*, Cambium, Phloem, Procambium, Signalling, Xylem

INTRODUCTION

Cell migration is fundamental to the development of animal body plans. By contrast, plant cell walls do not allow cells to migrate, and consequently plant growth and development is entirely a result of differential growth. As such, initiation and elaboration of plant organs occurs via coordinated changes to the orientation and occurrence of cell divisions, and by cell expansion. In *Arabidopsis* embryos, pattern is established early in development. Twenty-eight-cell embryos have already specified the provascular tissue that consists of four cells the centre of the embryo. A layer of endodermal tissue surrounds the provasculature, and an outer layer of epidermal cells has also been specified (ten Hove et al., 2015). Extra tissue types, cortex and pericycle, are subsequently derived from specific rounds of asymmetric cell division (Kajala et al., 2014). In the hypocotyl, the vascular tissue undergoes a transition from diarch to radial symmetry 6-10 days post-germination. Here, cells adjacent to the xylem divide to generate the vascular cambium (Smetana et al., 2019), such that the tissue pattern along the radial axis becomes epidermis-cortex-endodermis-pericycle-phloem-cambium-xylem. As the hypocotyl further expands, the epidermis and cortex are lost in a process that corresponds with periderm specification and proliferation at around 3 weeks post-germination (Wunderling et al., 2018). Thus, a morphology periderm-phloem-cambium-xylem is generated and maintained through the remainder of life of the plant (Chaffey et al., 2002).

Coordination of tissue expansion must occur as the hypocotyl transitions from diarch to radial symmetry, and as organs increase in size. This coordination must incorporate cell division, because cell numbers increase from tens to hundreds to thousands of cells. It must also incorporate cell size, which differs according to cellular function in differentiated cells. Consequently, the *Arabidopsis* hypocotyl represents an interesting model for studying how patterns are maintained through very large increases in plant size, a mechanism that is poorly understood. This organisation contrasts with that of the *Arabidopsis* inflorescence stem, where radial growth is much more limited. Here, radial pattern is defined in the rib zone below the shoot apex, rather than built upon a pre-existing embryonic pattern. The tissue types along the radial axis of the stem also differ. Epidermis, cortex and endodermis are present outside the phloem, procambium and xylem (Fig. 1A). Pith constitutes the cell type at the centre of the stem.

Evidence points to the presence of mechanisms that coordinate the order of tissue layers. In the *Arabidopsis* root, removal of the root tip results in a reorganisation of the organ to enable the formation of a new meristem. Strikingly, stable patterning of tissue layers is established in the reorganised tissue separately from the activity of the stem cell niche. This suggests that tissue layer organisation is independent of stem cell growth (Efroni et al., 2016). Non-cell autonomous signalling represents one mechanism through which tissue layer organisation could be coordinated. A ligand secreted by one tissue could provide positional information to a receptor located in an adjacent cell type. Ligand-receptor pairs that signal between tissue layers and are required for tissue layer organisation have been described. TRACHEARY ELEMENT DIFFERENTIATION INHIBITORY FACTOR (TDIF) is a ligand that is encoded for by three genes, *CLAVATA3-LIKE/ESR-RELATED 41* (*CLE41*), *CLE42* and *CLE44*. TDIF is excreted from the phloem and perceived by a receptor kinase, PHLOEM

[1]Department of Biosciences, Durham University, South Road, Durham, DH1 3LE, UK. [2]College of Life Science, Henan Agricultural University, 95 Wenhua Road, Zhengzhou 450002, China. [3]Faculty of Biology, Medicine & Health, University of Manchester, Manchester M13 9PT, UK. [4]Department of Mathematical Sciences, Durham University, South Road, Durham DH1 3LE, UK.
*Present address: School of Life Science, Beijing Institute of Technology, 5 South Zhongguancun Street, Haidian District, Beijing 100081, People's Republic of China. ‡Present address: The John Innes Centre, Colney Lane, Norwich NR4 7UH, UK. §Present address: Department of Plant Sciences, University of Cambridge, Downing Street, Cambridge CB2 3EA, UK.
¶These authors contributed equally to this work.

**Author for correspondence (peter.etchells@durham.ac.uk)

W.W., 0000-0002-3711-5181; J.P.E., 0000-0002-8524-4949

Received 19 February 2019; Accepted 23 April 2019

Development (2019) 146, dev177105. doi:10.1242/dev.177105

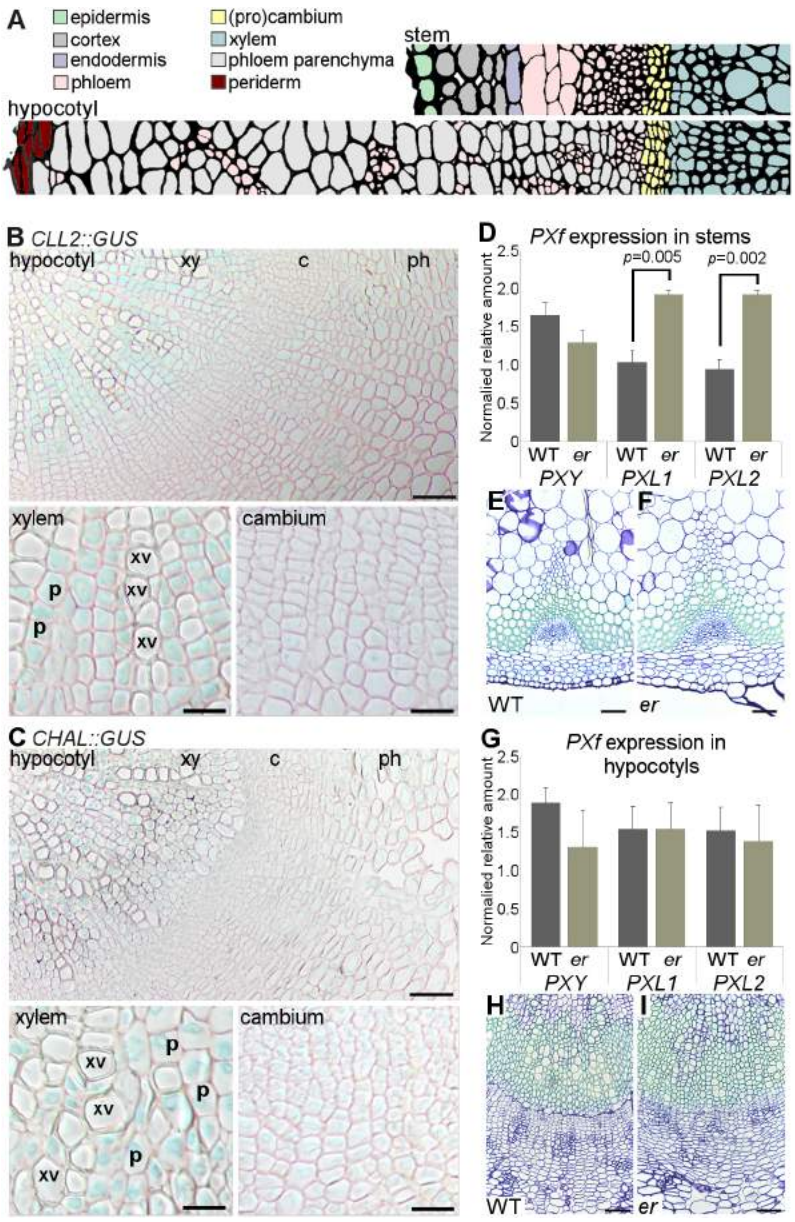

Fig. 1. Analysis of *CLL2*, *CHAL*, *PXL1* and *PXL2* expression. (A) Tissue types in the *Arabidopsis* stem and hypocotyl. (B,C) Spatial expression of *CLL2* (B) and *CHAL* (C) in hypocotyl transverse sections determined using *GUS* transcriptional fusions. (D) Graph showing qRT-PCR results for expression of *PXL1* and *PXL2* normalised to *ACT2* in wild-type and *er* mutant inflorescence stems from 5-week-old plants. (E,F) Wild-type (E) and *er* (F) stem vascular bundles. (G) Graph showing qRT-PCR results for expression of *PXY*, *PXL1* and *PXL2* normalised to *ACT2* in wild-type and *er* mutant hypocotyls at 5 weeks of age. (H,I) Transverse sections of wild-type (H) and *er* (I) hypocotyls. In qRT-PCRs (D,G), *P* values were calculated using Student's *t*-test. Scale bars: 50 µm in B,C (upper), E,F,H,I; 20 µm in B,C (lower). xy, xylem; c, cambium; ph, phloem; p, xylem parenchyma; xv, xylem vessels.

INTERCALATED WITH XYLEM (PXY), which is expressed in the cambium. Loss of TDIF-PXY results in a failure to correctly organise tissue layers in the vascular tissue. *pxy* mutants are characterised by disruption to the spatial separation of xylem, cambium and phloem. Reductions in cell division in the cambium and premature xylem differentiation are also a consequence of loss of *PXY* (Etchells and Turner, 2010; Fisher and Turner, 2007; Han et al., 2018; Hirakawa et al., 2010; Hirakawa et al., 2008; Ito et al., 2006; Kondo et al., 2014; Suer et al., 2011). TDIF-PXY signalling thus represents a mechanism through which differential growth in vascular tissue could be coordinated, regulating as it does, tissue organisation, cell division and differentiation.

TDIF-PXY genetically interacts with a second ligand-receptor pair to maintain the spatial separation of vascular tissues. In stems, the *ERECTA* (*ER*) receptor is expressed in the phloem, and its cognate ligands, *CHALLAH-LIKE 2*/*EPIDERMAL PATTERNING FACTOR-LIKE 4* (*CLL2*/*EPFL4*) and *CHALLAH* (*CHAL*/*EPFL6*) are expressed in the endodermis (Abrash et al., 2011; Uchida et al., 2012). *pxy er* mutant stems show organisation defects greater than those of *pxy* single mutants (Etchells et al., 2013). Thus, in stems, the genetic interaction between EPFL-ER and TDIF-PXY represents a non-cell autonomous signalling system that organises tissue layers between endodermis, phloem, cambium and xylem. In hypocotyls, changes to the organisation of vascular tissues in *er pxy* hypocotyls are also apparent (Etchells et al., 2013). However, *ER* expression is reported to be much broader, being present in phloem, cambium and xylem parenchyma (Ikematsu et al., 2017). The spatial expression domains of *CHAL* and *CLL* genes have not been described in hypocotyls.

In the *Arabidopsis* genome, paralogues of both *PXY* and *ER* are present. The *PXY* family, hereafter referred to as *PXf*, comprises *PXY*, *PXY-LIKE1* (*PXL1*) and *PXY-LIKE2* (*PXL2*). TDIF is reported to bind the ligand binding pocket of PXL1 and PXL2 (Zhang et al., 2016), and *pxl1* and *pxl2* enhance the vascular organisation defects that are characteristic of *pxy* mutants (Etchells et al., 2013; Fisher and Turner, 2007). The *ER* paralogues are *ER-LIKE1* (*ERL1*) and *ERL2* (Shpak et al., 2004). The *ERECTA* family (*ERf*) have wide-ranging roles in regulation of plant growth and development.

Development (2019) 146, dev177105. doi:10.1242/dev.177105

Redundantly, these three genes function in cell elongation, cell division, inflorescence architecture (Shpak et al., 2004; Torii et al., 1996), floral patterning (Bemis et al., 2013), shoot apical meristem fate (Kimura et al., 2018; Uchida et al., 2013) and stomatal spacing (Shpak et al., 2005). In the context of plant vascular development, they promote vascular expansion in the stem (Uchida and Tasaka, 2013). By contrast, in hypocotyls they repress radial expansion and also control the timing of xylem fibre formation (Ikematsu et al., 2017; Ragni et al., 2011). A hallmark of loss of *ER*f genes is an increase in cell size, particularly with respect to the radial axis (Shpak et al., 2004; Shpak et al., 2003).

In this article, we have investigated the genetic relationships between *PX*f and *ER*f receptors. We generated *pxy pxl1 pxl2 er erl1 erl2* sextuple mutants using a combination of classical genetics and genome editing. In hypocotyls, the sextuple mutant failed to make the transition to secondary growth. Further analysis of these lines demonstrated that *PX*f and *ER*f genetically interact to coordinate tissue integrity at the levels of both cell size and cell division. Gene expression analysis in stems and hypocotyls suggested that members of *PXY* and *ER* gene families regulated expression of paralogues both within and between these families. However, this regulation was distinct in hypocotyls and stems. In stems, *PX*f and *ER* also influenced the expression of non-vascular-expressed *EPFL4* and *EPFL6*. This suggests that coordination of growth regulators occurs between vascular and non-vascular tissue layers. Our results demonstrate that although interactions between members of both families are crucial in both stem and hypocotyl, the paralogues have specialised functions within vascular tissue of differing ontogenies.

RESULTS

PXL1 and *PXL2* expression is elevated in *er* stems.

In *Arabidopsis* stems and hypocotyls, tissue is arranged in concentric rings with the vasculature at the centre (Fig. 1A). *PXY* and *ER* genetically interact to control vascular development. In stems, ER ligands, CHAL and CLL2 (Abrash et al., 2011), are expressed in the endodermis whereas *ER* is expressed in the phloem (Uchida et al., 2012). TDIF-encoding genes are expressed in the phloem, and TDIF signals to PXY, which is expressed in the procambium (Etchells and Turner, 2010; Fisher and Turner, 2007; Hirakawa et al., 2008). In mature hypocotyls, endodermis is not present and the *CLL2* and *CHAL* domains of expression are not known. To better understand the spatial relationships between the PXY and ER receptors and ER ligands in hypocotyls, we determined the *CHAL* and *CLL2* expression pattern in 5-week-old plants using transcriptional reporters (Abrash et al., 2011). Both *CHAL::GUS* and *CLL2::GUS* lines demonstrated clear expression maxima both in xylem parenchyma and in the differentiating xylem adjacent to the cambium (Fig. 1B,C). Expression in the cambium itself was minimal. Thus, active ER ligand-receptor complexes occur in different locations in stems compared with hypocotyls. In stem tissue, active ER ligand-receptor complexes would be in the phloem, whereas in hypocotyls they must predominate in differentiating xylem.

To better understand the influence that *ER* might have upon PXY signalling, we tested whether expression levels of genes involved in PXY signalling differed in *er* mutants. We have previously shown that TDIF-encoding *CLE41*, *CLE42* and *CLE44* levels are unchanged in *er* (Etchells et al., 2013), so we analysed expression of the *PX*f family of receptors. qRT-PCR was used to test levels of *PX*f gene expression in stems and hypocotyls of 5-week-old wild-type and *er* plants (Fig. 1D-I). In hypocotyls, the level of *PX*f gene expression was unchanged in *er* mutants compared with wild type (Fig. 1G). By contrast, *PXL1* and *PXL2* expression, but not that of *PXY* was found to be elevated in *er* mutant stems (Fig. 1D). These observations suggest that *ER* signalling may regulate vascular development by setting *PXL1* and *PXL2* levels in the stem. They also underline that there are differences in regulatory relationships between patterning genes in stem and hypocotyl.

Genetic interactions between *ER* and *PX*f in stems and hypocotyls

We sought to further investigate the role of *PXL1* and *PXL* in vascular development. In transverse sections, *pxl1 pxl2* double mutants were indistinguishable from wild type (Fig. S1); however, we have previously shown that *pxl1* and *pxl2* enhance the *pxy* phenotype (Etchells et al., 2013; Fisher and Turner, 2007) (Figs 2A,B and 3D). Thus, as *PXL* gene expression was observed to be elevated in *er* stems, but neither *er* (Fig. 1E-F) nor *pxl1 pxl2* (Fig. S1) lines had vascular stem phenotypes except in a *pxy* mutant background, we addressed the function of *PXL1* and *PXL2* regulation by *ER* in the absence of *pxy*. *er px*f quadruple mutants (*er pxy pxl1 pxl2*) were generated and compared with wild-type, *pxy*, *er*, *er pxy* and *px*f lines. In inflorescence stems, *er px*f lines had considerably fewer cells per vascular bundle than either *px*f, *er* or *pxy er* counterparts (Fig. 2A; Tables S1 and S2). Therefore *PXL1* and *PXL2* do function redundantly with *ER* to regulate vascular proliferation in the stem, at least in the absence of *PXY*. In hypocotyls, a reduction in radial growth was observed in *px*f *er* lines relative to *px*f and *er*; however, *px*f *er* and *pxy er* lines were indistinguishable (Fig. 3; Tables S1 and S3). Thus, *pxl1* and *pxl2* do not enhance *pxy er* hypocotyl phenotypes, a result consistent with our observation that *PXL1* and *PXL2* expression was unchanged in *er* mutant hypocotyls (Fig. 1G).

Although changes to vascular proliferation were apparent in *er px*f inflorescence stems, by far the most dramatic defect was observed when the vascular bundle shape was assessed (Fig. 2B-F). In wild-type *Arabidopsis* stems, the distribution of vascular bundles is such that there is a greater distribution of vascular tissue along radial axis of the stem than along the tangential (Fig. 2C). We found the tangential:radial length ratio of wild-type vascular bundles to be 0.61. In *px*f and *pxy er* lines, this ratio was 0.91 and 1.36, respectively. In *er px*f stems, a dramatic redistribution of vascular cell types had occurred along the tangential axis (Fig. 2F), such that the ratio of tangential:radial length of vascular tissue was 2.30 (Fig. 2B; Table S1). In some plant stems, this led to an almost complete ring of vascular tissue, with phloem cells scattered around the circumference of the vascular cylinder (arrows in Fig. 2F), rather than present in discrete vascular bundles (Fig. 2C,D). Thus, *PXL1* and *PXL2* are crucial for regulating radial pattern in the stem, particularly in the absence of *ER* and *PXY*, and these data support the idea that *ER* and *PX*f constitute a mechanism for organising vascular cell layers.

Stem *ER*f expression is subject to the presence of *ER* and *PX*f.

Having observed that *PX*f genes were differentially expressed in *er* mutants (Fig. 1D), and that *PXL1* and *PXL2* contribute to the control of stem radial pattern (Fig. 2), we also sought to determine whether expression of members of the *ER* gene family were changed in response to perturbation of *PX*f or *ER* genes. In stems and hypocotyls of *px*f lines, *ER* expression did not differ from wild-type levels, as determined by qRT-PCR. Expression levels of *ERL1* and *ERL2* were also indistinguishable in wild-type, *er* and *px*f stems (Fig. 4A-C). By contrast, *ERL1* expression was significantly reduced when *er px*f lines were compared with *er* single mutants.

Development (2019) 146, dev177105. doi:10.1242/dev.177105

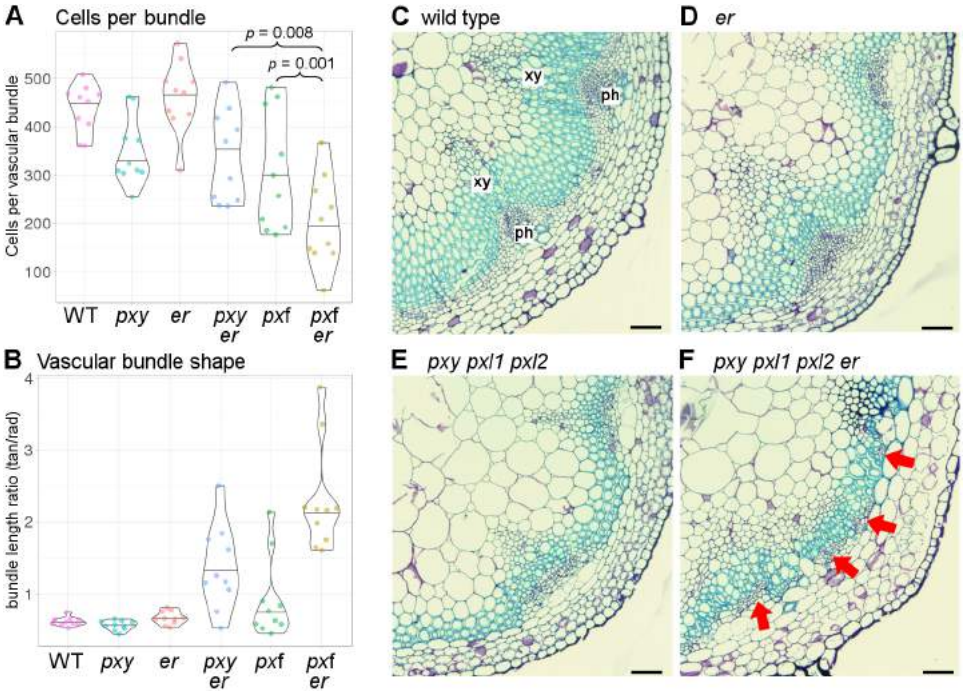

Fig. 2. Comparison of vascular tissue in stems of *pxf er* lines and controls. (A) Violin plot showing mean cells per vascular bundle. (B) Violin plot showing representation of vascular bundle arrangement (bundle tangential/radial axes ratio). (C-F) Transverse sections through wild-type (C), *er* (D), *pxf* (E) and *pxf er* (G) stems. Arrows in F indicate phloem distributed around the stem, rather than in discrete bundles, as seen in other genotypes (C-E). *P* values were calculated using ANOVA with an LSD post-hoc test (A). Scales bars: 50 µm. xy, xylem; ph, phloem.

Thus *ERL1* expression in *er* mutants is maintained by the *PXF* in stems (Fig. 4A). Expression levels of the ER ligands that function in the stem, *CHAL* and *CLL2*, were also tested in this experiment, as was that of *CLL1*, which genetically interacts *CHAL* and *CLL2* (Abrash et al., 2011; Uchida et al., 2012; Uchida and Tasaka, 2013). Inflorescence stem expression of *CHAL* and *CLL2*, but not that of *CLL1*, demonstrated significant reductions in expression in *er pxf* lines when compared with *er* (Fig. 4D-F). Thus, *PXF* and *ER* genetically interact to maintain *EPFL* ligand expression in stems in addition to that of their cognate receptor, *ERL1* (Fig. 4A).

Co-regulation of *ERf* expression by *ER* and *PXF* in hypocotyls

In hypocotyls, *ERL1* acts redundantly with *ER* to repress hypocotyl growth and control the timing of xylem fibre differentiation (Ikematsu et al., 2017). *ERL2* has not been assigned a function in hypocotyl development as its expression has been reported as absent from hypocotyls in 9-day-old seedlings and 3-week-old plants (Ikematsu et al., 2017; Uchida et al., 2013). To understand how *PXY* and *ER* might influence *ERf* expression, *ERf*:*GUS* reporter constructs (Shpak et al., 2004) were crossed into *pxy* and *er* mutants. To our surprise, in 5-week-old plants, we did detect *ERL2::GUS* reporter expression in the hypocotyls of wild type, which, at this growth stage, demonstrated a very similar pattern to that observed for *ERL1* and *ER* (Fig. 5A,D,G). Thus, *ERL2* expression is a feature of late hypocotyl development. *ER*, *ERL1* and *ERL2* expression was present in most hypocotyl cell types, with two maxima; the first in the cambium and xylem initials, and the second in the periderm (Fig. 5A,D,G; arrowheads). No change in the pattern of *ERL1* or *ERL2::GUS* expression was observed in *er* mutants (Fig. 5C,F). However, the clearly defined expression maxima that were observed in *ER::GUS*, *ERL1::GUS* and *ERL2::GUS* lines in both wild type and *er* mutants, lacked definition in the absence of *PXY* (Fig. 5B,E,H). Here, for all three reporters, expression was

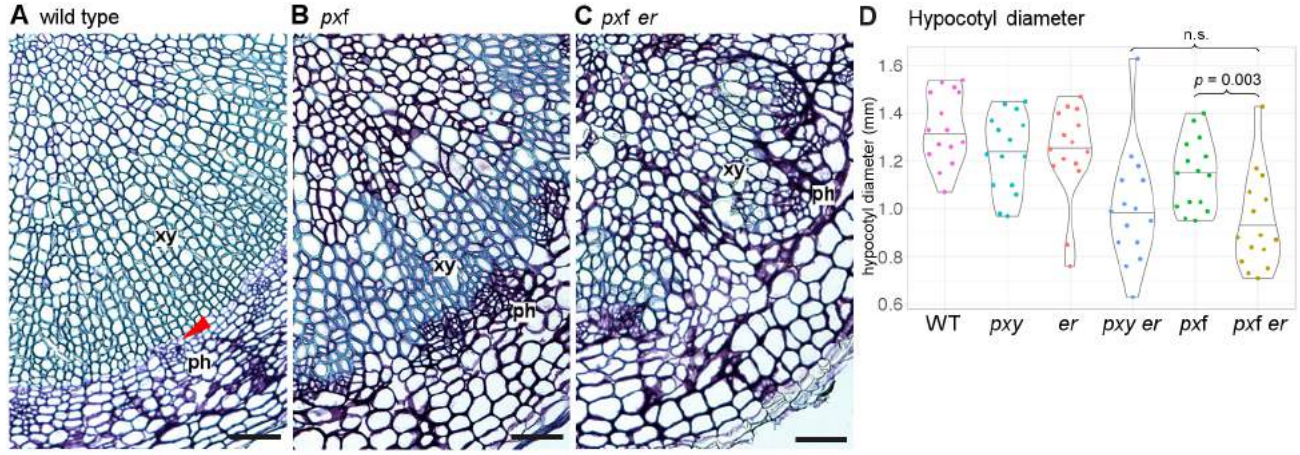

Fig. 3. Vascular tissue in hypocotyls of *pxf er* lines and controls. (A-C) Transverse sections through *Arabidopsis* hypocotyls. (A) Wild type. (B) *pxf*. (C) *pxf er*. (D) Violin plot showing reductions in hypocotyl diameter in *er pxf* lines compared with controls. Statistical significance was calculated using ANOVA plus Tukey. xy, xylem; ph, phloem. Red arrowhead in A marks dividing cambium. Scale bars: 50 µm.

Development (2019) 146, dev177105. doi:10.1242/dev.177105

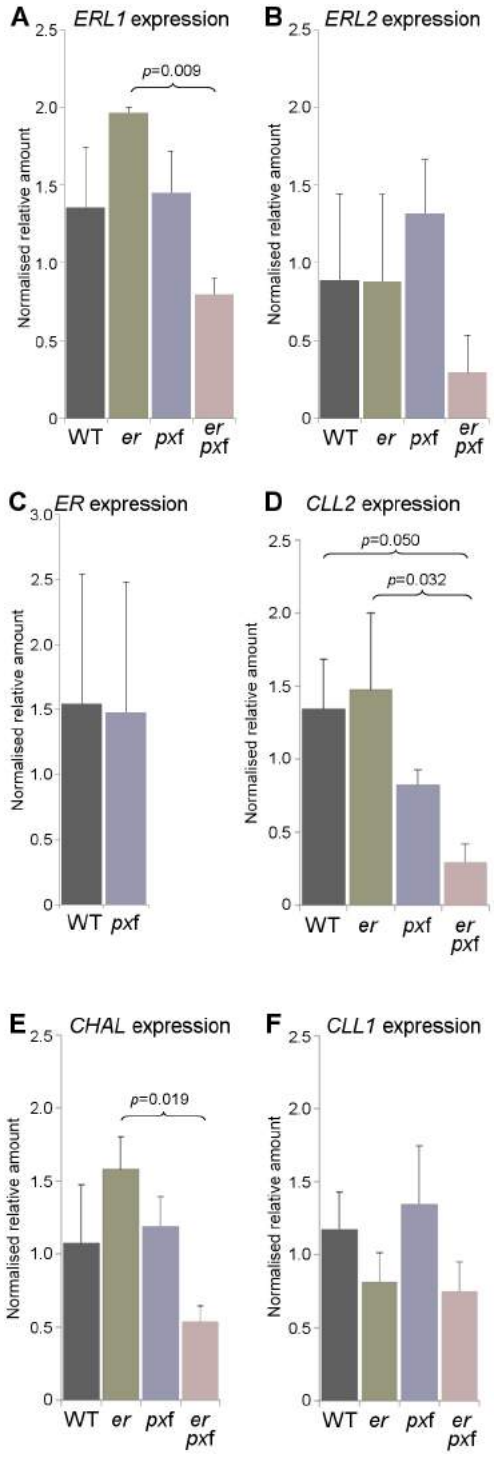

Fig. 4. qRT-PCRs showing *ER*f and *EPFL* expression in stems. (A-C) Stem expression of *ERL1* (A), *ERL2* (B) and *ER* (C) in wild type, *er*, *pxf* and *pxf er* mutants in stems. Expression was normalised to *18S* rRNA. (D-F) Expression of *CLL2* (D), *CHAL* (E) and *CLL1* (F) in hypocotyls (normalised to *18S rRNA*). *P* values were calculated using ANOVA with an LSD post-hoc test. Significant differences are marked with brackets.

observed to be more even across the hypocotyl, thus PXY signalling is either required to define *ER*f expression maxima, or cell types in which *ER*f are expressed are found throughout the hypocotyl in *pxy* mutants. The latter seems unlikely as there are fewer vascular cells in *pxy* mutants.

Having defined the pattern of *ER*f expression in a subset of genotypes, we sought to address changes to levels of *ER*f expression using qRT-PCR (Fig. 5I-K). In common with our observation in the stem (Fig. 4), hypocotyl *ERL1* and *ERL2* expression levels did not differ between wild-type, *er* and *pxf* lines (Fig. 5J-K). By contrast, a striking increase in *ERL1* and *ERL2* gene expression was observed

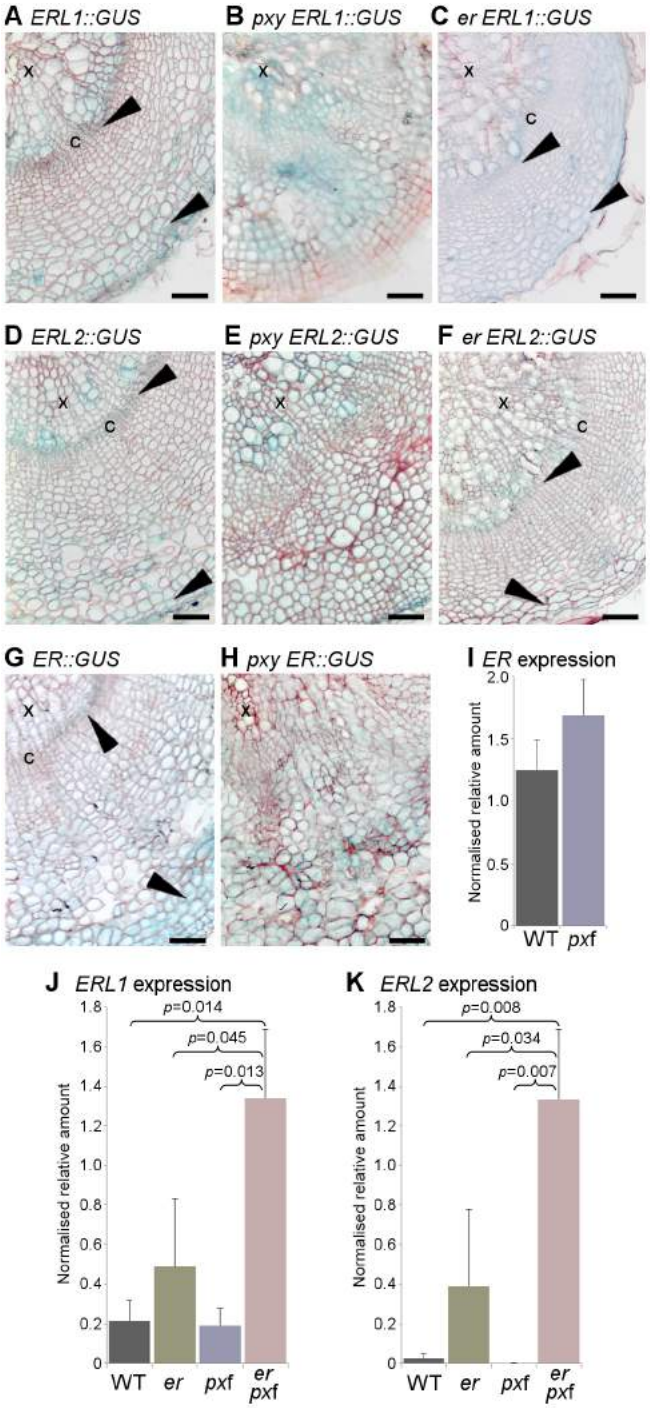

Fig. 5. *ER*f expression in hypocotyls of *pxy* and *er* lines. (A-C) *ERL1::GUS* in wild type (A), *pxy* (B) and *er* (C). (D-F) *ERL2::GUS* in wild type (D), *pxy* (E) and *er* (F). (G,H) *ER::GUS* in wild type (G) and *pxy* (H). Black arrowheads indicate expression maxima. x, xylem; c, cambium. Scale bars: 50 µm. (I-K) Expression of *ER* (I), *ERL1* (J) and *ERL2* (K) in wild-type, *er*, *pxf* and *pxf er* hypocotyls (normalised to 18S rRNA). *P* values were calculated using ANOVA and an LSD post-hoc test.

Development (2019) 146, dev177105. doi:10.1242/dev.177105

in *pxf er* hypocotyls relative to all other genotypes tested (Fig. 5J,K). As such, opposite regulation of *ERL1* and *ERL2* by *ER* and *PXf* genes occurred in the hypocotyls (Fig. 4J-K) and stem (Fig. 2A-B). This highlights a difference in the nature of the *PXf-ER* genetic interactions in stems and hypocotyls. In hypocotyls, no changes were observed in levels of *CHAL*, *CLL1* and *CLL2* expression levels in *er*, *pxf* or *er pxf* lines (Fig. S2).

Hypocotyl size and organisation in *PXf ERf* mutants

The *PXf* promotes radial growth in hypocotyls (Etchells et al., 2013; Fisher and Turner, 2007; Hirakawa et al., 2008) (Fig. 3D; Tables S1 and S3), whereas *ER* and *ERL1* signalling represses it (Ikematsu et al., 2017). Thus, our gene expression data demonstrating that *PXf* plays a part in repression of ERL gene expression in hypocotyls (Fig. 5J,K) are consistent with existing phenotypic data because the *PXf* might be expected to repress expression of negative regulators of hypocotyl radial growth. In addition to repressing radial growth, *ER* and *ERL1* have also been described as preventing premature fibre formation, as *er erl1* hypocotyls develop fibre cells in the location where parenchyma are present in wild type. *ERL2* was thought not to function in the hypocotyl given its very low expression levels in the early stages of development (Ikematsu et al., 2017). Because we found *ERL2* to be expressed in hypocotyls at 5 weeks (Fig. 5D,K), we tested whether *ERL2* functioned similarly to *ERL1* by analysing *er erl2* lines. Neither change to fibre formation, nor to hypocotyl radial growth were observed (Fig. S3); thus, in contrast to *ERL1* (Ikematsu et al., 2017), a function for *ERL2* in hypocotyl development is not apparent in a double mutant background with *er*.

To address the function of the elevated ERL gene expression that we observed in *pxf er* hypocotyls (Fig. 5J,K), we removed ERL gene function from this genotype by generating *pxf er erl1*, *pxf er erl2* and *pxf erf* quintuple and sextuple mutants. *PXY* and *ERL1* are tightly linked on chromosome 5, separated by just 270 kb, so to overcome this linkage we employed a CRISPR/cas9 construct that contained two guide RNAs against *ERL1* (Fig. S4). Thus, *pxf er erl1* and *pxf erf* plants were generated by genome editing. Secondary growth in these lines and controls was determined by measuring the hypocotyl radius in 6-week-old plants (Fig. 6A, Fig. S5C). Radii of *pxf er* and *pxf er erl1* lines did not show a significant difference. By contrast, radii of *pxf er erl2* and *pxf erf* hypocotyls were significantly smaller than those of *pxf er erl1* plants (Fig. 6A). Thus, *ERL1* and *ERL2* expression is required in *pxf er* hypocotyls to maintain hypocotyl growth rates; however, pairwise comparisons suggested that *ERL2* played a greater role than *ERL1* in this respect, as *pxf er erl1* hypocotyls were larger than those of *pxf er erl2* lines.

During vascular cylinder development in the embryo, the hypocotyl forms in a diarch pattern with a row of xylem cells that are flanked by two phloem poles (Dolan et al., 1993). As secondary growth proceeds, this organisation develops radial symmetry with phloem present around the circumference of the vascular cylinder (Chaffey et al., 2002). We analysed hypocotyl morphology in 5-week-old plants. Strikingly, development was perturbed to such a degree in *pxf erf* mutants that the position of the original phloem poles remained apparent (arrows in Fig. 6F; see Fig. S5 for higher magnification). This demonstrates that vascular development was retarded to such a degree that these plants could not make the transformation to true radial growth. Such phenotypes were not observed in *pxf*, *erf* or *pxf er erl2* lines (Fig. 6B-E).

Next, we looked to identify recent cell divisions in our mutant hypocotyls by analysing thin sections. In wild-type and *erf* lines, cell divisions were always oriented perpendicular to the hypocotyl

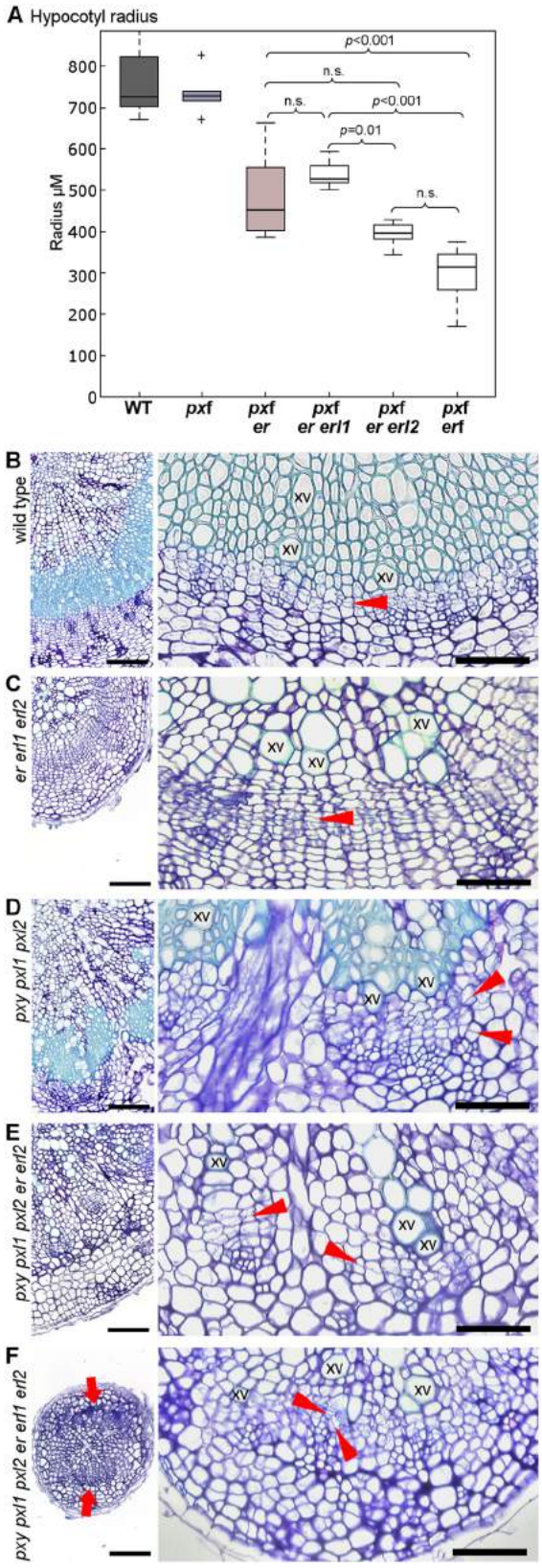

Fig. 6. Transverse sections of hypocotyls from *pxf erf* lines. (A) Boxplot showing hypocotyl radii of *pxf* lines with differing numbers of *erf* mutations. (B) Wild-type, (C) *erf*, (D) *pxf*, (E) *pxf er erl2* and (F) *pxf erf* vascular tissue. Sites of phloem poles in *pxf erf* are marked with red arrows in the left-hand panel of F (see Fig. S5 for higher magnification). Red arrowheads in B-F align with cell divisions. Scale bars: 100 µm (left); 50 µm (right); xv, xylem vessel.

Development (2019) 146, dev177105. doi:10.1242/dev.177105

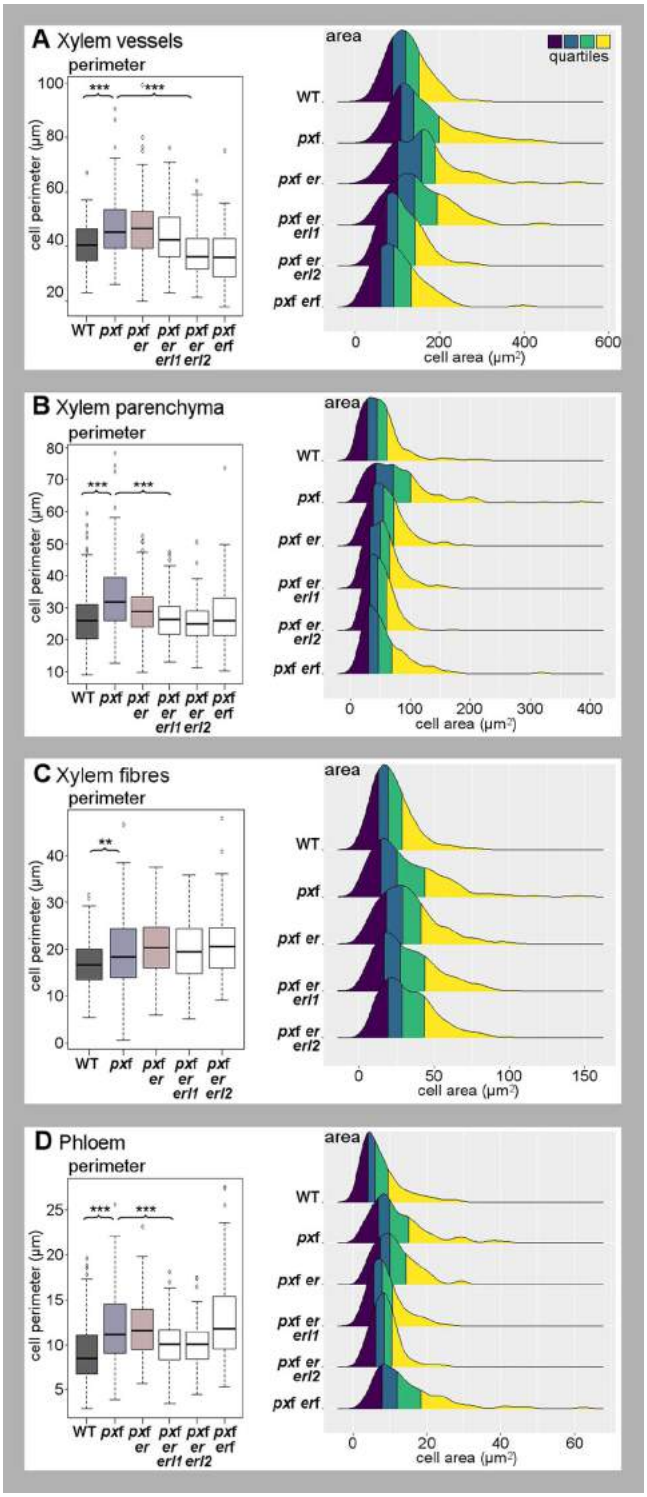

Fig. 7. Comparisons of hypocotyl cell morphology. (A-D) Boxplots on left show mean cell perimeter for xylem vessels (A), xylem parenchyma (B), fibres (C) and phloem cells (D). Boxes represent the 25th to 75th percentile, the horizontal line marks the median. Whiskers' endpoints are the min/max points within the interval spanning Q1-1.5*IQR (lower) and Q3-1.5*IQR (upper). IQR = Q3-Q1 (the length of the box). Asterisks mark significant differences (ANOVA plus Tukey; ***P<0.001, **P<0.01; see Table S4 for pairwise comparisons of P values). Ridgeline plots on the right show the distributions of cell areas divided into quartiles. Areas of *pxf* lines were greater than those of *pxf er erl2* lines in xylem vessels, phloem and parenchyma (P≤0.001) but not fibres. Differences were calculated with ANOVA and a Tukey post-hoc test; see Tables S4 and S5 for pairwise comparisons of P values.

radial axis (Fig. 6B,C, arrowheads). This aspect of normal vascular development known to perturbed in lines that lack *pxy* and its paralogues (Fig. 6D) (Fisher and Turner, 2007). Recent cell divisions were clearly identifiable in the absence of the *PXf*, *ER* and *ERL2*, and they remained present, albeit lacking orientation and at a much reduced frequency in *pxf erf* lines (Fig. 6E-F). Thus, although not an absolute necessity for formation of either phloem or xylem vessels, these receptor-kinase families are absolutely essential in specifying their positioning and in coordinating cell division in a manner that allows organised radial expansion and pattern maintenance (Fig. 6).

Cell size in hypocotyls is balanced by *PXf* and *ERf*

One common characteristic of mutants with reduced cell division is an increase in cell size, relative to wild-type plants. This compensates for fewer cells, such that final organ size is often similar to that of wild-type plants (Horiguchi and Tsukaya, 2011). In the course of our hypocotyl analysis, cell sizes and shapes appeared to differ among our mutant lines, and, in particular, cells in *pxf* lines appeared larger than those of other lines (Fig. 3A,B). Consequently, cell morphology was calculated from images of anatomical sections by selecting cell representatives from the different genotypes and using a MATLAB code to analyse the cells as connected components with measurable features (Fig. S6A,B). Cell area and perimeter were investigated for xylem vessels, fibres, xylem parenchyma and phloem cells in wild-type, *pxf*, *pxf er erl1*, *pxf er erl2*, and *pxf erf* lines (Fig. 7) with one exception. Fibre morphology could not be assessed in *pxf erf*, as insufficient fibre cells were present (Fig. 6F). In hypocotyls, all *pxf* cell types tested demonstrated increases in cell perimeter relative to wild type (Fig. 7; Table S4). *pxf er* and *pxf* cells demonstrated no statistically significant differences in vessel, fibre and phloem cell perimeters, but *pxf er* xylem parenchyma perimeters were smaller than those of *pxf* lines. Strikingly, removal of further members of the ERf restored vessel, parenchyma and phloem cell perimeters to wild-type sizes (Fig. 7A,B,D; Table S4). Thus members of the *ERf* are required to promote increases in cell size in the absence of *PXf*.

The one cell type that was the exception to this cell size regulation was xylem fibres. Here, the increase in fibre perimeter that was characteristic of *pxf* mutant hypocotyl cells was not rescued by *erf* mutants (Fig. 7C; Table S4). These observations were supported by cell area measurements. For the four cell types tested, *pxf* cell areas were larger than those of wild-type plants but, with the exception of fibres, removal of *er erl1* or *er erl2* from *pxf* restored cell areas to those observed in wild type (Fig. 7; Table S5).

Xylem cells are characterised by rigid secondary cell walls, so we hypothesised that parenchyma may be subject to changes in cell shape to accommodate the increased xylem cell size. To test this hypothesis, we calculated the ellipticity of the parenchyma and other hypocotyl cell types by determining their major to minor axis ratios in wild-type, *pxF* and *pxF er erl2* lines. However, this parameter varied little between genotypes (Fig. S6C-F).

Phenotypes of *pxf erf* sextuple mutant stems

To complete our analysis of *pxf erf* sextuple mutant morphology, we examined vascular tissue in inflorescence stems. Inflorescence stem vascular morphology was similar in *pxf erf* lines and *pxf er erl2* counterparts (Fig. 8). Both were characterised by very large reductions in vascular bundle size. Characteristic xylem and phloem cell types were present, but only very small xylem vessels were observed, relative to those found in wild-type, *erf* and *pxf* lines (Figs 8D,E and 9A; Tables S6 and S7). Furthermore, tissue layer

Development (2019) 146, dev177105. doi:10.1242/dev.177105

organisation defects were apparent beyond those previously observed. In particular, the clearly defined organisation of endodermal and adjacent phloem cap cells were lacking, with the phloem cap appearing to extend into the cortex (Fig. 8D) or be absent altogether (Fig. 8E). Thus, tissue layer defects occurred outwith vascular cell types. These similarities in vascular morphology were independent of plant size because gross morphology of *pxf erf* sextuple lines was considerably smaller than *pxf er erl2* counterparts (Fig. S7).

Having observed large reductions in xylem vessel size in stems (Fig. 9A), we tested whether *PXF* and *ERf* genes genetically interacted to control cellular morphology of other vascular cell types in the stem (Fig. 9B,C). In stems, xylem vessels and cells in the phloem were smaller in *pxf* lines than in wild type, as determined by measuring both cell perimeter and cell area, and in contrast to measurements in the hypocotyl. Removing *ER* from *pxf* lines resulted in no change to the size of these cells, but loss of *ERL2* from *pxf er* plants caused a further reduction in cell size (Fig. 9A,C; Tables S6 and S7). Thus, in phloem and xylem vessels, *pxf* and *erf* families interact to maintain cell size. Xylem fibre sizes differed from this trend. Here, *pxf er* cells were significantly larger than wild type, but this phenotype was suppressed in *pxf er erl2* plants as fibre perimeter and area was unchanged from wild type (Fig. 9B; Tables S6 and S7). We were unable to assess fibre morphology in *pxf erf* vascular bundles, as too few were identifiable in these lines (Fig. 8E). Taken together, our results demonstrate that a genetic interaction between PXf and ERf signalling coordinates organ size at the level of cell size, in addition to coordination of proliferation and pattern maintenance in both stems and hypocotyls.

DISCUSSION

Coordination of growth between cell layers

Plant growth and development require coordination between expanding tissue layers, particularly where tissue types are organised in concentric rings. Clearly, expansion of inner layers must be coordinated with expansion of outer layers. How does coordination between tissue layers occur? It was proposed some time ago that the *ERf* could perform this function (Shpak et al., 2004), and this initial suggestion has subsequently been supported by observations that, in the inflorescence stem, endodermis derived EPFL ligands signal to ER in the phloem to regulate cell division in the adjacent procambium (Uchida et al., 2012; Uchida and Tasaka, 2013) (Fig. 10A). Our observation that *PXL* expression is higher in the stem of *er* mutants (Fig. 1D) suggests that these endodermis-derived signals could act through ER to attenuate *PXf*-regulated vascular expansion (Fig. 10A). The alternative conclusion would be that *PXL* expression is higher in *er* mutants due to a change in stem morphology, but we regard this as unlikely for two reasons. First, there are negligible differences in vascular proliferation and organisation in *er* stem vascular tissue compared with wild type that could account for such changes in gene expression (Figs. 1E,F and 2A,B). Second, there is clear evidence that *pxl1* and *pxl2* genetically interact with *er*. This interaction is apparent in a *pxy* mutant background, as *pxf er* lines demonstrated fewer cells in stem vascular bundles than either *pxy er* or *pxf* lines (Fig. 2; Table S2).

Our experimentation with *pxf er* lines led to observations that *PXf* receptors, redundantly with *ER*, are required for normal expression levels of ERL receptors and their *EPFL* ligands in the stem (Fig. 3). As *CLL2* and *CHAL* are endodermis expressed, changes in the expression levels of these genes could be due to coordination of vascular tissue expansion in stems across multiple tissue layers via a series of feedback loops (Fig. 10). As the endodermal stem layer remains clearly defined in *er pxf* lines, it is unlikely that the reduction in *CHAL*/ and *CLL2* expression in these lines is due to the disruption of endodermal cell fate (Fig. 2F). However, owing to severe disruptions to vascular morphology adjacent to the endodermis, we cannot rule out that such changes are a consequence of the disruption to xylem, phloem and procambium organisation. Disruption to *pxf er* quadruple mutants was severe to such a degree that in stems, vascular tissue was no longer found in discrete bundles, but scattered around the stem adjacent to the endodermis (Fig. 2).

Oriented cell divisions and the development of organ boundaries in the rib zone of the shoot apical meristem, from which stem vascular tissue is derived, have been reported to be regulated by a homeodomain transcription factor, REPLUMLESS (RPL). Pertinent to the results obtained here, RPL was found to occupy the promoters of *PXY*, *CLE41*, *CLE42*, *ER*, *ERL1*, *ERL2* and *CHAL* in ChIP-Seq experiments (Bencivenga et al., 2016). RPL is localised to the cytoplasm unless present in a heterodimer with class I KNOX protein, such as BREVIPEDICELLUS (Bhatt et al., 2004). *rpl bp* double mutants, particularly those in the L*er* background that lacks a functional copy of *ER*, demonstrate considerable defects in vascular development (Etchells et al., 2012; Smith and Hake, 2003). Thus, events in the rib zone that are controlled by RPL could set up the initial pattern in the stem. Our genetic analysis demonstrates that however the pattern is initiated, it is maintained by interacting

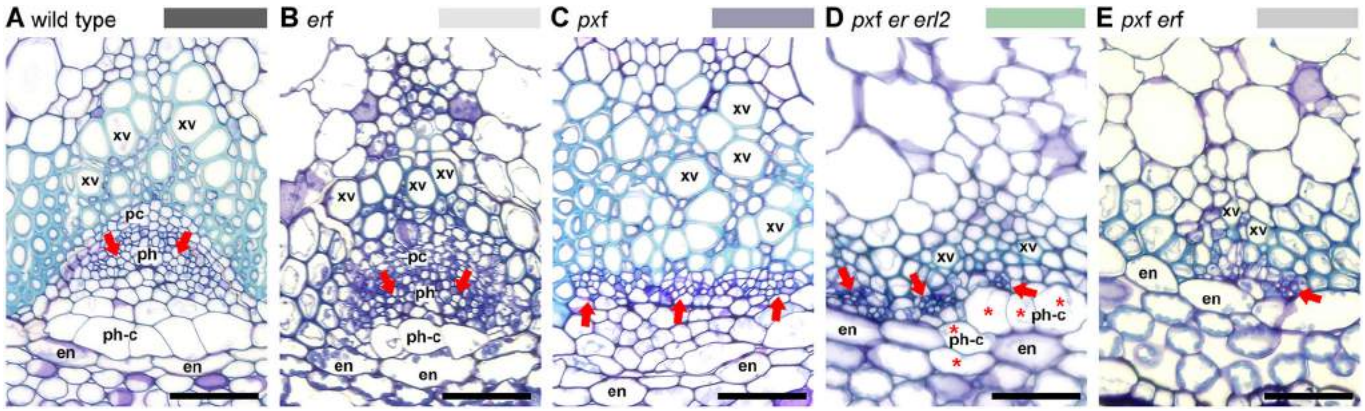

Fig. 8. Stem tissue from *pxf erf* lines. (A) Wild-type, (B) *erf*, (C) *pxf*, (D) *pxf er erl2*, (E) *pxf erf* vascular bundles. Phloem arrangement is marked with red arrows. Cells with phloem cap-like morphology are marked with asterisks. Scale bars: 50 µm; xv, xylem vessel; pc, procambium; ph, phloem; ph-c, phloem cap; en, endodermis.

Development (2019) 146, dev177105. doi:10.1242/dev.177105

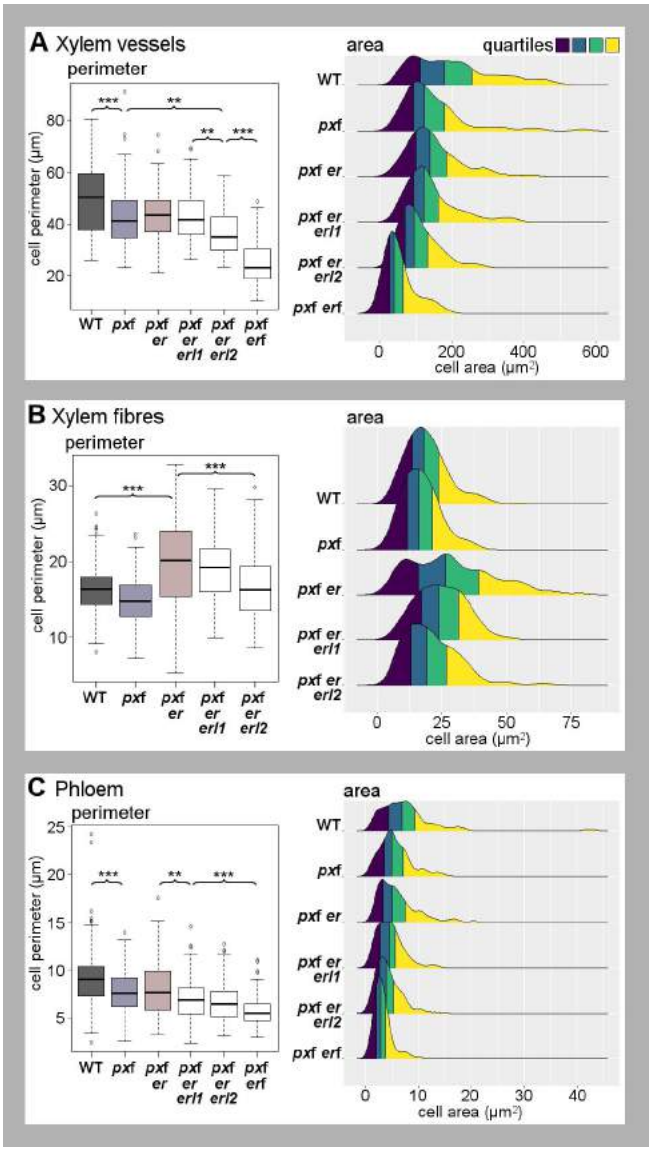

Fig. 9. Comparisons of morphology of cells in stem vascular bundles. (A-C) Boxplots on left show mean cell perimeter for xylem vessels (A), xylem fibres (B) and phloem cells (C). Boxes represent the 25th to 75th percentile, the horizontal line marks the median. Whiskers' endpoints are the min/max points within the interval spanning Q1-1.5*IQR (lower) and Q3-1.5*IQR (upper). Asterisks mark significant differences (ANOVA plus Tukey; ***P<0.001, **P<0.01; see Table S6 for pairwise comparisons of P values). Ridgeline plots on the right show the distributions of cell areas divided into quartiles. Areas of *pxf er* lines were greater than those of *pxf er erl2* lines in all three cell types ($P \leq 0.05$). Differences were calculated with ANOVA and a Tukey post-hoc test; see Table S7 for pairwise comparisons of P values.

signalling pathways characterised by members of the ERECTA and PXY families.

ERL genes are prominent in regulating cell size

Evidence that mechanisms exist to adjust cell morphology in order to maintain tissue size and organisation include the observation that cell expansion differs according to the rate of cell division. Here, overall organ size in mutants with fewer cells is often comparable to or only subtly different from those of wild-type plants due to an increase in cell size (De Veylder et al., 2002; Hemerly et al., 1999; Shpak et al., 2004; Ullah et al., 2001). Furthermore, such mechanisms can act non-

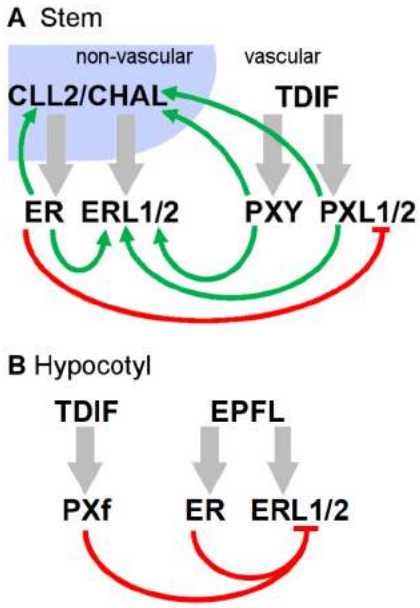

Fig. 10. Hypothesis of gene expression regulation in stems and hypocotyls. (A) In the stem, *ER* represses *PXL* gene expression. *PXf* and *ER* act as activators of ERL and *EPFL* gene expression. (B) In hypocotyls, negative regulation of *PXf* and *ER* targets predominate. Green arrows indicate a positive influence on gene expression; red blunt-ended lines indicate repression. Grey arrows indicate ligand-receptor interactions.

cell autonomously. Expression of *KRP1* reduces cell division (Hemerly et al., 1995). When it is specifically expressed in the epidermal cell layer, concomitant changes to palisade cell size and density also occur (Lehmeier et al., 2017). Thus, where the cell cycle has been manipulated in one cell layer, influence on cell size and organisation occurs in adjacent tissues, contributing to tissue integrity. We found that the interaction between *PXf* and *ERf* was crucial to regulation of cell size in multiple cell types. The ability to adjust cell size to compensate for the profound reductions in cell division in *pxf er* lines was particularly dependent on *ERL2* (Figs 7 and 9). This is in contrast to the consequences of losing the *ERECTA* family alone, as cell size adjustments are a feature of *erf* mutants (Shpak et al., 2004). However, the influence of *ERL2*, *ER* and *ERL1* differed by cell type and organ. In hypocotyls, vascular cells were larger in either *pxf* or *pxf er* lines compared with wild type. In hypocotyl xylem vessels, parenchyma and phloem cells, this increase in size was dependent on ERL gene expression as increases in cell size were lost in *pxf er erl1* and *pxf er erl2* lines (Fig. 7A,B,D). In stem vascular bundles, the only cell type with an increase in size in response to fewer to cell divisions were the fibres. This phenotype was also suppressed by removal of ERL genes. These observations support the idea that one function of the genetic interaction between *ERf* and *PXf* is coordination of tissue expansion. We propose that with these signalling mechanisms removed, the positional information that must be interpreted for cell morphology adjustments to occur is missing.

Genetic interactions may underpin physical interactions

In stems, the receptor kinases that are the focus of this study are expressed in discrete domains. By contrast, in hypocotyls, expression patterns of ER and PXY overlap on the xylem side of the cambium (Hirakawa et al., 2008; Ikematsu et al., 2017; Shi et al., 2019; Smetana et al., 2019). As the domain of ERL gene expression is expanded in *pxy* mutants (Fig. 5B,E,H), the presence

Development (2019) 146, dev177105. doi:10.1242/dev.177105

of PXL receptors in cells that also express ERf proteins is increasingly likely. A direct interaction between members of these receptor families is therefore possible. A recent *in vitro* global analysis of receptor kinase interactions did not include direct interactions between ERf and PXf family members because putative interactions did not pass cut-offs for inclusion in the high confidence bidirectional dataset (Smakowska-Luzan et al., 2018). Nevertheless strong *in vitro* interactions between ER and PXY, and ER and PXL1 proteins were observed in one orientation, and between PXL2 and ERL2 in both directions [Youssef Belkhadir, personal communication; data available in BAR ePlant (Waese et al., 2017)]. The determination of whether these interactions are genuine and, if so, the circumstances under which they occur *in vivo* will be an important focus for future research. ERf activity in the epidermis has previously been reported to be buffered by a second receptor, TOO MANY MOUTHS (TMM). Loss of this buffering in *tmm* mutants leads to opposite stomatal spacing phenotypes in spatially separate cotyledon, where stomata cluster, compared with hypocotyls where stomata are absent. Differing ligand availability in cotyledon and hypocotyl is thought to account for this difference (Abrash et al., 2011). CHAL and CLL2 have been demonstrated to act as ERf ligands in the inner tissues of stems (Uchida et al., 2012). We have shown that these ligands are expressed in developing xylem in hypocotyls (Fig. 1B,C). Thus, in stem vascular tissue, active ligand-ER complexes most likely reside in the phloem, whereas in hypocotyls they would be predominant in xylem initials. It remains to be determined whether the difference in ERL gene regulation by *ER* and *PXf* in stem and hypocotyl could be due to differing complements of co-receptors and ligands in these differing locations.

Our observation that ERL gene expression is de-repressed in the absence of *PXf* and *ER* in hypocotyls (Fig. 5J-K) supports the idea that these components genetically interact. Perhaps the most striking of our findings was the observation that *ER* and *PXf* regulation of ERL gene expression in the hypocotyl occurred in a manner opposite to that observed in the stem (compare Figs 4A,B and 5J,K), where *ER* and *PXf* combine to repress ERL gene expression. Thus, while *PXf* and *ERf* are required non-cell autonomously for tissue organisation and expansion in both stems and hypocotyls, the regulatory networks through which development is controlled in these two organs differs (Fig. 10). One explanation for differences in regulation is that tissue layer organisation varies by location. In hypocotyls, cambium division must occur concomitantly with factors that control periderm division. By contrast, in stems there is no such continually expanding tissue outside the vascular tissue, so vascular proliferation in stems must be under much tighter regulation.

PXf and *ERf* are an absolute requirement for hypocotyl secondary growth

Factors controlling the transition to secondary growth in *Arabidopsis* hypocotyls have recently been described. It first arises in cells adjacent to xylem, and central to this transition was an accumulation of auxin and expression of *HD-ZipIII* transcription factors. These factors, in turn, activate expression of *PXY* signalling (Smetana et al., 2019). Nevertheless, *pxy* mutants, and indeed *pxf* triple mutants, do ultimately make the transition to secondary growth (Figs 3 and 6). Thus, other factors must act with PXY to regulate the transition secondary growth and radial pattern in hypocotyls. *pxy er* double mutants, *erf* triple mutants, *pxf er* quads, and both *pxf er erl1* and *pxf er erl2* quintuple lines all made the transition to full secondary growth (Figs 4 and 6). By contrast, *pxf erf* sextuple mutants did not. As such, these lines demonstrated a phenotype that, as far as we are aware, has never previously been described. The observation of this novel phenotype further supports the idea that these receptor families coordinate development through a genetic interaction, and that the phenotypes cannot be explained simply by a correlative loss of cell division-promoting factors. Thus, PXf and ERf signalling act redundantly to regulate radial growth transition; consequently, complete removal of *PXf* and *ERf* families results not only in prominent proliferation defects, but also in dramatic defects to patterning (Fig. 6).

Concluding remarks

In *Arabidopsis*, stem and hypocotyl differ in that the hypocotyl undergoes radial growth, but the vast majority of the stem does not. Radial hypocotyl growth is largely the consequence of expansion of a pattern that is laid down in the embryo, but in stems, *de novo* patterning must occur below the shoot apical meristem. Nevertheless, in both stem and hypocotyl, the xylem, (pro)cambium and phloem must be specified in adjacent tissue layers in a coordinated manner. Our mutant analysis demonstrates that interactions between *PXf* and *ERf* are central to maintaining this organisation by regulating cell division (Figs 6 and 8) and coordinating cell size (Figs 7 and 9) in these different contexts.

MATERIALS AND METHODS

Accession numbers

AGI accession numbers for the genes studies in this manuscript are as follows: At3g24770 (*CLE41*), At5g61480 (*PXY*), At1g08590 (*PXL1*), At4g28650 (*PXL2*), At2g26330 (*ER*), At5g62230 (*ERL1*), At5g07180 (*ERL2*), At4g14723 (*CLL2*/*EPFL4*), At3g22820 (*CLL1*/*EPFL5*) and At2g30370 (*CHAL*/*EPFL6*).

Gene expression

For qRT-PCR, RNA was isolated using Trizol reagent (Life Technologies) prior to DNAse treatment with RQ1 (Promega). cDNA synthesis was performed using Tetro reverse transcriptase (Bioline). All samples were measured in technical triplicates on biological triplicates. qPCR reactions were performed using qPCRBIO SyGreen Mix (PCR Biosystems) using a CFX connect real-time system (Bio-Rad) with the standard sybr green detection programme. A melting curve was produced at the end of every experiment to ensure that only single products were formed. Gene expression was determined using a version of the comparative threshold cycle (Ct) method using average amplification efficiencies of each target, as determined using LinReg PCR software (Ramakers et al., 2003). Samples were normalised to *18S* rRNA or *ACT2*. Primers for qRT-PCR are described in Table S1. Significant differences in gene expression were identified with ANOVA and an LSD post-hoc test for four-way comparisons or using Student's *t*-test for two-way comparisons.

Plant lines

Previously described parental lines *pxy-3 pxl1-1 pxl2-1* (referred to hereafter as *pxf*) and *pxy-5 er-124* (Etchells et al., 2013) were crossed to generate *pxy-3 pxl1-1 pxl2-1 er-124* (*er pxf*). The quadruple mutants were selected in F3 by PCR using primers listed in Table S8. To generate *pxf er erl2* quintuple mutants, parental lines *er-105 erl1-2/+ erl2-1* (*erf*) (Shpak et al., 2004) and *pxy-3 pxl1-1 pxl2-1* (Etchells et al., 2013) were crossed. Plants homozygous for *er* were selected by visual phenotype in the F2, which was also sprayed with glufosinate to select for plants carrying an *erl2-1* allele. Families homozygous for glufosinate resistance in the F3 were screened for *pxy-3*, *pxl1-1* and *pxl2-1* to generate *pxf er erl2*. *er* and *erl2* mutants were subsequently confirmed by PCR.

erl1 genome edited lines were generated using an egg cell-specific CRISPR/Cas9 construct (Wang et al., 2015; Xing et al., 2014). Briefly, target sequences TCCAATTGCAGAGACTTGCAAGG and TCTTGCT-GGCAATCATCTAACGG were identified using the CRISPR-PLANT

Development (2019) 146, dev177105. doi:10.1242/dev.177105

website (Xie et al., 2014) and tested for off-targets (Bae et al., 2014). Primers incorporating the target sequences (Table S8) were used in a PCR reaction with plasmid pCBC-DT1T2 as a template to generate a PCR product incorporating a guide RNA against *ERL1*. A golden gate reaction was used to incorporate the purified PCR product into pHEE2E-TRI. The resultant *ERL1* CRISPR/cas9 clone was transferred to *Arabidopsis* by floral dip (Clough and Bent, 1998). *erl1*^{GE} mutants were selected in the T1 generation by sequencing PCR products generated from primers specific to ERL1 genomic DNA that flanked the guide RNA target sites.

For spatial expression of *ER*f genes in *pxy* or *er*, previously described *ER::GUS*, *ERL1::GUS* and *ERL2::GUS* reporters were used (Shpak et al., 2004). These were crossed to *pxy-3* or *er-124*. *pxy* mutants were selected in the F2 using primers described Table S8. Reporter lines were picked that also demonstrated GUS expression as judged by *GUS* histochemical staining, and the presence of *GUS* reporter construct was subsequently confirmed by PCR using primers (Table S8). For determination of ER-ligand expression, previously described *CHAL::GUS* and *CLL2::GUS* lines were used (Abrash et al., 2011).

Analysis of vascular tissue anatomy

Vascular morphology was assessed using tissue embedded in JB4 resin. For vascular bundles, inflorescence stem tissue from 0.5 cm above the rosette was assessed. Tissue was fixed in FAA, dehydrated in ethanol and infiltrated with JB4 infiltration medium, prior to embedding. Sections (4 µm) taken using a Thermo Fisher Scientific Finesse ME 240 microtome were stained in 0.02% aqueous Toluidine Blue and mounted with histomount.

GUS-stained tissue was harvested to ice-cold phosphate buffer. Samples were treated with ice-cold acetone for 5 min and then returned to phosphate buffer. GUS staining buffer (50 mM phosphate buffer, 0.2% triton, 2 mM potassium ferrocyanide, 2 mM potassium ferricyanide and 2 mM X-Gluc) was added and samples were infiltrated using a vacuum, before incubation overnight at 37ºC. Samples were progressively incubated in: FAA, then 70%, 85% and 95% ethanol for 30 min each prior to embedding in Technovit 7100 according to the manufacturer's instructions. Embedded samples were allowed to polymerize at room temperature for 2 h and at 37°C overnight. The inhibition layer was removed by wiping with a lint-free cloth. Samples were sectioned, counterstained with 0.1% Neutral Red and mounted using histomount.

Quantitative morphology calculations

To capture measurements for the cell perimeters and areas, images from six different individuals were selected for each genotype tested. A minimum of 10 cells of each cell type (xylem vessels, xylem fibres, phloem and parenchyma) were selected from a wedge with a 60° central angle from each image (Fig. S6A). Cells of each type were selected along the full length of the radial axis to ensure that cells of all sizes and phenotypic variation were represented. A MATLAB code (available on request) was generated to extract the intrinsic properties of each cell type. To that end, the code was designed to split each image into binary sub-images, wherein the interior of the cell type of interest was represented as white objects on black background (Fig. S6B). The cells (the white objects) from each image were then analysed as connected components of the image and their area and perimeter extracted. To remove noise, i.e. data obtained from objects that were wrongly classified as connected components within the algorithm (e.g. stray pixels), the code was devised to discard data that yielded unrealistically small values for perimeter and area (perimeter value of 0 µm, area smaller than 1 µm^2). The data were converted from pixels to µm using a calibration factor, in order to yield results consistent with laboratory observations. For each cell type, an equal number of cells was selected on a random basis from each plant within each genotype to avoid small variations between the number of representatives obtained from each individual plant.

To test the significance of the variation between the cell areas and perimeters between the different genotypes, a nested ANOVA was performed in R at 5% significance level. To perform the nested ANOVA, the data were classified according to genotype (treatment) and plant ID (plants within that treatment), with the response variable either the area or perimeter. A post-hoc Tukey HSD test was performed to determine the significance of the pairwise differences between the means of the areas/perimeters between the different genotypes. To determine the reliability of the results, the residuals from the data were tested for normality. Histograms and quantile-quantile plots for the residuals of each cell type were used to judge the distribution, followed by a Shapiro-Wilk normality test. The residuals for the data for all cell types withstood the Shapiro-Wilk normality test at 5% significance level, confirming that the results of the ANOVA analysis were reliable.

Mean hypocotyl diameters were measured using callipers. The radius was calculated from hypocotyl images of six plants from each genotype. A MATLAB code was used to measure the length of the shorter radius. The length of the radii in pixels was subsequently converted to µm. A Lilliefors test at 5% significance level was used to confirm that the radii for each genotype were normally distributed. A one-way ANOVA followed by a post-hoc Tukey HSD test was used to determine pairwise variation between the means.

Acknowledgements

We thank Miguel de Lucas, Keith Lindsey and Jen Topping for critical reading of the manuscript, and Youssef Belkhadir for comments on the preprint. The authors are grateful to Keiko Torii for sharing *er* and *erl* mutants, and *ER*f reporter lines, and to the Nottingham Arabidopsis Stock Centre for providing other genetic resources.

Competing interests

The authors declare no competing or financial interests.

Author contributions

Conceptualization: J.P.E.; Software: K.S.B., I.H.J.; Formal analysis: J.P.E.; Investigation: N.W., K.S.B., R.E.D., X.Y.W., J.T.K., K.A.C., J.P.E.; Writing - original draft: J.P.E.; Writing - review & editing: K.S.B., R.E.D., I.H.J., S.R.T.; Supervision: W.W., I.H.J., S.R.T., J.P.E.; Project administration: J.P.E.; Funding acquisition: S.R.T., J.P.E.

Funding

This work was funded by the European Union (329978, a Marie Skladowska Curie Fellowship to J.P.E.), by the Biotechnology and Biological Sciences Research Council (BB/H019928 to J.P.E. and S.R.T., and a NLD-DTP studentship to K.S.B., J.P.E. and I.H.J.), and by an N8 AgriFood programme grant to J.P.E. and S.R.T. The authors gratefully acknowledge a travel grant from Henan Agricultural University to N.W.

Supplementary information

Supplementary information available online at
http://dev.biologists.org/lookup/doi/10.1242/dev.177105.supplemental

References

Abrash, E. B., Davies, K. A. and Bergmann, D. C. (2011). Generation of signaling specificity in arabidopsis by spatially restricted buffering of ligand–receptor interactions. *Plant Cell* **23**, 2864-2879. doi:10.1105/tpc.111.086637

Bae, S., Park, J. and Kim, J.-S. (2014). Cas-OFFinder: a fast and versatile algorithm that searches for potential off-target sites of Cas9 RNA-guided endonucleases. *Bioinformatics* **30**, 1473-1475. doi:10.1093/bioinformatics/btu048

Bemis, S. M., Lee, J. S., Shpak, E. D. and Torii, K. U. (2013). Regulation of floral patterning and organ identity by Arabidopsis ERECTA-family receptor kinase genes. *J. Exp. Bot.* **64**, 5323-5333. doi:10.1093/jxb/ert270

Bencivenga, S., Serrano-Mislata, A., Bush, M., Fox, S. and Sablowski, R. (2016). Control of oriented tissue growth through repression of organ boundary genes promotes stem morphogenesis. *Dev. Cell* **39**, 198-208. doi:10.1016/j.devcel.2016.08.013

Bhatt, A. M., Etchells, J. P., Canales, C., Lagodienko, A. and Dickinson, H. (2004). VAAMANA–a BEL1-like homeodomain protein, interacts with KNOX proteins BP and STM and regulates inflorescence stem growth in Arabidopsis. *Gene* **328**, 103-111. doi:10.1016/j.gene.2003.12.033

Chaffey, N., Cholewa, E., Regan, S. and Sundberg, B. (2002). Secondary xylem development in Arabidopsis: a model for wood formation. *Physiol. Plant* **114**, 594-600. doi:10.1034/j.1399-3054.2002.1140413.x

Clough, S. J. and Bent, A. F. (1998). Floral dip: a simplified method for Agrobacterium-mediated transformation of Arabidopsis thaliana. *Plant J.* **16**, 735-743. doi:10.1046/j.1365-313x.1998.00343.x

De Veylder, L., Beeckman, T., Beemster, G. T. S., Engler, J. D., Ormenese, S., Maes, S., Naudts, M., Van der Schueren, E., Jacqmard, A., Engler, G. et al. (2002). Control of proliferation, endoreduplication and differentiation by the Arabidopsis E2Fa-DPa transcription factor. *EMBO J.* **21**, 1360-1368. doi:10.1093/emboj/21.6.1360

Dolan, L., Janmaat, K., Willemsen, V., Linstead, P., Poethig, S., Roberts, K. and Scheres, B. (1993). Cellular-organization of the arabidopsis-thaliana root. *Development* **119**, 71-84.

Efroni, I., Mello, A., Nawy, T., Ip, P.-L., Rahni, R., DelRose, N., Powers, A., Satija, R. and Birnbaum, K. D. (2016). Root regeneration triggers an embryo-like sequence guided by hormonal interactions. *Cell* **165**, 1721-1733. doi:10.1016/j.cell.2016.04.046

Etchells, J. P. and Turner, S. R. (2010). The PXY-CLE41 receptor ligand pair defines a multifunctional pathway that controls the rate and orientation of vascular cell division. *Development* **137**, 767-774. doi:10.1242/dev.044941

Etchells, J. P., Moore, L., Jiang, W. Z., Prescott, H., Capper, R., Saunders, N. J., Bhatt, A. M. and Dickinson, H. G. (2012). A role for BELLRINGER in cell wall development is supported by loss-of-function phenotypes. *BMC Plant Biol.* **12**, 212. doi:10.1186/1471-2229-12-212

Etchells, J. P., Provost, C. M., Mishra, L. and Turner, S. R. (2013). WOX4 and WOX14 act downstream of the PXY receptor kinase to regulate plant vascular proliferation independently of any role in vascular organisation. *Development* **140**, 2224-2234. doi:10.1242/dev.091314

Fisher, K. and Turner, S. (2007). PXY, a receptor-like kinase essential for maintaining polarity during plant vascular-tissue development. *Curr. Biol.* **17**, 1061-1066. doi:10.1016/j.cub.2007.05.049

Han, S., Cho, H., Noh, J., Qi, J., Jung, H.-J., Nam, H., Lee, S., Hwang, D., Greb, T. and Hwang, I. (2018). BIL1-mediated MP phosphorylation integrates PXY and cytokinin signalling in secondary growth. *Nat. Plants* **4**, 605-614. doi:10.1038/s41477-018-0180-3

Hemerly, A., Engler, J. D. A., Bergounioux, C., Van Montagu, M., Engler, G., Inzé, D. and Ferreira, P. (1995). Dominant negative mutants of the Cdc2 kinase uncouple cell division from iterative plant development. *EMBO J.* **14**, 3925-3936. doi:10.1002/j.1460-2075.1995.tb00064.x

Hemerly, A. S., Ferreira, P. C. G., Van Montagu, M. and Inze, D. (1999). Cell cycle control and plant morphogenesis: is there an essential link? *BioEssays* **21**, 29-37 doi:10.1002/(SICI)1521-1878(199901)21:1

Hirakawa, Y., Shinohara, H., Kondo, Y., Inoue, A., Nakanomyo, I., Ogawa, M., Sawa, S., Ohashi-Ito, K., Matsubayashi, Y. and Fukuda, H. (2008). Non-cell-autonomous control of vascular stem cell fate by a CLE peptide/receptor system. *Proc. Natl. Acad. Sci. USA* https://www.ncbi.nlm.nih.gov/pubmed/?term=Non-cell-autonomous+control+of+vascular+stem+cell+fate+by+a+CLE+peptide%2Freceptor+system **105**, 15208-15213. doi:10.1073/pnas.0808444105

Hirakawa, Y., Kondo, Y. and Fukuda, H. (2010). TDIF peptide signaling regulates vascular stem cell proliferation via the WOX4 homeobox gene in arabidopsis. *Plant Cell* **22**, 2618-2629. doi:10.1105/tpc.110.076083

Horiguchi, G. and Tsukaya, H. (2011). Organ size regulation in plants: insights from compensation. *Front. Plant Sci.* https://www.ncbi.nlm.nih.gov/pubmed/?term=Organ+size+regulation+in+plants%3A+insights+from+compensation **2**, 24. doi:10.3389/fpls.2011.00024

Ikematsu, S., Tasaka, M., Torii, K. U. and Uchida, N. (2017). ERECTA-family receptor kinase genes redundantly prevent premature progression of secondary growth in the Arabidopsis hypocotyl. *New Phytol.* **213**, 1697-1709. doi:10.1111/nph.14335

Ito, Y., Nakanomyo, I., Motose, H., Iwamoto, K., Sawa, S., Dohmae, N. and Fukuda, H. (2006). Dodeca-CLE peptides as suppressors of plant stem cell differentiation. *Science* **313**, 842-845. doi:10.1126/science.1128436

Kajala, K., Ramakrishna, P., Fisher, A., Bergmann, D. C., De Smet, I., Sozzani, R., Weijers, D. and Brady, S. M. (2014). Omics and modelling approaches for understanding regulation of asymmetric cell divisions in arabidopsis and other angiosperm plants. *Ann. Bot.* **113**, 1083-1105. doi:10.1093/aob/mcu065

Kimura, Y., Tasaka, M., Torii, K. U. and Uchida, N. (2018). ERECTA-family genes coordinate stem cell functions between the epidermal and internal layers of the shoot apical meristem. *Development* **145**, dev156380. doi:10.1242/dev.156380

Kondo, Y., Ito, T., Nakagami, H., Hirakawa, Y., Saito, M., Tamaki, T., Shirasu, K. and Fukuda, H. (2014). Plant GSK3 proteins regulate xylem cell differentiation downstream of TDIF–TDR signalling. *Nat. Commun.* **5**, 3504. doi:10.1038/ncomms4504

Lehmeier, C., Pajor, R., Lundgren Marjorie, R., Mathers, A., Sloan, J., Bauch, M., Mitchell, A., Bellasio, C., Green, A., Bouyer, D. et al. (2017). Cell density and airspace patterning in the leaf can be manipulated to increase leaf photosynthetic capacity. *Plant J.* **92**, 981-994. doi:10.1111/tpj.13727

Ragni, L., Nieminen, K., Pacheco-Villalobos, D., Sibout, R., Schwechheimer, C. and Hardtke, C. S. (2011). Mobile gibberellin directly stimulates arabidopsis hypocotyl xylem expansion. *Plant Cell* **23**, 1322-1336. doi:10.1105/tpc.111.084020

Ramakers, C., Ruijter, J. M., Deprez, R. H. L. and Moorman, A. F. M. (2003). Assumption-free analysis of quantitative real-time polymerase chain reaction (PCR) data. *Neurosci. Lett.* **339**, 62-66. doi:10.1016/S0304-3940(02)01423-4

Shi, D., Lebovka, I., López-Salmerón, V., Sanchez, P. and Greb, T. (2019). Bifacial cambium stem cells generate xylem and phloem during radial plant growth. *Development* **146**, dev171355. doi:10.1242/dev.171355

Shpak, E. D., Lakeman, M. B. and Torii, K. U. (2003). Dominant-negative receptor uncovers redundancy in the Arabidopsis ERECTA leucine-rich repeat receptor-like kinase signaling pathway that regulates organ shape. *Plant Cell* **15**, 1095-1110. doi:10.1105/tpc.010413

Shpak, E. D., Berthiaume, C. T., Hill, E. J. and Torii, K. U. (2004). Synergistic interaction of three ERECTA-family receptor-like kinases controls Arabidopsis organ growth and flower development by promoting cell proliferation. *Development* **131**, 1491-1501. doi:10.1242/dev.01028

Shpak, E. D., McAbee, J. M., Pillitteri, L. J. and Torii, K. U. (2005). Stomatal patterning and differentiation by synergistic interactions of receptor kinases. *Science* **309**, 290-293. doi:10.1126/science.1109710

Smakowska-Luzan, E., Mott, G. A., Parys, K., Stegmann, M., Howton, T. C., Layeghifard, M., Neuhold, J., Lehner, A., Kong, J., Grünwald, K. et al. (2018). An extracellular network of Arabidopsis leucine-rich repeat receptor kinases. *Nature* **553**, 342. doi:10.1038/nature25184

Smetana, O., Mäkilä, R., Lyu, M., Amiryousefi, A., Sánchez Rodríguez, F., Wu, M.-F., Solé-Gil, A., Leal Gavarrón, M., Siligato, R., Miyashima, S. et al. (2019). High levels of auxin signalling define the stem-cell organizer of the vascular cambium. *Nature* **565**, 485-489. doi:10.1038/s41586-018-0837-0

Smith, H. M. S. and Hake, S. (2003). The interaction of two homeobox genes, BREVIPEDICELLUS and PENNYWISE, regulates internode patterning in the arabidopsis inflorescence. *Plant Cell* **15**, 1717-1727. doi:10.1105/tpc.012856

Suer, S., Agusti, J., Sanchez, P., Schwarz, M. and Greb, T. (2011). WOX4 imparts auxin responsiveness to cambium cells in arabidopsis. *Plant Cell* **23**, 3247-3259. doi:10.1105/tpc.111.087874

ten Hove, C. A., Lu, K.-J. and Weijers, D. (2015). Building a plant: cell fate specification in the early Arabidopsis embryo. *Development* **142**, 420-430. doi:10.1242/dev.111500

Torii, K. U., Mitsukawa, N., Oosumi, T., Matsuura, Y., Yokoyama, R., Whittier, R. F. and Komeda, Y. (1996). The arabidopsis ERECTA gene encodes a putative receptor protein kinase with extracellular leucine-rich repeats. *Plant Cell* **8**, 735-746. doi:10.1105/tpc.8.4.735

Uchida, N. and Tasaka, M. (2013). Regulation of plant vascular stem cells by endodermis-derived EPFL-family peptide hormones and phloem-expressed ERECTA-family receptor kinases. *J. Exp. Bot.* **64**, 5335-5343. doi:10.1093/jxb/ert196

Uchida, N., Lee, J. S., Horst, R. J., Lai, H.-H., Kajita, R., Kakimoto, T., Tasaka, M. and Torii, K. U. (2012). Regulation of inflorescence architecture by intertissue layer ligand–receptor communication between endodermis and phloem. *Proc. Natl. Acad. Sci. USA* **109**, 6337-6342. doi:10.1073/pnas.1117537109

Uchida, N., Shimada, M. and Tasaka, M. (2013). ERECTA-Family Receptor Kinases Regulate Stem Cell Homeostasis via Buffering its Cytokinin Responsiveness in the Shoot Apical Meristem. *Plant Cell Physiol.* **54**, 343-351. doi:10.1093/pcp/pcs109

Ullah, H., Chen, J.-G., Young, J. C., Im, K.-H., Sussman, M. R. and Jones, A. M. (2001). Modulation of cell proliferation by heterotrimeric G protein in arabidopsis. *Science* **292**, 2066-2069. doi:10.1126/science.1059040

Waese, J., Fan, J., Pasha, A., Yu, H., Fucile, G., Shi, R., Cumming, M., Kelley, L. A., Sternberg, M. J., Krishnakumar, V. et al. (2017). ePlant: visualizing and exploring multiple levels of data for hypothesis generation in plant biology. *Plant Cell* **29**, 1806-1821. doi:10.1105/tpc.17.00073

Wang, Z.-P., Xing, H.-L., Dong, L., Zhang, H.-Y., Han, C.-Y., Wang, X.-C. and Chen, Q.-J. (2015). Egg cell-specific promoter-controlled CRISPR/Cas9 efficiently generates homozygous mutants for multiple target genes in Arabidopsis in a single generation. *Genome Biol.* **16**, 144. doi:10.1186/s13059-015-0715-0

Wunderling, A., Ripper, D., Barra-Jimenez, A., Mahn, S., Sajak, K., Targem, M. B. and Ragni, L. (2018). A molecular framework to study periderm formation in Arabidopsis. *New Phytol.* **219**, 216-229. doi:10.1111/nph.15128

Xie, K., Zhang, J. and Yang, Y. (2014). Genome-wide prediction of highly specific guide RNA spacers for CRISPR–Cas9-mediated genome editing in model plants and major crops. *Mol. Plant* **7**, 923-926. doi:10.1093/mp/ssu009

Xing, H.-L., Dong, L., Wang, Z.-P., Zhang, H.-Y., Han, C.-Y., Liu, B., Wang, X.-C. and Chen, Q.-J. (2014). A CRISPR/Cas9 toolkit for multiplex genome editing in plants. *BMC Plant Biol.* **14**, 327. doi:10.1186/s12870-014-0327-y

Zhang, H., Lin, X., Han, Z., Qu, L.-J. and Chai, J. (2016). Crystal structure of PXY-TDIF complex reveals a conserved recognition mechanism among CLE peptide-receptor pairs. *Cell Res.* **26**, 543. doi:10.1038/cr.2016.45

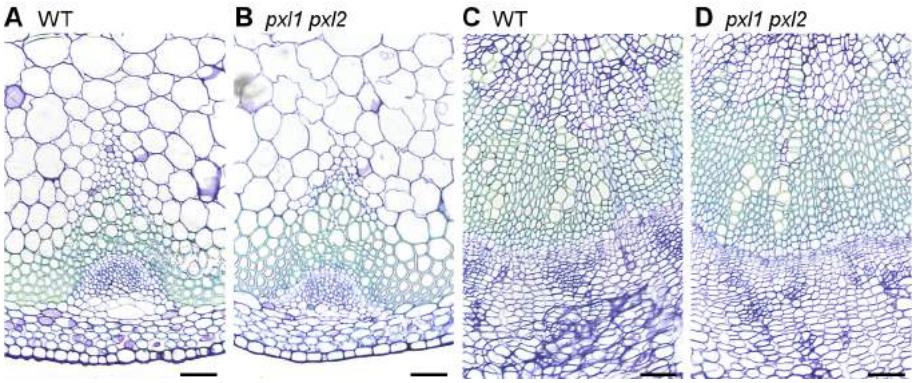

Figure S1. *pxl1 pxl2* vascular tissue is indistinguishable from wild type. Inflorescence stem vascular bundles from wild type plants (A) and *pxl1 pxl2* lines (B). Hypocotyl transverse sections from wild type (C) and *pxl1 pxl2* plants (D). Scales are 50 µM.

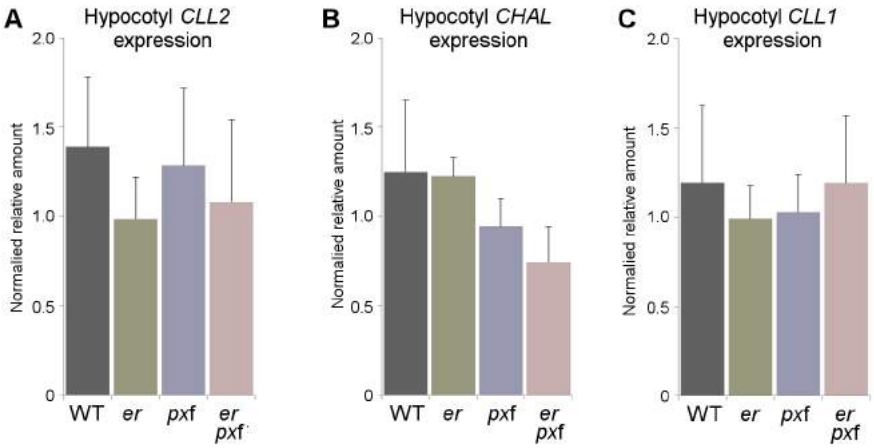

Figure S2. *EPFL* expression in hypocotyls. (A-C) Hypocotyl expression of *CLL2* (A), *CHAL* (B) and *CLL1* (C) in wild type, *er*, and *pxf* mutants (expression normalised to 18S rRNA). No significant differences in expression were observed, using ANOVA and LSD post-hoc test.

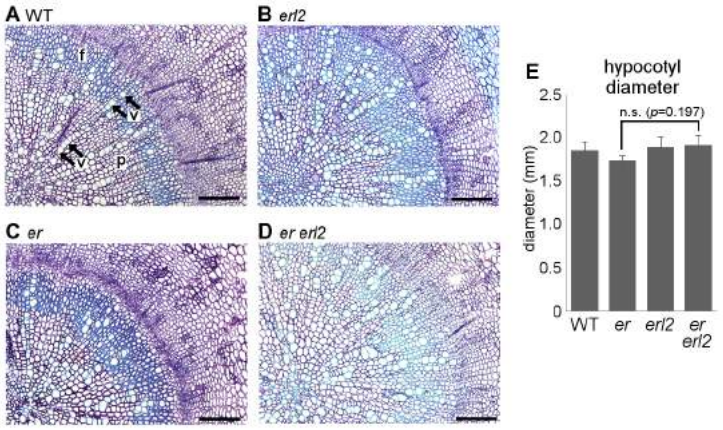

Figure S3. *er* and *erl2* mutant hypocotyl phenotypes. (A-D) Hypocotyl transverse sections of wild type (A), *erl2* (B), *er* (C), and *er erl2* (D) lines. (E) Graph showing hypocotyl diameter or *er erl2* lines and controls at 5 weeks old. Xylem fibres are marked 'f'; black arrows (v) mark vessels; 'p' marks parenchyma. Scales are 100 µM. *p* values were calculated with ANOVA and LSD post-hoc test.

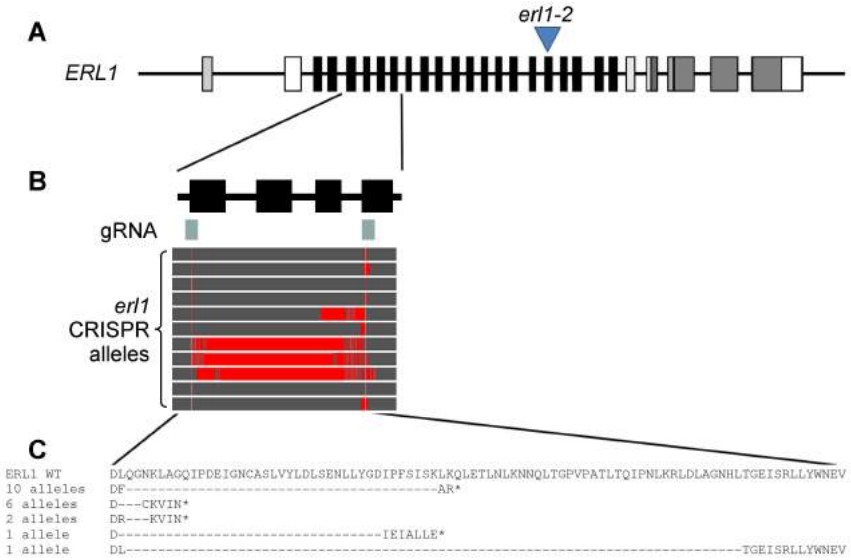

Figure S4. Diagram showing CRISPR/Cas9 generated *erl1* alleles. (A) Diagram showing intron-exon structure of *ERL1* with position of commonly used *erl1-2* allele marked with a blue triangle. (B) Close up of exons 5-8 showing positions of guide RNA (grey-green boxes), and the alleles identifies in the family analysed. Grey represents alignment with wild type sequence; red shows no alignment. (C) Translation of wild type and mutant *erl1* alleles. All but one has premature stop codons; the remaining allele has a large deletion of the LRR domain.

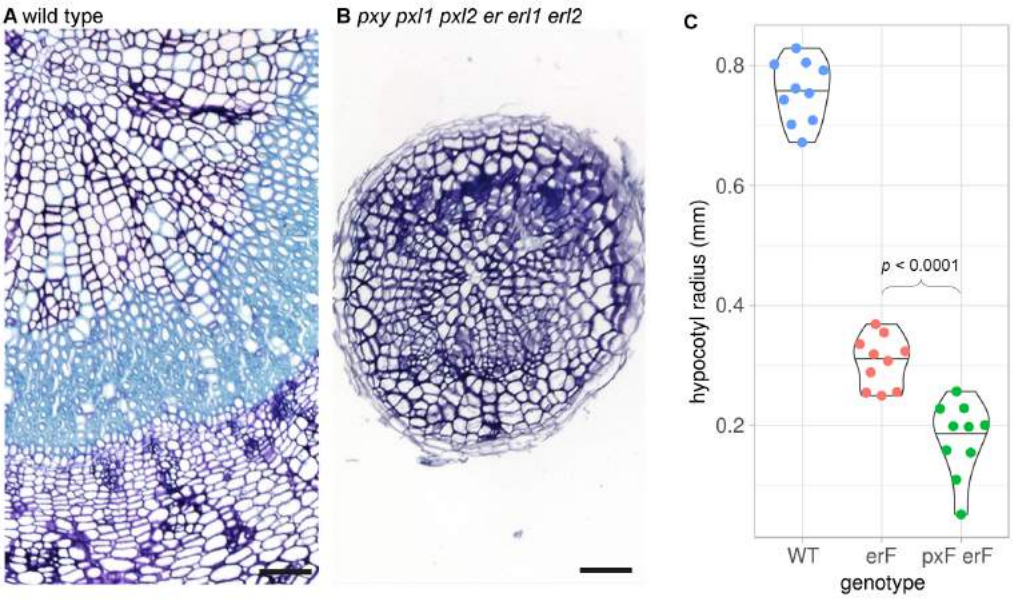

Figure S5. *pxf erf* hypocotyls. Close-up of wild type (A) and *px*f *er*f (B) hypocotyls. Scales are 50 µM. (C) Violin plot showing comparison of *px*f and *px*f *er*f hypocotyl radii. *p* values were calculated with ANOVA and LSD post-hoc test.

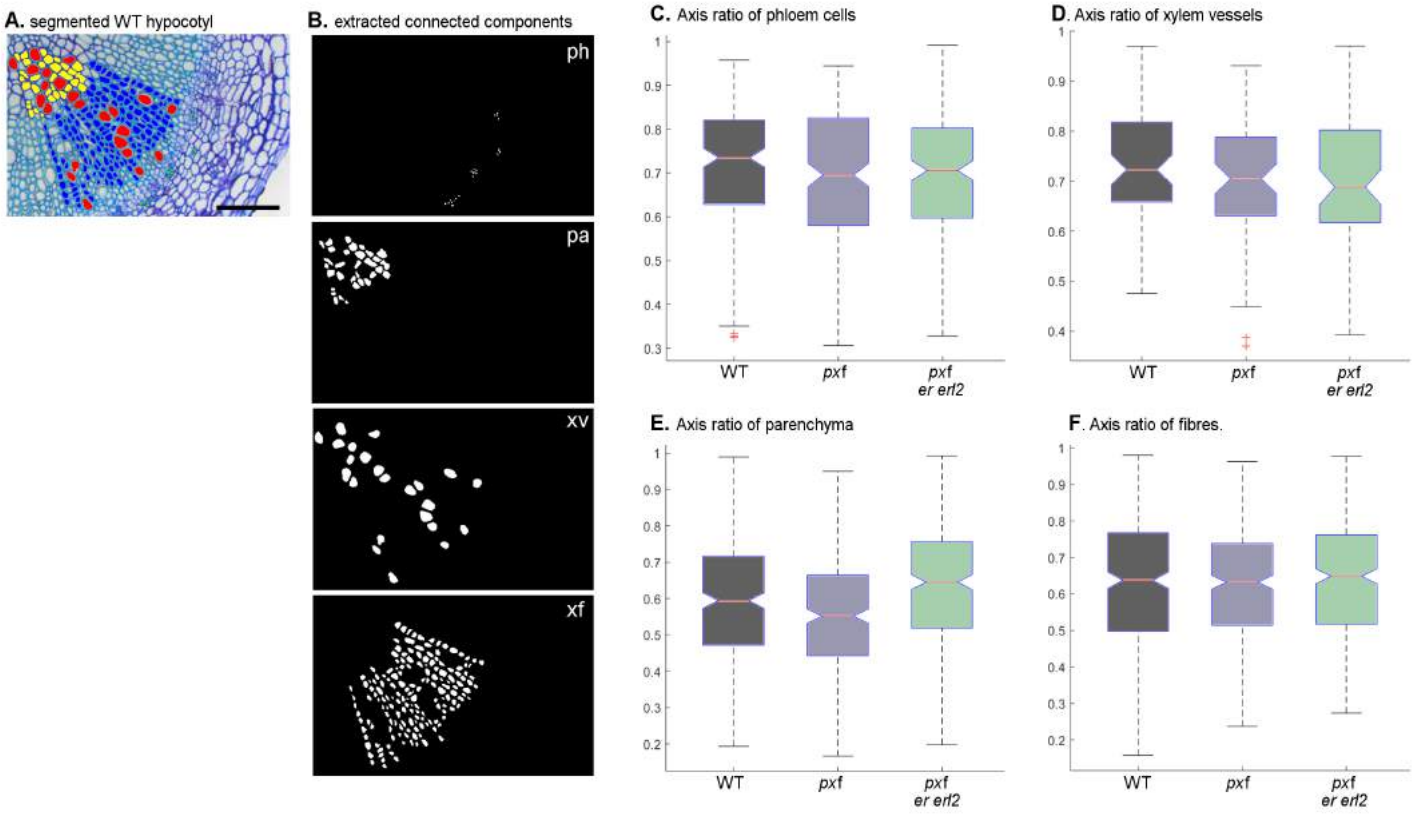

Figure S6. Example of extracted connected components. (A-B) Wild type hypocotyl with cell types segmented (xylem parenchyma are yellow; xylem fibres are blue; xylem vessels are red; phloem are green; A). Scale is 100 µM. (B) extracted connected components. (C-F) Notched box plot showing comparison of elipticity from extracted connected components for phloem (C), xylem vessels (D), parenchyma (E), and fibres (F) from wild type, *pxf*, and *pxf er erl2* lines.

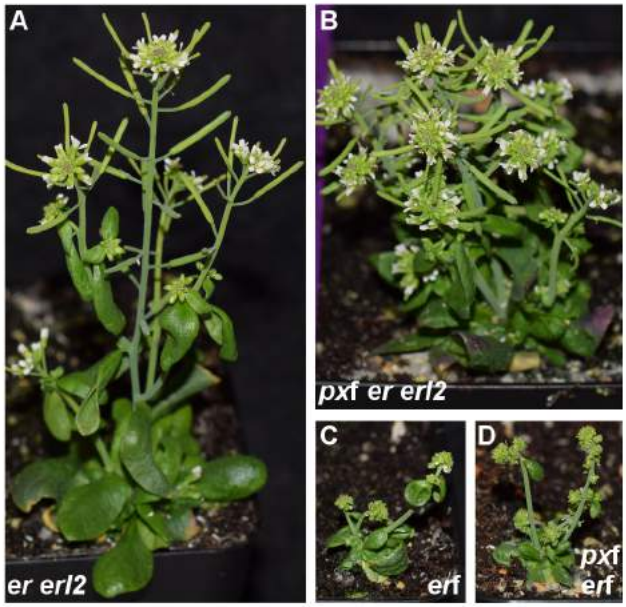

Figure S7. Gross morphology of a subset of mutant lines. (A) *er erl2*. (B) *pxf er erl2*. (C) *erf*. (D) *pxf erf* at 6 weeks old. Images were taken at the same magnification.

Table S1. Vascular proliferation and morphology characteristics of *pxf er* mutant combinations.

Genotype	Vascular bundle size and shape		Hypocotyl diameter (mm)
	cells per bundle	ratio tangential:radial	
Wild type	438.2 ± 15.74	0.61 ± 0.02	1.34 ± 0.04
pxy	347.6 ± 21.79	0.56 ± 0.02	1.24 ± 0.04
er	463.1 ± 23.05	0.67 ± 0.03	1.27 ± 0.05
pxy er	338.2 ± 30.13	1.36 ± 0.18	1.01 ± 0.06
er erl1 erl2	182.3 ± 20.60	0.65 ± 0.06	0.85 ± 0.04
pxy pxl1 pxl2	305.3 ± 38.35	0.91 ± 0.18	1.14 ± 0.04
pxy pxl1 pxl2 er	202.5 ± 28.84	2.30 ± 0.23	0.97 ± 0.06

values are ± S.E.M.

Table S2. *p* values from comparisons of cells per vascular bundle for each genotype tested (ANOVA + LSD).

compared genotypes		*p* value
WT	*er*	0.507
	er pxf	<0.001
	pxy	0.018
	pxy er	0.009
	pxf	0.001
er	WT	0.507
	er pxf	<0.001
	pxy	0.003
	pxy er	0.001
	pxf	<0.001
pxf er	WT	<0.001
	er	<0.001
	pxy	<0.001
	pxy er	0.001
	pxf	0.008
pxy	WT	0.018
	er	0.003
	er pxf	<0.001
	pxy er	0.802
	pxf	0.262
pxy er	WT	0.009
	er	0.001
	er pxf	0.001
	pxy	0.802
	pxf	0.382
pxf	WT	0.001
	er	<0.001
	er pxf	0.008
	pxy	0.262
	pxy er	0.382

Table S3. *p* values from comparisons of hypocotyl diameter for each genotype tested (ANOVA + LSD).

compared genotypes		*p* value
WT	*er*	0.048
	er pxf	<0.001
	pxy	0.028
	pxy er	<0.001
	pxf	0.001
er	WT	0.048
	er pxf	0.001
	pxy	0.816
	pxy er	<0.001
	pxf	0.142
pxf er	WT	<0.001
	er	0.001
	pxy	0.002
	pxy er	0.240
	pxf	0.062
pxy	WT	0.028
	er	0.816
	er pxf	0.002
	pxy er	<0.001
	pxf	0.214
pxy er	WT	<0.001
	er	<0.001
	er pxf	0.002
	pxy	<0.001
	pxf	0.214
pxf	WT	0.001
	er	0.142
	er pxf	0.062
	pxy	0.214
	pxy er	0.003

Table S4. *p* values from comparisons of cell perimeters measured from the vascular cells of each genotype tested (ANOVA + Tukey). Values in grey boxes were not significantly different at the 95% confidence level.

Statistical differences between hypocotyl cell perimeters

Compared genotypes	**xylem**			**phloem**
	vessel	fibres	parenchyma	
WT - *pxf*	0.001	0.007	< 0.0001	< 0.0001
WT - *pxf er*	0.001	< 0.0001	0.014	< 0.0001
WT - *pxf er erl1*	0.515	< 0.0001	1.000	0.374
WT - *pxf er erl2*	0.232	< 0.0001	0.826	0.388
WT - *pxf erf*	0.031	n.d.	0.567	< 0.0001
pxf - *pxf er*	1.000	0.132	< 0.0001	1.000
pxf - *pxf er erl1*	0.192	0.652	< 0.0001	0.001
pxf - *pxf er erl2*	< 0.0001	0.036	< 0.0001	0.001
pxf - *pxf erf*	< 0.0001	n.d.	< 0.0001	0.204
pxf er - *pxf er erl1*	0.193	0.863	0.037	0.001
pxf er - *pxf er erl2*	< 0.0001	0.987	< 0.0001	0.001
pxf er - *pxf erf*	< 0.0001	n.d.	0.579	0.188
pxf er erl1 - *pxf er erl2*	0.001	0.570	0.639	1.000
pxf er erl1 - *pxf erf*	< 0.0001	n.d.	0.769	< 0.0001
pxf er erl2 - *pxf erf*	0.967	n.d.	0.048	< 0.0001

Table S5. *p* values from pairwise comparisons of cell areas calculated from vascular cell types in the hypocotyl (ANOVA + Tukey). Values in grey boxes were not significantly different at the 95% confidence level.

Compared genotypes	vessel	xylem fiber	parenchyma	phloem
WT - *pxf*	0.001	< 0.0001	< 0.0001	< 0.0001
WT - *pxf er*	0.001	< 0.0001	0.051	< 0.0001
WT - *pxf er erl1*	0.068	< 0.0001	0.908	0.632
WT - *pxf er erl2*	0.787	< 0.0001	1.000	0.732
WT - *pxf erf*	0.231	n.d.	0.333	< 0.0001
pxf - *pxf er*	1.000	0.973	< 0.0001	0.922
pxf - *pxf er erl1*	0.819	0.995	< 0.0001	0.001
pxf - *pxf er erl2*	< 0.0001	0.798	< 0.0001	0.001
pxf - *pxf erf*	< 0.0001	n.d.	< 0.0001	0.036
pxf er - *pxf er erl1*	0.833	1.000	0.456	0.033
pxf er - *pxf er erl2*	< 0.0001	0.987	0.034	0.020
pxf er - *pxf erf*	< 0.0001	n.d.	0.963	0.001
pxf er erl1 - *pxf er erl2*	0.001	0.953	0.848	1.000
pxf er erl1 - *pxf erf*	< 0.0001	n.d.	0.922	< 0.0001
pxf er erl2 - *pxf erf*	0.941	n.d.	0.255	< 0.0001

Table S6. Pairwise comparisons of cell perimeters from vascular cells in the inflorescence stem. *p* values were calculated using ANOVA + Tukey. Values in grey boxes were not significantly different at the 95% confidence level.

Genotypes compared	**Xylem**		**phloem**
	vessel	fibres	
WT - *pxf*	0.001	0.136	< 0.0001
WT - *pxf er*	0.004	< 0.0001	0.012
WT - *pxf er erl1*	0.002	< 0.0001	< 0.0001
WT - *pxf er erl2*	< 0.0001	0.996	< 0.0001
WT - *pxf erf*	< 0.0001	n.d.	< 0.0001
pxf - *pxf er*	0.999	< 0.0001	0.773
pxf - *pxf er erl1*	1.000	< 0.0001	0.227
pxf - *pxf er erl2*	0.008	0.055	0.009
pxf - *pxf erf*	< 0.0001	n.d.	< 0.0001
pxf er - *pxf er erl1*	1.000	0.528	0.006
pxf er - *pxf er erl2*	0.002	< 0.0001	< 0.0001
pxf er - *pxf erf*	< 0.0001	n.d.	< 0.0001
pxf er erl1 - *pxf er erl2*	0.004	< 0.0001	0.843
pxf er erl1 - *pxf erf*	< 0.0001	n.d.	0.001
pxf er erl2 - *pxf erf*	< 0.0001	n.d.	0.058

Table S7. *p* values from pairwise comparisons of vascular cell area from inflorescence stems (ANOVA + Tukey). Values in grey boxes were not significantly different at the 95% confidence level.

Genotypes compared	Xylem		phloem
	vessel	fibres	
WT - *pxf*	0.0004	0.420	<0.0001
WT - *pxf er*	0.0003	<0.0001	<0.0001
WT - *pxf er erl1*	<0.0001	0.001	0.632
WT - *pxf er erl2*	<0.0001	0.855	0.732
WT - *pxf erf*	<0.0001	n.d.	<0.0001
pxf - *pxf er*	0.999	<0.0001	0.922
pxf - *pxf er erl1*	0.993	<0.0001	0.001
pxf - *pxf er erl2*	0.015	0.052	0.0005
pxf - *pxf erf*	<0.0001	n.d.	0.036
pxf er - *pxf er erl1*	0.995	0.021	0.033
pxf er - *pxf er erl2*	0.016	<0.0001	0.020
pxf er - *pxf erf*	<0.0001	n.d.	0.001
pxf er erl1 - *pxf er erl2*	0.076	0.040	0.999
pxf er erl1 - *pxf erf*	<0.0001	n.d.	<0.0001
pxf er erl2 - *pxf erf*	0.001	0.855	<0.0001

Table S8. Primers used in this manuscript

Name	sequence	function
ERL2_F	TGTGGATAACGAGGCCAACT	qRT-PCR
ERL2_R	ATGTGTCCTGAGTCCATGCA	qRT-PCR
ER_F	CACGGCTCACTGAGAAATCC	qRT-PCR
ER_R	TCACTTCATTGTTCCCCGTC	qRT-PCR
ERL1_F	ACTGGGAAGAAAGCAGTGGA	qRT-PCR
ERL1_R	CCTCTGGATCAACTGCTTCC	qRT-PCR
EPFL4_F	CTTCTCCGCCTCCTCCATAG	qRT-PCR
EPFL4_R	ACTCCTTATGAACCCACCCG	qRT-PCR
EPFL5_F	GTCCTCCCAACTCTCATCGT	qRT-PCR
EPFL5_R	ACCCGACCTAGCTATCTCCT	qRT-PCR
EPFL6_F	AGAAATTCTCAGCCGTCGGA	qRT-PCR
EPFL6_R	ACGGTACTCTTGCCTTCCTC	qRT-PCR
PXY_F	AGCATGGGTAGGTCGTGTAG	qRT-PCR
PXY_R	CAACACATCTCTCATCGGCG	qRT-PCR
PXL1_F	GACGTGGTTGAGTGGATTCG	qRT-PCR
PXL1_R	GGTGCAGAGAAGAGCGATTC	qRT-PCR
PXL2_F	AACGGAAACCTTGGTGATGC	qRT-PCR
PXL2_R	TCATGGTGGAGGTAAGCGAG	qRT-PCR
qRT_18s_rRNAf	CATCAGCTCGCGTTGACTAC	qRT-PCR
qRT_18s rRNAr	GATCCTTCCGCAGGTTCAC	qRT-PCR
qACT2f	GCCATCCAAGCTGTTCTCTC	qRT-PCR
qACT2r	ACCCTCGTAGATTGGCACAG	qRT-PCR
JL202 LB	CATTTTATAATAACGCTGCGGACATCTAC	genotyping
ERL1_LP	TTCATGTGCAGCCTTGAATC	genotyping
ERL1_RP	GCAATTGGCCAAGTTCAGTT	genotyping
ERL2_LP	TTCCCATGAACATTGCTGAA	genotyping
ERL2_RP	CCGGAAGTGATTGGTCTGAT	genotyping
ER-1	tttgtttttgtgcgtgtgtg	genotyping
ER-2	ATCATTCGGCTGTCTTTTGG	genotyping
GABI-LB	ATATTGACCATCATACTCATTGC	genotyping
pxl2-1(salk)F	ACCTCTATGCCACACACCAAG	genotyping
pxl2-1(salk)R	CAAGCTCTGACGGAATCTCAC	genotyping
salk_LBa1	TGGTTCACGTAGTGGGCCATCG	genotyping
pxl1-1(salk)F	AATCGATGGTCTATCCTTCGG	genotyping
pxl1-1(salk)R	TATGCGGTGGAGTTCTACCAC	genotyping
ER-GUSF	accactgtaaatttccgccag	genotyping
ER-GUSR	aagacttcgcgctgatacca	genotyping
ERL1-GUSF	acgccgttacttatctccgt	genotyping
ERL1-GUSR	atccagactgaatgcccaca	genotyping
ERL2-GUSF	tagaaccgtcgccgtcaaat	genotyping
ERL2-GUSR	ttcacgggttggggtttcta	genotyping
ERL1 DT1-BsF	ATATATGGTCTCGATTGCCAATTGCAGAGACTTGCAGTT	erl1-GE clone
ERL1 DT1-F0	TGCCAATTGCAGAGACTTGCAGTTTTAGAGCTAGAAATAGC	erl1-GE clone
ERL1 DT2-R0	AACTTAGATGATTGCCAGCAAGCAATCTCTTAGTCGACTCTAC	erl1-GE clone
ERL1 DT2-BsR	ATTATTGGTCTCGAAACTTAGATGATTGCCAGCAAGCAA	erl1-GE clone
VErl1_F	GAATTTGTCCAGTCTGAATCTTGG	erl1-GE genotyping
VErl1_R	CAAGTACCACAAACCGGTTAGC	erl1-GE genotyping

Appendix E

Appendix E1: Morris method rankings

Appendix E1.1: Morris method individual ranking for the network with the PXY-MP loop

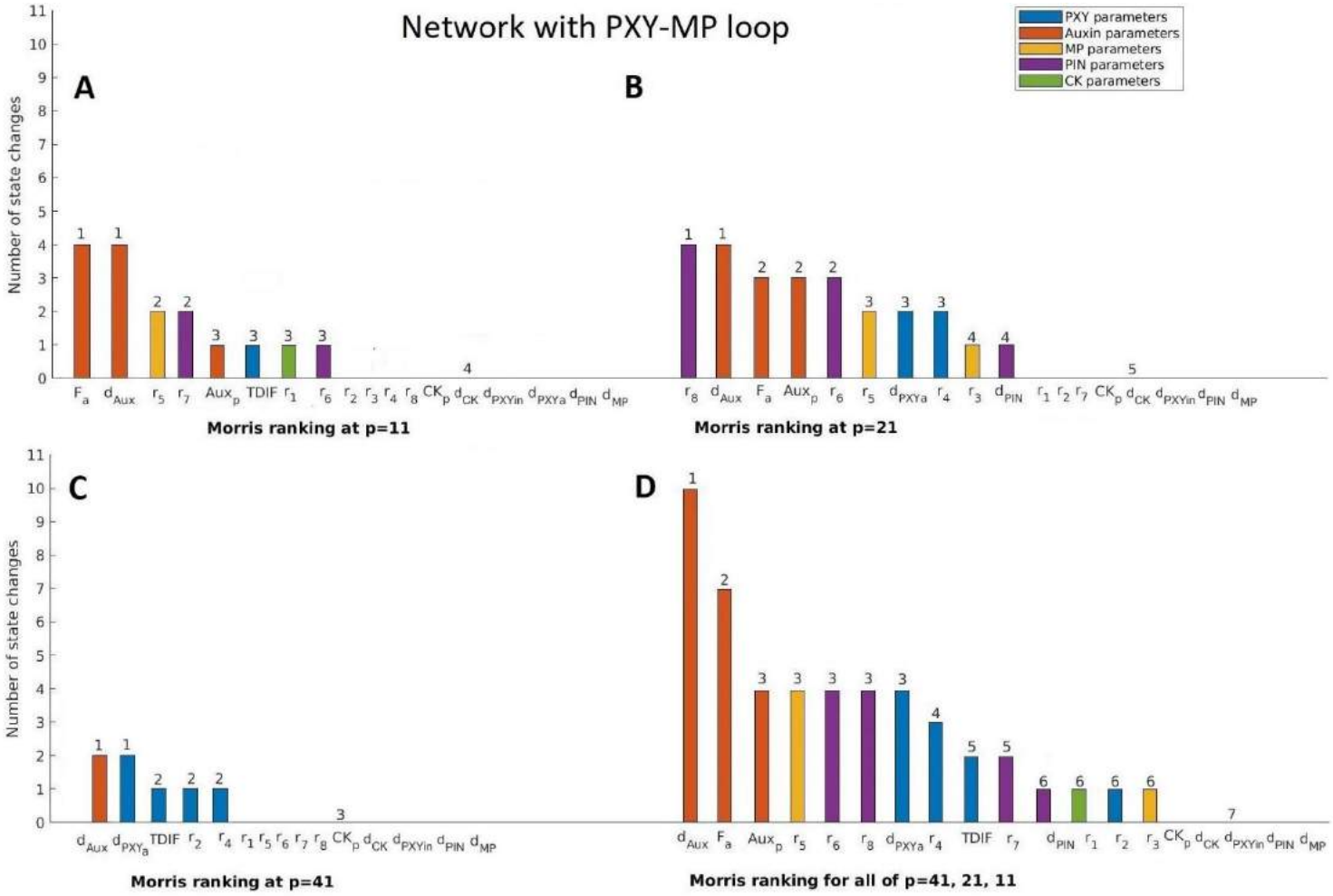

Figure 1S: Individual parameter sensitivity values for Morris levels for p=11 (A), p=21 (B), p=41 (C) and all three levels combined (D). ranking for the network with the PXY-MP feedback loop. Rank numbers are set above the bars, parameter names are below the bars. Rank 1 corresponds to the parameter that the network is most sensitive to, highest rank corresponds to parameter the network is least sensitive to. Bars of the same colours belong to the same parameter group, such that PXY-related parameters are blue, auxin-related parameters are orange, MP-related parameters are yellow, PIN related parameters are purple, and CK-related parameters are green.

Appendix E1.2: Morris method individual ranking for the network without the PXY-MP loop

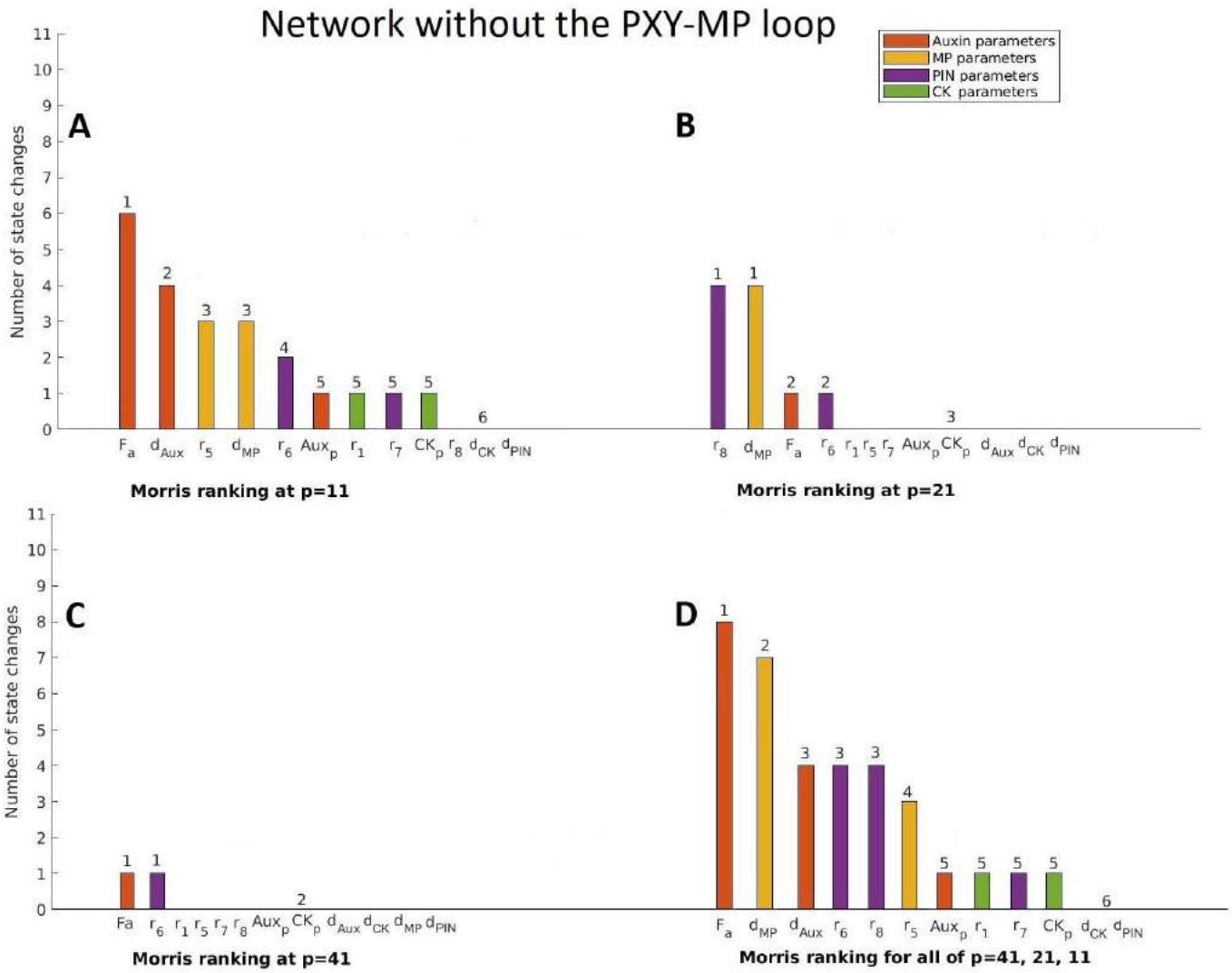

Figure 2S: Individual parameter sensitivity values for Morris levels for p=11 (A), p=21 (B), p=41 (C) and all three levels combined (D). ranking for the network without the PXY-MP feedback loop. Rank numbers are set above the bars, parameter names are below the bars. Rank 1 corresponds to the parameter that the network is most sensitive to, highest rank corresponds to parameter the network is least sensitive to. Bars of the same colours belong to the same parameter group, such that auxin-related parameters are orange, MP-related parameters are yellow, PIN related parameters are purple, and CK-related parameters are

Appendix E2: Probability density functions of the distribution of values of parameters that satisfy both networks vs only the network with the loop

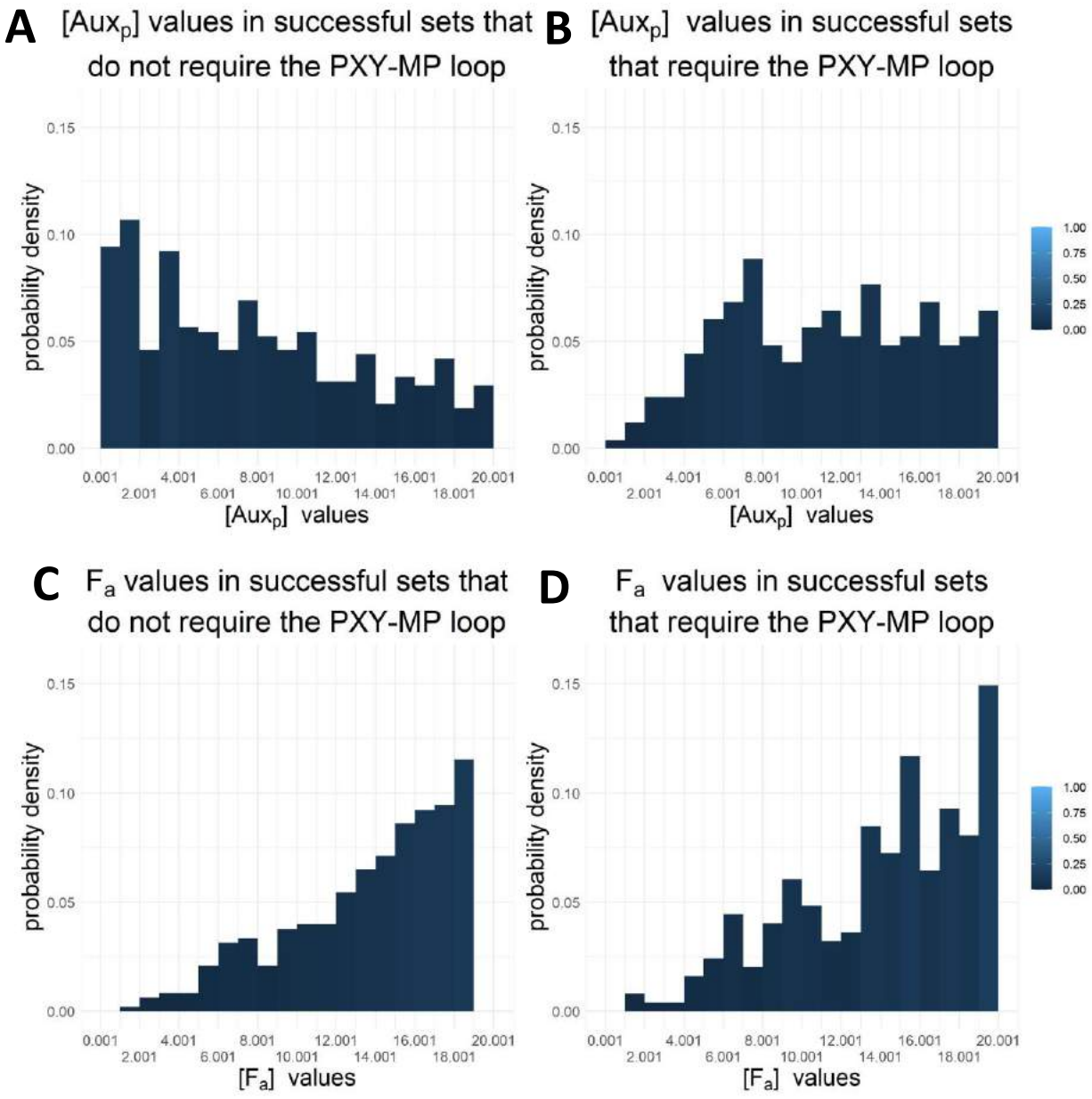

(graph continued on the next page…)

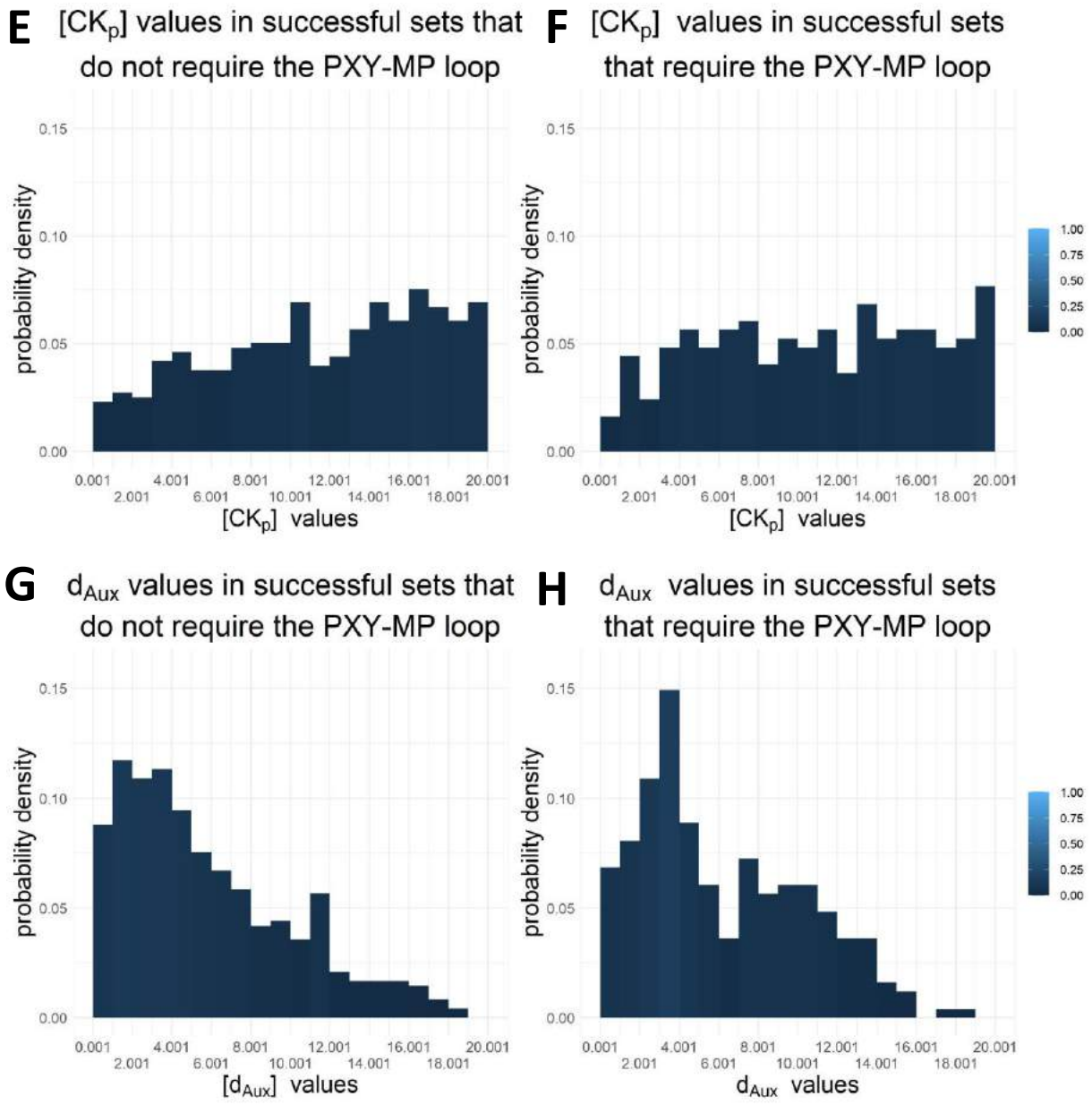

(graph continued on the next page…)

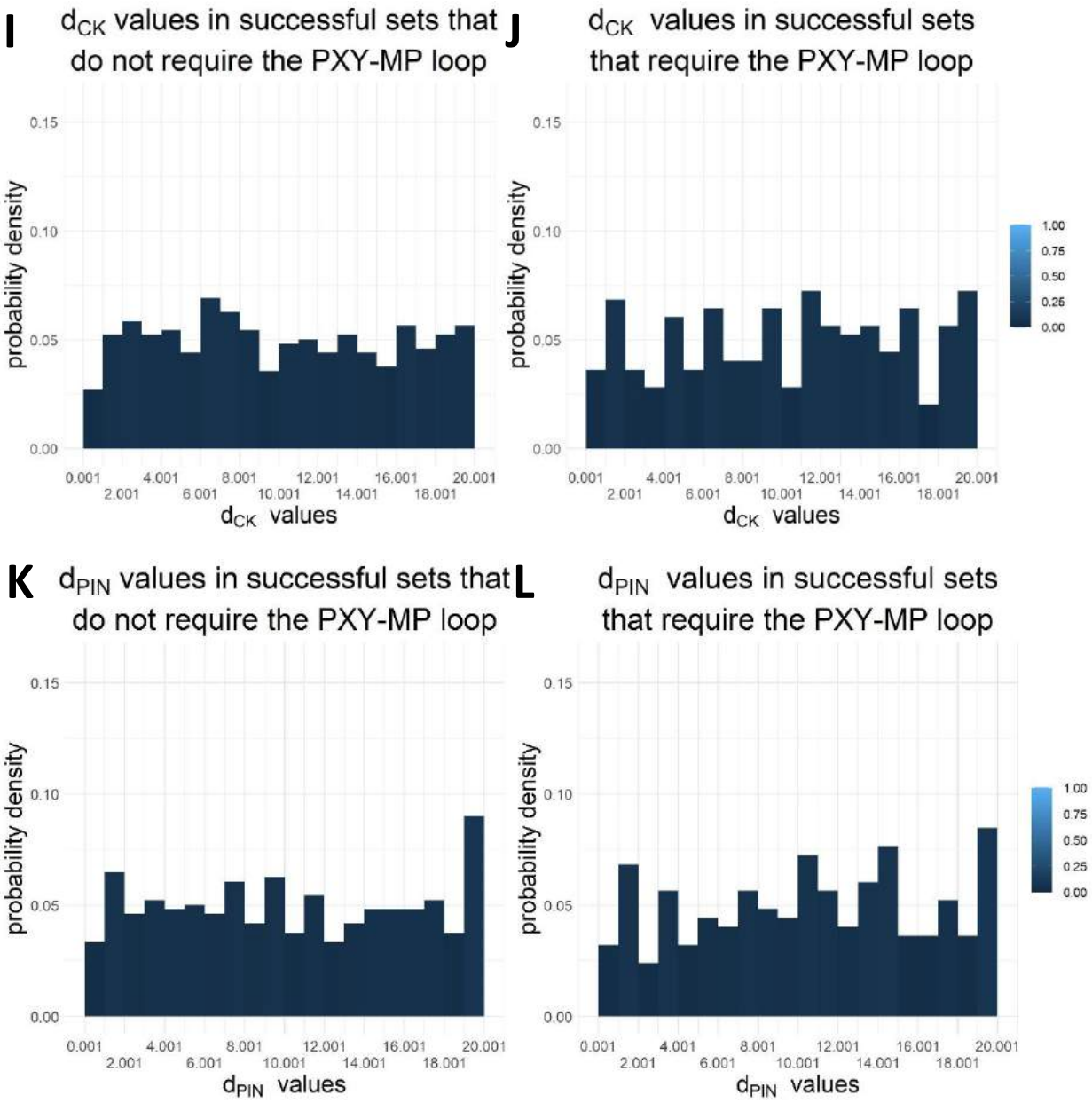

(graph continued on the next page…)

M

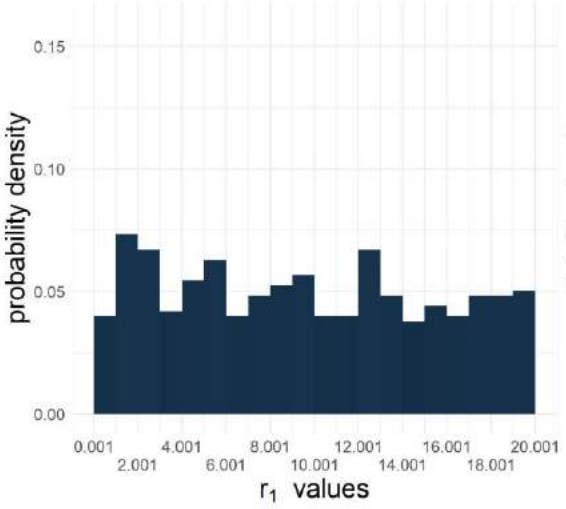
r1 values in successful sets that do not require the PXY-MP loop
probability density
0.15
0.10
0.05
0.00
0.001
2.001
4.001
6.001
8.001
10.001
12.001
14.001
16.001
18.001
20.001
r1 values

N

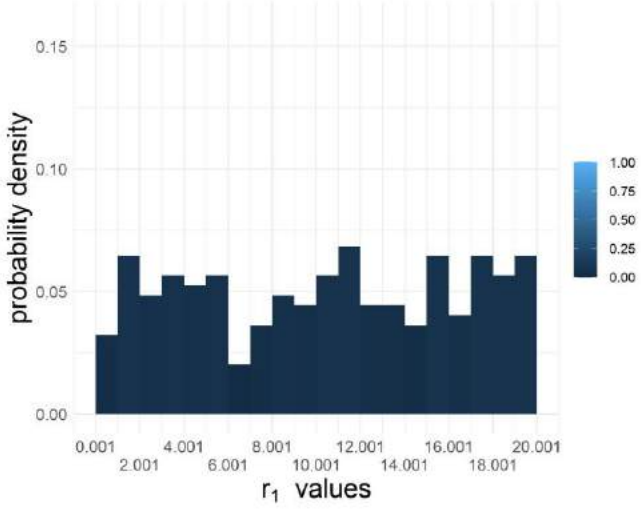
r1 values in successful sets that require the PXY-MP loop
probability density
0.15
0.10
0.05
0.00
0.001
2.001
4.001
6.001
8.001
10.001
12.001
14.001
16.001
18.001
20.001
r1 values
1.00
0.75
0.50
0.25
0.00

O

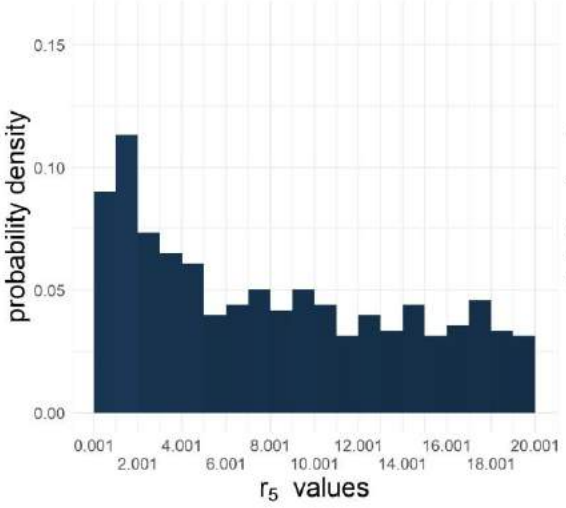
r5 values in successful sets that do not require the PXY-MP loop
probability density
0.15
0.10
0.05
0.00
0.001
2.001
4.001
6.001
8.001
10.001
12.001
14.001
16.001
18.001
20.001
r5 values

P

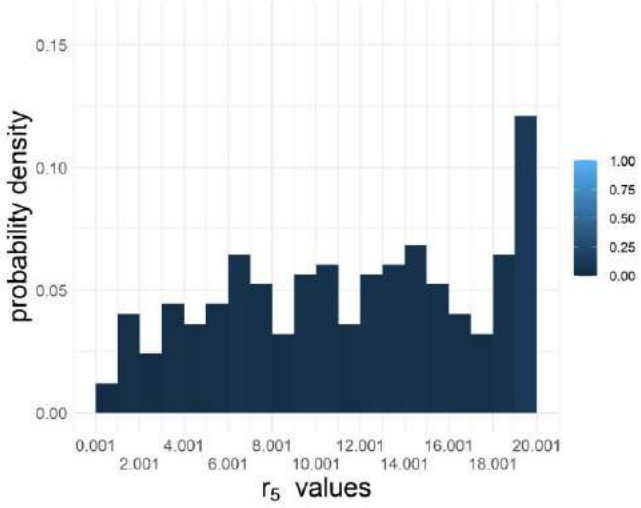
r5 values in successful sets that require the PXY-MP loop
probability density
0.15
0.10
0.05
0.00
0.001
2.001
4.001
6.001
8.001
10.001
12.001
14.001
16.001
18.001
20.001
r5 values
1.00
0.75
0.50
0.25
0.00

Q

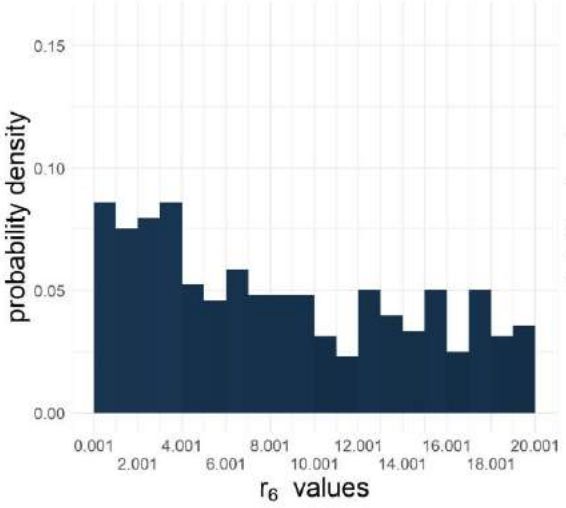
r6 values in successful sets that do not require the PXY-MP loop
probability density
0.15
0.10
0.05
0.00
0.001
2.001
4.001
6.001
8.001
10.001
12.001
14.001
16.001
18.001
20.001
r6 values

R

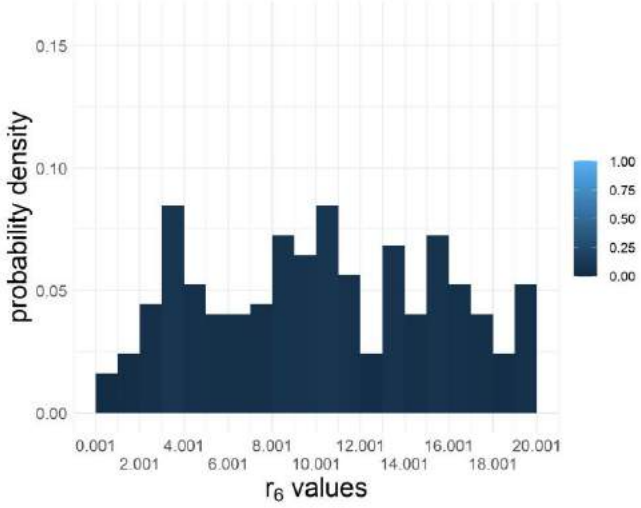
r6 values in successful sets that require the PXY-MP loop
probability density
0.15
0.10
0.05
0.00
0.001
2.001
4.001
6.001
8.001
10.001
12.001
14.001
16.001
18.001
20.001
r6 values
1.00
0.75
0.50
0.25
0.00

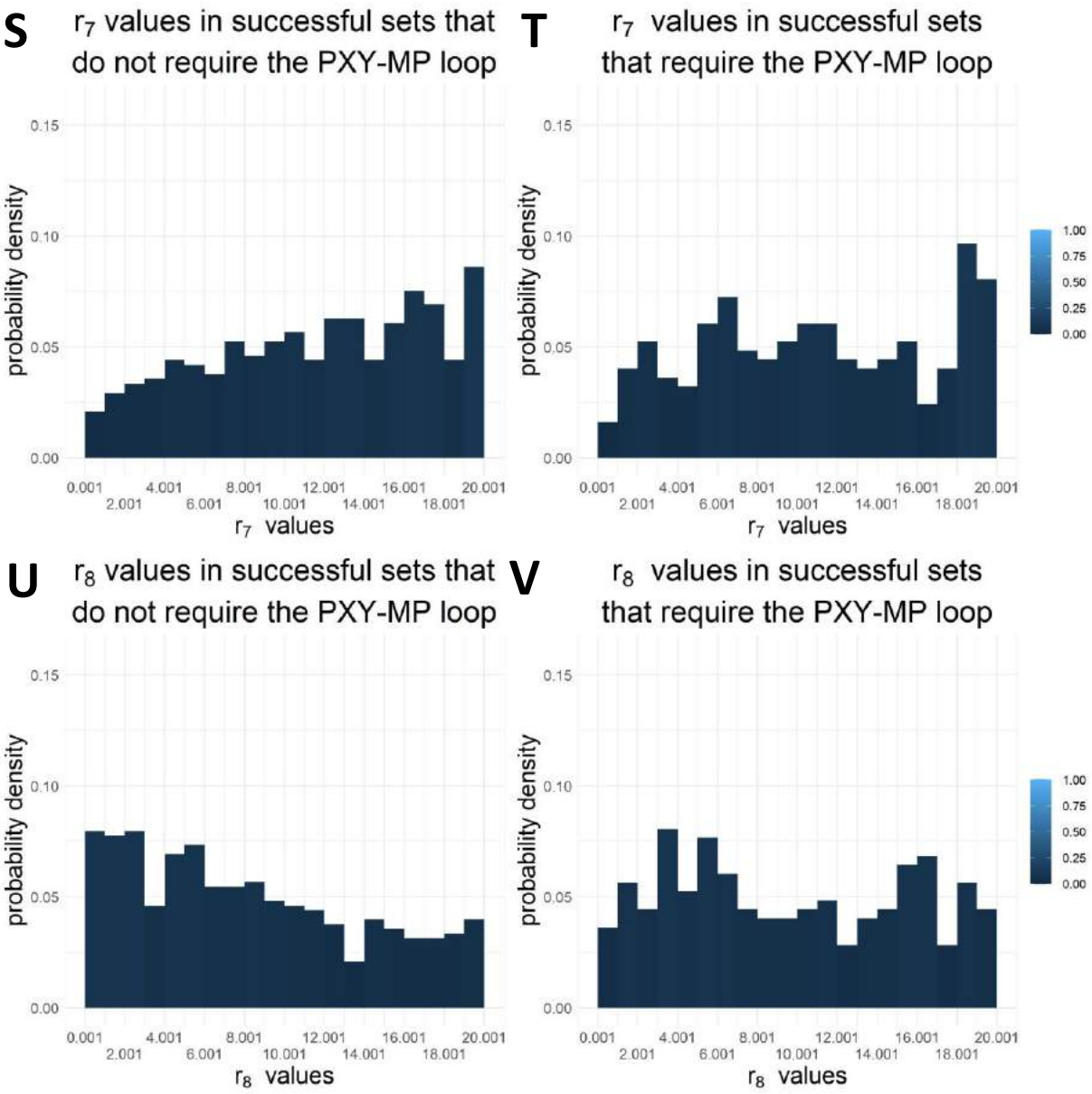

Figure 3S: Probability density functions of the distribution of $Aux_p, F_a, d_{Aux}, d_{PIN}, d_{CK}, r_1, r_5, r_7, r_8$ in the successful parameter set that do not require the PXY-MP negative feedback loop (left) and in those that require a PXY-MP negative feedback loop (right). Bin count = 20. Each bin contains 2 possible choices of values, except the last one which contains 3. Darker blue is lower probability, lighter is higher.

Note that for the parameters of the PXY-MP negative feedback loop and the final steady state concentration $[PXY_a]$ (Figure 31 A) only the distribution for the parameter sets which require the PXY-MP negative feedback loop were considered. This is the case as any values can be sampled for $r_2,\ r_3,\ r_4,\ TDIF,\ d_{PXY_a},\ d_{PXY_{in}}$ parameters and any $[PXY_a]$, yet the parameter set as a whole would not fail to pattern.

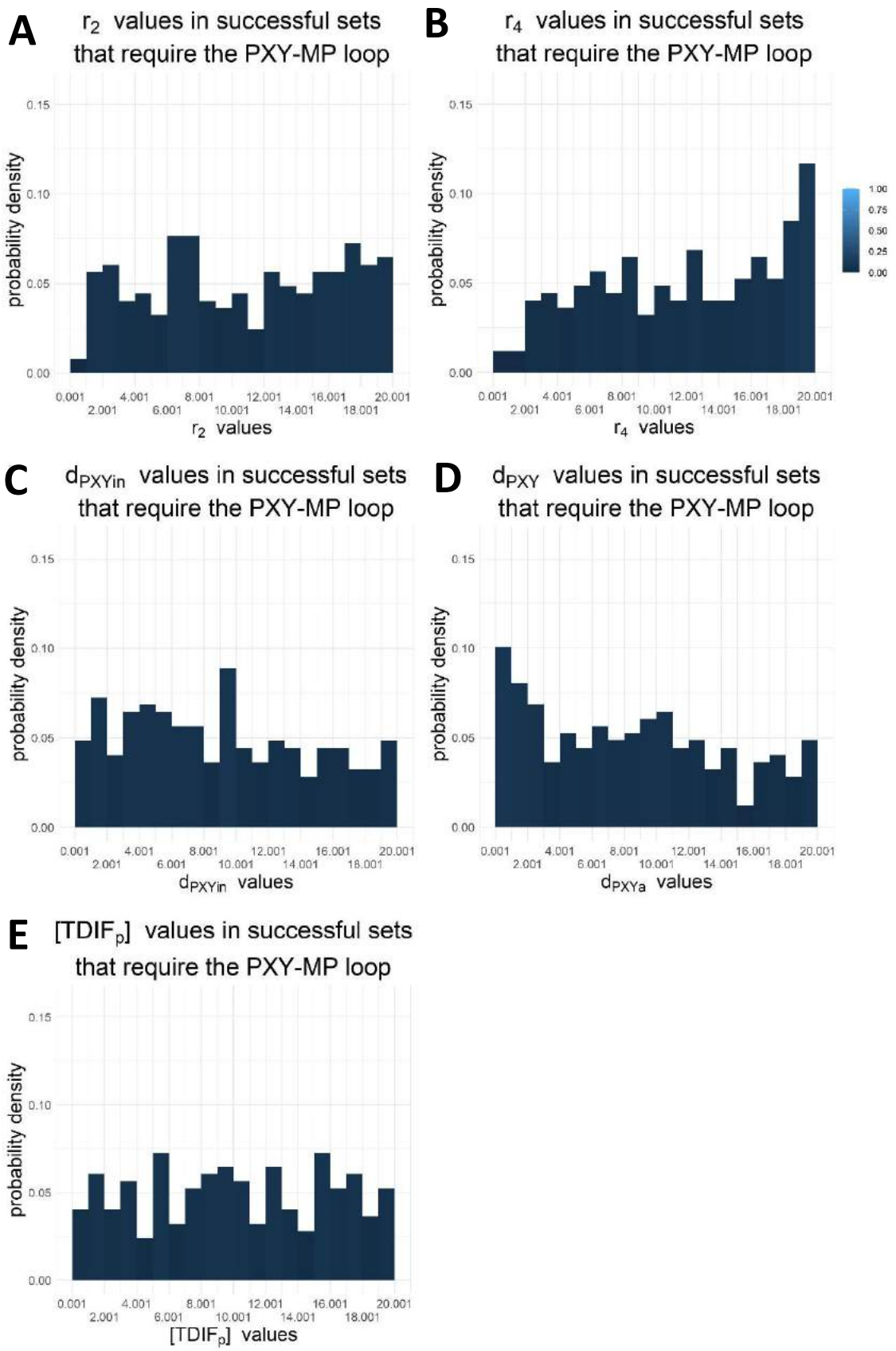

Figure 4S: Probability density functions of the distribution of r_2 (A), r_4 (B), $d_{PXY_{in}}$ (C), d_{PXY_a} (D) and $[TDIF_p]$ (E) in the successful parameter set that do require the PXY-MP negative feedback loop. Bin count = 20. Each bin contains 2 possible choices of values, except the last one which contains 3. Darker blue is lower probability, lighter is higher.

Appendix E3: Closed form analysis

The full system of equations is given by

$$\frac{\mathrm{d}[Aux_c]}{\mathrm{d}t} = F_a[Aux_p] - r_8[PIN_c][Aux_c] + \frac{1}{2}r_8[PIN_x][Aux_x] - d_{Aux}[Aux_c] \quad (1)$$

$$\frac{\mathrm{d}[Aux_x]}{\mathrm{d}t} = \frac{1}{2}r_8[PIN_c][Aux_c] - r_8[PIN_x][Aux_x] - d_{Aux}[Aux_x] \quad (2)$$

$$\frac{\mathrm{d}[PIN_c]}{\mathrm{d}t} = r_6[MP_c] - r_7[CK_c][PIN_c] - d_{PIN}[PIN_c] \quad (3)$$

$$\frac{\mathrm{d}[PIN_x]}{\mathrm{d}t} = r_6[MP_x] - r_7[CK_x][PIN_x] - d_{PIN}[PIN_x] \quad (4)$$

$$\frac{\mathrm{d}[MP_c]}{\mathrm{d}t} = r_5[Aux_c] - r_3[PXY_a][MP_c] - d_{MP}[MP_c] \quad (5)$$

$$\frac{\mathrm{d}[MP_x]}{\mathrm{d}t} = r_5[Aux_x] - d_{MP}[MP_x] \quad (6)$$

$$\frac{\mathrm{d}[PXY_{in}]}{\mathrm{d}t} = r_4[MP_c] - r_2[PXY_{in}][TDIF_p] - d_{PXY_{in}}[PXY_{in}] \quad (7)$$

$$\frac{\mathrm{d}[PXY_a]}{\mathrm{d}t} = r_2[PXY_{in}][TDIF_p] - d_{PXY_a}[PXY_a] \quad (8)$$

$$\frac{\mathrm{d}[CK_c]}{\mathrm{d}t} = D_{ck}\frac{\partial^2[CK]}{\partial x^2} - r_1[Aux_c][CK_c] - d_{CK}[CK_c] \quad (9)$$

$$\frac{\mathrm{d}[CK_x]}{\mathrm{d}t} = D_{ck}\frac{\partial^2[CK]}{\partial x^2} - r_1[Aux_x][CK_x] - d_{CK}[CK_x]. \quad (10)$$

For the correct hormone pattern to be obtained, the following inequalities must be satisfied:

$$\left[CK_p\right] > [CK_c] > [CK_x] \quad (11)$$

$$[Aux_c] > \left[Aux_p\right] \quad (12)$$

$$[Aux_c] > [Aux_x] \quad (13)$$

Inequality (11) was shown to always hold in Chapter 4, section 4.4.1. Here, successful patterning conditions will be derived for which inequalities (11) and (12) are satisfied. This will be done for both cases: without the PXY-MP negative feedback loop (r_2, r_3, r_4, $[TDIF_p]$, d_{PXY_a}, , $d_{PXY_{in}}$ are equal to zero) and and with it. The aim was to derive conditions which, if

satisfied, would ensure successful patterning. The successful patterning conditions would be derived in such way as to minimise their dependence on final steady state concentrations.

Appendix E3.1: Network with no PXY-MP feedback loop

Consider the system without the PXY-MP negative feedback loop. In this case the equations governing the active and inactive PXY concentrations are omitted. In addition, no change in concentration occurs over time at steady state, thus diffusion terms are equal to zero, and $[CK_P] > [CK_c] > [CK_x]$ is always true (see Chapter 4, section 4.4.1). The full system of equations is reduced to

$$F_a[Aux_p] - r_8[PIN_c][Aux_c] + \frac{1}{2}r_8[PIN_x][Aux_x] - d_{Aux}[Aux_c] = 0$$

$$\frac{1}{2}r_8[PIN_c][Aux_c] - r_8[PIN_x][Aux_x] - d_{Aux}[Aux_x] = 0$$

$$r_6[MP_c] - r_7[CK_c][PIN_c] - d_{PIN}[PIN_c] = 0$$

$$r_6[MP_x] - r_7[CK_x][PIN_x] - d_{PIN}[PIN_x] = 0$$

$$r_5[Aux_c] - d_{MP}[MP_c] = 0$$

$$r_5[Aux_x] - d_{MP}[MP_x] = 0.$$

For ease of writing, the brackets that denote component concentration are dropped.

With these alterations, the above system of equations becomes

$$F_a Aux_p - r_8 PIN_c Aux_c + \tfrac{1}{2}r_8 PIN_x Aux_x - d_{Aux} Aux_c = 0 \quad (14)$$

$$\tfrac{1}{2}r_8 PIN_c Aux_c - r_8 PIN_x Aux_x - d_{Aux} Aux_x = 0 \quad (15)$$

$$r_6 MP_c - r_7 CK_c PIN_c - d_{PIN} PIN_c = 0 \quad (16)$$

$$r_6 MP_x - r_7 CK_x PIN_x - d_{PIN} PIN_x = 0 \quad (17)$$

$$r_5 Aux_c - d_{MP} MP_c = 0 \quad (18)$$

$$r_5 Aux_x - d_{MP} MP_x = 0 \quad (19)$$

In the following discussion, the system (14)-(19) will be examined to obtain conditions for which (12) and (13) hold.

Inequality $Aux_c > Aux_x$

Here, inequality $Aux_c > Aux_x$ is proven to always hold at steady state. To do this, proof by contradiciton is used. The inequality $Aux_c > Aux_x$ is assumed to be broken, i.e. $Aux_c \leq Aux_x$ is assumed to hold. It will be shown that for non-negative components and parameters, $Aux_c \leq Aux_x$ can never hold. Two sub-cases are considered: the case where $Aux_c < Aux_x$ and the simpler special case $Aux_c = Aux_x$. The case $Aux_c = Aux_x$ is solved similarly to $Aux_c < Aux_x$, showing that in this case no auxin is supported throughout the entire system and thus no pattern is observed.

The approach in both cases is similar. First, equations (18) and (19) are examined to show that $Aux_c \leq Aux_x$ leads to the condition $MP_c \leq MP_x$. Next, $MP_c \leq MP_x$ is used in combination with $CK_c > CK_x$ and equations (16) and (17) to produce an inequality $PIN_c < PIN_x$. Finally, it is observed that equations (14) and (15), together with $Aux_c \leq Aux_x$ contradict $PIN_c < PIN_x$, thus disproving the initial assumption that $Aux_c \leq Aux_x$ and showing that $Aux_c > Aux_x$ must always hold.

$Aux_c < Aux_x$ assumption for the network without the PXY-MP negative feedback loop

Consider equations (18) and (19). Rearrange for Aux_c and Aux_x as follows

$$r_5 Aux_c - d_{MP} MP_c = 0 \tag{18}$$

$$Aux_c = \frac{d_{MP} MP_c}{r_5}. \tag{20}$$

For (19), the following representation can be achieved

$$r_5 Aux_x - d_{MP} MP_x = 0 \tag{19}$$

$$Aux_x = \frac{d_{MP} MP_x}{r_5} \tag{21}$$

Since $Aux_c < Aux_x$ was assumed, combine (20) and (21)

$$\frac{d_{MP}MP_c}{r_5} = Aux_c < Aux_x = \frac{d_{MP}MP_x}{r_5}.$$

Thus

$$\frac{d_{MP}MP_c}{r_5} < \frac{d_{MP}MP_x}{r_5}.$$

Or,

$$MP_c < MP_x. \tag{22}$$

Next, combine (22) with equation (17), which re-arrange as follows

$$r_6MP_x - r_7CK_xPIN_x - d_{PIN}PIN_x = 0 \tag{17}$$

$$r_6MP_x - PIN_x(r_7CK_x + d_{PIN}) = 0$$

$$r_6MP_x = PIN_x(r_7CK_x + d_{PIN})$$

$$r_6MP_c < r_6MP_x = PIN_x(r_7CK_x + d_{PIN}),$$

for $MP_c, MP_x \geq 0$.

$$r_6MP_c < PIN_x(r_7CK_x + d_{PIN})$$

$$r_6MP_c - PIN_x(r_7CK_x + d_{PIN}) < 0 \tag{23}$$

Notice that $CK_c > CK_x$ always holds. Thus,

$$PIN_x(r_7CK_x + d_{PIN}) < PIN_x(r_7CK_c + d_{PIN})$$

$$-PIN_x(r_7CK_x + d_{PIN}) > -PIN_x(r_7CK_c + d_{PIN})$$

$$r_6MP_c - PIN_x(r_7CK_x + d_{PIN}) > r_6MP_c - PIN_x(r_7CK_c + d_{PIN})$$

From (23)

$$r_6MP_c - PIN_x(r_7CK_x + d_{PIN}) < 0 \tag{23}$$

resulting in,

$$0 > r_6MP_c - PIN_x(r_7CK_x + d_{PIN}) > r_6MP_c - PIN_x(r_7CK_c + d_{PIN}).$$

Thus,

$$r_6 MP_c - PIN_x(r_7 CK_c + d_{PIN}) < 0. \quad (24)$$

Now, from (16),

$$r_6 MP_c - r_7 CK_c PIN_c - d_{PIN} PIN_c = 0 \quad (16)$$

$$r_6 MP_c = r_7 CK_c PIN_c + d_{PIN} PIN_c. \quad (25)$$

Substitute (25) into (24)

$$r_6 MP_c - PIN_x(r_7 CK_c + d_{PIN}) < 0 \quad (24)$$

$$(r_7 CK_c PIN_c + d_{PIN} PIN_c) - PIN_x(r_7 CK_c + d_{PIN}) < 0$$

$$-PIN_x(r_7 CK_c + d_{PIN}) + PIN_c(r_7 CK_c + d_{PIN}) < 0$$

$$(PIN_c - PIN_x)(r_7 CK_c + d_{PIN}) < 0 \quad (26)$$

In (26), $r_7 CK_c + d_{PIN} \geq 0$ for all parameters and components non-negative. Thus, for (26) to be true, it must be that the following inequality holds

$$PIN_c - PIN_x < 0$$

$$PIN_c < PIN_x \quad (27)$$

Now, return to equations (14) and (15) armed with $PIN_c < PIN_x$. Consider (14),

$$F_a Aux_p - r_8 PIN_c Aux_c + \tfrac{1}{2} r_8 PIN_x Aux_x - d_{Aux} Aux_c = 0 \quad (14)$$

Since $Aux_c < Aux_x$, according to the assumption, then $d_{Aux} Aux_x > d_{Aux} Aux_c > 0$, thus, from (14), obtain

$$0 = F_a Aux_p - r_8 PIN_c Aux_c + \frac{1}{2} r_8 PIN_x Aux_x - d_{Aux} Aux_c$$
$$> F_a Aux_p - r_8 PIN_c Aux_c + \frac{1}{2} r_8 PIN_x Aux_x - d_{Aux} Aux_x$$

So,

$$F_a Aux_p - r_8 PIN_c Aux_c + \tfrac{1}{2} r_8 PIN_x Aux_x - d_{Aux} Aux_x < 0. \quad (28)$$

Consider equation (15)

$$\tfrac{1}{2} r_8 Aux_c PIN_c - r_8 Aux_x PIN_x - d_{Aux} Aux_x = 0 \quad (15)$$

$$d_{Aux}Aux_x = \frac{1}{2}r_8Aux_cPIN_c - r_8Aux_xPIN_x \quad (29)$$

Substitute (29) into (28)

$$F_aAux_p + \frac{1}{2}r_8Aux_xPIN_x - r_8Aux_cPIN_c - d_{Aux}Aux_x < 0 \quad (28)$$

$$F_aAux_p + \frac{1}{2}r_8Aux_xPIN_x - r_8Aux_cPIN_c - \frac{1}{2}r_8Aux_cPIN_c + r_8Aux_xPIN_x < 0$$

$$F_aAux_p + \frac{3}{2}r_8Aux_xPIN_x - \frac{3}{2}r_8Aux_cPIN_c < 0 \quad (30)$$

Since from the assumption, $Aux_c < Aux_x$, and $\frac{3}{2}r_8Aux_xPIN_x > 0$, it is clear that $\frac{3}{2}r_8Aux_xPIN_x > \frac{3}{2}r_8Aux_cPIN_x > 0$. Substitute into (30) as follows

$$F_aAux_p + \frac{3}{2}r_8Aux_xPIN_x - \frac{3}{2}r_8Aux_cPIN_c < 0 \quad (30)$$

$$0 > F_aAux_p + \frac{3}{2}r_8Aux_xPIN_x - \frac{3}{2}r_8Aux_cPIN_c$$

$$> F_aAux_p + \frac{3}{2}r_8Aux_cPIN_x - \frac{3}{2}r_8Aux_cPIN_c$$

$$F_aAux_p + \frac{3}{2}r_8Aux_cPIN_x - \frac{3}{2}r_8Aux_cPIN_c < 0$$

$$F_aAux_p + \frac{3}{2}r_8Aux_c(PIN_x - PIN_c) < 0 \quad (31)$$

Now, $F_aAux_p \geq 0$, $r_8Aux_c \geq 0$ and since (27) showed $PIN_x > PIN_c$, then $PIN_x - PIN_c > 0$. It then follows that the left-hand side of (31) must always be non-negative. This is a contradiction. Thus, the original assumption that $Aux_x > Aux_c$ must have been false. It remains to show that furthermore $Aux_c \neq Aux_x$ and $Aux_x < Aux_c$ will have been shown to always hold.

$Aux_c = Aux_x$ assumption for the network without the PXY-MP negative feedback loop

Thus far it has been shown that $Aux_x > Aux_c$ cannot hold in the network without the PXY-MP negative feedback loop. The above analysis is reworked for the special case when

$Aux_c = Aux_x$ to show that this can never hold, either. The approach is similar to the previous case, with the exception of some inequalities being replaced with equalities. Identical notation is used when the equations are the same, and $(* a)$ notation (where $*$ is an equation number) where the only difference is the sign ($=$ rather than $>$ or $<$) in the equation. As before, equations (18) and (19) are used first to show that $Aux_c = Aux_x$ implies $MP_c = MP_x$. Next, equations (16) and (17) show that $PIN_x > PIN_c$. Finally, (14) and (15) are used to confirm that together, these conclusions require no auxin presence in any of the cells, thus removing the existence of a pattern altogether and making the system uninformative.

Consider equations (18) and (19). Rearrange for Aux_c and Aux_x as follows

$$r_5 Aux_c - d_{MP} MP_c = 0 \quad (18)$$

$$Aux_c = \frac{d_{MP} MP_c}{r_5} \quad (20)$$

For (19),

$$r_5 Aux_x - d_{MP} MP_x = 0 \quad (19)$$

$$Aux_x = \frac{d_{MP} MP_x}{r_5} \quad (21)$$

Since $Aux_c = Aux_x$ was assumed, combine (20) and (21)

$$\frac{d_{MP} MP_c}{r_5} = Aux_c = Aux_x = \frac{d_{MP} MP_x}{r_5}$$

Thus

$$\frac{d_{MP} MP_c}{r_5} = \frac{d_{MP} MP_x}{r_5},$$

or,

$$MP_c = MP_x \quad (22a)$$

Next, combine (22a) with equation (17), which re-arranges as follows

$$r_6 MP_x - r_7 CK_x PIN_x - d_{PIN} PIN_x = 0 \quad (17)$$

$$r_6 MP_x - PIN_x(r_7 CK_x + d_{PIN}) = 0$$

$$r_6 MP_x = PIN_x(r_7 CK_x + d_{PIN})$$

$$r_6 MP_c = r_6 MP_x = PIN_x(r_7 CK_x + d_{PIN})$$

for $MP_c, MP_x \geq 0$.

$$r_6 MP_c = PIN_x(r_7 CK_x + d_{PIN})$$

$$r_6 MP_c - PIN_x(r_7 CK_x + d_{PIN}) = 0 \quad (23)$$

Note that $CK_c > CK_x$ holds. Thus,

$$PIN_x(r_7 CK_x + d_{PIN}) < PIN_x(r_7 CK_c + d_{PIN})$$

$$-PIN_x(r_7 CK_x + d_{PIN}) > -PIN_x(r_7 CK_c + d_{PIN})$$

$$r_6 MP_c - PIN_x(r_7 CK_x + d_{PIN}) > r_6 MP_c - PIN_x(r_7 CK_c + d_{PIN})$$

From (23)

$$r_6 MP_c - PIN_x(r_7 CK_x + d_{PIN}) = 0 \quad (23a)$$

This results in

$$0 \geq r_6 MP_c - PIN_x(r_7 CK_x + d_{PIN}) > r_6 MP_c - PIN_x(r_7 CK_c + d_{PIN})$$

Thus,

$$r_6 MP_c - PIN_x(r_7 CK_c + d_{PIN}) < 0 \quad (24)$$

Now, from (16),

$$r_6 MP_c - r_7 CK_c PIN_c - d_{PIN} PIN_c = 0 \quad (16)$$

$$r_6 MP_c = r_7 CK_c PIN_c + d_{PIN} PIN_c \quad (25)$$

Substitute (25) into (24)

$$r_6 MP_c - PIN_x(r_7 CK_c + d_{PIN}) < 0 \quad (24)$$

$$r_7 CK_c PIN_c + d_{PIN} PIN_c - PIN_x(r_7 CK_c + d_{PIN}) < 0$$

$$-PIN_x(r_7 CK_c + d_{PIN}) + PIN_c(r_7 CK_c + d_{PIN}) < 0$$

$$(PIN_c - PIN_x)(r_7 CK_c + d_{PIN}) < 0 \quad (26)$$

In (26), $r_7 CK_c + d_{PIN} \geq 0$ for all parameters and components non-negative. Thus, for (26) to be true, it must be that the following inequality holds

$$PIN_c - PIN_x < 0$$

$$PIN_c < PIN_x \tag{27}$$

Now, return to equations (14) and (15) armed with $PIN_c < PIN_x$. Consider (14),

$$F_a Aux_p + \frac{1}{2} r_8 Aux_x PIN_x - r_8 Aux_c PIN_c - d_{Aux} Aux_c = 0 \tag{14}$$

Since $Aux_c = Aux_x$, according to the assumption, then $d_{Aux} Aux_x = d_{Aux}$, $Aux_c \geq 0$, thus, from (14), it follows that

$$0 = F_a Aux_p + \frac{1}{2} r_8 Aux_x PIN_x - r_8 Aux_c PIN_c - d_{Aux} Aux_c$$
$$= F_a Aux_p + \frac{1}{2} r_8 Aux_x PIN_x - r_8 Aux_c PIN_c - d_{Aux} Aux_x.$$

So,

$$F_a Aux_p + \frac{1}{2} r_8 Aux_x PIN_x - r_8 Aux_c PIN_c - d_{Aux} Aux_x = 0 \tag{28a}$$

Consider equation (15)

$$\frac{1}{2} r_8 Aux_c PIN_c - r_8 Aux_x PIN_x - d_{Aux} Aux_x = 0 \tag{15}$$

$$d_{Aux} Aux_x = \frac{1}{2} r_8 Aux_c PIN_c - r_8 Aux_x PIN_x \tag{29}$$

Substitute (29) into (28a)

$$F_a Aux_p + \frac{1}{2} r_8 Aux_x PIN_x - r_8 Aux_c PIN_c - d_{Aux} Aux_x = 0 \tag{28a}$$

$$F_a Aux_p + \frac{1}{2} r_8 Aux_x PIN_x - r_8 Aux_c PIN_c - \frac{1}{2} r_8 Aux_c PIN_c + r_8 Aux_x PIN_x = 0$$

$$F_a Aux_p + \frac{3}{2} r_8 Aux_x PIN_x - \frac{3}{2} r_8 Aux_c PIN_c = 0 \tag{30a}$$

Since from the assumption, $Aux_c = Aux_x$, and $\frac{3}{2} r_8 Aux_x PIN_x \geq 0$,it's clear that $\frac{3}{2} r_8 Aux_x PIN_x = \frac{3}{2} r_8 Aux_c PIN_x \geq 0$, thus the following still holds. Substitute into (40a) as follows

$$F_a Aux_p + \frac{3}{2} r_8 Aux_x PIN_x - \frac{3}{2} r_8 Aux_c PIN_c = 0$$

$$0 = F_a Aux_p + \frac{3}{2} r_8 Aux_x PIN_x - \frac{3}{2} r_8 Aux_c PIN_c = F_a Aux_p + \frac{3}{2} r_8 Aux_c PIN_x - \frac{3}{2} r_8 Aux_c PIN_c$$

$$F_a Aux_p + \frac{3}{2} r_8 Aux_c PIN_x - \frac{3}{2} r_8 Aux_c P_c = 0$$

$$F_a Aux_p + \frac{3}{2} r_8 Aux_c (PIN_x - PIN_c) = 0$$

Now, $F_a Aux_p \geq 0$, $r_8 Aux_c \geq 0$ and since (27) showed $PIN_x > PIN_c$, then $PIN_x - PIN_c > 0$. Thus, both $F_a Aux_p = 0$ and $r_8 Aux_c = 0$ are needed, suggesting that there is no input of auxin into the system and no active transport of auxin from the cambium or the xylem (since $Aux_c = Aux_x$, it follows that if $r_8 Aux_c = 0$, then $r_8 Aux_x = 0$). As there is no other source of auxin into the system other than the phloem, this leads to an uninformative system where no auxin enters and no pattern can be observed altogether. This is a contradiction. Thus, the original assumption that $Aux_x = Aux_c$ must have been false.

Together with the previous analysis, showing that $Aux_c < Aux_x$ cannot be true, it follows that and $Aux_x < Aux_c$ holds always. □

Inequality $Aux_c > Aux_p$:

In the previous section, it was shown that $Aux_c > Aux_x$ is always true, using proof by contradiction. In this section, successful patterning conditions for $Aux_c > Aux_p$ are derived.

First, $Aux_c PIN_c > Aux_x PIN_x$ is shown to hold. Using this together with equation (14) an inequality for F_a is found which is irrespective of Aux_c and Aux_x and depends only on one other final steady state concentration, PIN_c. The inequalities (11) and (12) are then used ($CK_p > CK_c > CK_x$ and $Aux_c > Aux_p$) to remove the dependence on PIN_c.

Consider equation (15),

$$\frac{1}{2} r_8 Aux_c PIN_c - r_8 Aux_x PIN_x - d_{Aux} Aux_x = 0. \quad (15)$$

For $d_{Aux} Aux_x > 0$,

$$0 = \frac{1}{2} r_8 Aux_c PIN_c - r_8 Aux_x PIN_x - d_{Aux} Aux_x < \frac{1}{2} r_8 Aux_c PIN_c - r_8 Aux_x PIN_x$$

$$\frac{1}{2} r_8 Aux_c PIN_c - r_8 Aux_x PIN_x > 0$$

$$\frac{1}{2} r_8 Aux_c PIN_c > r_8 Aux_x PIN_x$$

$$Aux_c PIN_c > 2 Aux_x PIN_x.$$

Thus,

$$Aux_c PIN_c > 2 Aux_x PIN_x > Aux_x PIN_x$$

$$Aux_c PIN_c > Aux_x PIN_x \quad (32)$$

Consider equation (14)

$$F_a Aux_p + \tfrac{1}{2} r_8 Aux_x PIN_x - r_8 Aux_c PIN_c - d_{Aux} Aux_c = 0 \quad (14)$$

Using (32),

$$F_a Aux_p + \frac{1}{2} r_8 Aux_x PIN_x - r_8 Aux_c PIN_c - d_{Aux} Aux_c = 0$$

$$0 = F_a Aux_p + \frac{1}{2} r_8 Aux_x PIN_x - r_8 Aux_c PIN_c - d_{Aux} Aux_c$$
$$< F_a Aux_p + \frac{1}{2} r_8 Aux_c PIN_c - r_8 Aux_c PIN_c - d_{Aux} Aux_c$$

$$F_a Aux_p + \frac{1}{2} r_8 Aux_c PIN_c - r_8 Aux_c PIN_c - d_{Aux} Aux_c > 0$$

$$F_a Aux_p - \frac{1}{2} r_8 Aux_c PIN_c - d_{Aux} Aux_c > 0$$

Since the case when $Aux_c > Aux_p$ and $F_a > 0$ is examined here, it follows that $F_a Aux_c > F_a Aux_p$

$$F_a Aux_p - \frac{1}{2} r_8 Aux_c PIN_c - d_{Aux} Aux_c > 0$$

$$F_a Aux_c - \frac{1}{2} r_8 Aux_c PIN_c - d_{Aux} Aux_c > F_A Aux_p - \frac{1}{2} r_8 Aux_c PIN_c - d_{Aux} Aux_c > 0$$

$$F_a Aux_c - \frac{1}{2} r_8 Aux_c PIN_c - d_{Aux} Aux_c > 0$$

Dividing throughout by $Aux_c > 0$

$$F_a - \frac{1}{2} r_8 PIN_c - d_{Aux} > 0 \quad (33)$$

Next, rearrange equation (16) to get PIN_c,

$$r_6 MP_c - r_7 CK_c PIN_c - d_{PIN} PIN_c = 0$$

$$r_7 CK_c PIN_c + d_{PIN} PIN_c = r_6 MP_c$$

$$PIN_c(r_7 CK_c + d_{PIN}) = r_6 MP_c$$

obtaining,

$$PIN_c = \frac{r_6 MP_c}{r_7 CK_c + d_{PIN}} \quad (34)$$

Substituting (34) into (33),

$$F_a - \frac{1}{2} r_8 PIN_c - d_{Aux} > 0 \quad (33)$$

$$F_a - \frac{1}{2} r_8 \frac{r_6 MP_c}{r_7 CK_c + d_{PIN}} - d_{Aux} > 0 \quad (35)$$

Note that $CK_p > CK_c$, thus $\frac{r_6 MP_c}{r_7 CK_p + d_{PIN}} < \frac{r_6 MP_c}{r_7 CK_c + d_{PIN}}$ and so from (35), it follows that

$$\frac{r_6 MP_c}{r_7 CK_p + d_{PIN}} < \frac{r_6 MP_c}{r_7 CK_c + d_{PIN}}$$

$$-\frac{r_6 MP_c}{r_7 CK_p + d_{PIN}} > -\frac{r_6 MP_c}{r_7 CK_c + d_{PIN}}$$

$$-\frac{1}{2} r_8 \frac{r_6 MP_c}{r_7 CK_p + d_{PIN}} > -\frac{1}{2} r_8 \frac{r_6 MP_c}{r_7 CK_c + d_{PIN}}$$

$$F_a - \frac{1}{2} r_8 \frac{r_6 MP_c}{r_7 CK_p + d_{PIN}} - d_{Aux} > F_a - \frac{1}{2} r_8 \frac{r_6 MP_c}{r_7 CK_c + d_{PIN}} - d_{Aux}$$

$$F_a - \frac{1}{2} r_8 \frac{r_6 MP_c}{r_7 CK_p + d_{PIN}} - d_{Aux} > F_a - \frac{1}{2} r_8 \frac{r_6 MP_c}{r_7 CK_c + d_{PIN}} > 0$$

Or,

$$F_a - \frac{1}{2} r_8 \frac{r_6 MP_c}{r_7 CK_p + d_{PIN}} - d_{Aux} > 0. \quad (36)$$

Notice that an expression for MP_c can be obtained from (18)

$$r_5 Aux_c - d_{MP} MP_c = 0$$

$$MP_c = \frac{r_5 Aux_c}{d_{MP}}$$

Substitute that into (36)

$$F_a - \frac{1}{2} r_8 \frac{r_6 MP_c}{r_7 CK_p + d_{PIN}} - d_{Aux} > 0$$

$$F_a - \frac{1}{2} r_8 \frac{r_6}{r_7 CK_p + d_{PIN}} \left(\frac{r_5 Aux_c}{d_{MP}}\right) - d_{Aux} > 0$$

finally obtaining

$$F_a - \frac{1}{2} r_8 \frac{r_5 r_6 Aux_c}{d_{MP}(r_7 CK_p + d_{PIN})} - d_{Aux} > 0. \quad (37)$$

Notice that all parameters and components in $\frac{1}{2} r_8 \frac{r_5 r_6 Aux_c}{d_{MP}(r_7 CK_p + d_{PIN})}$ are positive, thus $\frac{1}{2} r_8 \frac{r_5 r_6 Aux_c}{d_{MP}(r_7 CK_p + d_{PIN})} > 0$. Here, the case where $Aux_c > Aux_p$ needs to be satisfied is discussed. Thus, $\frac{1}{2} r_8 \frac{r_5 r_6 Aux_c}{d_{MP}(r_7 CK_p + d_{PIN})} > \frac{1}{2} r_8 \frac{r_5 r_6 Aux_p}{d_{MP}(r_7 CK_p + d_{PIN})} > 0$ holds. This inequality is combined with (37) in order to find a successful patterning condition that does not depend on Aux_c as follows

$$\frac{1}{2} r_8 \frac{r_5 r_6 Aux_c}{d_{MP}(r_7 CK_p + d_{PIN})} > \frac{1}{2} r_8 \frac{r_5 r_6 Aux_p}{d_{MP}(r_7 CK_p + d_{PIN})} > 0$$

$$-\frac{1}{2} r_8 \frac{r_5 r_6 Aux_c}{d_{MP}(r_7 CK_p + d_{PIN})} < -\frac{1}{2} r_8 \frac{r_5 r_6 Aux_p}{d_{MP}(r_7 CK_p + d_{PIN})} < 0$$

$$F_a - \frac{1}{2} r_8 \frac{r_5 r_6 Aux_c}{d_{MP}(r_7 CK_p + d_{PIN})} - d_{Aux} < F_a - \frac{1}{2} r_8 \frac{r_5 r_6 Aux_p}{d_{MP}(r_7 CK_p + d_{PIN})} - d_{Aux} < F_a - d_{Aux}$$

$$F_a - \frac{1}{2} r_8 \frac{r_5 r_6 Aux_c}{d_{MP}(r_7 CK_p + d_{PIN})} - d_{Aux} > 0$$

$$F_a - \frac{1}{2} r_8 \frac{r_5 r_6 Aux_c}{d_{MP}(r_7 CK_p + d_{PIN})} - d_{Aux} < F_a - \frac{1}{2} r_8 \frac{r_5 r_6 Aux_p}{d_{MP}(r_7 CK_p + d_{PIN})} - d_{Aux} < F_a - d_{Aux}$$

Thus, this results in

$$F_a - \frac{1}{2} r_8 \frac{r_5 r_6 Aux_p}{d_{MP}(r_7 CK_p + d_{PIN})} - d_{Aux} > F_a - \frac{1}{2} r_8 \frac{r_5 r_6 Aux_c}{d_{MP}(r_7 CK_p + d_{PIN})} - d_{Aux} > 0 \quad (38)$$

$$F_a - \frac{1}{2} r_8 \frac{r_5 r_6 Aux_p}{d_{MP}(r_7 CK_p + d_{PIN})} - d_{Aux} > 0$$

$$F_a > \frac{1}{2} r_8 \frac{r_5 r_6 Aux_p}{d_{MP}(r_7 CK_p + d_{PIN})} + d_{Aux} \quad (39)$$

The above equation (39) is a condition dependent on parameters only, as required. A summary table for the successful patterning conditions for the network without the PXY-MP negative feedback loop are shown in Table 1S □.

Network with no PXY-MP negative feedback loop		
Conditions for cambial auxin maxima	$Aux_c > Aux_p$	$Aux_c > Aux_x$
	$F_a > \frac{1}{2} r_8 \frac{r_5 r_6 Aux_p}{d_{Mp}(r_7 CK_p + d_{PIN})} + d_{Aux}$	Always true

Table 1S: A summary table for the successful patterning conditions the network without the PXY-MP negative feedback loop. Column 1 shows headings. Column 2 shows the conditions for auxin accumulation in the cambium over the phloem. Column 3 shows the auxin concentration in the cambium in both system exceeds the auxin concentration in the xylem

In the next section, successful patterning conditions are derived for the network with the PXY-MP negative feedback loop.

Appendix E3.2: Network with PXY-MP feedback loop

Consider now the system of equations which involve the PXY-MP negative feedback loop. Just as before, for ease of writing, the brackets that denote the components'

concentration will be dropped. Successful parameter conditions for satisfying inequalities (12) and (13) ($[Aux_c] > [Aux_x]$ and $[Aux_c] > [Aux_p]$) will be derived. As before, the aim is to obtain such conditions independently of final steady state concentrations of any of the components. At steady state, the system of equations to be solved is given by

$$F_a Aux_p - r_8 PIN_c Aux_c + \frac{1}{2} r_8 PIN_x Aux_x - d_{Aux} Aux_c = 0 \quad (14)$$

$$\frac{1}{2} r_8 PIN_c Aux_c - r_8 PIN_x Aux_x - d_{Aux} Aux_x = 0 \quad (15)$$

$$r_6 MP_c - r_7 CK_c PIN_c - d_{PIN} PIN_c = 0 \quad (16)$$

$$r_6 MP_x - r_7 CK_x PIN_x - d_{PIN} PIN_x = 0 \quad (17)$$

$$r_5 Aux_c - r_3 PXY_a MP_c - d_{MP} MP_c = 0 \quad (40)$$

$$r_5 Aux_x - d_{MP} MP_x = 0 \quad (19)$$

$$r_4 MP_c - r_2 PXY_{in} TDIF - d_{PXY_{in}} PXY_{in} = 0 \quad (41)$$

$$r_2 PXY_{in} TDIF - d_{PXY_a} PXY_a = 0 \quad (42)$$

Notice that for both cases, with and without the PXY-MP negative feedback loop, equations (14)-(17) and (19) are present. In the following discussion successful patterning conditions will be derived for which the above system (14)-(17), (19), (40)-(42), obeys conditions $Aux_c > Aux_x$ and $Aux_c > Aux_p$. As will be seen in the case for $Aux_c > Aux_p$, the successful patterning condition will depend on the final steady state PXY_a as, due to the additional $r_3 PXY_a MP_c$ term, MP_c could not be rewritten in terms of auxin alone and subected to $Aux_c > Aux_p$. Thus, a purely parameter-based condition could not be found. Other strategies for solving the system to obtain a parameter based successful patterning condition resulted in a larger number of final steady state dependencies. Thus, at the day of writing, the analysis presented in this section is the best effort made.

Inequality $Aux_c > Aux_x$:

Here, it is shown that for the system (14)-(17), (19), (40)-(42) the inequality $Aux_c > Aux_x$ always holds at steady state. To do this, proof by contradition is used and the equality $Aux_c > Aux_x$ is assumed to be broken, i.e. $Aux_c \leq Aux_x$ is assumed to hold. It is shown that for non-negative components and parameters, $Aux_c \leq Aux_x$ can never hold. Two sub-cases are considered: the case where $Aux_c < Aux_x$ and the special case $Aux_c = Aux_x$. The case $Aux_c = Aux_x$ is solved similarly to $Aux_c < Aux_x$, showing that in such case no auxin is supported throughout the entire system and thus no pattern is observed.

Equations (19) and (40) are examined first to show that $Aux_c \leq Aux_x$ leads to the condition $MP_c \leq MP_x$. Next, $MP_c \leq MP_x$ is used in combination with $CK_c > CK_x$ and equations (16) and (17) to produce an inequality $PIN_c < PIN_x$. Finally, equations (14) and (15), together with $Aux_c \leq Aux_x$ are shown to contradict $PIN_c < PIN_x$, thus disproving the initial assumption that $Aux_c \leq Aux_x$ holds and showing that $Aux_c > Aux_x$ must always hold.

Consider the assumption $Aux_c < Aux_x$ first.

$Aux_c < Aux_x$ assumption for the network with the PXY-MP

Assume $Aux_c < Aux_x$.

First, consider equations (19) and (40).

$$r_5 Aux_x - d_{MP} MP_x = 0 \tag{19}$$

Equation (21) is obtained again

$$Aux_x = \frac{d_{MP} MP_x}{r_5} \tag{21}$$

From (40), an expression for Aux_c, for $r_5 \neq 0$ can be obtained as follows

$$r_5 Aux_c - r_3 PXY_a MP_c - d_{MP} MP_c = 0 \tag{40}$$

$$r_5 Aux_c = r_3 PXY_a MP_c + d_{MP} MP_c$$

$$Aux_c = \frac{r_3 PXY_a MP_c + d_{MP} MP_c}{r_5} = \frac{(r_3 PXY_a + d_{MP}) MP_c}{r_5} \tag{43}$$

Using (21) and (43) and the assumption $Aux_x > Aux_c$

$$\frac{d_{MP}MP_x}{r_5} = Aux_x > Aux_c = \frac{(r_3PXY_a + d_{MP})MP_c}{r_5}.$$

Thus,

$$d_{MP}MP_x > (r_3PXY_a + d_{MP})MP_c.$$

Set $d_{MP} \neq 0$

$$d_{MP}MP_x > (r_3PXY_a + d_{MP})MP_c.$$

$$MP_x > \left(\frac{r_3PXY_a}{d_{MP}} + 1\right) MP_c \quad (44)$$

Since $r_3, d_{MP} > 0$ (here, $r_3 \neq 0$ while above $d_{MP} \neq 0$) and $PXY_a \geq 0$, notice that $\frac{r_3PXY_a}{d_{MP}} \geq 0$ so $\left(\frac{r_3PXY_a}{d_{MP}} + 1\right) \geq 1$, so

$$MP_x > \left(\frac{r_3PXY_a}{d_{MP}} + 1\right) MP_c \quad (45)$$

$$MP_x > \left(\frac{r_3PXY_a}{d_{MP}} + 1\right) MP_c \geq MP_c$$

Thus, inequality (22) is obtained again

$$MP_x > MP_c \quad (22)$$

Next, consider equations (16) and (17). Recall equation (17)

$$r_6MP_x - r_7CK_xPIN_x - d_{PIN}PIN_x = 0 \quad (17)$$

which can be rewritten as follows

$$r_6MP_x - P_x(r_7CK_x + d_{PIN}) = 0$$

$$r_6MP_x = P_x(r_7CK_x + d_{PIN})$$

Since $MP_x > MP_c$ from equation (22), it follows that $r_6MP_c < r_6MP_x$ for non-negative r_6,

$$r_6MP_c < r_6MP_x = PIN_x(r_7CK_x + d_{PIN})$$

for $MP_c, MP_x \geq 0$. So,

$$r_6MP_c < PIN_x(r_7CK_x + d_{PIN}),$$

which once again gives (23).

$$r_6 MP_c - PIN_x(r_7 CK_x + d_{PIN}) < 0 \quad (23)$$

Note that $CK_c > CK_x$ holds. Thus,

$$PIN_x(r_7 CK_x + d_{PIN}) < PIN_x(r_7 CK_c + d_{PIN})$$

$$-PIN_x(r_7 CK_x + d_{PIN}) > -PIN_x(r_7 CK_c + d_{PIN})$$

$$r_6 MP_c - P_x(r_7 CK_x + d_{PIN}) > r_6 MP_c - PIN_x(r_7 CK_c + d_{PIN}).$$

From (23)

$$r_6 MP_c - PIN_x(r_7 CK_x + d_{PIN}) < 0.$$

Thus,

$$0 > r_6 MP_c - PIN_x(r_7 CK_x + d_{PIN}) > r_6 MP_c - PIN_x(r_7 CK_c + d_{PIN})$$

It follows that the same inequality (24) is obtained, as before

$$r_6 MP_c - PIN_x(r_7 CK_c + d_{PIN}) < 0 \quad (23)$$

Now, from (16)

$$r_6 MP_c - r_7 CK_c PIN_c - d_{PIN} PIN_c = 0 \quad (16)$$

$$r_6 MP_c = r_7 CK_c PIN_c + d_{PIN} PIN_c$$

$$r_6 MP_c = r_7 CK_c PIN_c + d_{PIN} PIN_c. \quad (25)$$

Substituting (25) into (24) then gives

$$r_6 MP_c - PIN_x(r_7 CK_c + d_{PIN}) < 0 \quad (24)$$

$$P_c(r_7 CK_c + d_{PIN}) - PIN_x(r_7 CK_c + d_{PIN}) < 0,$$

which yields inequality (26)

$$(PIN_c - PIN_x)(r_7 CK_c + d_{PIN}) < 0. \quad (26)$$

Clearly, $(r_7 CK_c + d_{PIN}) > 0$, suggesting $PIN_c - PIN_x < 0$ must hold. In particular,

$$PIN_c < PIN_x \quad (27)$$

must be true. In what follows, (27) is shown to lead to a contradiction with the initial assumption that $Aux_c < Aux_x$ holds.

Consider equation (14)

$$F_a Aux_p + \frac{1}{2} r_8 Aux_x PIN_x - r_8 Aux_c PIN_c - d_{Aux} Aux_c = 0. \quad (14)$$

Since the initial assumption states that $Aux_c < Aux_x$, then $d_{Aux} Aux_x > d_{Aux} Aux_c$, thus, from (14), (28) is obtained

$$0 = F_a Aux_p + \frac{1}{2} r_8 Aux_x PIN_x - r_8 Aux_c PIN_c - d_{Aux} Aux_c$$

$$> F_a Aux_p + \frac{1}{2} r_8 Aux_x PIN_x - r_8 Aux_c PIN_c - d_{Aux} Aux_x$$

$$F_a Aux_p + \tfrac{1}{2} r_8 Aux_x PIN_x - r_8 Aux_c PIN_c - d_{Aux} Aux_x < 0 \quad (28)$$

Consider equation (15), the substitution (29) is used as follows

$$\tfrac{1}{2} r_8 Aux_c PIN_c - r_8 Aux_x PIN_x - d_{Aux} Aux_x = 0 \quad (15)$$

$$d_{Aux} Aux_x = \tfrac{1}{2} r_8 Aux_c PIN_c - r_8 Aux_x PIN_x \quad (29)$$

Substituting (29) into (28) gives

$$F_a Aux_p + \tfrac{1}{2} r_8 Aux_x PIN_x - r_8 Aux_c PIN_c - d_{Aux} Aux_x < 0 \quad (28)$$

$$F_a Aux_p + \frac{1}{2} r_8 Aux_x PIN_x - r_8 Aux_c PIN_c - (\frac{1}{2} r_8 Aux_c PIN_c - r_8 Aux_x PIN_x) < 0$$

$$F_a Aux_p + \frac{1}{2} r_8 Aux_x PIN_x - r_8 Aux_c PIN_c - \frac{1}{2} r_8 Aux_c PIN_c + r_8 Aux_x PIN_x < 0$$

$$F_a Aux_p + \tfrac{3}{2} r_8 Aux_x PIN_x - \tfrac{3}{2} r_8 Aux_c PIN_c < 0 \quad (30)$$

Since, $Aux_c < Aux_x$, and $\frac{3}{2} r_8 Aux_x PIN_x \geq 0$,it follows that $\frac{3}{2} r_8 Aux_x P_x > \frac{3}{2} r_8 Aux_c PIN_x$, thus

$$\frac{3}{2} r_8 Aux_x PIN_x > \frac{3}{2} r_8 Aux_c PIN_x$$

$$\frac{3}{2} r_8 Aux_c PIN_x < \frac{3}{2} r_8 Aux_x PIN_x$$

$$\frac{3}{2} r_8 Aux_c PIN_x - \frac{3}{2} r_8 Aux_c P_c < \frac{3}{2} r_8 Aux_x P_x - \frac{3}{2} r_8 Aux_c P_c$$

$$F_a Aux_p + \frac{3}{2} r_8 Aux_c PIN_x - \frac{3}{2} r_8 Aux_c PIN_c < F_a Aux_p + \frac{3}{2} r_8 Aux_x PIN_x - \frac{3}{2} r_8 Aux_c PIN_c$$

$$F_a Aux_p + \frac{3}{2} r_8 Aux_c PIN_x - \frac{3}{2} r_8 Aux_c PIN_c < F_a Aux_p + \frac{3}{2} r_8 Aux_x PIN_x - \frac{3}{2} r_8 Aux_c PIN_c < 0$$

Thus,

$$F_a Aux_p + \tfrac{3}{2} r_8 Aux_x PIN_x - \tfrac{3}{2} r_8 Aux_c PIN_c < 0 \quad (30)$$

$$F_a Aux_p + \frac{3}{2} r_8 Aux_c PIN_x - \frac{3}{2} r_8 Aux_c PIN_c < F_a Aux_p + \frac{3}{2} r_8 Aux_x PIN_x - \frac{3}{2} r_8 Aux_c PIN_c < 0,$$

which yields (31)

$$F_a Aux_p + \tfrac{3}{2} r_8 Aux_c (PIN_x - PIN_c) < 0 \quad (31)$$

Now, $F_a Aux_p \geq 0$, $r_8 Aux_c \geq 0$ and since (27) showed $PIN_x > PIN_c$, then $PIN_x - PIN_c > 0$. It then follows that the left-hand side of (31) must always be non-negative. This is a contradiction. Thus, the original assumption that $Aux_x > Aux_c$ must have been false. It remains to show that furthermore $Aux_c \neq Aux_x$ to prove that $Aux_x < Aux_c$ always holds.

$Aux_c = Aux_x$ assumption for the network with the PXY-MP negative feedback loop

Thus far it has been hown that $Aux_x > Aux_c$ cannot hold in the network without the PXY-MP negative feedback loop. The above analysis is reworked for the special case when $Aux_c = Aux_x$ to show that this can never hold, either. The approach is similar to the previous case, with the exception of some inequalities being replaced with equalities. Identical notation is used when the equations are the same, and $(* a)$ notation (where $*$ is an equation number) where the only difference is the sign ($=$ rather than $>$ or $<$) in the equation. As

First, consider equations (19) and (40). From (19), an expression for Aux_x is obtained, for $r_5 \neq 0$

$$r_5 Aux_x - d_{MP} MP_x = 0 \quad (19)$$

Equation (21) is obtained again

$$Aux_x = \frac{d_{MP} MP_x}{r_5} \quad (21)$$

For (21) and for $r_5 \neq 0$, an expression for Aux_c is derived

$$r_5 Aux_c - r_3 PXY_a MP_c - d_{MP} MP_c = 0 \quad (40)$$

$$r_5 Aux_c = r_3 PXY_a MP_c + d_{MP} MP_c$$

$$Aux_c = \frac{r_3 PXY_a MP_c + d_{MP} MP_c}{r_5} = \frac{(r_3 PXY_a + d_{MP}) MP_c}{r_5} \quad (43)$$

Using (21) and (43) and the assumption $Aux_x = Aux_c$

$$\frac{d_{MP} MP_x}{r_5} = Aux_x = Aux_c = \frac{(r_3 PXY_a + d_{MP}) MP_c}{r_5}$$

$$\frac{d_{MP} MP_x}{r_5} = \frac{(r_3 PXY_a + d_{MP}) MP_c}{r_5}$$

$$d_{MP} MP_x = (r_3 PXY_a + d_{MP}) MP_c$$

Set $d_{MP} \neq 0$

$$d_{MP} MP_x = (r_3 PXY_a + d_{MP}) MP_c$$

$$MP_x = \left(\frac{r_3 PXY_a}{d_{MP}} + 1\right) MP_c \quad (44a)$$

Since $r_3, d_{MP} > 0$ ($r_3 \neq 0$ in the network with the PXY-MP negative feedback loop, and above $d_{MP} \neq 0$ was set) and $PXY_a \geq 0$, it follows that $\frac{r_3 PXY_a}{d_{MP}} \geq 0$ so $\left(\frac{r_3 PXY_a}{d_{MP}} + 1\right) MP_c \geq 1$, so from (44a)

$$MP_x = \left(\frac{r_3 PXY_a}{d_{MP}} + 1\right) MP_c \quad (44a)$$

$$MP_x = \left(\frac{r_3 PXY_a}{d_{MP}} + 1\right) MP_c \geq MP_c$$

Thus, obtain relationship (22a)

$$MP_x \geq MP_c \quad (22a)$$

Next, consider equations (16) and (17).

$$r_6 MP_x - r_7 CK_x PIN_x - d_{PIN} PIN_x = 0 \quad (17)$$

$$r_6 MP_x - PIN_x (r_7 CK_x + d_{PIN}) = 0$$

$r_6 MP_x = PIN_x(r_7 CK_x + d_{PIN})$

Since $MP_x \geq MP_c$, it follows that $r_6 MP_c \geq r_6 MP_x$ for non-negative r_6

$r_6 MP_c \leq r_6 MP_x = PIN_x(r_7 CK_x + d_{PIN})$

for $MP_c, MP_x \geq 0$.

$r_6 MP_c \leq PIN_x(r_7 CK_x + d_{PIN})$

$r_6 MP_c - PIN_x(r_7 CK_x + d_{PIN}) \leq 0$ (23a)

Note that $CK_c > CK_x$. Thus, for non-negative PIN_x, r_7, CK_x, CK_p and d_{PIN}, the following holds

$PIN_x(r_7 CK_x + d_{PIN}) < PIN_x(r_7 CK_c + d_{PIN})$

$-PIN_x(r_7 CK_x + d_{PIN}) > -PIN_x(r_7 CK_c + d_{PIN})$

$r_6 MP_c - PIN_x(r_7 CK_x + d_{PIN}) > r_6 MP_c - PIN_x(r_7 CK_c + d_{PIN})$

From (23)

$r_6 MP_c - PIN_x(r_7 CK_x + d_{PIN}) \leq 0$ (23)

it follows that

$0 \geq r_6 MP_c - PIN_x(r_7 CK_x + d_{PIN}) > r_6 MP_c - PIN_x(r_7 CK_c + d_{PIN})$.

Thus, the same inequality (24) is obtained as before

$r_6 MP_c - PIN_x(r_7 CK_c + d_{PIN}) < 0$ (24)

Now, from (16),

$r_6 MP_c - r_7 CK_c PIN_c - d_{PIN} PIN_c = 0$ (16)

$r_6 MP_c = r_7 CK_c PIN_c + d_{PIN} PIN_c$

$r_6 MP_c = r_7 CK_c PIN_c + d_{PIN} PIN_c$ (25)

Substituting (25) into (24) then gives

$r_6 MP_c - PIN_x(r_7 CK_c + d_{PIN}) < 0$ (24)

$PIN_c(r_7 CK_c + d_{PIN}) - PIN_x(r_7 CK_c + d_{PIN}) < 0$

Which yields inequality (26) for the system with a PXY-MP negative feedback loop

$$(PIN_c - PIN_x)(r_7 CK_c + d_{PIN}) < 0. \quad (26)$$

For non-negative components and parameters $(r_7 CK_c + d_{PIN}) > 0$, suggesting $PIN_c - PIN_x < 0$ must hold. In particular,

$$PIN_c < PIN_x \quad (27)$$

must be true. In what follows, (27) will be shown to lead to a contradiction.

Consider equation (14)

$$F_a Aux_p + \tfrac{1}{2} r_8 Aux_x PIN_x - r_8 Aux_c PIN_c - d_{Aux} Aux_c = 0 \quad (14)$$

Since, according to the assumption in this case $Aux_c = Aux_x$, then $d_{Aux} Aux_x = d_{Aux} Aux_c$, thus, from (14), (28a) is obtained

$$\begin{aligned} 0 &= F_a Aux_p + \frac{1}{2} r_8 Aux_x P_x - r_8 Aux_c P_c - d_{Aux} Aux_c \\ &\geq F_a Aux_p + \frac{1}{2} r_8 Aux_x P_x - r_8 Aux_c P_c - d_{Aux} Aux_x \end{aligned}$$

$$F_a Aux_p + \tfrac{1}{2} r_8 Aux_x PIN_x - r_8 Aux_c PIN_c - d_{Aux} Aux_x = 0 \quad (28a)$$

Consider equation (15) and once again, use the substitution (29)

$$\tfrac{1}{2} r_8 Aux_c PIN_c - r_8 Aux_x PIN_x - d_{Aux} Aux_x = 0 \quad (15)$$

$$d_{Aux} Aux_x = \tfrac{1}{2} r_8 Aux_c PIN_c - r_8 Aux_x PIN_x \quad (29)$$

Substituting (29) into (28) gives

$$F_a Aux_p + 1\tfrac{1}{2} r_8 Aux_x P_x - r_8 Aux_c P_c - d_{Aux} Aux_x = 0 \quad (28a)$$

$$F_a Aux_p + \frac{1}{2} r_8 Aux_x P_x - r_8 Aux_c P_c - (\frac{1}{2} r_8 Aux_c P_c - r_8 Aux_x P_x) = 0$$

$$F_a Aux_p + \frac{1}{2} r_8 Aux_x P_x - r_8 Aux_c P_c - \frac{1}{2} r_8 Aux_c P_c + r_8 Aux_x P_x = 0$$

$$F_a Aux_p + \tfrac{3}{2} r_8 Aux_x P_x - \tfrac{3}{2} r_8 Aux_c P_c = 0 \quad (30a)$$

Since, $Aux_c = Aux_x$, and $\frac{3}{2}r_8 Aux_x PIN_x = 0$,it follows that $\frac{3}{2}r_8 Aux_x PIN_x = \frac{3}{2}r_8 Aux_c PIN_x$, thus

$$F_a Aux_p + \frac{3}{2}r_8 Aux_c PIN_x - \frac{3}{2}r_8 Aux_c PIN_c = F_a Aux_p + \frac{3}{2}r_8 Aux_x PIN_x - \frac{3}{2}2r_8 Aux_c PIN_c$$

Thus,

$$F_a Aux_p + \frac{3}{2}r_8 Aux_x PIN_x - \frac{3}{2}r_8 Aux_c PIN_c = 0 \quad (30a)$$

$F_a Aux_p + \frac{3}{2}r_8 Aux_c PIN_x - \frac{3}{2}r_8 Aux_c PIN_c = F_a Aux_p + \frac{3}{2}r_8 Aux_x PIN_x - \frac{3}{2}r_8 Aux_c PIN_c = 0$, which yields (31a)

$$F_a Aux_p + \frac{3}{2}r_8 Aux_c (PIN_x - PIN_c) = 0 \quad (31a)$$

Now, $F_a Aux_p \geq 0$, $r_8 Aux_c \geq 0$. Recall (27), i.e. $PIN_c < PIN_x$. Therefore, for (31a) to hold both $F_a Aux_p = 0$ and $r_8 Aux_c = 0$ must hold, i.e. no auxin enters into the system and no active transport out of the cambium or xylem occurs (since $r_8 Aux_c = 0$ and $Aux_x = Aux_c$, it follows that $r_8 Aux_x = 0$). Thus, the original assumption that $Aux_x = Aux_c$ must have been false.

Combining both of the above discussions,it follows that $Aux_x > Aux_c$ and $Aux_x = Aux_c$ can never be true, thus $Aux_x < Aux_c$ is true always □.

f

Inequality $Aux_c > Aux_p$:

In the previous section, it was shown that $Aux_c > Aux_x$ is always true, using proof by contradiction. In this section, successful patterning conditions for $Aux_c > Aux_p$ are derived.

The first two equations in this system with the PXY-MP negative feedback loop are the same as in the case where there is no PXY-MP negative feedback loop. Thus, similar approach is used. From (15), $Aux_c PIN_c > Aux_x PIN_x$ is shown t hold.

$$\frac{1}{2}r_8 Aux_c PIN_c - r_8 Aux_x PIN_x - d_{Aux} Aux_x = 0 \quad (15)$$

For $d_{Aux} Aux_x > 0$,

$$0 = \frac{1}{2} r_8 Aux_c PIN_c - r_8 Aux_x PIN_x - d_{Aux} Aux_x < \frac{1}{2} r_8 Aux_c PIN_c - r_8 Aux_x PIN_x$$

$$\frac{1}{2} r_8 Aux_c PIN_c - r_8 Aux_x PIN_x > 0$$

$$\frac{1}{2} r_8 Aux_c PIN_c > r_8 Aux_x PIN_x$$

$$Aux_c PIN_c > 2 Aux_x PIN_x$$

Thus,

$$Aux_c PIN_c > 2 Aux_x PIN_x > Aux_x PIN_x$$

Thus, the same relationship as in inequality (32) was derived, i.e.

$$Aux_c PIN_c > Aux_x PIN_x \tag{32}$$

Next, consider equation (14)

$$F_a Aux_p + \tfrac{1}{2} r_8 Aux_x PIN_x - r_8 Aux_c PIN_c - d_{Aux} Aux_c = 0. \tag{14}$$

Using (32), the following is obtained

$$F_a Aux_p + \frac{1}{2} r_8 Aux_x PIN_x - r_8 Aux_c PIN_c - d_{Aux} Aux_c = 0$$

$$0 = F_a Aux_p + \frac{1}{2} r_8 Aux_x PIN_x - r_8 Aux_c PIN_c - d_{Aux} Aux_c$$
$$< F_A Aux_p + \frac{1}{2} r_8 Aux_c PIN_c - r_8 Aux_c PIN_c - d_{Aux} Aux_c$$

$$F_a Aux_p + \frac{1}{2} r_8 Aux_c PIN_c - r_8 Aux_c PIN_c - d_{Aux} Aux_c > 0$$

$$F_a Aux_p - \frac{1}{2} r_8 Aux_c PIN_c - d_{Aux} Aux_c > 0$$

Since this is the case for $Aux_c > Aux_p$ and furthermore $F_a > 0$, it follows that $F_a Aux_c > F_a Aux_p$

$$F_a Aux_p - \frac{1}{2} r_8 Aux_c PIN_c - d_{Aux} Aux_c > 0$$

$$F_a Aux_c - \frac{1}{2} r_8 Aux_c PIN_c - d_{Aux} Aux_c > F_A Aux_p - \frac{1}{2} r_8 Aux_c PIN_c - d_{Aux} Aux_c > 0$$

$$F_a Aux_c - \frac{1}{2} r_8 Aux_c PIN_c - d_{Aux} Aux_c > 0$$

Dividing throughout by Aux_c obtain an equivalent to the previous inequality (33) for $Aux_c > 0$,

$$F_a - \tfrac{1}{2} r_8 PIN_c - d_{Aux} > 0 \quad (33)$$

Next, rearrange equation (16) to obtain PIN_c,

$$r_6 MP_c - r_7 CK_c PIN_c - d_{PIN} PIN_c = 0 \quad (16)$$

$$r_7 CK_c PIN_c + d_{PIN} PIN_c = r_6 MP_c$$

$$PIN_c (r_7 CK_c + d_{PIN}) = r_6 MP_c$$

Thus,

$$PIN_c = \frac{r_6 MP_c}{r_7 CK_c + d_{PIN}} \quad (34)$$

Substituting (34) into (33)

$$F_a - \tfrac{1}{2} r_8 PIN_c - d_{Aux} > 0 \quad (33)$$

$$F_a - \tfrac{1}{2} r_8 \frac{r_6 MP_c}{r_7 CK_c + d_{PIN}} - d_{Aux} > 0 \quad (35)$$

Note that $CK_p > CK_c$, thus $\frac{r_6 r_8 MP_c}{r_7 CK_p + d_{PIN}} < \frac{r_6 r_8 MP_c}{r_7 CK_c + d_{PIN}}$ and so from (35), the following is obtained

$$\frac{r_6 MP_c}{r_7 CK_p + d_{PIN}} < \frac{r_6 MP_c}{r_7 CK_c + d_{PIN}}$$

$$-\frac{r_6 MP_c}{r_7 CK_p + d_{PIN}} > -\frac{r_6 MP_c}{r_7 CK_c + d_{PIN}}$$

$$-\frac{1}{2} r_8 \frac{r_6 MP_c}{r_7 CK_p + d_{PIN}} > -\frac{1}{2} r_8 \frac{r_6 MP_c}{r_7 CK_c + d_{PIN}}$$

$$F_a - \frac{1}{2} r_8 \frac{r_6 MP_c}{r_7 CK_p + d_{PIN}}) - d_{Aux} > F_a - \frac{1}{2} r_8 \frac{r_6 MP_c}{r_7 CK_c + d_{PIN}} - d_{Aux}$$

$$F_a - \frac{1}{2} r_8 \frac{r_6 MP_c}{r_7 CK_p + d_{PIN}}) - d_{Aux} > F_a - \frac{1}{2} r_8 \frac{r_6 MP_c}{r_7 CK_c + d_{PIN}} > 0$$

$$F_a - \frac{1}{2} r_8 \frac{r_6 MP_c}{r_7 CK_p + d_{PIN}} - d_{Aux} > 0 \quad (36)$$

Now, for the system (14)-(17),(19), (40)-(42), a different equation for MP_c is given,i.e.

$$r_5 Aux_c - r_3 PXY_a MP_c - d_{MP} MP_c = 0 \quad (40)$$

And, indeed

$$Aux_c = \frac{r_3 PXY_a MP_c + d_{MP} MP_c}{r_5} \quad (46)$$

$$Aux_c = \frac{(r_3 PXY_a + d_{MP}) MP_c}{r_5}$$

$$MP_c = \frac{r_5 Aux_c}{r_3 PXY_a + d_{MP}} \quad (47)$$

Substituting (47) into (36)

$$F_a - \frac{1}{2} r_8 \frac{r_6 MP_c}{r_7 CK_p + d_{PIN}} - d_{Aux} > 0 \quad (36)$$

$$F_a - \frac{1}{2} r_8 \frac{r_6}{r_7 CK_p + d_{PIN}} \left(\frac{r_5 Aux_c}{r_3 PXY_a + d_{MP}} \right) - d_{Aux} > 0.$$

Since this is the case for $Aux_p < Aux_c$

$$F_a - \frac{1}{2} r_8 \frac{r_6}{r_7 CK_p + d_{PIN}} \left(\frac{r_5 Aux_p}{r_3 PXY_a + d_{MP}} \right) - d_{Aux}$$

$$> F_a - \frac{1}{2} r_8 \frac{r_6}{r_7 CK_p + d_{PIN}} \left(\frac{r_5 Aux_c}{r_3 PXY_a + d_{MP}} \right) - d_{Aux} > 0$$

$$F_a - \frac{1}{2} r_8 \frac{r_6}{r_7 CK_p + d_{PIN}} \left(\frac{r_5 Aux_p}{r_3 PXY_a + d_{MP}} \right) - d_{Aux} > 0. \quad (48)$$

Thus, the successful patterning condition for $Aux_c > Aux_p$ to be satisfied for the network with the PXY-MP negative feedback loop is given by (48). The successful patterning condition (48) is not independent of final steady state concentrations of components and depends on PXY_a.Thus, an additional relatioship for PXY_a was identified such that it depends only parameters. This derivation is given below.

First, PXY_a will be written in terms of PXY_{in} using equation (42). Next, (41) will be rearranged to find PXY_{in} in terms of MP_c. Finally, MP_c will be written in terms of Aux_c and subjected to the requirement $Aux_c > Aux_p$ in order to find a condition for PXY_a.

A detailed approach is discussed below:

$$r_5 Aux_c - r_3 PXY_a MP_c - d_{MP} MP_c = 0 \quad (40)$$

$$r_4 MP_c - d_{PXY_{in}} PXY_{in} - r_2 PXY_{in} TDIF_p = 0 \quad (41)$$

$$r_2 PXY_{in} TDIF_p - d_{PXY_a} PXY_a = 0 \quad (42)$$

From (42),

$$r_2 PXY_{in} TDIF_p - d_{PXY_a} PXY_a = 0 \quad (41)$$

$$r_2 PXY_{in} TDIF_p = d_{PXY_a} PXY_a$$

$$d_{PXY_a} PXY_a = r_2 PXY_{in} TDIF_p$$

Set $d_{Aux} \neq 0$

$$PXY_a = \frac{r_2 PXY_{in} TDIF_p}{d_{PXY_a}} \quad (49)$$

Next, use (41) for an equation for PXY_{in}

$$r_4 MP_c - d_{PXY_{in}} PXY_{in} - r_2 PXY_{in} TDIF_p = 0$$

$$r_4 MP_c - PXY_{in}(d_{PXY_{in}} + r_2 TDIF_p) = 0$$

$$PXY_{in}(d_{PXY_{in}} + r_2 TDIF_p) = r_4 MP_c$$

Set $d_{PXY_{in}} + r_2 TDIF_p \neq 0$. Thus,

$$PXY_{in} = \frac{r_4 MP_c}{d_{PXY_{in}} + r_2 TDIF} \quad (50)$$

Substitute (50) into (49) to find an equation for PXY_a in terms of MP_c

$$PXY_a = \frac{r_2 PXY_{in} TDIF_p}{d_{PXY_a}}$$

$$PXY_a = \frac{r_2 TDIF}{d_{PXY_a}} \frac{r_4 MP_c}{(d_{PXY_{in}} + r_2 TDIF_p)} \quad (51)$$

To find MP_c, use (40)

$$r_5 Aux_c - r_3 PXY_a MP_c - d_{MP} MP_c = 0 \quad (40)$$

$$r_5 Aux_c - MP_c(r_3 PXY_a + d_{MP}) = 0$$

$$MP_c(r_3 PXY_a + d_{MP}) = r_5 Aux_c$$

Set $r_3 PXY_a + d_{MP} \neq 0$

$$MP_c = \frac{r_5 Aux_c}{r_3 PXY_a + d_{MP}} \quad (52)$$

Now, (52) is substitutred into into (51) to get a quadratic for PXY_a

$$PXY_a = \frac{r_2 TDIF_p}{d_{PXY_a}} \frac{r_4 MP_c}{(d_{PXY_{in}} + r_2 TDIF_p)} \quad (51)$$

$$PXY_a = \frac{r_2 TDIF_p}{d_{PXY_a}} \frac{r_4}{(d_{PXY_{in}} + r_2 TDIF_p)} \frac{r_5 Aux_c}{r_3 PXY_a + d_{MP}}$$

$$PXY_a(r_3 PXY_a + d_{MP}) = \frac{r_2 TDIF_p}{d_{PXY_a}} \frac{r_4 r_5 Aux_c}{(d_{PXY_{in}} + r_2 TDIF_p)}$$

$$r_3 PXY_a^2 + d_{MP} PXY_a = \frac{r_2 TDIF_p}{d_{PXY_a}} \frac{r_4 r_5 Aux_c}{(d_{PXY_{in}} + r_2 TDIF_p)}$$

$$PXY_a^2 + \frac{d_{MP}}{r_3} PXY_a = \frac{r_2 TDIF_p}{r_3 d_{PXY_a}} \frac{r_4 r_5 Aux_c}{(d_{PXY_{in}} + r_2 TDIF_p)}$$

Thus,

$$PXY_a^2 + \frac{d_{MP}}{r_3} PXY_a - \frac{r_2 TDIF_p}{r_3 d_{PXY_a}} \frac{r_4 r_5 Aux_c}{(d_{PXY_{in}} + r_2 TDIF)} = 0 \quad (53)$$

Here, the case for $Aux_c > Aux_p$ to be satisfied is discussed. Thus, since all are parameters and component are non-negative

$$\frac{r_2 TDIF_p}{r_3 d_{PXY_a}} \frac{r_4 r_5 Aux_c}{(d_{PXY_{in}} + r_2 TDIF_p)} > \frac{r_2 TDIF_p}{r_3 d_{PXY_a}} \frac{r_4 r_5 Aux_p}{(d_{PXY_{in}} + r_2 TDIF_p)}$$

$$-\frac{r_2 TDIF_p}{r_3 d_{PXY_a}} \frac{r_4 r_5 Aux_c}{(d_{PXY_{in}} + r_2 TDIF_p)} < -\frac{r_2 TDIF_p}{r_3 d_{PXY_a}} \frac{r_4 r_5 Aux_p}{(d_{PXY_{in}} + r_2 TDIF_p)}$$

$$0 = PXY_a^2 + \frac{d_{MP}}{r_3} PXY_a - \frac{r_2 TDIF_p}{r_3 d_{PXY_a}} \frac{r_4 r_5 Aux_c}{(d_{PXY_{in}} + r_2 TDIF_p)}$$

$$< PXY_a^2 + \frac{d_{MP}}{r_3} PXY_a - \frac{r_2 TDIF_p}{r_3 d_{PXY_a}} \frac{r_4 r_5 Aux_p}{(d_{PXY_{in}} + r_2 TDIF_p)}$$

$$0 < PXY_a^2 + \frac{d_{MP}}{r_3} PXY_a - \frac{r_2 TDIF_p}{r_3 d_{PXY_a}} \frac{r_4 r_5 Aux_p}{(d_{PXY_{in}} + r_2 TDIF_p)}$$

Thus,

$$PXY_a^2 + \frac{d_{MP}}{r_3} PXY_a - \frac{r_2 TDIF_p}{r_3 d_{PXY_a}} \frac{r_4 r_5 Aux_p}{(d_{PXY_{in}} + r_2 TDIF_p)} > 0 \quad (54)$$

The above inequality can be solved for PXY_a. Consider the roots of the equation

$$PXY_a^2 + \frac{d_{MP}}{r_3} PXY_a - \frac{r_2 TDIF_p}{r_3 d_{PXY_a}} \frac{r_4 r_5 Aux_p}{(d_{PXY_{in}} + r_2 TDIF_p)} = 0 \quad (55)$$

Equation (55) can be factorized using the discriminant D

$$D = \left(\frac{d_{MP}}{r_3}\right)^2 - \left(-4 \frac{r_2 TDIF_p}{d_{PXY_a} r_3} \frac{r_4 r_5 Aux_p}{(d_{PXY_{in}} + r_2 TDIF_p)}\right)$$

$$= \left(\frac{d_{MP}}{r_3}\right)^2 + \left(4 \frac{r_2 TDIF_p}{d_{PXY_a} r_3} \frac{r_4 r_5 Aux_p}{(d_{PXY_{in}} + r_2 TDIF_p)}\right)$$

The roots of (55) PXY_{a_1},PXY_{a_2} then become

$$PXY_{a_1}, PXY_{a_2} = \frac{1}{2}\left(-\frac{d_{MP}}{r_3} \pm \sqrt{D}\right)$$

$$= \frac{1}{2}\left(-\frac{d_{MP}}{r_3} \pm \sqrt{\left(\frac{d_{MP}}{r_3}\right)^2 + \left(4 \frac{r_2 TDIF_p}{d_{PXY_a} r_3} \frac{r_4 r_5 Aux_p}{(d_{PXY_{in}} + r_2 TDIF_p)}\right)}\right)$$

Thus, factorise (55) as follows:

$$PXY_a^2 + \frac{d_{MP}}{r_3} PXY_a - \frac{r_2 TDIF_p}{r_3 d_{PXY_a}} \frac{r_4 r_5 Aux_p}{(d_{PXY_{in}} + r_2 TDIF_p)} = 0$$

$$\left(PXY_a + \frac{1}{2}\frac{d_{MP}}{r_3} - \frac{1}{2}\sqrt{\left(\frac{d_{MP}}{r_3}\right)^2 + \left(4 \frac{r_2 TDIF_p}{d_{PXY_a} r_3} \frac{r_4 r_5 Aux_p}{(d_{PXY_{in}} + r_2 TDIF_p)}\right)}\right) \times$$

$$\left(PXY_a + \frac{1}{2}\frac{d_{MP}}{r_3} + \frac{1}{2}\sqrt{\left(\frac{d_{MP}}{r_3}\right)^2 + \left(4 \frac{r_2 TDIF_p}{d_{PXY_a} r_3} \frac{r_4 r_5 Aux_p}{(d_{PXY_{in}} + r_2 TDIF_p)}\right)}\right) > 0$$

If $PXY_{a_1} = -\frac{1}{2}\frac{d_{MP}}{r_3} - \frac{1}{2}\sqrt{\left(\frac{d_{MP}}{r_3}\right)^2 + \left(4\frac{r_2 TDIF_p}{d_{PXY_a} r_3}\frac{r_4 r_5 Aux_p}{(d_{PXY_{in}} + r_2 TDIF_p)}\right)}$ and $PXY_{a_2} = -\frac{1}{2}\frac{d_{MP}}{r_3} + \frac{1}{2}\sqrt{\left(\frac{d_{MP}}{r_3}\right)^2 + \left(4\frac{r_2 TDIF_p}{d_{PXY_a} r_3}\frac{r_4 r_5 Aux_p}{(d_{PXY_{in}} + r_2 TDIF_p)}\right)}$, then the solution to the inequality is given by

$$PXY_a \in (-\infty; PXY_{a_1}) \cup (PXY_{a_2}; +\infty). \quad (56)$$

Notice, however, that PXY_a is non-negative. Thus, $PXY_a \in [0, +\infty)$. The intersection of $PXY_a \in [0, +\infty)$ with (56) give the final solution

$$PXY_a > -\frac{1}{2}\frac{d_{MP}}{r_3} + \frac{1}{2}\sqrt{\left(\frac{d_{MP}}{r_3}\right)^2 + \left(4\frac{r_2 TDIF_p}{d_{PXY_a} r_3}\frac{r_4 r_5 Aux_p}{(d_{PXY_{in}} + r_2 TDIF_p)}\right)}. \quad (57)$$

The summary of the successful patterning conditions for the network with the PXY-MP negative feedback loop given in Table 2.

Network with PXY-MP negative feedback loop		
Conditions for cambial auxin maxima	$Aux_c > Aux_p$	$Aux_c > Aux_x$
	$F_a - \frac{1}{2} r_8 \frac{r_6}{r_7 CK_p + d_{PIN}} \left(\frac{r_5 Aux_p}{r_3 PXY_a + d_{MP}}\right) - d_{Aux} > 0$ with $PXY_a > -\frac{d_{MP}}{2r_3} + \frac{1}{2}\sqrt{\left(\frac{d_{Mp}}{r_3}\right)^2 + 4\frac{r_2 TDIF_p}{d_{PXY_a} r_3}\frac{r_4 r_5 Aux_p}{\left(d_{PXY_{in}} + r_2 TDIF_p\right)}}$	Always true

Table 2S: A summary table for the successful patterning conditions the network with the PXY-MP negative feedback loop. Column 1 shows headings. Column 2 shows the conditions for

auxin accumulation in the cambium over the phloem. Column 3 shows the auxin concentration in the cambium in both system exceeds the auxin concentration in the xylem

Together,

Conditions for auxin pattern in both networks		
Conditions for cambial auxin maxima	$Aux_c > Aux_p$	$Aux_c > Aux_x$
No PXY-MP loop	$F_a - \frac{1}{2} r_8 \frac{r_5 r_6 Aux_p}{d_{MP}(r_7 CK_p + d_{PIN})} - d_{Aux} > 0$	Always true
With PXY-MP loop	$F_a - \frac{1}{2} r_8 \frac{r_6}{r_7 CK_p + d_{PIN}} \left(\frac{r_5 Aux_p}{r_3 PXY_a + d_{MP}}\right) - d_{Aux} > 0$ with $PXY_a > -\frac{d_{MP}}{2r_3} + \frac{1}{2}\sqrt{\left(\frac{d_{MP}}{r_3}\right)^2 + \frac{r_2 TDIF_p}{d_{PXY_a} r_3} \frac{r_4 r_5 Aux_p}{(d_{PXY_{in}} + r_2 TDIF)}}$	Always true

Table 3S: This table matches Table 3 from Chapter 4. A summary table for the successful patterning conditions the network without the PXY-MP negative feedback loop. Column 1 shows headings. Column 2 shows the conditions for auxin accumulation in the cambium over the phloem. Column 3 shows the auxin concentration in the cambium in both system exceeds the auxin concentration in the xylem